Imperial College London
Department of Physics

Vacuum Energy in (2+1)-Dimensional Quantum Field Theory on Curved Spaces

Lucas Samuel Wallis

Thesis for the degree of
Doctor of Philosophy

March 2022

Abstract

Relativistic quantum degrees of freedom in their vacuum state endow geometric backgrounds with an energy, as demonstrated by the Casimir Effect. We explore the vacuum energy (or free energy at finite temperature) of (2+1)-dimensional ultrastatic relativistic quantum field theories as a functional of their spatial geometry. These theories have physical realisations as, for example, the low-energy effective description of the electronic structure of graphene: four free massless Dirac fermions. We define a UV-finite unambiguous measure of free energy for these setups: the free energy difference. We compute it for the free scalar with curvature coupling and free Dirac fermion using heat kernel methods, deriving analytic expressions for perturbative and long-wavelength deformations of maximally-symmetric two-spaces (namely the plane and the round sphere) and, using a novel numerical approach, highly-accurate estimates in the case of large (axisymmetric) deformations to the sphere. We find that for these theories, as with holographic conformal field theories (CFTs) dual to vacuum Einstein gravity with a negative cosmological constant, it is universally negative for non-trivial deformations of maximally-symmetric two-spaces and can be made arbitrarily negative as the geometry becomes singular. In fact, we find that the differenced heat kernel has a definite sign — a much stronger result. We also observe a qualitative similarity between the (appropriately normalised) vacuum energies of a conformal scalar, massless Dirac fermion and holographic CFT on deformations of the two-sphere, and a remarkably close quantitive agreement between the latter two — very dissimilar in nature — theories. Finally, we show vacuum energy negativity for all perturbative deformations to Poincaré-invariant, power-counting-renormalisable theories on the plane. Our results indicate that relativistic quantum degrees of freedom universally disfavour smooth geometries and we note this effect has the potential to be measured experimentally.

Statement of Originality

I declare that, unless otherwise specified, the work presented in this thesis is my own and that the work of others has been appropriately acknowledged and referenced. A portion of the material presented here appears in the publications [1–4],

[1] Sebastian Fischetti, Lucas Wallis, and Toby Wiseman. "What Spatial Geometries do (2+1)-Dimensional Quantum Field Theory Vacua Prefer?" In: *Phys. Rev. Lett.* 120.26 (2018), p. 261601. DOI: 10.1103/PhysRevLett.120.261601. arXiv: 1803.04414 [hep-th].

[2] Krai Cheamsawat, Lucas Wallis, and Toby Wiseman. "Free energy dependence on spatial geometry for (2+1)-dimensional QFTs". In: *Class. Quant. Grav.* 36.19 (2019), p. 195011. DOI: 10.1088/1361-6382/ab353d. arXiv: 1811.05995 [hep-th].

[3] Sebastian Fischetti, Lucas Wallis, and Toby Wiseman. "Does the Round Sphere Maximize the Free Energy of (2+1)-Dimensional QFTs?" In: *JHEP* 10 (2020), p. 078. DOI: 10.1007/JHEP10(2020)078. arXiv: 2003.09428 [hep-th].

[4] Krai Cheamsawat, Sebastian Fischetti, Lucas Wallis, and Toby Wiseman. "A surprising similarity between holographic CFTs and a free fermion in (2 + 1) dimensions". In: *JHEP* 05 (2021), p. 246. DOI: 10.1007/JHEP05(2021)246. arXiv: 2012.14437 [hep-th].

to which each of the named authors contributed equally, and the work presented in Chapter 7 was done in collaboration with Andrew Tolley and Toby Wiseman. I wish to emphasise in particular that:

(i) the calculation of the free energy difference at finite temperature for perturbative deformations to holographic CFTs and long-wavelength deformations to theories which admit a hydrostatic description, originally presented in [2] and reviewed here in Section 4.2, were performed entirely by Krai Cheamsawat and Toby Wiseman and

(ii) the numerical calculations of the vacuum energy of holographic CFTs on non-perturbative deformations of the two-sphere, the results of which were originally presented in [4] and are included here in Chapter 6, were performed entirely by Krai Cheamsawat and Toby Wiseman.

Copyright Declaration

Acknowledgements

First and foremost, I'm extremely grateful to my supervisor, Toby Wiseman, for his expertise, guidance and generosity throughout this project. I would like to thank Krai Cheamsawat and Sebastian Fischetti for our enjoyable collaborations, Andrew Tolley and Arttu Rajantie for helpful discussions throughout the course of my research and the rest of the Theory Group for making Imperial a great place to work. I also wish to acknowledge the support of the Science and Technology Facilities Council Doctoral Training Partnership research studentship grant ST/R504816/1 that enabled this project. Particular thanks are also owed to my fellow PhD students and officemates with whom sharing copious amounts of coffee, countless amusing discussions over lunch and an Ethos made each day in the office a pleasure.

Finally, I'm fortunate to have been surrounded by friends and family whose continued support has been the basis for all my successes. I'm especially thankful to my parents for their unwavering support and encouragement, and to my partner, Rona, for her level-headed perspective and for keeping me sane throughout.

In memory of my father, Stephen Wallis.

Contents

List of Tables

List of Figures

Conventions

Units: Unless otherwise stated we use natural units, $\hbar = c = k_{\mathrm{B}} = 1$ with c the 'effective' speed of light of the relativistic fields (not necessarily equal to the actual speed of light).

Metrics and Tensors: We take the Minkowski metric to have signature $(-,+,\ldots,+)$. and use Einstein summation convention (unless otherwise stated).

We (generally) use upper-case Latin letters $(A, B, \ldots)$, lower-case Greek letters $(\mu, \nu, \ldots)$ and lower-case Latin letters $(i, j, \ldots)$ for bulk (normally four-dimensional), spacetime (normally three-dimensional) and spatial (normally two-dimensional) indices, respectively (the exception is Section 1.3 where the use should be clear from context).

Symmetrisation and antisymmetrisation over indices are normalised by the number of terms, i.e.

$$A_{(\mu_1\mu_2\ldots\mu_n)} \equiv \frac{1}{n!}\sum_{\sigma\in \mathrm{S}_n} A_{\mu_{\sigma(1)}\mu_{\sigma(2)}\cdots\mu_{\sigma(n))}} \text{ and } A_{[\mu_1\mu_2\ldots\mu_n]} \equiv \frac{1}{n!}\sum_{\sigma\in \mathrm{S}_n} \mathrm{sgn}(\sigma) A_{\mu_{\sigma(1)}\mu_{\sigma(2)}\cdots\mu_{\sigma(n)}}$$

where S_n is the symmetric group of degree n.

We define the Riemann curvature tensor of a connection to be

$$R^{\mu}{}_{\nu\rho\sigma} = \partial_\rho \Gamma^{\mu}_{\nu\sigma} - \partial_\sigma \Gamma^{\mu}_{\nu\rho} + \Gamma^{\tau}_{\nu\sigma}\Gamma^{\mu}_{\tau\rho} - \Gamma^{\tau}_{\nu\rho}\Gamma^{\mu}_{\tau\sigma}$$

in a coordinate basis, where $\Gamma^{\mu}_{\nu\rho}$ are the connection components and the Ricci curvature tensor to be $R_{\mu\nu} \equiv R^{\rho}{}_{\mu\rho\nu}$.

Integrals: When integral measures are omitted the measure is understood to be given by the natural volume form of the manifold.

Introduction

The equilibrium configuration of a physical system is determined by competition between several physical effects. Each effect has some energetic contribution that measures the potential for work to be done on the system, inducing a force that attempts to minimise its own contribution to the total energy. Identifying and understanding the nature and origin of these forces has been key to pushing physics forwards. Ancient Greek philosophers were aware of forces but their failure to account for friction left them unable to distill their effect on particle motion. These misunderstandings were challenged intially by Galileo in what eventually became the first of Newton's universal laws of motion. Efforts to understand the forces of electricity and magnetism resulted in Maxwell's equations and hidden within them was the idea of a force propagating at a finite speed of light. This was a key insight that Einstein based his 1905 paper "On Electrodynamics on moving bodies" on, in which he posited the special theory of relativity and, with it, the concept of 'spacetime' and the famous equivalence of mass and energy [5]. Attempting to incorporate gravity into this new framework led Einstein to his general theory of relativity — the remarkable idea that gravity is best understood as a fictitious force with its effects attributed to spacetime curvature induced by any energy and momentum present in the universe.

In the preceeding years our understanding of energy at the microscopic level had also undergone a paradigm shift. The tension between spectra of black body radiation and classical predictions led to the idea of energy being 'quantised'. This was unified with the Bohr model for electronic structure and wave-particle duality into a theory for non-relativistic physics at atomic scales: quantum mechanics. Although this theory was sufficient to explain why atoms radiate when subjected to an electromagnetic field, i.e. stimulated emission, it could not account for the rate at which such a process happened when no electromagnetic field was present. To do so, Dirac considered not only whether the energy levels of an electron should be quantised but also the electromagnetic field at each point in spacetime. This gave rise to what would eventually become quantum electrodynamics (QED), the first example of a quantum field theory (QFT) — the most successful theoretical framework we have for particle and condensed matter physics. Ultimately, it was the novel understanding of the 'vacuum' that came from applying the principles of quantum mechanics to the relativistic field theory that accounted for the spontaneous emission. The vacuum is the lowest energy state of the system and is empty

in that it contains no particles. In *quantum* field theory, however, no space can be truly empty. Just as in classical field theory, there are 'fields' that take some value at each point in spacetime, the electric and magnetic fields in this instance. In contrast with the classical case, these fields are subject to the laws of quantum mechanics, in particular Heisenberg's uncertainty principle, and thus *must* be constantly fluctuating — even in the vacuum state. It is these quantum fluctuations that 'stimulate' the spontaneous emission of photons and thus most of the light we see around us. The presence of vacuum fluctuations suggests that the vacuum should have some kind of energy, however naïve attempts to calculate the total energy of these modes by, for example, taking the vacuum expectation value of the Hamiltonian, leads to a divergent sum. This is, of course, a generic feature of QFTs. The canonical quantisation procedure leads to ambiguities in operator ordering and therefore matrix elements of composite operators. To fix them we often use prescriptions for operator ordering, such as normal ordering, that in the particular case of the Hamiltonian set its vacuum expectation value, the vacuum energy, to zero, the physical justification for this being that only energy *differences* are observable. However, while this philosophy may be appropriate for microscopic systems, it is not universally applicable in physics. Indeed, in trusting Einstein's theory of general relativity, we subscribe to the belief that *all* energy gravitates. This suggests that we should take the idea that vacuum energy has some meaningful value, at least as a functional of the geometry that supports it, seriously.

Among those who did was Hendrik Casimir. In 1948, he and Dik Polder presented a series of cumbersome calculations to show that there is an attractive force between a perfectly conducting plate and a well-separated neutral molecule and that a similar result holds between two such molecules [6]. Casimir was struck by how simple the results were, in contrast to the calculations themselves. He mentioned them to Niels Bohr who then, according to Casimir himself, "mumbled something about zero-point energy" [7] which was the catalyst for him to reformulate his results in terms of the energy of the QED vacuum. Taking this idea further led to the seminal work [8] in which he predicted the Casimir Effect, i.e. two parallel conducting plates placed nanometers apart in a vacuum should exert a small, but measurable, attractive force on each other owing to the energy of the QED vacuum, a phenomenon that has since been experimentally verified many times over [9, 10]. This was an early example of the macroscopic physics induced by quantum vacuum energy and, in particular, how the presence of a quantum field may back-react to alter the geometry of a macroscopic system. Indeed, Einstein's equation tells us that all energy couples to spacetime curvature and so we should expect the existence of quantum fields to have some effect on gravitational systems.

In cosmology, the kinematics of the universe from roughly 10^{-37}s after the beginning of the expansion until the present day are well established. However, the precise physics behind it remains disputed. The Lambda-Cold Dark Matter (Λ-CDM) model is

the dominant paradigm in modern cosmology due to its precise agreement with cosmological observations [11]. It assumes that on large scales the universe is homogeneous and isotropic (the cosmological principle), so that the geometry is characterised by a single function of time, the scale factor $a(t)$, and that general relativity holds so we can use the Einstein equation to map out its evolution. The input is then the matter content of the universe, whose contribution is characterised its abundance and equation of state ($P = w\rho$). This is made up of three different species: 'matter' ($w = 0$) made up baryons and cold dark matter, 'radiation' ($w = 1/3$) made up of photons and relativistic neutrinos and 'dark energy' ($w = -1$), whose origins are as yet unknown. While matter and radiation have a tendency to contract space, the negative pressure of dark energy leads to accelerated expansion. Thus, when light measured from Type Ia supernovae revealed that the expansion of the universe is accelerating [12, 13] it became accepted that dark energy must form a *significant* part of the energy budget of the universe. Current measurements [14] estimate that dark energy accounts for around 69% of the energy in the universe, yet its fundamental nature is still an active area of research. Vacuum energy is a very appealing candidate for several reasons. Firstly, it is a form of energy that does not dilute with volume. Indeed, a change in volume $\mathrm{d}V$ leads change in energy $\rho_{\mathrm{vac}}\mathrm{d}V$ thus an equation of state $w = -1$. Secondly, vacuum energy is an intrinsic feature of the quantum field theories that live throughout the cosmos, giving a natural argument for its origin. Thirdly, its energy contribution to the universe should be calculable. However, attempts to do so led to estimates of the dark energy that are up to 120 orders of magnitude larger that what is observed — a disagreement that has come to be known as the 'cosmological constant problem'.

Vacuum energy also finds its uses on the more theoretical end of the spectrum. A wormhole is a geometrical connection between two distinct asymptotically flat[1] regions. These can be distant regions of the same universe or belong to separate universes entirely. Wormholes have long been of interest to physicists and science fiction writers alike. The first wormhole solution found in General Relativity was the Einstein-Rosen bridge between the two asymptotically flat regions of Kruskal spacetime — the maximal analytic extension of a Schwarzschild black hole. It is not possible, however, to send a signal from one end of this wormhole to the other. What we should really be interested in are wormholes solutions for which this is possible — traversable wormholes. Any solutions of Einstein's equations that satisfy the averaged null energy condition (ANEC), i.e. given a complete null geodesic with tangent vector u and parameter λ, the expectation value of the stress tensor satisfies

$$\int_{-\infty}^{\infty} \mathrm{d}\lambda \langle T_{\mu\nu}\rangle u^\mu u^\nu \geqslant 0, \tag{1}$$

cannot contain a traversable wormhole due to topological censorship [16–18]. ANEC is

[1] or asymptotically AdS, of particular interest due to the AdS/CFT correspondence [15].

satisfied by classical matter thus, assuming Einstein gravity holds, some kind of exotic matter is required to support stable traversable wormhole solutions. The QFT vacuum can provide a source of negative energy (cf. the Casimir Effect) that permits the ANEC violation required to support wormholes. This has been used to construct traversable wormholes in four dimensions [19], however these wormholes are microscopic, and, as such, further efforts are being made to extend these ideas to the construction of humanly traversable wormholes [20]. As the only current lab confirmed form of exotic matter[2], quantum vacuum energy has a key role to play in the future development of exotic solutions in general relativity.

Looking beyond Einstein gravity, there are many physical scenarios that involve relativistic degrees of freedom on curved spaces embedded within a higher dimensional geometry. In braneworld models of the universe [23, 24], initially theorised to solve the Hierarchy Problem, the (3+1)-dimensional spacetime that we perceive is simply a 3-brane embedded in a manifold with additional spatial dimensions on which the Standard Model fields are localised. In the early universe, spontaneous symmetry breaking may have led to the formation of domain walls defects — (2+1)-dimensional regions of high energy density that are, effectively, topologically stabilised membranes that support quantum fields [25].

The purpose of this thesis will be to investigate the vacuum energy at zero temperature, or free energy at finite temperature, of ultrastatic quantum field theories on (2+1)-dimensional spaces as a functional of their spatial geometries. Our interest in these particular theories owes itself to some intriguing results from holography.

The setting for this work is quantum field theory in curved spacetime, where first principles computations are generically difficult. Through the AdS/CFT correspondence, these computations can be reformulated as tractable problems in classical geometry, at least for a large number of conformal field theories (CFTs) [26–28]. By probing these theories, one may find qualitative features worthy of further investigation. For holographic CFTs[3] with closed spatial geometries, it follows from a geometric argument that the renormalised CFT vacuum energy is found to be non-positive and zero if and only if the background has constant curvature [29]. Following this, it was also proved that constant curvature spaces are local maxima of vacuum energy for all unitary[4] CFTs when the spatial geometry is topologically $\mathbb{R}^2$ or S^2 [30]. These results raise an obvious question: how universal is vacuum/free energy non-positivity amongst (2+1)-dimensional QFTs? This question merits investigation as a theoretical one alone but also has a relatively straightforward connection to experiment. If true more generally, the negativity of free

[2] i.e. it does not obey many of the standard energy conditions assumed in general relativity to prove physically sensible behaviour (such as the Penrose Singularity Theorem [21], no closed timelike curves [22]).

[3] See Section 1.2 for a precise description of these theories

[4] 'Unitary' here (and throughout the rest of this thesis when referring to CFTs) means that the collection of physical states of the theory admit a positive-definite inner product and, in particular, form a Hilbert Space.

energy points to a peculiar property of (2+1)-dimensional QFTs — an energetic preference for crumpled geometries over smooth ones.

Increasingly, (2+1)-dimensional QFTs have found physical realisations in condensed matter physics where some effective descriptions of the electronic structure of two-dimensional crystalline materials have been in terms of quasi-relativistic quantum fields. Graphene is, thus far, the most famous example of such a material. It is the closest thing we have to a two-dimensional object — consisting of just a single layer of carbon atoms arranged in a 'honeycomb' structure. Though it is thought to be a generic product of rubbing graphite — i.e. using a pencil on paper — and thus ubiquitous, it took until 2004 before it was isolated [31]. Other well known forms of carbon are constructed from graphene: graphite is made from stacking layers of graphene on top of one another, carbon nanotubes are graphene rolled up into cylindrical form and 'buckyballs' can be made from graphene with the addition of some pentagons to the honeycomb lattice to make a sphere [32]. Where industry see the mechanical stiffness, exceptionally high electrical and thermal conductivity, strength and elasticity of graphene as an opportunity for innovation in technology [33, 34], physicists see an opportunity to stress test QED. This is because the low-energy effective description of the electronic structure matches that of a relativistic QFT, namely four (2+1)-dimensional massless Dirac fermions propagating at the Fermi velocity ($\approx 10^6$m/s) [35–37]. We will illustrate this here by reviewing some analysis of the band structure of graphene that was first undertaken by P.R. Wallace in 1947 [38], long before the isolation of two-dimensional crystalline materials was thought to be possible, as part of a toy model to understand graphite, and later on in 1984 by Semenoff who made the connection between QED and the electronic structure of graphene explicit [39].

A Physical Realisation: Graphene

The carbon atoms in graphene form a hexagonal lattice, best understood as two overlaid triangular sublattices, with adjacent sites lying on different sublattices, as shown in Figure 1, and whose sites are given by $\Lambda_{\mathrm{A}} = \left\{n_1\mathbf{a}_1 + n_2\mathbf{a}_2 | (n_1, n_2) \in \mathcal{A} \subset \mathbb{Z}^2\right\}$ and $\Lambda_{\mathrm{B}} = \left\{n_1\mathbf{a}_1 + n_2\mathbf{a}_2 + \mathbf{d} | (n_1, n_2) \in \mathcal{A} \subset \mathbb{Z}^2\right\}$ where the vectors $\mathbf{a}_1 = \sqrt{3}a\left(1, -\sqrt{3}\right)/2$ and $\mathbf{a}_2 = -\sqrt{3}a\left(1, \sqrt{3}\right)/2$ generate the sublattices, $\mathbf{d} = (0, a)$ moves between the two, $a\,(\approx 1.42\text{Å}$ for graphene) is the lattice spacing and $2N \equiv 2|\mathcal{A}|$ is the total number of lattice sites. Each carbon atom has four electrons, three of which bond it to its nearest neighbours, leaving one free electron from each — these give rise to the electronic properties of graphene. The best model to probe the collective behaviour of these electrons is the tight-binding model — the assumption being that each electron is 'tightly bound' to an atom on the lattice and has some small chance of tunnelling to a neigh-

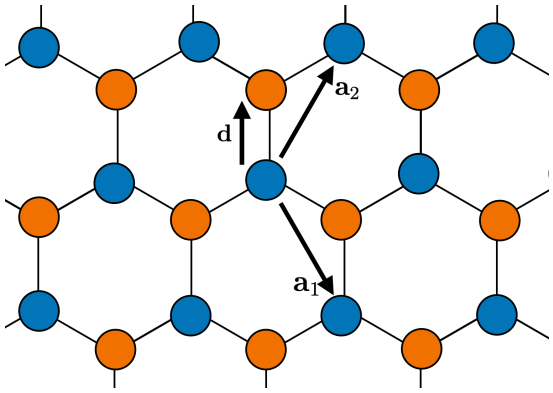

Figure 1: A diagram showing the 'honeycomb' lattice structure of graphene. The sites in the sublattice Λ_A are represented with blue nodes and sites in the sublattice Λ_B are represented by orange nodes. The vectors $\mathbf{a}_1$ and $\mathbf{a}_2$ generate the sublattices and $\mathbf{d}$ moves between them.

bouring atom. We will also neglect interactions between the electrons and only consider nearest-neighbour hopping. A complete treatment can be found in [40] but the main qualitative features are present in the leading order calculation, that will be covered in the rest of this section.

Consider the behaviour of a single electron. Writing $|\mathbf{r}, \sigma\rangle$ to denote the state representing the electron being bound to atomic site $\mathbf{r}$ with spin σ leads to a Hamiltonian of the form

$$H = -t \sum_{\mathbf{r}\in\Lambda_\mathrm{A},\sigma} |\mathbf{r}_\mathrm{A}, \sigma\rangle \left(\langle \mathbf{r}_\mathrm{B} + \mathbf{a}_1, \sigma| + \langle \mathbf{r}_\mathrm{B} + \mathbf{a}_2, \sigma| + \langle \mathbf{r}_\mathrm{B}, \sigma| \right) + \mathrm{h.c.}, \tag{2}$$

where $\mathbf{r}_\mathrm{A} \equiv \mathbf{r}$, $\mathbf{r}_\mathrm{B} \equiv \mathbf{r} + \mathbf{d}$ and $t \approx 2.8\mathrm{eV}$, which parametrises the probability of an electron 'hopping' to an adjacent side, is called the hopping parameter. This Hamiltonian has a spectrum given by

$$E(\mathbf{k}) = \pm t \sqrt{1 + 4\cos(3k_y a/2)\cos(\sqrt{3}k_x a/2) + 4\cos^2(\sqrt{3}k_x a/2)}. \tag{3}$$

with $\mathbf{k}$ taking values in the first Brillouin zone. The Pauli exclusion principle then plays a key role in the collective behaviour of all of the electrons. As electrons are fermions, there can only be one electron with a given $\mathbf{k}$ and spin at any given time. The number of permitted 'momenta' matches the number of unit cells in the lattice. For a honeycomb lattice there are two atoms in each unit cell, thus providing precisely correct number of electrons to fill the spin up and spin down slots available for each energy level with $E(\mathbf{k}) < 0$. The relevant low energy behaviour, therefore, belongs to states with momenta close to the solutions of $E(\mathbf{k}) = 0$, namely $\mathbf{K}_\pm = -\frac{2\pi}{3a}\left(\pm 1, \frac{1}{\sqrt{3}}\right)$. Suppressing spin labels for the

time being and switching to a momentum space basis

$$|\mathbf{k}_{A/B}\rangle \equiv \frac{1}{\sqrt{N}} \sum_{\mathbf{r}} \mathrm{e}^{i\mathbf{k}\cdot\mathbf{r}} |\mathbf{r}_{A/B}\rangle, \tag{4}$$

gives that the Hamiltonian density, $\mathcal{H}(\mathbf{k})$, near these modes is

$$\mathcal{H}(\mathbf{k}) \equiv \begin{pmatrix} \langle \mathbf{k}_A|\hat{H}|\mathbf{k}_A\rangle & \langle \mathbf{k}_A|\hat{H}|\mathbf{k}_B\rangle \\ \langle \mathbf{k}_B|\hat{H}|\mathbf{k}_A\rangle & \langle \mathbf{k}_B|\hat{H}|\mathbf{k}_B\rangle \end{pmatrix} = \pm\hbar v_{\mathrm{F}} \gamma^i_{\pm} p_i + \mathcal{O}(t(a|\mathbf{p}|)^2) \tag{5}$$

where $\mathbf{p} = \mathbf{k} - \mathbf{K}_{\pm}$, $\boldsymbol{\gamma}_{\pm} = (\sigma^1, \pm\sigma^2)$ and $v_{\mathrm{F}} = \frac{3t}{2a\hbar} \approx 10^6 \mathrm{m/s}$ is the Fermi velocity of these excitations. Thus, in the continuum/low-energy limit, the effective Hamiltonian is

$$\langle\psi|H|\psi\rangle = \hbar v_{\mathrm{F}} \int \mathrm{d}^2x \, \psi_+(\mathbf{x})^\dagger \gamma^i_+ \partial_i \psi_+(\mathbf{x}) - \psi_-(\mathbf{x})^\dagger \gamma^i_- \partial_i \psi_-(\mathbf{x}) \tag{6}$$

where $\psi_{\pm}$ are the position space wavefunctions that correspond to the modes near $\mathbf{K}_{\pm}$ respectively. Note that each of $\mathbf{K}_{\pm}$ will give rise to two such wavefunctions — one for spin up and one for spin down. Thus, in second quantised language, the low-energy effective description of the electronic structure of graphene matches that of a relativistic QFT, namely four (2+1)-dimensional massless Dirac fermions (spin up and down electrons at each of $\mathbf{K}_{\pm}$) propagating at the Fermi velocity.

Further, this analysis can be extended to the case of curved graphene sheets [41] to show the low-energy effective behaviour of the electrons is given by the curved space Dirac equation[5] (where the electrons experience a metric perturbation that is larger by a factor of $\beta \approx 3.3$ [43]) — a bona fide QFT in curved spacetime. This opens the door for a mutually beneficial relationship between two-dimensional materials and curved space QFT, where the latter can seek to explain observed phenomena in the former, such as the ripples observed in freely suspended graphene at room temperature [44], and the former can be used to create analogue systems that test predictions of the latter, such as the Unruh effect [45] and, of particular interest to us, any predictions one may have about the relationship between quantum vacuum energy and its background geometry. Perhaps even more promising on the experimental side of things is the growing interest in the use of optical lattices. They mimic crystalline materials using potential wells generated by the interference of lasers and the ultra-cold atoms they trap emulate charge carriers in a material. The greater control over parameters, compared with physical materials, afforded by optical lattices makes them an ideal candidate for experimental work. In particular, one can choose the lattice structure and tune the depth of these various wells, and in doing so create a system whose long-wavelength dynamics are governed by a (2+1)-dimensional relativistic QFT, with a curved background of one's choosing [46], offering a rare avenue

[5] We note that recent work suggests this may only hold subject to an (unnatural) fine tuning of the geometry [42].

for a testing (2+1)-dimensional curved space QFT predictions, in particular those given in this thesis, in the lab.

Plan for the Thesis

Chapter 1 will serve as a technical introduction to the subject of vacuum energy in QFT and exhibit the results that directly motivated the original work in the thesis. The calculation of the Casimir Energy [8], the use of the AdS/CFT correspondence to show the non-positivity of the vacuum energy of static (2+1)-dimensional holographic CFTs [29] and the universality of this result for all unitary CFTs [30] will be reviewed.

Chapter 2 will review the theory behind calculating the free energy: heat kernel methods. It will be shown how the partition function, and thus the free energy, of a free theory on a curved space can be written in terms of a functional determinant of a differential operator and then how heat kernel methods can be used to calculate it. The heat kernel, and in particular the heat kernel expansion, will be introduced and used to probe the free energy (or more generally the one-loop effective action) of a quantum field theory on a curved space. The rest of the thesis will focus on calculating and bounding the free energy of (2+1)-dimensional QFTs on a product of time with a static two-space and is largely based on [1–4].

In Chapter 3, the study of non-conformal field theories will be initiated with an analysis of free fields at finite temperature. A UV-finite, unambiguous measure of the free energy, the free energy difference, ΔF, will be defined for free fields. The corresponding differenced heat kernel, $\sigma\Delta K$, will then be shown to be negative for any small perturbation of flat space to leading order in the perturbation parameter, indicating a negative ΔF and, thus, a preference for crumpled geometries for all masses and at all temperatures. It will then be shown how this quantum effect could have a non-negligible effect on the shape of monolayer graphene. This chapter is based on work in [1, 3] and will closely follow the presentation there.

In Chapter 4, it will be shown that the free energy difference described in Chapter 3 can be generalised to define a quantity that is UV finite and unambiguous for non-free theories, for both compact and non-compact backgrounds. A review will be given of a holographic calculation that shows, using this definition ΔF, small spatial-metric perturbations also lower the free energy difference for flat holographic CFTs at finite temperature to leading order and that the same is true for long-wavelength deformations to theories that admit a hydrostatic description. A remarkable quantitative similarity between ΔF for a free massless Dirac fermion and a strongly-coupled holographic CFT, a priori two very different theories, will be noted. Finally, ΔF will be shown to be negative for free scalar and fermion theories on weakly curved deformations of flat space. This will be demonstrated by a derivation of an asymptotic expansion of ΔF to all orders in inverse

powers of the curvature scale of the deformation. This chapter is based on [2] and will closely follow the presentation there.

Chapter 5 will treat free fields on topologically spherical backgrounds. Just as in Chapter 3 for flat backgrounds, $\sigma\Delta K$ will be calculated and shown to be negative for small perturbations of the background. The focus will then turn to the global behaviour of ΔF as a functional of spatial geometry. It will be shown how pseudo-spectral methods can be used to yield accurate estimates for the spectra of differential operators. These will permit accurate numerical computations of $\sigma\Delta K$ for large (axisymmetric) deformations of the sphere that, along with some analytic results, will be used to provide a substantial body of evidence for the conjecture that $\sigma\Delta K$ (and thus ΔF for all masses and at all temperatures) is negative for any non-trivial deformation of the geometry. Finally, the free energy contribution of various singularities will be examined along with their implications for graphene-like materials. This chapter is based largely on [3] and will closely follow the presentation there.

In Chapter 6, the similarity between various field theories observed in Chapters 4 and 5 will be explored. For zero-temperature CFTs on topological two-spheres, the vacuum energy of holographic CFTs — computed numerically via the harmonic approach, which will be reviewed — the Dirac fermion and the conformally-coupled scalar will be compared for a range of large sphere deformations. A close qualitative similarity between all three and, in parallel with what will be seen in Chapter 4, a striking and unexplained close quantitative similarity between (appropriately normalised) Dirac fermion and holographic CFT vacuum energies will be observed. This chapter is based on [4] and will closely follow the presentation there.

Chapter 7 will return to zero-temperature theories on flat space. Canonical QFT methods will be used to compute the variation of the vacuum energy due small deformations of flat space. Assuming only power-counting renormalisability and Lorentz invariance of the flat-space theory, we will show such perturbations always *lower* the vacuum energy, thereby extending the previous results found for unitary CFTs and free theories. It will be shown that this result is special to ultrastatic theories in (2+1)-dimensions — the vacuum energy in higher dimensions is not necessarily unambiguous. This chapter is based on work done in collaboration with Andrew Tolley and Toby Wiseman.

The thesis will then conclude with a summary of, and the questions posed by, the work in this thesis.

Chapter 1

Calculating The Vacuum Energy

The vacuum energy is one the most basic quantities of a quantum field theory with a globally-timelike Killing vector field but nevertheless, as is often the case for observables in quantum field theory, is non-trivial to calculate from first principles. Given a generic theory, it is an impossible task. The objective of this work is to probe the vacuum energies of (2+1)-dimensional QFTs for as large a class of theories as possible. As such, previous vacuum energy calculations can provide key insight into the technical challenges involved in vacuum energy calculations and a steer in what is a priori an open-ended investigation topic. In this chapter, we will review three such vacuum energy computations.

Firstly, the calculation of the Casimir Energy will be reviewed [8]. To do this, the massless, free vector field will be quantised to show how the energy of its vacuum state is modified by the presence of conducting plates. Following appropriate regularisation, it is found that the vacuum energy is a *increasing* function of plate separation and thus that there is an attractive force between the conducting plates. Further, this force is purely quantum yet measurable for small plate separations [9, 10]. This setup gives a realistic physical example of a quantum vacuum energy driving changes to macroscopic geometry and, as the first quantum vacuum energy calculation of its kind, it serves as a useful introduction to many of the technical aspects that are generically present in vacuum energy computations.

In the latter half the chapter, the focus will turn to the subject of the rest of thesis: the vacuum energy of static (2+1)-dimensional QFTs as a functional of their spatial geometry. To initiate the investigation, we begin with a set of tractable theories. Thanks to the AdS/CFT correspondence, we know there exist a certain class of strongly-coupled CFTs with a large number of degrees of freedom whose renormalised stress tensor vacuum expectation values can be deduced from the asymptotic behaviour of a 'dual' Einstein metric with negative curvature. This gives a large number of static (2+1)-dimensional theories whose energies can be probed through classical geometry. We will do so for such theories with compact spatial geometry $(\Sigma, \bar{g})$. Under some reasonable assumptions, it turns out that the vacuum energy of these holographic CFTs is zero when $(\Sigma, \bar{g})$ has

constant curvature and is otherwise negative [29]. This raises the question of whether a similar result holds for *all* static (2+1)-dimensional QFTs. Further progress has been made in this area, with a proof that (2+1)-dimensional CFT vacuum energy is *locally* maximised by flat space and the round sphere for $(\Sigma, \bar{g})$ topologically flat and spherical, respectively [30]. These results will also reviewed in this chapter.

The plan for the chapter is as follows. In Section 1.1, a free massless vector in the presence of two parallel conducting plates will be quantised and its vacuum energy computed using cutoff, zeta and exponential regularisations. In Section 1.2, the AdS/CFT correspondence will be introduced and the boundary stress tensor will be defined and related to a renormalised CFT stress tensor for asymptotically locally AdS spaces. Section 1.3 will review the results on the non-positivity of vacuum energy for (2+1)-dimensional holographic CFTs on static backgrounds with compact spatial slices [29]. Section 1.4 will review the results on the local maximisation of (2+1)-dimensional CFT vacuum energy by flat space and the round sphere among spatial geometries with flat and spherical topology, respectively [30]. We conclude with a brief summary and discussion in Section 1.5.

1.1 The Casimir Effect

Consider a Maxwell field in the region between a pair of parallel conducting metal plates. This is represented by a real vector field $A_\mu(x)$ and action

$$S = \int \mathrm{d}^4x F_{\mu\nu}F^{\mu\nu}, \tag{1.1}$$

with a U(1) gauge invariance $A_\mu \mapsto A_\mu - \partial_\mu\alpha$ where $F_{\mu\nu} = \partial_\mu A_\nu - \partial_\nu A_\mu$ is the gauge invariant field strength tensor. We choose coordinates so that the plates lie in planes $z = 0$ and $z = d$ where d measures the distance between the plates. Since the plates are conducting the electric field must meet them right angles and the magnetic field must have no normal component at them. To quantise we work in the Coulomb gauge $A_0 = \nabla\cdot\mathbf{A} = 0$ and find that in the Schrödinger picture

$$\hat{\mathbf{A}}_\parallel(\mathbf{x}) = \sum_{n=1}^{\infty}\int \frac{\mathrm{d}^2k}{(2\pi)^2}\frac{1}{2E(\mathbf{k}_n)}\sum_\lambda \boldsymbol{\varepsilon}_\parallel^\lambda(\mathbf{k}_n)\left(\hat{a}_\lambda(\mathbf{k}_n)\mathrm{e}^{i\mathbf{k}\cdot\mathbf{x}} + \hat{a}_\lambda^\dagger(\mathbf{k}_n)\mathrm{e}^{-i\mathbf{k}\cdot\mathbf{x}}\right)\sin\left(\frac{\pi n z}{d}\right) \tag{1.2}$$

$$\hat{A}_z(\mathbf{x}) = \sum_{n=1}^{\infty}\int \frac{\mathrm{d}^2k}{(2\pi)^2}\frac{-i}{2E(\mathbf{k}_n)}\sum_\lambda \varepsilon_z^\lambda(\mathbf{k}_n)\left(\hat{a}_\lambda(\mathbf{k}_n)\mathrm{e}^{i\mathbf{k}\cdot\mathbf{x}} - \hat{a}_\lambda^\dagger(\mathbf{k}_n)\mathrm{e}^{-i\mathbf{k}\cdot\mathbf{x}}\right)\cos\left(\frac{\pi n z}{d}\right) \tag{1.3}$$

between the plates, where the subscript $\parallel$ denotes the projection of vector onto the (x, y) plane, $\mathbf{k}_n = (\mathbf{k}, \pi n/d)$, $E(\mathbf{k}_n) = |\mathbf{k}_n|$, the $\boldsymbol{\varepsilon}^\lambda$ are two orthonormal polarisation vectors satisfying

$$\mathbf{k}_n\cdot\boldsymbol{\varepsilon}^\lambda(\mathbf{k}_n) = 0 \text{ and } \sum_\lambda \boldsymbol{\varepsilon}^\lambda(\mathbf{k}_n)\boldsymbol{\varepsilon}^{\lambda\mathrm{T}}(\mathbf{k}_n) = \mathbf{1} - \frac{\mathbf{k}_n\mathbf{k}_n^\mathrm{T}}{\mathbf{k}_n^2} \tag{1.4}$$

for all $\mathbf{k} \in \mathbb{R}^2$, $n \in \mathbb{Z}_{\geqslant 1}$ and the annihilation and creation operators obey

$$\left[\hat{a}_\lambda(\mathbf{k}_n), \hat{a}^\dagger_{\lambda'}(\mathbf{p}_m)\right] = 2E(\mathbf{k}_n)(2\pi)^2\delta_{\lambda\lambda'}\delta^{(2)}(\mathbf{k}-\mathbf{p})\frac{2\delta_{mn}}{d} \tag{1.5}$$

with all other commutators vanishing, where we note the Coulomb gauge has residual gauge freedom that has allowed the removal of the constant z mode in $\hat{A}_z$. The vacuum state $|0\rangle$ obeys $a_\lambda(\mathbf{k}_n)|0\rangle = 0$ and the Hamiltonian is

$$H = d\int \mathrm{d}^2x\,\rho + \frac{d}{2}\sum_{n=1}\int \frac{\mathrm{d}^2k}{(2\pi)^2}\frac{1}{2E(\mathbf{k}_n)}\frac{E(\mathbf{k}_n)}{2}\sum_\lambda a^\dagger_\lambda(\mathbf{k}_n)a_\lambda(\mathbf{k}_n) + a_\lambda(\mathbf{k}_n)a^\dagger_\lambda(\mathbf{k}_n), \tag{1.6}$$

where ρ is a constant expressing the freedom to set the zero of the energy density. While in many problems we would now normal order, and consequently renormalise the energy to zero, this is not a valid operation in this setup. We wish to compare the energy at various plate separations, each of which have *different* annihilation and creation operators. To normal order would be to renormalise each plate separation differently thus rendering any comparison between them invalid — we therefore use natural ordering here. With this understanding, the energy per unit area of the plates in the vacuum state is given by

$$\mathcal{E}(d) = d\rho + \sum_{n=1}^{\infty}\int \frac{\mathrm{d}^2k}{(2\pi)^2}\sqrt{\mathbf{k}^2 + \left(\frac{\pi n}{d}\right)^2}. \tag{1.7}$$

This quantity is highly divergent. The key point to note however is that, at least naïvely, this quantity depends on the distance between the two plates — so there must be a force exerted on the plates (changing the geometry) in an attempt to reach the lowest energy configuration. To confirm this d dependence, we must compute this UV-divergent quantity. When working in QFT there is always implicitly a cutoff energy, Λ, up to which we trust our description of the physics and as such modes with momenta exceeding this cutoff should not be included in our calculations. Given that we are necessarily ignorant of the UV description, we should hope to derive an answer that does not depend on it. In this particular example, we expect that the presence of conducting plates should have little effect on high frequency radiation and thus $\mathcal{E}(d)$ should be UV insensitive. Thus, the quantity we are actually interested in is

$$\mathcal{E}(d) = d\rho + \sum_{n=1}^{\infty}\int \frac{\mathrm{d}^2k}{(2\pi)^2}\sqrt{\mathbf{k}^2 + \left(\frac{\pi n}{d}\right)^2}\,\eta(|\mathbf{k}_n|/\Lambda) \tag{1.8}$$

where $\eta \in \mathcal{C}^\infty(\mathbb{R}_{\geqslant 0}, [0,1])$ is a non-increasing function with $\eta(0) = 1$ that rapidly decays to zero at infinity, acting as a 'cutoff function'. For our final answer to be physical it cannot depend on the exact form of η and must also be finite as $\Lambda \to \infty$, indicating that $\mathcal{E}(d)$ is a meaningful IR quantity insensitive to the UV details of the theory. The goal, then,

is to probe the large Λ asymptotics of the energy and extract the well-defined UV-finite part. There are many different ways of calculating this.

Cutoff Regularisation was the method of chosen by Casimir himself in the original calculation [8]. As is intuitive, the idea is to directly calculate the cutoff dependence of $\mathcal{E}(d)$ at large Λ. Using the Euler-Maclaurin formula,

$$\sum_{n=1}^{N} f(n) = \int_0^N \mathrm{d}x f(x) - \sum_{k=1}^{K} \frac{B_k}{k!} f^{(k-1)}(0) + \mathcal{O}(N\|f\|_{\dot{C}^K}) \tag{1.9}$$

where B_k are the Bernoulli numbers, for a smooth function f whose value and derivatives vanish at $x = N$, a discrete sum over integer n can be expressed in terms of an integral over real n and some corrections. Supposing further that $\eta(x) = 1$ in some neighbourhood of $x = 0$ and $\eta(x)|_{x\geqslant 1} = 0$, applying (1.9) to $\mathcal{E}(d)$ gives

$$\mathcal{E}(d) = d\left(\rho + \frac{1}{\pi^2} C_{\eta,3}\Lambda^4\right) - \frac{1}{4\pi}\Lambda^3 C_{\eta,2} - \frac{1}{720}\frac{\pi^2}{d^3} + \mathcal{O}\left(\Lambda^{-1}\right) \tag{1.10}$$

where

$$C_{\eta,s} = \int_0^\infty \mathrm{d}x\, x^s \eta(x). \tag{1.11}$$

Interpreting each of these terms can now help us to extract the answer. Recall that an ambiguity in the zero of energy density allows us to choose the value of ρ thus we may choose it to cancel the $\mathcal{O}(\Lambda^4)$ term — this is not physically relevant as it gives uniform contribution to the energy density. Physically, the $\mathcal{O}(\Lambda^3)$ term is a surface tension term; it is independent of d and, therefore also irrelevant. In SI units, that leaves only

$$\mathcal{E}_{\mathrm{reg}}(d) = -\frac{\hbar c \pi^2}{720 d^3} \tag{1.12}$$

as $\Lambda \to \infty$, which we note is finite and insensitive to the precise details of the cutoff function, confirming our previous intuition that the Casimir Energy is a meaningful IR quantity. Thus, the closer the plates are to each other the *lower* the energy of the vacuum between them — they are attracted to each other due to the vacuum of the electromagnetic fields between them. Remarkably, this is a purely quantum (vanishes as $\hbar \to 0$) effect. While this does mean it is small effect the fact that $\mathcal{E}(d) \sim d^{-3}$ gave some hope that it might be measurable at small plate separation. The reason why the divergence can be neglected, and thus where the renormalised value of the Casimir energy comes from, are clear from this method but it is not the most computationally efficient and, despite the integrals being calculable in this simple example, is likely to run into difficulties for more complex setups. There exist other techniques which can be used like a black box that lean heavily on advanced mathematics to circumvent some of the complexity of harder

problems and yield the answer more directly.

Zeta Function Regularisation uses complex analysis to extract $\mathcal{E}_{\text{reg}}(d)$. It originated in number theory as a method to assign meaningful values to divergent series — a problem that has since become very common in physics. Early proponents of the method include Hawking [47], J.S.Dowker and Raymond Critchley [48] who used it to give finite values to path integrals of curved space QFTs with quadratic actions. It can be applied to this problem as follows. Suppose we introduce a complex parameter s and write

$$\mathcal{E}(d,s,\Lambda) \equiv \sum_{n=1}^{\infty} \int \frac{\mathrm{d}^2k}{(2\pi)^2} \left(\mathbf{k}^2 + \left(\frac{\pi n}{d}\right)^2\right)^{1/2-s} \eta(|\mathbf{k}_n|/\Lambda). \tag{1.13}$$

Then after evaluating $\mathcal{E}(d,s,\infty)$ in some region of s at which it is finite, analytically continuing this function to a region that contains $s = 0$ and evaluating this function at $s = 0$, $\mathcal{E}_{\text{reg}}(d)$ is recovered since

$$\sum_{n=1}^{\infty} \int \frac{\mathrm{d}^2k}{(2\pi)^2} \left(\mathbf{k}^2 + \left(\frac{\pi n}{d}\right)^2\right)^{1/2-s} = \left(\frac{\pi}{d}\right)^{3-2s} \frac{1}{2\pi} \frac{1}{2s-3} \zeta(2s-3). \tag{1.14}$$

and

$$\left(\frac{\pi}{d}\right)^{3-2s} \frac{1}{2\pi} \frac{1}{2s-3} \zeta(2s-3)\bigg|_{s=0} = -\frac{\pi^2}{720d^3}. \tag{1.15}$$

To see why this works in this instance, consider evaluating $\mathcal{E}(d,s,\Lambda)$ for $\Re(s) < 3/2$ using the Euler-Maclaurin formula (1.9). The summand in (1.13) is not necessarily smooth at $n = 0$ so instead consider the telescoped partial sum

$$\mathcal{E}(d,s,\Lambda) - \mathcal{E}(d,s,\Lambda/2) = \sum_{n=1}^{\infty} \int \frac{\mathrm{d}^2k}{(2\pi)^2} \left(\mathbf{k}^2 + \left(\frac{\pi n}{d}\right)^2\right)^{1/2-s} \left(\eta(|\mathbf{k}_n|/\Lambda) - \eta(2|\mathbf{k}_n|/\Lambda)\right) \tag{1.16}$$

and take

$$f(n) = \int \frac{\mathrm{d}^2k}{(2\pi)^2} \left(\mathbf{k}^2 + \left(\frac{\pi n}{d}\right)^2\right)^{1/2-s} \left(\eta(|\mathbf{k}_n|/\Lambda) - \eta(2|\mathbf{k}_n|/\Lambda)\right). \tag{1.17}$$

which is smooth everywhere and vanishing in a neighbourhood of $n = 0$. Applying (1.9)

to this function gives

$$\begin{aligned}&\mathcal{E}(d,s,2^{-m}\Lambda)-\mathcal{E}(d,s,2^{-m-1}\Lambda)\\&\quad=\frac{d}{\pi^2}\left(\frac{\Lambda}{2^m}\right)^{4-2s}C_{\eta,3-2s}(1-2^{2s-4})-\frac{1}{4\pi}\left(\frac{\Lambda}{2^m}\right)^{3-2s}C_{\eta,2-2s}(1-2^{2s-3})+\mathcal{O}\left(\Lambda^{-1}\right).\end{aligned}\tag{1.18}$$

Performing the sum over $m \geqslant 0$ leaves us with

$$\mathcal{E}(d,s,\Lambda)=F(s)+\frac{d}{\pi^2}\Lambda^{4-2s}C_{\eta,3-2s}-\frac{1}{4\pi}\Lambda^{3-2s}C_{\eta,2-2s}+\mathcal{O}\left(\Lambda^{-1}\right)\tag{1.19}$$

where $F(s)$ is the finite part of the sum over the $\mathcal{O}\left(\Lambda^{-1}\right)$ terms and can be concretely expressed as

$$F(s)=\lim_{\Lambda\to\infty}\left(\mathcal{E}(d,s,\Lambda)-\frac{d}{\pi^2}\Lambda^{4-2s}C_{\eta,3-2s}+\frac{1}{4\pi}\Lambda^{3-2s}C_{\eta,2-2s}\right).\tag{1.20}$$

It can be shown that the error terms are such that this limit converges uniformly on all compact subsets of $\{s \in \mathbb{C} : \Re(s) < 3/2\}$. It then follows from Morera's Theorem that $F(s)$ is complex analytic on that set. Comparing with cutoff regularisation calculation we see that $F(0)$ is the physically-meaningful value of the Casimir Energy. For sufficiently large Λ

$$C_{\eta,-s}\Lambda^{1-s}=\frac{1}{1-s}+\int_1^\Lambda \mathrm{d}x\, x^{-s}\eta(x/\Lambda)\tag{1.21}$$

thus $F(s)$ can also be rewritten as

$$\begin{aligned}F(s)=&-\frac{d}{\pi^2}\frac{1}{4-2s}-\frac{1}{4\pi}\frac{1}{3-2s}\\&+\lim_{\Lambda\to\infty}\left(\mathcal{E}(d,s,\Lambda)-\frac{d}{\pi^2}\int_1^\Lambda \mathrm{d}x\, x^{3-2s}\eta(x/\Lambda)-\frac{1}{4\pi}\int_1^\Lambda \mathrm{d}x\, x^{2-2s}\eta(x/\Lambda)\right)\end{aligned}\tag{1.22}$$

giving an analytic continuation to $\mathbb{C}\setminus\{2,3/2\}$. In particular, for $\Re(s) > 2$

$$F(s)=\lim_{\Lambda\to\infty}\mathcal{E}(d,s,\Lambda)=\sum_{n=1}^{\infty}\int\frac{\mathrm{d}^2k}{(2\pi)^2}\left(\mathbf{k}^2+\left(\frac{\pi n}{d}\right)^2\right)^{1/2-s}\tag{1.23}$$

which is the function we naïvely analytically continued at the start (1.14). The result being that introducing a complex parameter, calculating the sum in a region where the sum converges and then analytically continuing back to value you want gives the UV-finite part of the result.

Exponential Regularisation can also be used to extract $\mathcal{E}_{\text{reg}}(d)$. This is simply a case

of choosing a particular cutoff function, namely $\eta(x) = \mathrm{e}^{-x}$, and using that to probe the UV-finite part of the Casimir Energy. With this regulator,

$$\mathcal{E}(d) = d\rho + \sum_{n=1}^{\infty} \int \frac{\mathrm{d}^2 k}{(2\pi)^2} \sqrt{\mathbf{k}^2 + \left(\frac{\pi n}{d}\right)^2}\, \mathrm{e}^{-|\mathbf{k}_n|/\Lambda}, \tag{1.24}$$

so the integral and sum are straightforward to perform analytically. After doing so, an asymptotic expansion in Λ gives

$$\mathcal{E}(d) = d\left(\rho + \frac{3\Lambda^4}{\pi^2}\right) - \frac{\Lambda^3}{2\pi} - \frac{\pi^2}{720 d^3} + \mathcal{O}(\Lambda^{-2}), \tag{1.25}$$

thus reproducing the expected result. This is actually an example of a more general prescription for calculating vacuum energy for theories with quadratic actions on manifolds (with boundaries). Note the connection here to the cylinder kernel $T(t)$ defined in Chapter 2. Comparing (2.7) and (1.24) it is clear that the exponentially regulated Casimir Energy per unit area is related to the local cylinder kernel of an operator with spectrum $\{|\mathbf{k}_n| : \mathbf{k} \in \mathbb{R}^2, n \in \mathbb{Z}_{\geqslant 1}\}$ (each with degeneracy 2)[1] by

$$\mathcal{E}(d) = d\rho - \frac{1}{2} \frac{\mathrm{d}\bar{T}(t)}{\mathrm{d}t}\bigg|_{t=\Lambda^{-1}}, \tag{1.26}$$

where $\bar{T}$ denotes the local cylinder kernel integrated over a single ray that is perpendicular to the (x, y) plane[2]. The asymptotic structure of the cylinder kernel (2.23) then shows how a UV-finite answer can be extracted from this definition. In the limit $t \to 0^+$

$$\bar{T}(t) \sim \frac{2d}{\pi^2 t^3} - \frac{1}{2\pi t^2} + \bar{e}_4(-\nabla^2)t + \mathcal{O}(t^2). \tag{1.27}$$

The divergences are sourced by terms determined by heat kernel coefficients which are local integrals of geometric invariants. Comparing with (1.26), it seems natural to take the UV-finite Casimir Energy to be proportional to the coefficient of t in the asymptotic expansion of the cylinder kernel. As mentioned in Chapter 2, this term is non-local and thus, while the divergence structure can be deduced from local geometric data, the Casimir Energy itself is non-local in its dependence on the geometry. This will turn out to be an important feature of our vacuum energy calculations.

Armed with our insight into vacuum energy calculations from the Casimir Effect, we now turn to vacuum energy as a functional of background geometry for QFTs in curved spacetimes and the work that motivated the original work in this thesis. To do so, we

[1] The most straightforward example of which is given by a two copies of a Laplacian acting on a scalar field on the Euclidean background $\mathbb{R}^2 \times [0, d]$ with Dirichlet boundary conditions.

[2] This quantity is (x, y) independent by symmetry.

begin with a review of the framework that allowed for progress in this area: the AdS/CFT correspondence.

1.2 The AdS/CFT Correspondence

The gauge/gravity duality is a conjectured duality between gravitational theories in $(d+1)$ dimensions and gauge theories in d dimensions that 'live' at the boundary. The most developed instance of this duality is the AdS/CFT correspondence [26–28]. This involves a string theory on a product of asymptotically (locally) AdS_{d+1} (AlAdS) space with a compact manifold on one side and a CFT on the other. While there is no proof of the correspondence, there is an overwhelming amount of evidence in its favour and, thus far, it provides the most complete examples of quantum gravity theories. It is a strong/weak duality — meaning that in the strong-coupling regime of the CFT the string theory is weakly coupled, and vice-versa, allowing us to probe previously intractable sectors of each theory. In particular, the challenging computations involved in strongly-coupled QFT in curved spacetime can be exchanged in favour of working in classical gravity.

Our interest lies in how this correspondence can help us compute some vacuum energies of QFTs on curved backgrounds. These CFTs generally have two parameters: a coupling which measures the strength of interactions between the microscopic constituents, λ, and a measure of the number of degrees of freedom, the effective central charge, c_T — defined as the coefficient of the two-point function of the stress tensor on flat space (as seen later in Equation (1.56)). While the full equivalence is between strings propagating in AdS and the CFT with arbitrary parameters, we can simplify the dual gravity theory by tuning the parameters of the string theory.

Consider a string theory on a space which is asymptotically locally $\mathrm{AdS} \times X$ with AdS length ℓ, string coupling g_s and string tension $T = (2\pi\alpha')^{-1}$, where X is a compact manifold. By taking the string coupling $g_\mathrm{s} \ll 1$ we may ignore string loops and thus enter the regime of semiclassical string theory. Looking further at $\alpha' \ll g_\mathrm{s}\ell^2$ we lose the 'stringy' α' corrections to the theory which, after compactifying on X, leaves behind a (super)gravity theory whose details depend on X. The central charge of the CFT is related to the string theory parameters as

$$c_T \sim \frac{1}{g_\mathrm{s}^2}\left(\frac{\ell^2}{\alpha'}\right)^4 \tag{1.28}$$

so the classical gravity theory is dual to a CFT with a large number of degrees of freedom[3]. Further, these theories are generally strongly coupled — for example, the cou-

[3]This relation follows from Equation (1.36) after noting that $G_{(d+1)} = G_{10}/\mathrm{Vol}(X)$ where $G_{10} \sim \alpha'^4 g_\mathrm{s}^2$ and X typically has $\mathrm{Vol}(X) \sim \ell^{10-(d+1)}$ [49, 50].

pling $\lambda \sim (\ell^2/\alpha')^2$ in the case of IIB strings on spaces with $AdS_5 \times S^5$ asymptotics. In particular, there is an infinite class of strongly-coupled CFTs on d-dimensional curved spacetimes, $(\mathbb{R} \times \Sigma, g_{\text{CFT}})$, that have (low-energy) sectors that are dual to $(d+1)$-dimensional solutions of Einstein gravity with negative cosmological constant

$$R_{AB} = -\frac{d(d-1)}{2\ell^2} g_{AB}, \tag{1.29}$$

subject to the condition that the conformal boundary of g is conformally equivalent to g_{CFT}, the so-called 'universal sector' of the AdS/CFT correspondence[4]. From here on, we will refer to these theories as 'holographic CFTs'. Certain observables of the CFT on the boundary, such as the stress tensor, can be deduced from this 'bulk' spacetime solution. In fact, many of them, including the vacuum energy, are determined by the asymptotics of the bulk solution at the conformal boundary. This was used in [29] to show that the vacuum energy of all such holographic CFTs on (2+1)-dimensional static backgrounds with compact spatial slices are non-positive and zero only on spaces that are locally conformal to a product of time with a constant-curvature space, and again in [30] to show that, when the spatial slices are flat space or spheres, small perturbations to the spatial geometry lower the vacuum energy for *all* CFTs. We will review this work in the rest of the chapter. In each case, extracting the stress tensor of the CFT is key to proving the result. Following [51–53], we will show how this can be done with a classical gravity calculation.

Defining a local energy density for gravitational fields is not possible due to the equivalence principle. A 'quasi-local' energy density defined locally on the boundary of a spacetime region, however, can be. Inspired by Hamilton-Jacobi theory, Brown and York proposed that the quasi-local stress tensor [54] for a spacetime region with action S and prescribed boundary metric $h_{\mu\nu}$ should be

$$T_{\mu\nu} = -\frac{2}{\sqrt{-h}} \frac{\delta S}{\delta h^{\mu\nu}}. \tag{1.30}$$

This quantity, much like a QFT stress tensor when its UV regulator is taken to infinity, suffers from divergences as the boundary is taken to infinity. In the case of AlAdS spaces there is a prescription for subtracting the divergences [51] using local counterterms that depend only on the intrinsic geometry of the boundary leaving a result that is finite and unambiguous. It is this quantity that is dual to the expectation of the renormalised CFT stress tensor in the AdS/CFT dictionary.

Consider an AlAdS_{d+1} space satisfying (1.29). For simplicity, we will consider the case where d is odd so that there is no Weyl anomaly in the CFT stress tensor

[4]The precise details of the CFT depend on the details of the compact manifold and will not be of interest here.

and ultimately we are interested in the case $d = 3$. A more comprehensive analysis, including even d, can be found in [53]. To calculate the boundary stress tensor, we can use Fefferman-Graham coordinates[5] [55] in a neighbourhood of the conformal boundary to write the metric in the form

$$\mathrm{d}s^2 = \frac{\ell^2}{z^2}\left(\mathrm{d}z^2 + h_{\mu\nu}(z,x)\mathrm{d}x^\mu \mathrm{d}x^\nu\right), \tag{1.31}$$

where $z \geqslant 0$ is a 'radial' coordinate which measures distance from the conformal boundary at $z = 0$ and x^μ are local coordinates on the boundary and solve for $h_{\mu\nu}(z,x)$ order by order in z using the Einstein equation to find that

$$h_{\mu\nu}(z,x) = \bar{h}_{\mu\nu}(x) + z^2 h^{(2)}_{\mu\nu}(x) + \ldots + z^{2n} h^{(2n)}_{\mu\nu}(x) + \ldots + z^d t_{\mu\nu}(x) + \mathcal{O}(z^{d+1}) \tag{1.32}$$

where $\bar{h}_{\mu\nu}$ is the metric on the conformal boundary and $h^{(n)}_{\mu\nu}$, $0 < n < d/2$ are local tensors on the conformal boundary built from $\bar{h}_{\mu\nu}$ and its derivatives, for which some explicit expressions can be found in [53] e.g.

$$h^{(2)}_{\mu\nu}(x) = \frac{1}{d-2}\left(R_{\mu\nu}[\bar{h}] - \frac{1}{2(d-1)}R[\bar{h}]\bar{h}_{\mu\nu}\right), \tag{1.33}$$

where $R_{\mu\nu}[\bar{h}]$ and $R[\bar{h}]$ are the Ricci and scalar curvature of the boundary, respectively. The asymptotic equations of motion alone do not completely determine $t_{\mu\nu}$ but do impose that it must be trace free and conserved with respect to $\bar{h}$ and its Levi-Civita connection, respectively. The higher-order terms can all be expressed in terms of $\bar{h}_{\mu\nu}$ and $t_{\mu\nu}$. Finally, after ensuring that the action has been appropriately renormalised to subtract off divergences[6] the quasi-local boundary stress tensor for the conformal boundary is

$$T_{\mu\nu} = \frac{d\ell^{d-1}}{16\pi G_{(d+1)}} t_{\mu\nu} \tag{1.34}$$

where $G_{(d+1)}$ is Newton's constant of gravitation in $(d+1)$ dimensions, and so the AdS/CFT dictionary states that the expectation value of the dual CFT renormalised stress tensor is

$$\langle T^{\mathrm{CFT}}_{\mu\nu}\rangle = d c_{\mathrm{h}} t_{\mu\nu}, \tag{1.35}$$

where c_{h} is the 'holographic' central charge. This is related the central charge of the dual CFT, c_T, by

$$\frac{\pi^2}{48} c_T = c_{\mathrm{h}} = \frac{\ell^{d-1}}{16\pi G_{(d+1)}}. \tag{1.36}$$

From here, we may express the energy of the dual CFT in terms of bulk quantities.

[5] These coordinates are analogous to Gaussian normal coordinates for the conformal boundary of AlAdS spaces.

[6] This is done using holographic renormalisation prescription [56].

1.3 Vacuum Energy Non-positivity: Holographic CFTs

We now seek to use the AdS/CFT correspondence to probe the vacuum energy of (2+1)-dimensional holographic CFTs with closed spatial geometries. The work presented in this section is a review of the results in [29].

Given a CFT on a static background $\mathbb{R} \times \Sigma$ where the spatial geometry of Σ is a closed Riemann two-manifold, the metric can be written in the form

$$\mathrm{d}s^2 = N(x)^2 \left(-\mathrm{d}t^2 + \bar{g}_{ij}(x)\mathrm{d}x^i \mathrm{d}x^j\right) \equiv N(x)^2 g_{\mathrm{CFT}}(x) \tag{1.37}$$

where $v = \partial/\partial t$ is a globally timelike Killing vector field, x^i are local coordinates on Σ and $N(x) > 0$ everywhere and is thus conformally equivalent to the ultrastatic metric g_{CFT}. The energy of the theory is the Noether charge that is conserved under time translations:

$$E = \int_\Sigma \langle T^{\mathrm{CFT}}_{\mu\nu} \rangle n^\mu v^\nu. \tag{1.38}$$

where n is the unit normal to the spatial slices Σ. There is no Weyl anomaly in odd dimensions so the integrand here is a singlet under conformal transformations and thus the energy is conformal invariant. So, WLOG, we can restrict our attention to ultrastatic metrics. The energy of a (2+1)-dimensional holographic CFT is thus

$$E = 3c_{\mathrm{h}} \int \mathrm{d}^2x \sqrt{\bar{g}} t_{tt}(x). \tag{1.39}$$

This holographic renormalisation and compactness of the spatial geometry guarantee that this quantity is finite and scheme independent. This is a neat example of how the often complex task of extracting finite observables in curved space QFT is greatly simplified in AdS/CFT. We need only solve classical gravity equations to extract the energy of the dual CFT. The AdS/CFT dictionary also tells us how to express the entropy and temperature of the CFT in terms of bulk geometric quantities. This is ultimately what will allow us to write a simple geometric inequality in terms of the CFT data and show that $E \leqslant 0$ for all holographic CFTs. Firstly, some assumptions need to made about the structure of the bulk that, while allowing for analytic progress, are not so restrictive as to exclude cases of interest. These will be explained in the following subsection.

1.3.1 Bulk Spacetime Structure

In [29], the following assumptions are also made:

(i) The dual bulk solution to the CFT at finite temperature, T, is static and smooth away from the conformal boundary. Further, it may only have other boundaries at smooth Killing horizons with Hawking temperature T with respect to $\partial/\partial t$.

(ii) In the limit $T \to 0^+$, these bulks tend to the zero-temperature dual of the CFT vacuum and the energy and entropy are well behaved[7].

Any bulk solution satisfying these assumptions may written as a warped product of a Riemannian manifold $(\mathcal{M}, g)$:

$$\mathrm{d}s^2 = \frac{\ell^2}{Z(x)^2}\left(-\mathrm{d}t^2 + g_{ij}\mathrm{d}x^i\mathrm{d}x^j\right) \tag{1.40}$$

where $(\mathcal{M}, g)$, known as the *optical* geometry [58] (the projections of the null geodesics onto the optical geometry are geodesic), admits some local coordinates x^i and has boundary $\partial\mathcal{M} = \Sigma$ and $Z > 0$ everywhere apart from the conformal boundary where $Z = 0$ and $\mathrm{d}Z \neq 0$. This bulk ends on the conformal boundary $(\mathbb{R}\times\Sigma, g_{\mathrm{CFT}})$ and $N_{\mathrm{H}} \geqslant 0$ Killing horizon components with spatial sections $\mathcal{H}_{1\leqslant J\leqslant N_{\mathrm{H}}}$. Examining this optical geometry, in particular its curvature at the boundaries, is the key to bounding the energy. From the optical geometry's point of view, the boundary at $Z = 0$ is a true boundary at which the optical metric is $\bar{g}$ and the N_{H} Killing horizon components are asymptotic boundaries with spatial geometries $\mathcal{H}_J$.

1.3.2 Optical Geometry

Rewriting the Einstein equations (1.29) in terms of the optical Ricci curvature, R_{ij}, the optical scalar curvature, R, and their associated connection ∇ gives that

$$R_{ij} = -\frac{2}{Z}\nabla_i\nabla_j Z \tag{1.41}$$

$$R = \frac{6}{Z^2}\left(1 - (\nabla Z)^2\right) \tag{1.42}$$

where indices are raised, lowered and contracted with the optical metric. Using these equations and the Bianchi identities, it follows that optical Ricci scalar satisfies the elliptic equation

$$\nabla^2 R = R^2 - 3R_{ij}R^{ij} = -3\left(R_{ij} - \frac{1}{3}Rg_{ij}\right)^2. \tag{1.43}$$

The right-hand side of (1.43) is negative semidefinite for a smooth Riemannian optical metric and zero if and only if g_{ij} is an Einstein metric (seen by evaluating its divergence). Integrating this equation over $(\mathcal{M}, g)$ gives, via the divergence theorem, a left-hand side that involves exclusively boundary terms:

$$\int_\Sigma \mathrm{d}A^i\nabla_i R + \sum_{1\leqslant J\leqslant N_{\mathrm{H}}}\int_{\mathcal{H}_J}\mathrm{d}A^i\nabla_i R = -3\int_{\mathcal{M}}\sqrt{g}\mathrm{d}^3x\left(R_{ij} - \frac{1}{3}Rg_{ij}\right)^2. \tag{1.44}$$

[7]Note that this allows for some zero-temperature bulks that, while *not* smooth, are generic and have 'good' singularities e.g. toroidal-AdS, as described in [57].

Each of these boundary terms can then be expressed in terms of near boundary geometric quantities that can then be related to CFT data via the AdS/CFT dictionary. The first term is evaluated at the boundary that supports the dual CFT and can be written as

$$\int_\Sigma \mathrm{d}A^i \nabla_i R = 18 \int_\Sigma \sqrt{\bar{g}} t_{tt} = \frac{6}{c_\mathrm{h}} E, \tag{1.45}$$

and integrals over the Killing horizon components can be written in terms of each of their Euler characteristics, $\chi(\mathcal{H}_J)$, and entropy of the CFT, S, as

$$\sum_{1 \leqslant J \leqslant N_\mathrm{H}} \int_{\mathcal{H}_J} \mathrm{d}A^i \nabla_i R = -\frac{6}{c_\mathrm{h}} TS - 12\pi T \sum_{1 \leqslant J \leqslant N_\mathrm{H}} \chi(\mathcal{H}_J). \tag{1.46}$$

where we have used that $c_\mathrm{h} = \ell^2/(16\pi G_{(4)})$. Returning to the relationship (1.44) gives that the free energy, $F = E - TS$, of the CFT satisfies

$$\frac{F}{c_\mathrm{h}} - 2\pi T \sum_{1 \leqslant J \leqslant N_\mathrm{H}} \chi(\mathcal{H}_J) = -\frac{1}{2} \int_\mathcal{M} \sqrt{g} \mathrm{d}^3 x \left(R_{ij} - \frac{1}{3} R g_{ij} \right)^2 . \tag{1.47}$$

Ultimately, we are interested in the energy of the zero-temperature CFT vacuum. In the limit $T \to 0^+$, $F \to E$ and therefore, providing the assumptions given at the start of Section 1.3.1 hold, we find that

$$\frac{E}{c_\mathrm{h}} = -\frac{1}{2} \int_\mathcal{M} \sqrt{g} \mathrm{d}^3 x \left(R_{ij} - \frac{1}{3} R g_{ij} \right)^2 \tag{1.48}$$

and thus $E \leqslant 0$ for (2+1)-dimensional holographic CFTs with spatial geometry $(\Sigma, \bar{g})$, with equality if only if g_{ij} is an Einstein metric. Since $\lim_{z \to 0} R[g] = 3R[\bar{g}]$, this inequality is only saturated when $(\Sigma, \bar{g})$ has constant curvature.

1.4 Vacuum Energy Non-positivity: General CFTs

To generalise the result to further (2+1)-dimensional CFTs, we now investigate how the vacuum energy of a unitary CFT behaves under small deformations to its spatial geometry. This is most easily achieved by expressing the vacuum energy in terms of the partition function of the theory. The work in this section is a review of results from [30].

For each Lorentzian QFT on an ultrastatic background $(\mathbb{R} \times \Sigma, -\mathrm{d}t^2 + g)$ at finite temperature, T, there is an equivalent Euclidean QFT on the background $(S^1 \times \Sigma, G \equiv \mathrm{d}\tau^2 + g)$ with $\tau \sim \tau + \beta$ the Euclidean time coordinate and $\beta = T^{-1}$ the radius of the S^1, where the two are related by identifying $t = -i\tau$ and analytically continuing[8]. For the rest of this section, we will use the Euclidean description. We will also restrict our attention to

[8] See Appendix A.1 for more details on this.

perturbations of spaces that are (locally) conformally flat. This obviously includes $(\mathbb{R}^2, \delta)$ but also (S^2, Ω), where Ω is the unit round sphere metric since $(\mathbb{R}^3, \delta)$ and $(\mathbb{R} \times S^2, \mathrm{d}\tau^2 + \Omega)$ are Weyl equivalent: taking Euclidean three-space with spherical polars (r, θ, ϕ) and making a Weyl transformation $\omega(r, \theta, \phi) = 1/r$ and change of coordinate $r = \mathrm{e}^\tau$ gives a space with metric

$$\mathrm{d}s^2 = \frac{1}{r^2}\left(\mathrm{d}r^2 + r^2\mathrm{d}\Omega^2\right) = \mathrm{d}\tau^2 + \Omega_{ij}\mathrm{d}\theta^i\mathrm{d}\theta^j, \tag{1.49}$$

i.e. $(\mathbb{R} \times S^2, \mathrm{d}\tau^2 + \Omega)$. We also assume that, in the zero-temperature limit, any vacuum expectation value (VEV) on these spaces can be obtained via conformal transformations of the corresponding VEV on flat space (i.e. no Weyl anomaly is present).

The QFT vacuum state is defined by its partition function,

$$Z[G] = \int \mathcal{D}\Phi \mathrm{e}^{-S_\mathrm{E}[G,\Phi]} \tag{1.50}$$

where $S_\mathrm{E}[G, \Phi]$ is its Euclidean action and Φ represents all the quantum fields. The thermal vacuum free energy $F[g] = -T \ln Z[G]$[9] tends to E in the zero-temperature limit so looking at variations of the partition function due to metric perturbations is tantamount to calculating the change in E. The response of the partition function to changes in the metric is measured by the VEV of the stress tensor:

$$\langle T_{\mu\nu}\rangle_G \equiv -\frac{2}{\sqrt{G}}\frac{\delta \ln Z[G]}{\delta G^{\mu\nu}}. \tag{1.51}$$

Having started with a static Lorentzian CFT, we can reasonably expect that this VEV is independent of Euclidean time τ. To see that this definition of $E[g]$ is equivalent to the energy defined by Equation (1.38), note that a diffeomorphism that shifts $G^{\tau\tau}$ by a constant $\delta G^{\tau\tau}$ induces a constant shift in the inverse temperature, $\delta\beta = -\delta G^{\tau\tau}\beta/2$, so that (by L'Hôpital)

$$E[g] = -\lim_{\beta\to\infty}\frac{\partial \ln Z}{\partial\beta} = -\lim_{\beta\to\infty}\int_\Sigma \frac{1}{\sqrt{G}}\frac{\delta \ln Z}{\delta G^{\tau\tau}}\frac{\partial G^{\tau\tau}}{\partial\beta} = -\int_\Sigma \langle T_{\tau\tau}\rangle_G\Big|_{T=0}, \tag{1.52}$$

which matches (1.38) upon analytic continuation to Lorentzian time. Under a perturbation to the metric $G_{\mu\nu} \to G_{\mu\nu} + \varepsilon H_{\mu\nu}$, the partition function varies as

$$\begin{aligned}\ln Z[G + \varepsilon H] = \ln Z[G] &+ \frac{1}{2}\varepsilon\int \mathrm{d}^3x\sqrt{G(x)}\langle T_{\mu\nu}(x)\rangle_G(H^{\mu\nu}(x) - \varepsilon H^{\mu\rho}(x)H_\rho{}^\nu(x)) \\ &+ \frac{1}{8}\varepsilon^2\int \mathrm{d}^3x\mathrm{d}^3y\sqrt{G(x)}\sqrt{G(y)}\langle T_{\mu\nu}(x)T_{\rho\sigma}(y)\rangle_G H^{\mu\nu}(x)H^{\rho\sigma}(y) + \mathcal{O}(\varepsilon^3)\end{aligned} \tag{1.53}$$

where indices are raised and lowered with respect to the fiducial metric G and the two-

[9] Note this does not depend on any other sources which will remain the same as we vary G.

point function is defined by

$$\langle T_{\mu\nu}(x)T_{\rho\sigma}(y)\rangle_G \equiv \frac{4}{\sqrt{G(x)}\sqrt{G(y)}}\frac{\delta^2 \ln Z[G]}{\delta G^{\mu\nu}(x)\delta G^{\rho\sigma}(y)}. \tag{1.54}$$

Taking a functional derivative of (1.53) with respect to $H^{\mu\nu}(x)$ gives that

$$\langle T_{\mu\nu}(x)\rangle_{G+\varepsilon H} = \langle T_{\mu\nu}(x)\rangle_G - \varepsilon\langle T_{\sigma\nu}(x)\rangle_G H_\mu{}^\sigma(x) - \varepsilon\langle T_{\mu\rho}(x)\rangle_G H^\rho{}_\nu(x) + \frac{\varepsilon}{2}\int \mathrm{d}^3y\sqrt{G(y)}\langle T_{\mu\nu}(x)T_{\rho\sigma}(y)\rangle_G H^{\rho\sigma}(y) + \mathcal{O}(\varepsilon^2). \tag{1.55}$$

In the zero-temperature case this equality takes on a very useful form. At zero temperature, and in the absence of any further sources, we know due to conformal symmetry of the flat space vacuum that: (i) all one-point functions on the reference space must vanish and (ii) the contribution of the stress tensor two-point function on conformally flat spaces is determined up to the central charge, c_T, of the CFT[10]. Thus $\sqrt{G(x)}\langle T_{\mu\nu}(x)\rangle_{G+\varepsilon H}/c_T$ is *universal* among all the CFTs we are considering at zero temperature (up to $\mathcal{O}(\varepsilon^2)$ corrections). For static perturbation to the spatial geometry, $g_{ij}(x) \to g_{ij}(x) + \varepsilon h_{ij}(x)$, Equation (1.55) gives that

$$\lim_{\beta\to\infty}\frac{1}{\beta}\int \mathrm{d}^3x\sqrt{g(x)}\ \langle T_{ij}(x)\rangle_{g+\varepsilon h}h^{ij}(x) = \lim_{\beta\to\infty}\frac{\varepsilon}{2\beta}\int \mathrm{d}^3x\mathrm{d}^3y\sqrt{g(x)}\sqrt{g(y)}\langle T_{ij}(x)T_{k\ell}(y)\rangle_g h^{ij}(x)h^{k\ell}(y) + \mathcal{O}(\varepsilon^2) \tag{1.58}$$

or, by noting the integrand on the LHS is constant in Euclidean time and can be performed before taking the limit,

$$\lim_{\beta\to\infty}\frac{1}{\beta}\int \mathrm{d}^3x\sqrt{g(x)}\ \langle T_{ij}(x)\rangle_{g+\varepsilon h}h^{ij}(x) = \frac{\varepsilon}{2}\int \mathrm{d}^2x\mathrm{d}^3y\sqrt{g(x)}\sqrt{g(y)}\langle T_{ij}(x)T_{k\ell}(y)\rangle_g h^{ij}(x)h^{k\ell}(y)\Big|_{\beta=\infty} + \mathcal{O}(\varepsilon^2) \tag{1.59}$$

for any fixed Euclidean time x^0. Thus, by comparing (1.58) and (1.59), it follows that the change in vacuum energy, as given by the $\beta\to\infty$ limit of (1.53), due to this static perturbation to the spatial geometry can be written in terms of the VEV of the stress

[10] In particular, in conformally flat coordinates [59]

$$\sqrt{G(x)}\sqrt{G(y)}\langle T_{\mu\nu}(x)T_{\rho\sigma}(y)\rangle_G = \frac{c_T}{|x_1-x_2|^2}\mathcal{I}_{\mu\nu,\rho\sigma}(x_1-x_2) \tag{1.56}$$

where

$$\mathcal{I}_{\mu\nu,\rho\sigma}(x) \equiv \mathcal{I}_{\mu(\rho}(x)\mathcal{I}_{\sigma)\nu}(x) - \frac{1}{3}\delta_{\mu\nu}\delta_{\rho\sigma} \text{ and } \mathcal{I}_{\mu\nu}(x) = \delta_{\mu\nu} - \frac{2x_\mu x_\nu}{x^2}. \tag{1.57}$$

tensor of the deformed theory:

$$E[g+\varepsilon h] = E[g] - \frac{\varepsilon}{4}\int_\Sigma \mathrm{d}^2x\sqrt{g(x)}\ \langle T_{ij}(x)\rangle_{g+\varepsilon h} h^{ij}(x) + \mathcal{O}(\varepsilon^3). \tag{1.60}$$

Having written E in this way, its clear that it may be computed in many different ways. The universality of $\sqrt{G(x)}\langle T_{\mu\nu}(x)\rangle_{G+\varepsilon H}/c_T$ at zero temperature for G conformally flat means that we may straightforwardly deduce the result for *all* such CFTs from a single example. Holographic CFTs provide a prescription for reading off the finite and unambiguous VEV of the renormalised CFT stress tensor on these backgrounds, and thus, via (1.60), the change in E just from bulk quantities. This gives a simple path to the solution that can be applied for both flat and spherical calculations[11]. In the following two subsections, we will show how this is achieved for perturbations of flat space and the round sphere.

1.4.1 Flat Space

Consider a static perturbation to the spatial geometry of a (2+1)-dimensional holographic CFT (as described in Section 1.2) on flat space so that the metric becomes

$$g_{\mathrm{CFT}} = \mathrm{d}\tau^2 + (\delta_{ij} + \varepsilon h_{ij}(x))\mathrm{d}x^i\mathrm{d}x^j. \tag{1.61}$$

The VEV of the stress tensor on this background can be deduced from the bulk gravity solution. The flat space holographic CFT is dual to pure AdS_4 with conformal boundary $\mathbb{R}^3$,

$$\mathrm{d}s^2_{\mathrm{AdS}_4} = \frac{\ell^2}{z^2}\left(\mathrm{d}z^2 + \mathrm{d}\tau^2 + \delta_{ij}\mathrm{d}x^i\mathrm{d}x^j\right), \tag{1.62}$$

so we seek the leading-order correction in ε to this space that solves the Einstein equation with conformal boundary metric g_{CFT}. All two-spaces are (locally) conformally equivalent to a flat metric so we can WLOG restrict our attention to perturbations that are proportional to δ_{ij} and, as is often useful for linear problems, we decompose in harmonics of the background space so that

$$h_{ij}(x) = 2f(x)\delta_{ij} \text{ and } f(x) = \int \mathrm{d}^2k\tilde{f}(k^j)\mathrm{e}^{-ik^ix_i} \tag{1.63}$$

where $f(k) = f(-k)^\star$ (since f is real). Assuming a static bulk we can solve the $\mathcal{O}(\varepsilon)$ equations for a single Fourier mode $f(x) = \mathrm{e}^{-ik^ix_i}$ to get

$$\mathrm{d}s^2 = \mathrm{d}s^2_{\mathrm{AdS}_4} + \varepsilon\frac{\ell^2}{z^2}\left[2(1+kz)\delta_{ij}\mathrm{d}x^i\mathrm{d}x^j - k^2z^2\mathrm{d}z^2 + ikk_i\mathrm{d}x^i\mathrm{d}z\right]\mathrm{e}^{-kz}\mathrm{e}^{ik^ix_i} + \mathcal{O}(\varepsilon^2). \tag{1.64}$$

[11] Other methods involving, for example, the explicit form the two-point function of the stress tensor and zeta function regularisation, are shown in [30].

To deduce the stress tensor, we switch to Fefferman-Graham coordinates (Z, X^i) (1.31),

$$z = Z\left[1 + \varepsilon\left(-\frac{k^2}{4}Z^2 + \frac{1}{6}k^3Z^3 + \mathcal{O}(Z^4)\right)\mathrm{e}^{-ik^ix_i}\right] + \mathcal{O}(\varepsilon^2) \tag{1.65}$$

$$x = X^i + \varepsilon\left(-\frac{1}{6}ikk^iZ^3 + \mathcal{O}(Z^4)\right)\mathrm{e}^{-ik^ix_i} + \mathcal{O}(\varepsilon^2), \tag{1.66}$$

and read off the $\mathcal{O}(Z^3)$ terms in the metric. It follows that the VEV of a renormalised CFT stress tensor on a space deformed by a single Fourier mode is

$$\frac{1}{c_{\mathrm{h}}}\langle T_{ij}(x)\rangle_{\delta+2\varepsilon f\delta} = \varepsilon\mathrm{e}^{-ik^ix_i}k\left(k^2\delta_{ij} - k_ik_j\right) + \mathcal{O}(\varepsilon^2) \tag{1.67}$$

and thus for the general deformation (1.63) is

$$\langle T_{ij}(x)\rangle_{\delta+2\varepsilon f\delta} = \varepsilon c_{\mathrm{h}}\int \mathrm{d}^2k\tilde{f}(k)\mathrm{e}^{-ik^ix_i}k\left(k^2\delta_{ij} - k_ik_j\right) + \mathcal{O}(\varepsilon^2). \tag{1.68}$$

Plugging this universal quantity into (1.60), we see that for *any* (2+1)-dimensional CFT on flat space

$$E[\delta + \varepsilon h] = E[\delta] - \varepsilon^2\frac{\pi^4 c_T}{24}\int \mathrm{d}^2k|\tilde{f}(k)|^2k^3 + \mathcal{O}(\varepsilon^3). \tag{1.69}$$

Thus, given that unitary CFTs must have positive central charge, any non-trivial pertubation to the spatial geometry (i.e. not a rigid rescaling) must *lower* the vacuum energy of the CFT at leading order in ε. A similar argument can be copied for the round sphere.

1.4.2 S^2

We will now consider a static perturbation to the spatial geometry of a (2+1)-dimensional holographic CFT on $(\mathbb{R}\times S^2, \mathrm{d}\tau^2 + \Omega)$. Just as in the flat space case we, WLOG, restrict our attention to perturbations that are proportional to Ω_{ij},

$$g_{\mathrm{CFT}} = \mathrm{d}\tau^2 + \Big(1 + 2\varepsilon f(\theta^k)\Big)\,\Omega_{ij}\mathrm{d}\theta^i\mathrm{d}\theta^j. \tag{1.70}$$

The vacuum state of the holographic CFT on $(\mathbb{R}\times S^2, \mathrm{d}\tau^2 + \Omega)$ is dual to pure AdS_4 with conformal boundary $\mathbb{R}\times S^2$,

$$\mathrm{d}s^2_{\mathrm{AdS}_4} = \frac{\ell^2}{z^2}\left[(1+z^2)\mathrm{d}\tau^2 + \frac{\mathrm{d}z^2}{1+z^2} + \Omega_{ij}\mathrm{d}\theta^i\mathrm{d}\theta^j\right]. \tag{1.71}$$

We seek the leading-order correction in ε to this space which solves the Einstein equation with conformal boundary metric g_{CFT}. Once again, we ask how this responds to a single harmonic, in this case a spherical harmonic $f(\theta^i) = Y_{lm}(\theta^i)$, and deduce the general result

from linearity. Note that the $l = 0$ mode is simply a rigid rescaling of the geometry and thus, since we are working with a CFT, induces no change in E, and that the Ricci scalar of the deformed geometry is

$$R = 2 + 2\varepsilon(l-1)(l+2)Y_{lm} + \mathcal{O}(\varepsilon^2) \tag{1.72}$$

so the $l = 1$ modes do not alter the geometry at $\mathcal{O}(\varepsilon)$ — they each generate an isometry that rotates the sphere. Thus, we will not consider modes with $l = 0, 1$. Assuming a staticity, the leading-order correction to the bulk can be expressed in terms of a single function

$$\mathcal{S}(z) = \left[{}_2F_1\left(-\frac{l+1}{2}, \frac{l}{2}; \frac{1}{2}; -z^2\right) z^2 + 2p_l \, {}_2F_1\left(-\frac{l}{2}, \frac{l+1}{2}; \frac{3}{2}; -z^2\right) z^3 \right], \tag{1.73}$$

where

$$p_l \equiv \frac{l+1}{l} \left(\frac{\Gamma\left(\frac{l+1}{2}\right)}{\Gamma(l/2)} \right)^2, \tag{1.74}$$

that solves the ODEs in z given by the Einstein equations at $\mathcal{O}(\varepsilon)$, gives regular behaviour within the bulk and the correct asymptotic behaviour at the conformal boundary. In terms of this function, the bulk metric is

$$\begin{aligned} \mathrm{d}s^2 = \mathrm{d}s^2_{\mathrm{AdS}_4} + \varepsilon \frac{\ell^2}{z^2} \Bigg\{ & \frac{(l-1)(l+2)}{1+z^2} \mathrm{d}z^2 \\ & + \left(\Omega_{ij} \mathrm{d}\theta^i \mathrm{d}\theta^j \left[\frac{6}{z^2} + 4 - \left(\frac{2}{z} + z \right) \partial_z \right] + 2\varepsilon \mathrm{d}\theta^i \mathrm{d}z \left[-\frac{1+2z^2}{z(1+z^2)} + \frac{1}{2}\partial_z \right] \partial_i \right) \Bigg\} \mathcal{S}(z) Y_{lm}(\theta^k) \\ & + \mathcal{O}(\varepsilon^2). \end{aligned} \tag{1.75}$$

and so changing to Fefferman-Graham coordinates (Z, Θ^i) defined implicitly by

$$z = Z\left[1 + \frac{1}{4}Z^2 + \varepsilon(l+2)(l-1)\left(-\frac{1}{4}Z^2 + \frac{1}{3}p_l Z^3\right) Y_{lm} + \mathcal{O}(Z^4)\right] \tag{1.76}$$

$$\theta^i = \Theta^i + \frac{\varepsilon}{3} p_l \Omega^{ij} \partial_j Y_{lm} Z^3 + \mathcal{O}(Z^4), \tag{1.77}$$

and reading off the $\mathcal{O}(Z^3)$ terms from the metric gives that the VEV of a renormalised CFT stress tensor on $(\mathbb{R} \times S^2, \mathrm{d}\tau^2 + \Omega)$ deformed by a single spherical harmonic is

$$\frac{1}{c_{\mathrm{h}}} \langle T_{ij} \rangle_{(1+2\varepsilon f)\Omega} = 2\varepsilon p_l \left\{ [l(l+1) - 1]\Omega_{ij} + \nabla_i \nabla_j \right\} Y_{lm} + \mathcal{O}(\varepsilon^2), \tag{1.78}$$

where ∇ is the Levi-Civita connection on the round sphere. By linearity, the result for an arbitrary perturbation,

$$f(\theta^i) = \sum_{l\geqslant 0} \sum_{m=-l}^{l} f_{lm} Y_{lm}(\theta^i), \tag{1.79}$$

is

$$\langle T_{ij} \rangle_{(1+2\varepsilon f)\Omega} = 2\varepsilon c_{\mathrm{h}} \sum_{lm} f_{lm} p_l \left\{ [l(l+1) - 1]\Omega_{ij} + \nabla_i \nabla_j \right\} Y_{lm} + \mathcal{O}(\varepsilon^2). \tag{1.80}$$

Plugging this universal quantity into (1.60), we see that for *any* (2+1)-dimensional CFT on $\mathbb{R} \times S^2$

$$E[\Omega + \varepsilon h] = E[\Omega] - \varepsilon^2 \frac{\pi^2 c_T}{48} \sum_{lm} |f_{lm}|^2 p_l (l+2)(l-1) + \mathcal{O}(\varepsilon^3). \tag{1.81}$$

Thus, given that unitary CFTs must have positive central charge, any non-trivial perturbation to the spatial geometry (i.e. not a rigid rescaling or a rotation) must *lower* the vacuum energy of the CFT at leading order in ε, just as on flat space.

1.5 Summary and Discussion

We have reviewed three vacuum energy calculations. Firstly, the vacuum energy of a free Maxwell field in the presence of parallel conducting plates was calculated, revealing the surprising result that there is a measurable attractive force between the plates driven purely by quantum fluctuations in the vacuum. In doing this calculation we encountered many steps that will be repeated through the original work in this thesis. An initial attempt to compute the vacuum energy gave an answer with UV divergences. To resolve this, the integral/sum needed to be regularised and there was some choice about how to do this. A few of the different options were exhibited here: cutoff regularisation, zeta function regularisation and exponential regularisation. Ultimately, care needed to be taken to make sure that the final result was UV finite and scheme independent — necessary conditions for a truly-physical quantity. The generic presence of UV divergences, need for appropriate regularisation, and search for an unambiguous quantity and means of calculating it will all feature prominently throughout the rest of this thesis. Next, we considered static (2+1)-dimensional holographic CFTs with compact spatial geometry $(\Sigma, \bar{g})$. Under some reasonable assumptions, the metrics of their dual spacetimes can be written as warped products of Riemannian manifolds whose scalar curvatures (due to the Einstein equations and Bianchi identities) have non-positive Laplacians. Via the divergence theorem, an equation involving the curvatures at the (asymptotic) boundaries, whose terms can then be expressed in terms of the CFT data, was derived. It followed from this equation that

the vacuum energy of these holographic CFTs is zero when $(\Sigma, \bar{g})$ has constant curvature and is otherwise negative.

The above is an exposition in how holographic intuition derived from the AdS/CFT correspondence can lead to progress in field theory. Even the most basic questions in QFT can be infamously difficult thanks to, for example, a lack of rigorous definition of the path integrals and potential ambiguities that come with renormalisation. Holography rephrased one of these questions in terms of simple classical gravity calculations leading to a non-positivity bound on a finite, unambiguous vacuum energy for a certain class of QFTs — raising the question of whether this result could hold more broadly. Further, it was shown how holography was used *directly* to show that E is locally[12] maximised by flat space and round sphere for *all* unitary CFTs. Answering these questions that holography has led us to will be the focus of the rest of this thesis.

To make further progress, we now move beyond the AdS/CFT correspondence and the theories it describes. The simplest and most natural next step is to investigate 'free' theories. For that, we will make use of heat kernel methods.

[12] In the space of volume-preserving metrics.

Chapter 2

Heat Kernel Methods

The behaviour of a diffusion process encodes geometric data about the manifold it is taking place on. As such, the fundamental solution to the heat equation, the heat kernel, has been studied extensively by mathematicians and physicists alike. In particular, heat kernels are an important tool for probing the spectra of Laplacian(-like) operators and have proven useful in developing new results such as the Atiyah-Singer index theorem [60–62]. Heat kernels also arise as an auxiliary function for various objects in quantum theory. This was initially noted by Fock [63] who represented the Dirac Green's function as an integral of a heat kernel over 'proper time'. Schwinger noted this parametrisation could be used to perform gauge covariant computation in QED in the presence of background fields [64]. DeWitt built on this by making the heat kernel a key tool in a manifestly-covariant approach to QFT on curved space and quantum gravity [65–68], serving as a platform for many results on quantum corrections to classical physics, such as first-order corrections to black hole entropy [69], anomalies in chiral gauge theories [70] and the Casimir Energy [71]. A key feature of these heat kernels is their asymptotics in small proper-time [72, 73]. The structure of this asymptotic expansion has been established in many cases, ranging from closed manifolds to manifolds with boundaries and exotic boundary conditions. There are a number of techniques for calculating the expansion coefficients. Notably, the coefficients are determined to a large extent by local geometric data — depending on the the spin of the fields in a limited way — allowing for universal results.

In this thesis, the vacuum, or free energy at finite temperature, of free theories as a functional of spatial geometry will be calculated using heat kernel methods. This chapter will review them, with a particular focus on the heat kernel coefficients that make the analytic and numerical work possible. A more comprehensive review of heat kernel methods with a particular focus on their asymptotic expansions, including many of the results that will be presented in this chapter, can be found in [74].

We will begin by mapping out the path between fundamental solutions to a generalised form of the heat equation on a compact Riemannian manifold (with boundary)

— where the Laplacian is replaced by a second-order differential operator, D, that is self adjoint with respect to some inner product, $(\cdot,\cdot)$ — and the free energy of a Lorentzian QFT with a quadratic action, $(\phi, D\phi)$, at finite temperature. In short, the partition function of these QFTs can be evaluated exactly in terms of the functional determinant of D — an object which, with the help of an auxiliary variable, can be written in terms a heat kernel. The aforementioned heat kernel expansion and its properties will then be introduced. Knowledge of the expansion coefficients alone is sufficient to extract data from the corresponding QFT. Most importantly for this work, they explicitly predict the UV divergences of partition functions, but they they can also detect quantum anomalies — both of which will be shown here.

The plan for this chapter is as follows. In Section 2.1, the heat kernel will be defined and it will be shown how to write the free energy of a Euclidean QFT in terms of it. The closely related cylinder kernel will also be introduced. The heat kernel expansion will be introduced in Section 2.2 and it will be shown how the heat kernel coefficients can be used to regularise and compute quantum anomalies in Sections 2.3 and 2.4, respectively. The chapter will then conclude with a summary in Section 2.5.

2.1 The Heat Equation

Consider a vector bundle V over some compact Riemannian manifold, $(\mathcal{M}, g)$. For our purposes, a (local) heat kernel $K(t, x, y, D)$[1] is a solution to an equation of the form[2]

$$(\partial_t + D)K = 0, \quad \text{with } K(0, x, y, D) = \delta(x, y) \tag{2.1}$$

for $t \in \mathbb{R}^+$, x, $y \in \mathcal{M}$ and D is an operator of the form

$$D = -\left(g^{\mu\nu}\nabla_\mu\nabla_\nu + E\right) \tag{2.2}$$

where E is a linear map $V \to V$ and ∇ is the sum of the spin (ω_μ^{ab}) and Riemannian $(\Gamma_{\mu\nu}^{\rho})$ connections. D is self adjoint with respect to the inner product $(\cdot,\cdot)$. If $\mathcal{M}$ is a manifold with a boundary there will also be some homogeneous boundary conditions. We write these as $\mathcal{B}\phi|_{\partial\mathcal{M}} = 0$, $\phi \in V$ where $\mathcal{B} = \Pi_- + (\nabla_n + S)\Pi_+$. Here Π_- and Π_+ are complementary projectors that select the components that obey the Dirichlet and Robin boundary conditions, respectively, and ∇_n denotes a normal derivative at the boundary. Provided that D has non-negative spectrum $\{\lambda\}$, we can write the solution to Equation (2.1) as

$$K(t, x, y, D) = \sum_\lambda \phi_\lambda^\dagger(y)\mathrm{e}^{-t\lambda}\phi_\lambda(x) \tag{2.3}$$

[1] Note that t is *not* a coordinate on $\mathcal{M}$.
[2] Note the similarity here to the Schrödinger equation in imaginary time.

where $\{\phi_\lambda\}$ is a complete orthonormal basis of eigenfunctions of D in V. Tracing over the matrix indices and spacetime points then gives the global heat kernel:

$$\int \mathrm{d}^n x\sqrt{g}\mathrm{tr}_V K(t,x,x,D) = \sum_\lambda \mathrm{e}^{-t\lambda}(\phi_\lambda,\phi_\lambda) = \mathrm{Tr}_{L^2}\left(\mathrm{e}^{-tD}\right). \tag{2.4}$$

From now on we will refer to the object

$$K(t,D) \equiv \mathrm{Tr}_{L^2}\left(\mathrm{e}^{-tD}\right) \tag{2.5}$$

as the heat kernel, as opposed to the local heat kernel defined by (2.1). Similarly, solutions to the partial differential equation

$$\left(\partial_t^2 - D\right) T(t,x,y,D) = 0, \text{ with } T(0,x,y,D) = \delta(x,y), \tag{2.6}$$

give the related cylinder kernel

$$T(t,D) \equiv \mathrm{Tr}_{L^2}\left(\mathrm{e}^{-t\sqrt{D}}\right). \tag{2.7}$$

These heat kernels are of interest in quantum theory because they can be used to evaluate partition functions, and in particular the free energy, of QFTs on curved backgrounds.

Given a QFT on $(\mathcal{M},g)$ consisting of a field $\phi \in V$ with an action $S[g,\phi] = (\phi, D\phi)$ its partition function is

$$Z[g] = \int \mathcal{D}\phi\, \mathrm{e}^{-S[g,\phi]}. \tag{2.8}$$

For actions of this form, the partition function can be evaluated via change of variables. We will consider the case of a real scalar field, as an example. Each field configuration $\phi \in V$ can be expressed uniquely in terms of the complete orthonormal basis of eigenfunctions of D, i.e. there are unique real $\{a_\lambda\}$ such that

$$\phi(x) = \sum_\lambda a_\lambda \phi_\lambda(x), \tag{2.9}$$

thus we may make a change of variables from the values of ϕ at each position in $\mathcal{M}$ to its coefficients in this expansion. In terms of the new variables, the action can be written as $S[g,\phi] = \sum_\lambda \lambda\, a_\lambda^2$ and the measure transforms as $\int \mathcal{D}\phi \to \prod_\lambda \int_{\mathbb{R}} \mathrm{d}a_\lambda$ (up to constant that cancels out in the computation of any observable so is neglected here, as will any further similar constants that arise in this calculation) so that the partition function is a product of Gaussian integrals,

$$Z[g] = \prod_\lambda \left(\int_{\mathbb{R}} \mathrm{d}a_\lambda\, \mathrm{e}^{-\lambda a_\lambda^2}\right) = \prod_\lambda \sqrt{\frac{\pi}{\lambda}}. \tag{2.10}$$

This is an example of the generic form the partition function for free theories, $Z[g] = \prod_\lambda \lambda^\sigma$ — even those for whom D is not a second-order operator. For example, repeating the argument above for the Dirac operator gives $Z[g] = \prod_\lambda \lambda$, with the integration over Grassmann numbers accounting for the difference in power here. Thus, the partition function of a theory with action of the form $S[g, \phi] = (\phi, D\phi)$ can be written as

$$\ln Z[g] = \sigma \ln \det D. \tag{2.11}$$

for some theory dependent constant σ. This quantity that admits a representation in terms of the heat kernel (2.5). Noticing that

$$\ln \lambda = -\int_0^\infty \frac{\mathrm{d}t}{t} \mathrm{e}^{-t\lambda} \tag{2.12}$$

up to an infinite constant[3], it follows from expressing $\ln \det D$ in terms of the eigenvalues of D that

$$\ln \det D = -\int_0^\infty \frac{\mathrm{d}t}{t} K(t, D). \tag{2.13}$$

Recall from statistical mechanics that given some system in thermodynamic equilibrium with partition function $Z(\beta)$, its free energy is given by $F = -\beta^{-1} \ln Z$. Therefore, when the Euclidean QFT described above matches that of a Lorentzian QFT at finite temperature $T = \beta^{-1}$ (and in the absence of any other dynamical fields) the free energy of that thermodynamic system is given by

$$\beta F = \sigma \int_0^\infty \frac{\mathrm{d}t}{t} K(t, D). \tag{2.14}$$

Thus, we can calculate the free energy from the spectrum of D. We note that, while only free theories are considered here, the treatment above can be adapted to show that the one-loop correction to an effective action due to integrating out quantum fluctuations in the presence of background fields can also be expressed in terms of a functional determinant, and thus a heat kernel, in this way [74, 75]. Indeed, what we have presented here is just a special case in which this correction is exact. This treatment is included in Appendix A.2.

As is typical for QFTs, there are divergences we have to deal with. Looking at the definition of $K(t, D)$, its clear that $K(t, D) \to \infty$ as $t \to 0^+$, so the integral on the right hand side of Equation (2.13) does not converge. Fortunately, the asymptotics of the heat kernel in this region are well understood, which facilitates regulating this expression a great deal.

[3] This can be shown by differentiating both sides of (2.12) with respect to λ. The constant here does not matter as we will only consider differences of the quantity on the RHS, where the constant cancels.

2.2 The Heat Kernel Expansion

The 'heat kernel expansion' refers to the asymptotic expansion of $K(t, D)$ as $t \to 0^+$. For any D of the form (2.2) with (if applicable) boundary conditions on a compact[4] Riemannian manifold of dimension n

$$K(t, f, D) \sim \sum_{k \geqslant 0} a_k(f, D, \mathcal{B}) t^{(k-n)/2} \tag{2.15}$$

as $t \to 0^+$, where $K(t, f, D)$ is a generalised form of the heat kernel:

$$K(t, f, D) \equiv \mathrm{Tr}_{L^2}\left(f \mathrm{e}^{-tD}\right) \tag{2.16}$$

for any function $f : \mathcal{M} \to \mathbb{R}$ [76]. We note here that the expression (2.15) generically has $(n + 1)$ terms that give divergences in (2.14). The expressions for the asymptotic coefficients $a_k(f, D)$ are: (i) calculable, (ii) local integrals of mostly geometric invariants and (iii) available for the most part in the literature for small k. More concretely,

$$a_k(f, D, \mathcal{B}) = \int_{\mathcal{M}} \mathrm{d}^n x \sqrt{g} f(x) a_k(x, D, \mathcal{B}) + \sum_{j=0}^{k-1} \int_{\partial \mathcal{M}} \mathrm{d}^{n-1} x \sqrt{h} f^{(j)} a_{k,j}(x, D, \mathcal{B}) \tag{2.17}$$

where $a_k(x, D, \mathcal{B})$ consists of dimension k terms built from E, the Riemann tensor $R^{\mu}{}_{\nu\rho\sigma}$, the curvature two-form, Ω, defined in terms of the 'gauge' part of the connection, ω, as

$$\Omega \equiv \mathrm{d}\omega + \omega \wedge \omega, \tag{2.18}$$

and their derivatives, $f^{(j)}$ denotes the j-th normal derivative of f at the boundary, h is the induced metric on the boundary and $a_{k,j}(x, D, \mathcal{B})$ is built from dimension $k - j - 1$ combinations of $E, R^{\mu}{}_{\nu\rho\sigma}, \Omega$, boundary quantities such as the extrinsic curvature K_{ab} and S, and their derivatives. The minor dependence on the vector bundle in which the fields live is a real strength of these coefficients — one calculation can be used for different theories on the same background. To illustrate their simplicity, here are the heat kernel

[4] It is also possible to define heat kernels on non-compact manifolds that also admit an asymptotic expansion with coefficients (2.17) but a little more care in needed. A naïve treatment yields IR divergent coefficients such as $a_0(f, D)$ (2.19). The local heat kernel and its coefficients carry over seamlessly to the non-compact case thus to avoid such difficulties one can work with a 'subtracted' heat kernel where, instead of just working with the global heat kernel $K(t, D)$, one first subtracts an appropriate 'reference' local heat kernel, based on some other different operator, from it and then integrate up this subtracted quantity. The same tools can then be used, such as the heat kernel expansion, but now with 'subtracted' quantities, such as subtracted heat kernel coefficients, as the subtraction renders them finite.

coefficients $a_k(f, D, \mathcal{B})$ for $0 \leqslant k \leqslant 4$ on manifolds with boundaries [74]:

$$a_0(f, D, \mathcal{B}) = \frac{1}{(4\pi)^{(n/2)}} \int_{\mathcal{M}} \mathrm{d}^n x \sqrt{g} \mathrm{tr}_V(f), \tag{2.19}$$

$$a_1(f, D, \mathcal{B}) = \frac{1}{4(4\pi)^{(n-1)/2}} \int_{\partial\mathcal{M}} \mathrm{d}^{n-1} x \sqrt{h} \mathrm{tr}_V(\chi f), \tag{2.20}$$

$$\begin{aligned} a_2(f, D, \mathcal{B}) = \frac{1}{6(4\pi)^{(n/2)}} \Bigg[& \int_{\mathcal{M}} \mathrm{d}^n x \sqrt{g} f \mathrm{tr}_V (6E + R) \\ & + \int_{\partial\mathcal{M}} \mathrm{d}^{n-1} x \sqrt{h} \mathrm{tr}_V (2fK_{aa} + 3\chi\nabla_n f + 12fS) \Bigg], \end{aligned} \tag{2.21}$$

where R is the scalar curvature and $\chi \equiv \Pi_+ - \Pi_-$ and further for a manifold without a boundary

$$\begin{aligned} a_4(f, D) = \frac{1}{360(4\pi)^{(n/2)}} \int \mathrm{d}^n x \sqrt{g} f \mathrm{tr}_V \big(& 60\nabla^2 E + 12\nabla^2 R + 60RE + 180E^2 \\ & + 5R^2 - 2R_{\mu\nu}R^{\mu\nu} + 2R_{\mu\nu\rho\sigma}R^{\mu\nu\rho\sigma} + 30\Omega_{\mu\nu}\Omega^{\mu\nu} \big) \end{aligned} \tag{2.22}$$

and $a_{2j+1}(f, D) = 0$ for all j, by dimensional analysis. As k increases, the number of allowed terms in the integrand of $a_k(f, D, \mathcal{B})$ increases too, making their calculation more complex. However, knowledge of only the leading order coefficients turns out to be sufficient for regularising the partition function and computing quantum anomalies, as well as estimating the heat kernel for small t.

The aforementioned global cylinder kernel also has an asymptotic expansion [71]. It is determined, in part, by the heat kernel coefficients of its operator:

$$T(t, D) \sim \sum_{k \geqslant 0} e_k(D, \mathcal{B}) t^{k-n} + \sum_{k \geqslant n+1; k-n \text{ odd}} f_k(D, \mathcal{B}) t^{k-n} \ln t \tag{2.23}$$

where

$$e_k(D, \mathcal{B}) = \frac{2^{n-k}}{\sqrt{\pi}} \Gamma\left(\frac{n-k+1}{2}\right) a_k(D, \mathcal{B}),\ f_k = 0 \text{ for } k-n \text{ even or negative} \tag{2.24}$$

$$f_k(D, \mathcal{B}) = (-1)^{(k-n+1)/2} \frac{2^{n-k+1}}{\sqrt{\pi}\Gamma\left(\frac{k-n+1}{2}\right)} a_k(D, \mathcal{B}) \text{ for } k-n \text{ odd and positive.} \tag{2.25}$$

but the rest of the coefficients are not determined by the heat kernel expansion — they depend globally on the background.

2.3 Regularisation

As mentioned in Section 2.2, the heat kernel diverges at $t = 0$ so it must be regulated in order to extract anything meaningful from it. To see where issues come from, we introduce

a UV cutoff, Λ. This is equivalent to changing the lower limit in the heat kernel integral from $0 \to \Lambda^{-2}$ (by dimensional analysis[5]). For simplicity, we consider an odd-dimensional manifold without boundary. To isolate the divergent pieces, rewrite the integral as

$$\int_{\Lambda^{-2}}^{\infty} \frac{\mathrm{d}t}{t} K(t,D) = \int_{\Lambda^{-2}}^{\infty} \frac{\mathrm{d}t}{t} \left(K(t,D) - \sum_{n>k\geqslant 0} a_k(D) t^{(k-n)/2} \right) - \sum_{n>k\geqslant 0} \frac{2a_k(D)}{k-n} \Lambda^{n-k} \tag{2.26}$$

In the limit $\Lambda \to \infty$,

$$\int_{\Lambda^{-2}}^{\infty} \frac{\mathrm{d}t}{t} K(t,D) \sim - \sum_{n>k\geqslant 0} \frac{2a_k(D)}{k-n} \Lambda^{n-k} + \mathcal{O}(\Lambda^0). \tag{2.27}$$

The RHS depends on the theory only through the heat kernel coefficients, which do not depend on the dynamical fields. It follows that by introducing local counterterms into the original action of the form

$$\begin{aligned} S[g,\phi] &\to S[g,\phi] + S_{\mathrm{CT}}[g] \\ &= S[g,\phi] + \sigma \sum_{n>k\geqslant 0} \frac{2a_k(D)}{k-n} \Lambda^{n-k} \end{aligned} \tag{2.28}$$

that we get a finite $\ln Z$:

$$\ln Z[g] = -\sigma \int_0^{\infty} \frac{\mathrm{d}t}{t} \left(K(t,D) - \sum_{n>k\geqslant 0} a_k(D) t^{(k-n)/2} \right) \tag{2.29}$$

Alternatively, we can renormalise using zeta function regularisation. The fundamental object in this setup is the the generalised zeta function, defined by

$$\zeta(s,f,D) \equiv \mathrm{Tr}(f D^{-s}) = \frac{1}{\Gamma(s)} \int_0^{\infty} \frac{\mathrm{d}t}{t} t^s K(t,f,D) \tag{2.30}$$

for $\Re(s) > n/2$. By comparing this with the expression for the functional determinant (2.13), it follows that the renormalised functional determinant is given by the analytic continuation of $\zeta(s,f,D)$ to $s=0$:

$$\ln \det D = -\lim_{s\to 0} \mu^{2s} \zeta(s,D)\Gamma(s) \tag{2.31}$$

where μ is a constant with mass dimension 1 and, as was the case for the heat kernel, $\zeta(s,D) \equiv \zeta(s,1,D)$. This analytic continuation can be carried out with the help of heat kernels and their coefficients.

We begin by working in the region $\Re(s) > n/2$ and separating out the problematic

[5] The argument of the heat kernel has dimension $[t] = -[\lambda] = -[D] = -2$

terms in analogy with (2.26):

$$\Gamma(s)\zeta(s,f,D) = \int_0^\nu \frac{\mathrm{d}t}{t} t^s \sum_{n\geqslant k\geqslant 0} a_k(f,D) t^{(k-n)/2} + \int_0^\nu \frac{\mathrm{d}t}{t} t^s \left(K(t,f,D) - \sum_{n\geqslant k\geqslant 0} a_k(f,D) t^{(k-n)/2} \right) + \int_\nu^\infty \frac{\mathrm{d}t}{t} t^s K(t,f,D) \quad (2.32)$$

where ν is some arbitrary parameter. The first set of terms here can then be integrated up giving

$$\Gamma(s)\zeta(s,f,D) = \sum_{n\geqslant k\geqslant 0} \frac{a_k(f,D)}{s-(k-n)/2} \nu^{s-(k-n)/2} + \int_0^\nu \frac{\mathrm{d}t}{t} t^s \left(K(t,f,D) - \sum_{n\geqslant k\geqslant 0} a_k(f,D) t^{(k-n)/2} \right) + \int_\nu^\infty \frac{\mathrm{d}t}{t} t^s K(t,f,D). \quad (2.33)$$

This expression has a potential pole at $s=0$ with residue

$$a_n(f,D) = \mathrm{Res}_{s=0}\left(\Gamma(s)\zeta(s,f,D)\right) = \zeta(0,f,D). \quad (2.34)$$

For odd dimensions (where $a_n(f,D)=0$) (2.33) can be analytically continued to $s=0$. Evaluating it at $s=0$ and taking the arbitrary parameter $\nu\to\infty$ gives a renormalised functional determinant that recovers the counterterm renormalised partition function (2.29). In even dimensions, there is generally a pole at $s=0$ that would need to be subtracted off in some way, leaving some scheme dependence behind. The takeaway from this is that the heat kernel coefficients contain most of the data necessary for regularisation.

2.4 An Application: Quantum Anomalies

A quantum anomaly is a symmetry of a classical action that fails to be a symmetry of the corresponding quantum theory for any renormalisation scheme. The canonical example this phenomenon is the axial symmetry of a massless Dirac fermion coupled to a gauge field in $d=4$. Consider the example of QED with a massless electron, that is, a U(1) gauge field coupled to massless Dirac fermion:

$$S[A,\psi] = \int \mathrm{d}^4x \left[-\frac{1}{4} F_{\mu\nu}F^{\mu\nu} + i\overline{\psi}\not{D}\psi \right] \quad (2.35)$$

$$= \int \mathrm{d}^4x \left[-\frac{1}{4} F_{\mu\nu}F^{\mu\nu} + i\psi_{\mathrm{L}}^\dagger \sigma^\mu D_\mu \psi_{\mathrm{L}} + i\psi_{\mathrm{R}}^\dagger \overline{\sigma}^\mu D_\mu \psi_{\mathrm{R}} \right] \quad (2.36)$$

where $F \equiv \mathrm{d}A$, $D_\mu = \partial_\mu - ieA_\mu$ is the gauge covariant derivative and $\psi = (\psi_\mathrm{L}, \psi_\mathrm{R})$. This action is invariant under the global transformation $\psi \to \mathrm{e}^{i\alpha\gamma^5}\psi$. However, in the quantum theory the mass parameter of the fermion receives quantum corrections and thus axial symmetry is broken. This is called a chiral anomaly. Another kind of symmetry which is often broken by quantisation is conformal symmetry. Pure Yang-Mills theory

$$S = -\frac{1}{4g_\mathrm{YM}^2}\int \mathrm{d}^4\, x F^a_{\mu\nu}F^{a\,\mu\nu} \tag{2.37}$$

in four dimensions is classically scale invariant but the Yang-Mills coupling runs when this theory is quantised [77, 78]. In some instances, the presence of an anomaly can have grave consequences. For global symmetries, such as the chiral and conformal anomalies described above, this is not the case. For a local symmetry, however, an anomaly leads to a fundamental inconsistency. Gauge invariance is required to cancel unphysical degrees of freedom and as such must be preserved by quantisation. This requirement that local symmetries not be anomalous can lead to constraints on theories. As this is a truly quantum effect, the one-loop effective action, and therefore the heat kernel, are useful tools for deducing these constraints. The heat kernel expansion turns out to be particularly suited to computing Weyl anomalies.

Consider a quantum field theory on an n-dimensional Riemannian manifold $(\mathcal{M}, g)$ whose classical action is Weyl invariant i.e. invariant under a Weyl transformation $g_{\mu\nu} \mapsto \mathrm{e}^{2\rho(x)}g_{\mu\nu}$. The self-adjoint second-order differential operator that determines the one-loop correction to the effective action, D, must transform as $D \mapsto \mathrm{e}^{-2\rho(x)}D$. Whether this symmetry is preserved at the quantum level is determined by the trace of the stress tensor since

$$\delta \ln Z = -\frac{1}{2}\int_\mathcal{M} \mathrm{d}^n x\sqrt{g}\langle T_{\mu\nu}\rangle \delta g^{\mu\nu} = \int_\mathcal{M} \mathrm{d}^n x\sqrt{g}\langle T_\mu{}^\mu\rangle\delta\rho. \tag{2.38}$$

Thus a quantum field theory is Weyl invariant at the quantum level if and only if $\langle T_\mu{}^\mu\rangle = 0$. By varying the expression for $\ln Z$ written in terms of the functional determinant (2.31), we can deduce an expression for the trace of the renormalised stress tensor at one-loop. Under an infinitesimal Weyl transformation $\delta g_{\mu\nu} = 2(\delta\rho)g_{\mu\nu}$, $\delta D = -2\delta\rho D$ and so the zeta function (2.30) varies as

$$\delta\zeta(s, D) = 2s\zeta(s, \delta\rho, D) \tag{2.39}$$

giving a functional determinant (2.31) that varies *unambiguously*[6] as

$$\delta \ln\det D = -2\zeta(0, \delta\rho, D) = -2a_n(\delta\rho, D). \tag{2.40}$$

[6]Even in the case of even-dimensional manifolds where the zeta function regularised partition function is scheme dependent.

Spin	a	b	c	d
0	1	1	$30\xi - 6$	$90(\xi - 1/6)^2$
$\frac{1}{2}$	$-\frac{7}{2}$	-11	6	90
1	-13	62	18	0
2	212	0	0	$\frac{717}{4}$

Table 2.1: A table displaying the coefficients of the various terms of the four-dimensional Weyl anomaly (2.42), as can be deduced from the heat kernel coefficients, for fields with spin 0, $1/2, 1$ and 2.

Comparing (2.38) with (2.40) gives that at one-loop the trace of the renormalised stress tensor of a classically Weyl-invariant theory is determined by a heat kernel coefficient density:

$$\langle T_\mu{}^\mu(x)\rangle = -2\sigma a_n(x, D), \tag{2.41}$$

where σ is a constant that depends on the spin of the field. While generally giving one-loop results, this expression is exact for free theories. For example, it can be used to read off the Weyl anomaly induced by placing free quantum fields on a four-dimensional curved background [74],

$$\langle T_\mu{}^\mu(x)\rangle = -\frac{\sigma}{1440\pi^2}\left[aC_{\mu\nu\rho\sigma}C^{\mu\nu\rho\sigma} + b\left(R_{\mu\nu}R^{\mu\nu} - \frac{1}{3}R^2\right) + c\nabla^2 R + dR^2\right] \tag{2.42}$$

where $C_{\mu\nu\rho\sigma}$ is the Weyl tensor and the coefficients a, b, c and d are given in Table 2.1 for the scalar field, Dirac fermion, vector field and graviton. It can even be used to derive the effective action in two dimensions, where all metrics are conformally flat. For example, the effective action for a free scalar field on a Riemannian two-manifold $(\Sigma, \mathrm{e}^{2\rho}\delta)$ with scalar curvature $R = -2\mathrm{e}^{-2\rho}\partial^2\rho$ varies as $\delta\Gamma/\delta\rho(x) = -a_2(x, \mathrm{e}^{-2\rho}\partial^2) = \partial^2\rho(x)/(12\pi)$ under a change to the metric $\delta g = 2\delta\rho g$ which can be integrated (subject to $\Gamma|_{\rho=0} = 0$) and written covariantly to give

$$\Gamma = -\frac{1}{96\pi}\int_\Sigma \mathrm{d}^2x\sqrt{g}\,R\frac{1}{\nabla^2}R. \tag{2.43}$$

This is of course the result of integrating out the quantum fluctuations of the bosonic string propagating on flat space governed by the Polyakov action. A similar calculation can also be performed to deduce the effective action for two dimensional QED [79].

2.5 Summary and Discussion

In this chapter, we have introduced heat kernel methods as a tool for quantum field theory on curved space. We have shown that the partition function of Euclidean QFT (and thus the free energy of a Lorentzian QFT at finite temperature) on a compact Riemannian

manifold with a quadratic action, $(\phi, D\phi)$, where D is an (elliptic) self-adjoint second-order differential operator, can be expressed in terms of the (global) heat kernel, $K(t, f, D)$, integrated over the auxiliary parameter t. The asymptotics of $K(t)$ as $t \to 0^+$ were then detailed for manifolds with boundaries, the key observation being that the coefficients in the expansion are local integrals of geometric invariants and the potential terms, and have a largely universal form, as demonstrated by the first few coefficients. While deriving the form of the coefficients can be involved, they are calculable and readily available in the literature. It was then shown how the heat kernel coefficients determine the UV divergences and thus provide a route to renormalisation. Finally, we discussed quantum anomalies and, in particular, how knowledge of a single heat kernel coefficient alone can determine the Weyl anomaly.

The heat kernel coefficients considered in this chapter, on manifolds with boundaries, will be sufficient for most of the geometries discussed in this thesis. What is known about them, however, goes far beyond the cases discussed here, with work detailing the application of heat kernel coefficients to different backgrounds, such as those with conical [80] and domain wall [81] defects, and more general operators, such as those with more derivatives [82, 83]. We refer the reader to [74] for a more comprehensive overview of the heat kernel expansion and its applications.

Knowledge of heat kernel coefficients alone is sufficient to deduce some observables in quantum theory but the vacuum energy is not one of them. While the locality of the heat kernel coefficients is a strength for computing them, it limits them here since, as observed in Chapter 1, vacuum energy is intrinsically non-local. Fortunately, heat kernel methods methods also give a path to calculating the vacuum energy — via the heat kernel itself and therefore the eigenvalues of D. These can seldom be solved for analytically but to investigate the global behaviour of free energy as a functional of spatial geometry we need to probe a wide range of theories. In this thesis, this will be achieved by using perturbation theory and numerical methods to calculate the eigenvalues and thus the vacuum energy. The heat kernel coefficients will then play an important role in extracting the UV-finite part of the vacuum energy and, in the numerical work, ensuring a high degree of numerical accuracy.

Chapter 3

Free Theories on Flat Space

The presence of matter gives a surface embedded in an ambient space an energy; it may be external to the surface — like the pressure of air on a soap bubble — or may comprise the material nature of the surface itself — like a membrane with surface tension and bending energy. The equilibrium configuration of such a surface is determined by these energies. For example, the presence of surface tension tends to make membranes favour (smooth) minimal-area configurations, while finite-temperature thermodynamic effects may render membranes unstable to crumpling or rippling [84–86]

In this chapter (based on work in [1, 3]) we initiate a study of the free energy contribution to the equilibrium configuration of a surface due to free relativistic quantised matter fields living on it. In particular, we include zero-temperature (Casimir) effects. Recall from the Introduction that such relativistic quantum fields occur in various physical settings: for example, in graphene and related materials, the electronic structure gives rise to an effective description in terms of relativistic Dirac fermions propagating on the two-dimensional crystal [35–37] and, with great experimental potential, optical lattices in the lab [46].

The setting is then (2+1)-dimensional QFT on a product of time with a (static) two-space. Aided by the heat kernel methods detailed in Chapter 2, we will study both the free non-minimally-coupled scalar and the free Dirac fermion and see that such fields *lower* the free energy of the surface on which they live when the surface is deformed (perturbatively) away from being intrinsically flat, as was shown to be case for unitary CFTs in Section 1.4. This energy difference is UV finite (and thus well defined) and present at any temperature including $T = 0$ (and thus a purely quantum vacuum energy) both for massless and massive fields, and any scalar non-minimal coupling. It is then natural to wonder: is a classical membrane action able to counteract this quantum preference for crumpling? We will perform a naïve analysis of this question for monolayer graphene, which is indeed seen to ripple on short scales [44, 87]. We will show that at room temperature the quantum vacuum energy of the Dirac fermions give a scale at which one would expect crumpling effects on the order of the lattice spacing. The effective mem-

brane description that would validate our analysis breaks down at this scale but, while our results make no definitive statement about the rippling of graphene, they indicate that any proper treatment of equilibrium configurations of graphene-like materials should account for these quantum effects — even at room temperature.

A plan for this chapter is as follows. Section 3.1 will detail how a UV-finite free energy difference can be defined and expressed in terms of heat kernels for free fields on our geometries of interest. Section 3.2 will set out how to compute the leading-order perturbative corrections to these heat kernels for free theories on small deformations of compact homogeneous spaces. The results of carrying out this calculation for our theories to deduce the free energy difference for perturbations of flat space will be presented in Section 6.3. Finally, we conclude with a discussion of the possible implications of these results for the equilibrium geometries of membranes that support relativistic quantum degrees of freedom in Section 3.4.

3.1 Free Energy Difference: Free Fields

We consider a spacetime that is a product of time with a two-space (Σ, g) (for now taken to be general). Since we are interested in QFT at finite temperature T we work in Euclidean time, so the metric is

$$\mathrm{d}s^2 = \mathrm{d}\tau^2 + g_{ij}(x)\mathrm{d}x^i\mathrm{d}x^j \tag{3.1}$$

with τ periodic with period $\beta = 1/T$. We consider a free scalar and a free Dirac fermion with (Euclidean) actions

$$S_{\mathrm{E}}[g,\phi] = \frac{1}{2}\int \mathrm{d}\tau \int \mathrm{d}^2x\sqrt{g}\,\phi(-\nabla^2 + \xi R + M^2)\phi \text{ and} \tag{3.2}$$

$$S_{\mathrm{E}}[g,\bar{\psi},\psi] = \int \mathrm{d}\tau \int \mathrm{d}^2x\sqrt{g}\,\bar{\psi}(i\not{D} - iM)\psi, \tag{3.3}$$

respectively, where ξ is a curvature coupling, M is a mass, ∇ is the Levi-Civita connection, R is the scalar curvature and $\not{D}$ is understood as being defined by the spin connection (our conventions can be found in Appendix A.3).

The free energy $F[g]$ is a functional of the geometry (Σ, g) (and temperature T) and is given in terms of the partition function, $Z[g]$, as $F[g] = -T\ln Z[g]$. We are specifically interested in the difference between the free energy on (Σ, g) and some reference background space $(\overline{\Sigma}, \bar{g})$ at the same temperature, that satisfies

$$\mathrm{e}^{-\beta\Delta F} = \frac{Z[g]}{Z[\bar{g}]} = \frac{\int \mathcal{D}\Phi\,\mathrm{e}^{-S_{\mathrm{E}}[g,\Phi]}}{\int \mathcal{D}\Phi\,\mathrm{e}^{-S_{\mathrm{E}}[\bar{g},\Phi]}} = \left\langle \mathrm{e}^{-\Delta S_{\mathrm{E}}} \right\rangle_{\bar{g}}, \tag{3.4}$$

where Φ stands for the matter field (scalar or fermion) being integrated over in the path integral, $\Delta F \equiv F[g] - F[\bar{g}]$ and $\Delta S_{\mathrm{E}} \equiv S_{\mathrm{E}}[g,\Phi] - S_{\mathrm{E}}[\bar{g},\Phi]$ are the differences between

the free energy and action on $(S^1 \times \Sigma, \mathrm{d}\tau^2 + g)$ and $(S^1 \times \overline{\Sigma}, \mathrm{d}\tau^2 + \bar{g})$, respectively, and the expectation value is defined by the path integral on the background geometry $(S^1 \times \overline{\Sigma}, \mathrm{d}\tau^2 + \bar{g})$. To evaluate ΔF, we recall from Section 2.1 that for free fields the path integrals in (3.4) yield functional determinants. This goes through as in Section 2.1 for the scalar. For the fermion, a direct path integral yields $Z = \det(i\not{D} - iM)$ and by exploiting the direct product structure of the metric (3.1) along with the fact that the two-dimensional rotation group only has a single generator, we may eliminate the spinor structure and reduce the determinant to that of an elliptic operator with the determinant taken over the space of complex functions with antiperiodicity on the thermal circle. We leave full details of this to Appendix A.3. The result being that the partition function in each case can be written as

$$Z = (\det\mathcal{L})^{\sigma} \text{ with } \mathcal{L} = -\partial_\tau^2 + L + M^2, \tag{3.5}$$

where $\sigma = -1/2$ $(+1)$ for the scalar (fermion), L is an elliptic self-adjoint scalar operator on Σ given explicitly in (3.28) below, and the determinant is evaluated over Matsubara frequencies on the thermal circle (with appropriate periodicity or antiperiodicity in the scalar and fermion cases respectively).

The free energy can then be evaluated via heat kernel methods as shown in Chapter 2: defining the heat kernel as $K_{\mathcal{L}}(t) \equiv \mathrm{Tr}(\mathrm{e}^{-t\mathcal{L}}) = \sum_i \mathrm{e}^{-t\lambda_i}$ (with λ_i the eigenvalues of $\mathcal{L}$), gives that

$$\beta\Delta F = \sigma \int_0^\infty \frac{\mathrm{d}t}{t} \Delta K_{\mathcal{L}}(t), \tag{3.6}$$

where $\Delta K_{\mathcal{L}}(t) \equiv K_{\mathcal{L}}(t) - K_{\overline{\mathcal{L}}}(t)$. This expression is UV divergent unless $\Delta K_{\mathcal{L}}(t)$ vanishes at $t = 0$; this condition can be ensured by an appropriate choice of background $(\overline{\Sigma}, \bar{g})$. Specifically, the heat kernel expansion (2.15) gives

$$K_{\mathcal{L}}(t) = \beta \left[\frac{c_1 \mathrm{Vol}[g]}{t^{3/2}} + \frac{c_2 \chi(\Sigma) + c_3 \mathrm{Vol}[g] M^2}{t^{1/2}} + \mathcal{O}(t^{1/2}) \right], \tag{3.7}$$

where $\mathrm{Vol}[g]$ and $\chi(\Sigma)$ are the volume[1] and Euler characteristic of (Σ, g), respectively, and c_1, c_2, and c_3 are dimensionless constants independent of the geometry (though they depend on the choice of matter field). Thus, requiring that ΔF be UV finite only imposes that we choose a background geometry $(\overline{\Sigma}, \bar{g})$ with the same volume and topology as (Σ, g). It is worth emphasising that although the undifferenced functional determinant $\det\mathcal{L}$ is UV divergent, we do not need to invoke any renormalisation to evaluate the *differenced* free energy[2]. It is also worth noting that in higher dimensions, the expansion (3.7) con-

[1] Suitably IR regulated if Σ is non-compact.

[2] Note that since $\det\mathcal{L}$ is UV divergent, ΔF is not necessarily the same as a difference of separately renormalised free energies on (Σ, g) and $(\overline{\Sigma}, \bar{g})$, which could contain renormalisation ambiguities that render it unphysical.

tains non-topological curvature invariants of (Σ, g); thus obtaining a UV-finite free energy difference would rely on a careful matching of these invariants on (Σ, g) and $(\overline{\Sigma}, \bar{g})$ (in contrast with the heuristic expectation that "energy differences are always UV finite"). It turns out that choosing (Σ, g) and $(\overline{\Sigma}, \bar{g})$ to have the same volume and topology renders the differenced free energy a UV-finite object for general (2+1)-dimensional ultrastatic setups — not just the free theories considered here. This will be shown later in Chapter 4. The mass and temperature dependence can be factored out of the heat kernels using (3.5) to give

$$\beta\Delta F = \sigma \int_0^\infty \frac{\mathrm{d}t}{t} \mathrm{e}^{-M^2 t} \Theta(T^2 t) \Delta K_L(t), \tag{3.8}$$

where the sum over Matsubara frequencies yields

$$\Theta(\zeta) = \sum_{n=-\infty}^{\infty} \mathrm{e}^{-(2\pi)^2 (n-\sigma+1/2)^2 \zeta}. \tag{3.9}$$

Now we specialise to our case of interest. Ultimately, we wish to take (Σ, g) to be a deformation of flat space, $(\overline{\Sigma}, \bar{g})$. Since these are two dimensional we introduce conformally flat coordinates x^i, in terms of which the metrics on g and $\bar{g}$ take the form

$$g = \mathrm{e}^{2f(x)} \delta_{ij} \mathrm{d}x^i \, \mathrm{d}x^j \,, \quad \bar{g} = \delta_{ij} \mathrm{d}x^i \, \mathrm{d}x^j. \tag{3.10}$$

In order to have good control over the spectrum of $\mathcal{L}$ (which is essential for computing the heat kernel), we compactify these to tori $(\mathbf{T}^2, g_d)$, $(\mathbf{T}^2, \bar{g}_d)$ via the identifications $x^i \sim x^i + d_i$ with $d_1 = d$ and $d_2 = rd$. We consider a family of deformations $f_d(x)$ so that as $d \to \infty$ (with r fixed) we recover (3.10) with the x^i uncompactified. Moreover, at any finite d, we may choose f_d such that $\mathrm{Vol}[g_d] = \mathrm{Vol}[\bar{g}_d]$. By the arguments above, this condition will ensure that for every d, the free energy difference between the deformed and flat tori will be UV finite.[3]

Our object of interest is the free energy difference with this IR regulator removed:

$$\beta\Delta F_\infty[f] \equiv \sigma \lim_{d\to\infty} \int_0^\infty \frac{\mathrm{d}t}{t} \Delta K_{\mathcal{L}}[f_d; d](t), \tag{3.11}$$

with $\Delta K_{\mathcal{L}}[f_d; d](t) \equiv K_{\mathcal{L}}[f_d; d](t) - K_{\mathcal{L}}[0; d](t)$. For notational convenience we will now suppress the arguments of these functionals and drop the subscripts d on f_d and ∞ on ΔF_∞. Using (3.5), we finally obtain

$$\beta\Delta F[f] = \sigma \lim_{d\to\infty} \int_0^\infty \frac{\mathrm{d}t}{t} \mathrm{e}^{-M^2 t} \Theta(T^2 t) \Delta K_L(t). \tag{3.12}$$

[3] For finite d one may choose between periodic and antiperiodic boundary conditions for the fermion on the torus cycles; since our torus is only an IR regulator, and this distinction vanishes in the limit $d \to \infty$, we take the (simpler) periodic boundary conditions.

3.2 Perturbation Theory

For this section, we consider the case where $(\overline{\Sigma}, \bar{g})$ is compact, homogeneous and of arbitrary topology and $\overline{\Sigma} = \Sigma$. The expression (3.8) for the differenced free energy in terms of the heat kernel of L is convenient because it simply requires computing the variation in the spectrum of L as the spatial geometry g is varied:

$$\Delta K_L(t) = \mathrm{Tr}(\mathrm{e}^{-tL}) - \mathrm{Tr}(\mathrm{e}^{-t\overline{L}}) = \sum_I \left(\mathrm{e}^{-t\lambda_I} - \mathrm{e}^{-t\bar{\lambda}_I}\right), \tag{3.13}$$

where I indexes the eigenvalues of L and $\overline{L}$. In this section, we will take the metric on (Σ, g) to be conformal to $(\Sigma, \bar{g})$:

$$g = \mathrm{e}^{2f}\bar{g}, \tag{3.14}$$

where f is some scalar field on Σ. We expand $f = \varepsilon f^{(1)} + \varepsilon^2 f^{(2)} + \mathcal{O}(\varepsilon^3)$; the reference metric corresponds to taking $\varepsilon = 0$. The volume-preservation condition thus requires that[4]

$$\int \mathrm{d}^2x\sqrt{\bar{g}}\, f^{(1)} = 0 \text{ and } \int \mathrm{d}^2x\sqrt{\bar{g}}\left(\left(f^{(1)}\right)^2 + f^{(2)}\right) = 0. \tag{3.15}$$

Similarly, we write the resulting expansion of L and of its eigenvalues λ_I and eigenvectors h_I as

$$L = \overline{L} + \varepsilon L^{(1)} + \varepsilon^2 L^{(2)} + \mathcal{O}(\varepsilon^3), \tag{3.16}$$

$$h_I = \bar{h}_I + \varepsilon h_I^{(1)} + \varepsilon^2 h_I^{(2)} + \mathcal{O}(\varepsilon^3), \tag{3.17}$$

$$\lambda_I = \bar{\lambda}_I + \varepsilon\lambda_I^{(1)} + \varepsilon^2\lambda_I^{(2)} + \mathcal{O}(\varepsilon^3). \tag{3.18}$$

Hence from (3.13), the perturbed heat kernel is

$$\Delta K_L(t) = \varepsilon\,\Delta K^{(1)}(t) + \varepsilon^2\Delta K^{(2)}(t) + \mathcal{O}(\varepsilon^3), \tag{3.19}$$

where

$$\Delta K^{(1)}(t) = -t\sum_I \mathrm{e}^{-\bar{\lambda}_I t}\lambda_I^{(1)}, \text{ and } \Delta K^{(2)}(t) = t\sum_I \mathrm{e}^{-\bar{\lambda}_I t}\left(\frac{t}{2}\left(\lambda_I^{(1)}\right)^2 - \lambda_I^{(2)}\right). \tag{3.20}$$

Homogeneity of $(\Sigma, \bar{g})$ implies that the leading variation of ΔK_L is quadratic[5], so $\Delta K^{(1)} = 0$ which we indeed find shortly. Now, defining the matrix elements

$$L_{IJ}^{(n)} \equiv \left\langle \bar{h}_I \middle| L^{(n)} \middle| \bar{h}_J \right\rangle \equiv \int \mathrm{d}^2x\sqrt{\bar{g}}\,\bar{h}_I^* L^{(n)}\bar{h}_J, \tag{3.21}$$

[4] The reason for giving f a non-trivial expansion in ε, rather than just defining ε via $f = \varepsilon f^{(1)}$ exactly, is that the second-order volume preservation constraint fixes $f^{(1)} = 0$ exactly unless a non-zero $f^{(2)}$ is turned on as well.

[5] See Section 4.1 for further details

a standard consistency condition in degenerate perturbation theory requires that $L^{(1)}_{IJ}$ be diagonal on any degenerate subspaces of $\overline{L}$ (that is, we must have $L^{(1)}_{IJ} = 0$ for any I, J with $I \neq J$ but $\bar{\lambda}_I = \bar{\lambda}_J$)[6]. Then standard perturbation theory yields the perturbations of the eigenvalues:

$$\lambda^{(1)}_I = L^{(1)}_{II}, \qquad \lambda^{(2)}_I = \sum_{\substack{J \\ \bar{\lambda}_J \neq \bar{\lambda}_I}} \frac{L^{(1)}_{IJ} L^{(1)}_{JI}}{\bar{\lambda}_I - \bar{\lambda}_J} + L^{(2)}_{II}. \tag{3.22}$$

It is important to note that while consistency of the perturbation theory requires an appropriate choice of the unperturbed eigenfunctions $\bar{h}_I$ the final expression for the heat kernel is insensitive to this choice. To see this, let us write the index I as the pair (ℓ, m), with ℓ labeling each degenerate subspace of degeneracy b_ℓ and m indexing its elements[7]. Then we may relate the eigenfunctions $\bar{h}_{\ell,m}$ to any other basis $\tilde{h}_{\ell,m}$ by a unitary transformation on each degenerate subspace:

$$\bar{h}_{\ell,m} = \sum_{m'} c^{\ell}_{m'm} \tilde{h}_{\ell,m'}, \tag{3.23}$$

where $c^{\ell}_{m'm}$ are the components of a unitary matrix chosen to ensure that $L^{(1)}_{\ell,m,\ell,m'} = 0$ for $m \neq m'$. We then have

$$\boldsymbol{L}^{(n)}_{\ell,\ell'} = (\boldsymbol{c}^{\ell})^{\dagger} \widetilde{\boldsymbol{L}}^{(n)}_{\ell,\ell'} \boldsymbol{c}^{\ell'}, \text{ where } \widetilde{L}^{(n)}_{\ell,m,\ell',m'} \equiv \left\langle \tilde{h}_{\ell m} \middle| L^{(n)} \middle| \tilde{h}_{\ell',m'} \right\rangle, \tag{3.24}$$

where bold characters denote matrices on the degenerate subspaces, so that e.g. $\boldsymbol{c}^{\ell}$ is the $b_\ell \times b_\ell$-dimensional matrix with elements $c^{\ell}_{m'm}$, $\boldsymbol{L}^{(1)}_{\ell,\ell'}$ is the $b_\ell \times b_{\ell'}$-dimensional matrix with elements $L^{(1)}_{\ell,m,\ell',m'}$, etc. Hence,

$$\Delta K^{(1)} = -t \sum_{\ell} \mathrm{e}^{-\bar{\lambda}_\ell t} \mathrm{tr} \left(\boldsymbol{L}^{(1)}_{\ell,\ell} \right) = -t \sum_{\ell} \mathrm{e}^{-\bar{\lambda}_\ell t} \mathrm{tr} \left(\widetilde{\boldsymbol{L}}^{(1)}_{\ell,\ell} \right) \tag{3.25}$$

with the final expression following from the basis-independence of the trace. Likewise, we have

$$\Delta K^{(2)} = t \sum_{\ell}^{\infty} \mathrm{e}^{-\bar{\lambda}_\ell t} \left[\frac{t}{2} \sum_{m} \left(L^{(1)}_{\ell,m,\ell,m} \right)^2 - \mathrm{tr} \left(\boldsymbol{L}^{(2)}_{\ell,\ell} + \sum_{\ell',\ell' \neq \ell} \frac{\boldsymbol{L}^{(1)}_{\ell,\ell'} \boldsymbol{L}^{(1)}_{\ell',\ell}}{\bar{\lambda}_\ell - \bar{\lambda}_{\ell'}} \right) \right], \tag{3.26}$$

[6] Should $L^{(1)}$ not be sufficient to break all degeneracy, then $L^{(2)}_{IJ}$ must be diagonal on any remaining degenerate subspaces, and so on to higher orders. Here we will only need to worry about the diagonalisation of $L^{(1)}$.

[7] This choice of labels is of course in analogy with the indexing of the spherical harmonics $Y_{\ell,m}$, which are eigenfunctions of the Laplacian on the round sphere with degenerate eigenvalues λ_ℓ, but this discussion is completely general.

but since $\boldsymbol{L}^{(1)}_{\ell,\ell}$ is required to be diagonal, the first sum in the square brackets can be written simply as $\mathrm{Tr}((\boldsymbol{L}^{(1)}_{\ell,\ell})^2)$. Then again using (3.24) and cyclicity of the trace, we find that

$$\Delta K^{(2)} = t\sum_{\ell} \mathrm{e}^{-\bar{\lambda}_\ell t}\mathrm{tr}\left[\frac{t}{2}\left(\widetilde{\boldsymbol{L}}^{(1)}_{\ell,\ell}\right)^2 - \widetilde{\boldsymbol{L}}^{(2)}_{\ell,\ell} - \sum_{\ell',\ell'\neq\ell}\frac{\widetilde{\boldsymbol{L}}^{(1)}_{\ell,\ell'}\widetilde{\boldsymbol{L}}^{(1)}_{\ell',\ell}}{\bar{\lambda}_\ell - \bar{\lambda}_{\ell'}}\right]. \tag{3.27}$$

All dependence on $\boldsymbol{c}^\ell$ has vanished due to the traces, and hence for the purposes of computing the heat kernel we may compute the matrix elements $\widetilde{L}^{(n)}_{\ell,m,\ell',m'}$ in any desired basis $\tilde{h}_{\ell,m}$.

3.3 Results

We now specialise the case where $(\overline{\Sigma}, \bar{g})$ is a flat torus as described at the end of Section 3.1. In this case, the operators L are given explicitly in terms of f as

$$L_{\mathrm{s}} = -\mathrm{e}^{-2f}\left(\overline{\nabla}^2 + 2\xi(\overline{\nabla}^2 f)\right), \tag{3.28a}$$

$$L_{\mathrm{f}} = L_{\mathrm{s}}|_{\xi=1/4} - \mathrm{e}^{-2f}\left(i\,\bar{\star}\,(\mathrm{d}f\wedge\mathrm{d}) - \frac{(\overline{\nabla}_i f)^2}{4}\right), \tag{3.28b}$$

with $\overline{\nabla}$ and $\bar{\star}$ the covariant derivative and Hodge dual on the flat background $f=0$, and the subscripts s and f denoting the scalar and fermion.

In order to perform our computations we Fourier decompose the perturbation

$$f^{(1)}(x) = \frac{(2\pi)^2}{rd^2}\sum_{\mathbf{N}} \tilde{f}^{(1)}_{\mathbf{N}}\mathrm{e}^{2\pi i\left(n_1x^1 + n_2x^2/r\right)/d}, \tag{3.29}$$

$$\to \int \mathrm{d}^2k\,\tilde{f}^{(1)}(\mathbf{k})\mathrm{e}^{i\mathbf{k}\cdot\mathbf{x}} \text{ as } d\to\infty, \tag{3.30}$$

where the sum runs over all pairs of integers $\mathbf{N} = \{n_1, n_2\}$, and the second line defines $k_i = \lim_{d\to\infty} 2\pi n_i/d_i$.

An explicit calculation on the torus for fixed d reveals that (for both the scalar and fermion) while the eigenvalues are indeed shifted at first order in ε, their contribution to the heat kernel, $\Delta K^{(1)}$, vanishes. The leading-order perturbation to the heat kernel is thus given by the second-order term $\Delta K^{(2)}$. A lengthy but ultimately straightforward calculation yields the finite-d expressions presented in Appendix A.4. In the limit $d\to\infty$, these become

$$\Delta K^{(2)}(t) = t\int \mathrm{d}^2k\,k^4\left|\tilde{f}^{(1)}(\mathbf{k})\right|^2 I(k^2t) \tag{3.31}$$

with $k = |\mathbf{k}|$,

$$I_{\mathrm{s}}(\zeta) = -\frac{\pi}{4\zeta^2}\left[6 + \zeta(1-8\xi) - \left(6 + 2\zeta(1-4\xi) + \frac{\zeta^2}{2}(1-4\xi)^2\right)\mathcal{F}\left(\frac{\sqrt{\zeta}}{2}\right)\right], \tag{3.32a}$$

$$I_{\mathrm{f}}(\zeta) = \frac{\pi}{4\zeta^2}\left[(6+\zeta)\,\mathcal{F}\left(\frac{\sqrt{\zeta}}{2}\right) - 6\right], \tag{3.32b}$$

and $\mathcal{F}(\zeta) = \zeta^{-1}\mathrm{e}^{-\zeta^2}\int_0^\zeta d\zeta'\,\mathrm{e}^{(\zeta')^2}$. Thus, using (3.12) we find

$$\Delta F = -\varepsilon^2 \int \mathrm{d}^2k\, a(k,T)\left|\tilde{f}^{(1)}(\mathbf{k})\right|^2, \tag{3.33}$$

with

$$a(k,T) \equiv -\sigma T k^4 \int_0^\infty \mathrm{d}t\,\mathrm{e}^{-M^2t}\Theta(T^2t)I(k^2t). \tag{3.34}$$

A few comments are in order. Firstly, we see the leading variation in ΔF is quadratic in ε. Next, as $d \to \infty$ the volume constraint $\mathrm{Vol}[g_d] = \mathrm{Vol}[\bar{g}_d]$ becomes the condition that the variation of the volume $\int \mathrm{d}^2x\sqrt{g}$ vanishes; for $f^{(1)}$ this simply imposes no constant Fourier component. We have that $I(\zeta)$ is finite and $\Theta(\zeta)$ is $\mathcal{O}(\zeta^{-1/2})$ at small ζ, and thus ΔF is UV finite. Likewise, since $I(\zeta)$ and $\Theta(\zeta)$ are finite at large ζ, ΔF is also IR finite for $M > 0$; in fact, the large-ζ decay of $I(\zeta)$ also implies IR finiteness in the massless case $M = 0$ for both the fermion and minimally-coupled scalar ($\xi = 0$)[8]. Finally, a key physical point is that $\sigma I(\zeta) < 0$ for all $\zeta > 0$ (and all ξ for the scalar). This can be seen by explicitly plotting it[9]. Noting that $-\sigma I_{\mathrm{s}}(\zeta)$ is a concave quadratic in ξ for each ζ, we can deduce negativity from a plot of its minimum value. This is presented, along with $-\sigma I_{\mathrm{f}}(\zeta)$, in Figure 3.1. Because $\Theta(\zeta) > 0$, the negativity of $\sigma I(\zeta)$ implies that for *any* (non-constant) f the free energy difference is strictly *negative* to leading order in ε: $\Delta F < 0$.

The form of the expression (3.34), along with the asymptotic behaviours of $\Theta(\zeta)$ and $I(\zeta)$, allows for the derivation of some scaling relations. Specifically, defining $\ell_M = \hbar/(cM)$ to be the (reduced) Compton wavelength, $\ell_T = \hbar c/(k_B T)$ to be a thermal wavelength, and ℓ to be the characteristic length scale of f, ΔF scales as detailed in Table 3.1. Thus, at small temperatures — in which ΔF becomes the energy difference ΔE — the effect, as we observed for the classical Casimir Effect in Section 1.1, is a *purely* quantum one: $\Delta E \sim -\varepsilon^2\hbar c/\ell$ for $\ell \ll \ell_M$.

We note also that the small-temperature limit $\ell_T \gg \max[\ell, \ell_M]$ is analytically

[8]For the massless scalar with non-minimal coupling $\xi \neq 0$, ΔF_{s} is IR divergent since the flat space zero eigenvalue acquires a negative contribution due to the scalar curvature coupling. This is reflected in the $\ln(\ell_M/\ell)$ corrections mentioned in Table 3.1.

[9]It is possible to prove that $I_{\mathrm{f}} < 0$ without resorting to plotting it; we have not been able to find as elegant of a proof for I_{s}.

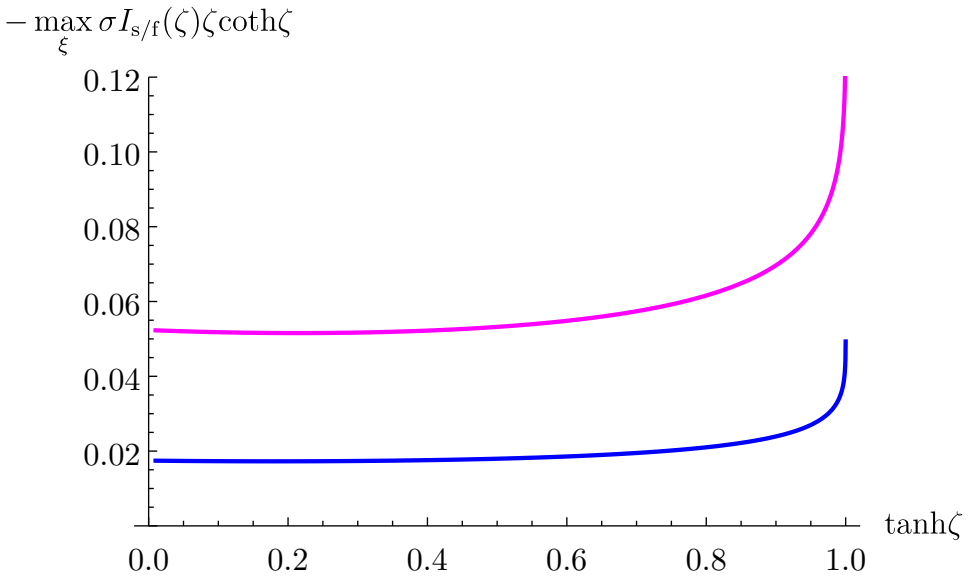

Figure 3.1: The plots of the $-\max_\xi \sigma I_{\mathrm{s/f}}(\zeta)\zeta\coth\zeta$ with $\sigma I_{\mathrm{s}}(\zeta)$ given by (3.32a) (and $\sigma = -1/2$) plotted in blue and $\sigma I_{\mathrm{f}}(\zeta)$ given by (3.32b) (and $\sigma = +1$) plotted in magenta.

	$-\Delta F_{\mathrm{s}}/(\varepsilon^2\hbar c/\ell)$	$-\Delta F_{\mathrm{f}}/(\varepsilon^2\hbar c/\ell)$
$\ell_T \gg \ell \gg \ell_M$	ℓ_M/ℓ	ℓ_M/ℓ
$\ell_T \gg \ell_M \gg \ell$	1	1
$\ell \gg \ell_T \gg \ell_M$	ℓ_M/ℓ	ℓ_M/ℓ
$\ell \gg \ell_M \gg \ell_T$	$\ell_M^2/(\ell\ell_T)$	ℓ_T/ℓ
$\ell_M \gg \ell_T \gg \ell$	1	1
$\ell_M \gg \ell \gg \ell_T$	ℓ/ℓ_T	ℓ_T/ℓ

Table 3.1: The scaling of ΔF for the minimally-coupled free scalar field and Dirac fermion for different relative magnitudes of ℓ, ℓ_M, and ℓ_T. Note that for the non-minimally-coupled scalar (i.e. $\xi \neq 0$), factors of $\ln(\ell_M/\ell)$ appear in the last two rows.

tractable. Poisson resummation gives that $\Theta(T^2 t) = \beta/\sqrt{4\pi t}$ up to terms that are exponentially suppressed in β^2/t, allowing us to compute $a(k)$ explicitly as[10]

$$a_{\mathrm{s}}(k,0) = \frac{\pi k^3}{128}\left[\frac{2(3-32\xi)M}{k} - \frac{24M^3}{k^3} + \left(3 - 32\xi + 128\xi^2 - 8(1-16\xi)\frac{M^2}{k^2} + \frac{48M^4}{k^4}\right)\operatorname{arccot}\left(\frac{2M}{k}\right)\right], \quad (3.35a)$$

$$a_{\mathrm{f}}(k,0) = \frac{\pi k^3}{64}\left[\frac{2M}{k} + \frac{24M^3}{k^3} + \left(1 - \frac{8M^2}{k^2} - \frac{48M^4}{k^4}\right)\operatorname{arccot}\left(\frac{2M}{k}\right)\right]. \quad (3.35b)$$

[10] In the massless limit these agree precisely with the energy in Equation (1.69) for the massless scalar CFT ($\xi = 1/8$) and free Dirac fermion CFT (with their appropriate central charges $c_{\mathrm{s}} = (3/2)/(4\pi)^2$ and $c_{\mathrm{f}} = 3/(4\pi)^2$ respectively).

3.4 Membrane Crumpling

In this chapter, we have shown that free (2+1)-dimensional relativistic degrees of freedom on (small) deformations of flat space that have UV-finite free energy difference from flat space always energetically prefer the deformation, for any temperature. Let us now consider how this effect competes with a membrane's bending energy (which at zero temperature favours a flat geometry) if it carries such degrees of freedom.

Consider three-dimensional flat space with Cartesian coordinates $\{X^i, Z\}$ and parametrise a surface in it by $X^i = x^i + \varepsilon^2 v^i(x^j)$, $Z = \varepsilon\, h(x^i)$. Then for small ε and suitable v^i, the intrinsic metric on the membrane in the coordinates x^i is as in Equation (3.10) with $-\overline{\nabla}^2 f = \varepsilon^2 \det(\partial_i \partial_j h)$[11]. The bending energy due to extrinsic curvature is

$$H = \varepsilon^2 \kappa \int \mathrm{d}^2x (\overline{\nabla}^2 h)^2, \tag{3.36}$$

where κ is the bending rigidity. When the membrane is deformed from flat over a region of characteristic size $\ell \ll \ell_M$, then the (positive) bending energy E_{B} and (negative) vacuum energy E_{Q} (at zero temperature) for N free relativistic quantum fields behave parametrically as

$$E_{\mathrm{B}} \sim \varepsilon^2 \kappa, \qquad E_{\mathrm{Q}} \sim -\varepsilon^4 N \frac{\hbar c}{\ell}. \tag{3.37}$$

The ground state equilibrium configuration of the membrane should minimise $E = E_{\mathrm{B}} + E_{\mathrm{Q}}$. At first glance, it may seem that, because E_{B} is lower order in ε than E_{Q}, a perturbative analysis guarantees that $E > 0$ for any deformation of flat space. The fact that E_{B} and E_{Q} have different scale dependence, however, with E_{Q} dominating at sufficiently-small scales, invalidates this argument. Defining $\ell_{\mathrm{crumple}} \equiv N\hbar c/\kappa$ and noting that ε and $\ell_{\mathrm{crumple}}/\ell$ are independent, if $\ell/\ell_{\mathrm{crumple}} \lesssim \varepsilon^2 \ll 1$ then E_Q can be comparable to and even dominate E_B while still being in the perturbative regime. Whether or not E actually decreases for (sufficiently-large) deformations of flat space — thus implying that the membrane's equilibrium configuration is crumpled at a sufficiently-small scale relative to ℓ_{crumple} — depends on non-linear and higher-derivative contributions to its bending energy and whether or not these are relevant at scales up to ℓ_{crumple} at amplitudes $\mathcal{O}(\varepsilon^4)$. Thus, ℓ_{crumple} defines a scale below which a membrane has the potential to crumple.

For illustrative purposes, we will consider the case of a graphene monolayer. In this setup, the bending rigidity is $\kappa \sim 1$ eV, the unit cell has size $\ell_{\mathrm{cell}} \sim 1$ Å, and the relativistic fields are four Dirac fermions with effective speed $c \sim c_{\mathrm{light}}/300$, with c_{light} the actual speed of light [36, 41, 87, 88]. Our effective membrane description is valid for $\ell \gg \ell_{\mathrm{cell}}$, while from Table 3.1 the scaling properties (3.37) are valid at room temperature for $\ell \ll \ell_{T=300\,K} \sim 10^3 \ell_{\mathrm{cell}}$. Computing the potential crumpling scale, we find $\ell_{\mathrm{crumple}} \sim 10\ell_{\mathrm{cell}}$.

[11] The constant part of f is not determined by this relation, thus we may choose it so that $f^{(1)}$ has no constant Fourier component.

This is sufficiently close to ℓ_{cell} to make our effective membrane description suspect. Hence, while this naïve analysis is insufficient to imply the existence of a crumpled equilibrium configuration for graphene, it *does* indicate that *long range quantum properties* of the conduction electrons in graphene are important for understanding the energetics of its equilibrium monolayers even at room temperature; such effects are presumably difficult to incorporate into Monte Carlo or *ab initio* quantum simulations. Indeed, it is intriguing to note that for freely-suspended graphene at room temperature, low-amplitude ripples are seen on short scales ~ 50 Å, close to our ℓ_{crumple} [44].

One of the obstructions to E_{Q} competing with E_{B} here is the suppression of E_{Q} by a further factor ε^2. For spherical (as opposed to planar) membranes, the vacuum energy due an embedding comes in at the same order in ε as the bending energy. Thus, E_{Q} may have a better chance of outcompeting E_{B} on a spherical graphene monolayer. A more detailed analysis of this setup will be carried out in Section 5.1.

For now, we turn to the question of whether, as with the free-field case we have considered in this chapter, a UV-finite free energy difference may be defined (and calculated) for *general* (2+1)-dimensional QFTs.

Chapter 4

Free Energy Difference: A UV-Finite Measure of Free Energy

The vacuum energy of a relativistic QFT on a static spacetime provides an energy measure on the geometry. We might then ask what type of geometry a QFT prefers energetically. An important subtlety is that the one-point function of the stress tensor must be renormalised, and this introduces ambiguity into the resulting energy. Typically, the leading UV divergence in this VEV is removed and the ambiguity in the counterterm, a cosmological constant, is chosen so that the one-point function vanishes on flat spacetime. However, there are subleading divergences which require local curvature counterterms to remove. These counterterms trivially vanish on flat spacetime so their finite remainder cannot be fixed by requiring that they vanish there. Thus, a notion of energy, or equivalently at finite temperature, free energy, in curved spacetime is ambiguous unless one has a UV-complete theory. Worse still, even on flat space if the theory is renormalised to have vanishing energy at zero temperature, then the total free energy at *finite* temperature will be IR divergent due to infinite volume, leading one typically to work instead with free energy density.

While the free energy is ambiguous, and on a non-compact space will generally be infinite, we can instead — guided by the intuition provided by the free field case in the previous chapter — consider the free energy *difference* between two spacetimes. We will consider (2+1)-dimensional QFT on an ultrastatic spacetime, so that the free energy is a functional of temperature and the two-space. For free scalar and fermion fields it was shown in Chapter 3 that the difference in free energy between two spaces with the same volume and topology is a physical quantity that is UV finite. Indeed, it may be computed without any renormalisation in this free-field setting. Further, it was shown that the free energy difference for a two-space that is a perturbation of flat space, relative to a flat space, is both UV and IR finite and quadratic in the amplitude of the metric perturbation, and for any deformation and mass and at all temperatures (and curvature coupling for the scalar) the sign of the free energy variation was the same — flat space is energetically

disfavoured. For a general unitary (2+1)-dimensional CFT the same energetic revulsion to flat space was shown at zero temperature in Section 1.4.

In this chapter (based on [2]), we will extend the arguments of Chapter 3. Considering relativistic (2+1)-dimensional QFTs on ultrastatic spacetimes we will carefully define a free energy difference for arbitrary deformations of flat space relative to flat space itself and argue this is generally UV finite. This will also be done, analogously, for deformations of compact spaces, where UV finiteness requires the volume of the deformed and undeformed spaces to be equal. For perturbations of flat space, and under reasonable assumptions, it is quadratic in the amplitude of the perturbation and can be computed from the linear response of the one-point function of the stress tensor to the perturbation, as was shown in the particular case of zero-temperature CFTs in Section 1.4.

As an illustration, we will then review two uses of this free energy difference. Firstly, an AdS/CFT calculation to compute this for holographic CFTs[1] will be reviewed. Computing the holographic stress tensor one-point function following Section 1.2 gives a similar result to that of the free field theories, namely that the leading variation of free energy is negative for any (non-trivial) perturbation and at any temperature. After a suitable normalisation by central charge, there is a rather remarkable similarity between the strongly-coupled holographic CFT free energy variation and that of the free fermion CFT (the massless Dirac case computed in Chapter 3). In the short-wavelength limit (relative to the thermal scale) this perturbative holographic calculation yields the universal zero-temperature result for a general CFT in Section 1.4. Secondly, a calculation of the (opposite) long-wavelength limit in the general (2+1)-dimensional finite temperature QFT case will be reviewed. In the holographic case, this limit can be solved using fluid/gravity methods where the behaviour is governed by hydrodynamics [89, 90]. More generally, we expect any (2+1)-dimensional QFT at finite temperature in our ultrastatic setting to have a hydrostatic description. This suggests one may understand the free energy variation in terms of a correction to the ideal-fluid stress tensor. We will identify the leading correction as a four-derivative curvature term. In this hydrostatic, or low-curvature, expansion setting, the free energy difference from flat space may be solved for in terms of the integral of the squared Ricci scalar of the deformed space, with a coefficient that in all the theories discussed above has definite sign. This implies that weakly-curved two-spaces are favoured over flat two-spaces — even in the regime where the deformation is not described by a small-amplitude metric perturbation.

For the free theories discussed in Chapter 3 we will then explicitly confirm this weak-curvature limit which follows simply from the heat kernel expansion (2.15) of the determinant that yields the partition function.

The plan for the chapter is as follows. In Section 4.1 we will define the UV-finite free energy difference described above for general (2+1)-dimensional QFTs. We will

[1] As defined in Section 1.3.

show that for perturbations of flat space the leading variation in free energy is quadratic in the perturbation amplitude. Then, in Section 4.2 we will review a computation of this quadratic variation for holographic CFTs at finite temperature, the derivation of the fluid/gravity limit for the free energy difference and an argument that for general (2+1)-dimensional QFTs the effect for low-curvature deformations of flat space can be understood from hydrostatics. Finally, in Section 4.3 these low-curvature results will be shown to be true for free fields. We will conclude with a summary and discussion of the physical interpretation of our free energy difference observable in Section 4.4.

4.1 Free Energy Variation

We consider a relativistic (2+1)-dimensional QFT on a product of time with a static Riemannian two-space, (Σ, g), in the finite temperature thermal vacuum state with temperature T. Moving to Euclidean time, we may regard this quantum thermal system as the QFT on the Riemannian geometry,

$$\mathrm{d}s^2 = \hat{g}_{\mu\nu}\mathrm{d}x^\mu \mathrm{d}x^\nu = \mathrm{d}\tau^2 + g_{ij}(x)\mathrm{d}x^i \mathrm{d}x^j \tag{4.1}$$

where $\tau \sim \tau + \beta$ with $\beta = 1/T$. All (scalar) couplings are constant in spacetime, and held fixed, and we do not turn on sources for any non-scalar operators (other than the stress tensor). The partition function Z, which is a functional of g_{ij} and β, defines the thermal vacuum free energy F as,

$$-\beta F = \ln Z[\beta, g]\,. \tag{4.2}$$

Let us introduce a UV cutoff Λ, and then write

$$Z[\beta, g] = \int_\Lambda \mathcal{D}\Phi \mathrm{e}^{-S_\mathrm{E}[\beta, g, \Phi]} \tag{4.3}$$

with $\mathcal{D}\Phi$ the integral over fields (obeying the thermal boundary conditions) and S_E the Euclidean action. The stress tensor one-point function of this theory in its thermal vacuum, defined as

$$\langle T_{\mu\nu}\rangle = -\frac{2}{\sqrt{\hat{g}}}\frac{\delta \ln Z}{\delta \hat{g}^{\mu\nu}}, \tag{4.4}$$

is UV divergent without suitable renormalisation. Since the only inhomogeneous deformation of the theory is due to the spatial geometry the divergences for a diffeomorphism-invariant regulator are given by all possible local geometric tensors which are symmetric, conserved and consistent with power counting, which in (2+1)-dimensions are a cosmo-

logical term and an Einstein tensor term,

$$\langle T_{\mu\nu}\rangle_{\hat{g}} = c_1\Lambda^3\hat{g}_{\mu\nu} + c_2\Lambda\hat{G}_{\mu\nu} + \mathcal{O}(\Lambda^0), \tag{4.5}$$

where $\hat{G}_{\mu\nu}$ is the Einstein tensor and $c_{1,2}$ are dimensionless coefficients that depend on the precise theory and its couplings, the nature of the cutoff and infrared mass scales. For example, in a theory with a mass m, they will be functions going as $c_{1,2}(\frac{m}{\Lambda})$ which tend smoothly to a constant as $\Lambda \to \infty$ (keeping the temperature and mass fixed). The leading divergence going as $\sim \Lambda^3$ leads to the famous 'cosmological constant' problem, but there is also the subleading curvature-induced divergence going as $\sim \Lambda$ too. The stress tensor is renormalised by suitable local geometric counterterms in the Euclidean action with coefficients that diverge as the cutoff is removed, in this case a cosmological and an Einstein-Hilbert term, $\int \mathrm{d}^3x\sqrt{\hat{g}}\left(a_1\Lambda^3 - \frac{1}{2}a_2\Lambda\hat{R}\right)$, so that $a_{1,2}(\frac{m}{\Lambda})$ are dimensionless functions. In a renormalisable theory, by tuning these as $\Lambda \to \infty$ we may remove the divergences in the stress tensor one-point function (and other correlators) provided the limits of $\Lambda^3\,(c_1 - a_1)$ and $\Lambda\,(c_2 - a_2)$ as $\Lambda \to \infty$ exist and are finite. However, that leaves a freedom in $a_{1,2}$ corresponding to adding a finite contribution of these counterterms to the action, i.e. $a_1 \to a_1 + \alpha_1\Lambda^{-3}$ and $a_2 \to a_2 + \alpha_2\Lambda^{-1}$ for any constants $\alpha_{1,2}$. Thus, one is left with a finite ambiguity in the stress tensor given by these two local terms. In curved spacetime QFT, one usually chooses a prescription to ensure that at zero temperature the stress tensor vanishes in flat spacetime, and this fixes the finite part associated to the coefficient a_1. However, since the Einstein-Hilbert term vanishes in flat space, there is no canonical choice for the finite part of a_2. Hence, the renormalised stress tensor, while finite in the $\Lambda \to \infty$ limit, suffers ambiguity parameterised by these pure-geometric counterterms in the action.[2] Computing, for example, the energy of a static curved space (Σ, g), such as a sphere, gives a finite but ambiguous result, which explicitly depends on the nature of the UV physics. In such a situation the energy of a given space (Σ, g) could be arbitrarily negative or positive depending on what finite counterterm contribution the UV theory chooses. Of course, at finite temperature on a non-compact space, such as the case of deformations of flat space that we are interested in here, the free energy will generally be IR divergent due to the non-zero thermal free energy density being integrated over an infinite volume.

However, as discussed in Chapter 3, we may consider the free energy difference, ΔF, between the theory on the ultrastatic spacetime with compact space (Σ, g) and a compact reference space $(\Sigma, \bar{g})$ of the same topology and volume, and at the same

[2]We note that these ambiguities do not arise in the case of a (2+1)-dimensional holographic CFT if the theory is only deformed by the metric, as we consider in later Section 4.2. However, we emphasise that the discussion above is for a general relativistic (2+1)-dimensional QFT.

temperature:

$$-\beta\Delta F[\beta, g, \bar{g}] = \ln Z[\beta, g] - \ln Z[\beta, \bar{g}]. \tag{4.6}$$

As shown in Chapter 3, for free scalar and fermion (2+1)-dimensional theories this difference is UV finite and, hence, an unambiguous low-energy quantity that is independent of details of the UV completion of the theory. Furthermore in the non-compact setting, for perturbations of flat space, this difference relative to flat space is also IR finite.

We may understand this quantity is UV finite for more general (2+1)-dimensional QFTs using the stress tensor divergence structure above. We begin with the case that our geometries of interest, (Σ, g) and $(\Sigma, \bar{g})$, are compact, as this will illustrate the idea. However, we are also interested in the case that $(\Sigma, \bar{g})$ is flat space, and (Σ, g) is a deformation of it. In this non-compact case there is an added subtlety we shall address after the compact discussion.

Take a smooth one-parameter family of (compact) geometries $(\Sigma, g(\varepsilon))$ with $g(0) = \bar{g}$. In local coordinates the metric on $(\Sigma, g(\varepsilon))$ is $g_{ij}(x;\varepsilon)$ with $g_{ij}(x;0) = \bar{g}_{ij}(x)$. We may define $\Delta F(\varepsilon)$ to be the difference of the free energy of $(\Sigma, g(\varepsilon))$ to that of $(\Sigma, \bar{g})$. Then, from the definition of the stress tensor, (4.4), its VEV determines the derivative of the partition function and hence the thermal vacuum free energy F as we deform in the parameter ε, as

$$\frac{\mathrm{d}F}{\mathrm{d}\varepsilon} = \frac{1}{2}\int \mathrm{d}^2x\sqrt{g}\langle T_{ij}\rangle_{g(\varepsilon)}\frac{\mathrm{d}g^{ij}}{\mathrm{d}\varepsilon}\,. \tag{4.7}$$

This is the generalisation of the fundamental thermodynamic relation, $\mathrm{d}F = -p\mathrm{d}V$, as is appropriate for this fixed-temperature setup. The above expression and those that follow are written covariantly in the two-dimensional geometry unless otherwise explicitly stated. Here, we have assumed that the one-point function of the stress tensor is independent of Euclidean time, as we expect for a good vacuum state, allowing us to perform the time integral trivially. If this were not the case, the Lorentzian continuation of the vacuum would be time dependent, as could happen for a free tachyonic scalar field. The Ricci scalar of ultrastatic metrics is simply that of their spatial geometry and so, since all two-spaces are Einstein, (2+1)-dimensional ultrastatic metrics have $\hat{G}_{ij} = 0$. Thus, substituting our ultrastatic geometry into the general (2+1)-dimensional divergence structure, (4.5), we see that in our situation of interest the divergence in the spatial components of the stress tensor becomes

$$\langle T_{ij}\rangle_g = c_1\Lambda^3 g_{ij} + \mathcal{O}(\Lambda^0) \tag{4.8}$$

and there is no contribution from the term involving c_2. For our ultrastatic geometry the corresponding Einstein-Hilbert counterterm simply becomes proportional to the Euler

characteristic of Σ, and hence in the variation of $\ln Z$ gives no contribution as the topology of $(\Sigma, g(\varepsilon))$ is invariant in ε. Thus, we see

$$\frac{\mathrm{d}F}{\mathrm{d}\varepsilon} = -c_1\Lambda^3\frac{\mathrm{d}}{\mathrm{d}\varepsilon}\left(\int \mathrm{d}^2x\sqrt{g}\right) + \mathcal{O}(\Lambda^0) \tag{4.9}$$

and, integrating along the flow,

$$\Delta F = -c_1\Lambda^3\left(\mathrm{Vol}[g] - \mathrm{Vol}[\bar{g}]\right) + \mathcal{O}(\Lambda^0) \tag{4.10}$$

and so provided the volume of the space (Σ, g), $\mathrm{Vol}[g]$, and reference geometry, $\mathrm{Vol}[\bar{g}]$, are equal then ΔF is manifestly finite in the $\Lambda \to \infty$ limit. In computing ΔF one can use the regularised (with a diffeomorphism-invariant regulator) but unrenormalised stress tensor and the result will have no ambiguity due to the finite part of $a_{1,2}$ cancelling entirely in the difference.

We now turn our focus to the case where the reference space $(\Sigma, \bar{g})$ is flat Euclidean two-space, and (Σ, g) is a perturbative metric deformation of this. This may be computed, as in Chapter 3, by considering a perturbation on a compactified space, such as a torus, and then taking the torus size to infinity keeping the perturbation scale fixed. Alternatively, as we will show later, one may compute directly in the infinite volume setting. Thus, we must now translate the argument above to this non-compact setting where we must be more careful in handling the infinite volumes of (Σ, g) and $(\Sigma, \bar{g})$.

We begin in a similar manner, by taking a one parameter family of geometries $(\Sigma, g(\varepsilon))$ such that $(\Sigma, g(0)) = (\Sigma, \bar{g})$ is flat space. Again, we take local coordinates and write $g_{ij}(x;\varepsilon)$ with $g_{ij}(x;0) = \bar{g}_{ij}(x)$. The subtlety is that the coordinates on the manifold are fixed, and we wish to present both the geometries (Σ, g) and $(\Sigma, \bar{g})$ in these same coordinates. Thus, we have two metrics and only one coordinate freedom. While the geometry $(\Sigma, \bar{g})$ is fixed as flat space, the explicit metric components may be evolved in the flow parameter ε by a diffeomorphism *relative* to those of (Σ, g) and this may potentially have physical effect. Thus, we write this metric as $\bar{g}_{ij}(x;\varepsilon)$ with $\bar{g}_{ij}(x;0) = \bar{g}_{ij}(x)$. Hence,

$$\frac{\mathrm{d}\bar{g}_{ij}(x;\varepsilon)}{\mathrm{d}\varepsilon} = 2\overline{\nabla}_{(i}v_{j)}, \tag{4.11}$$

where $\overline{\nabla}$ is the connection of $\bar{g}_{ij}(\varepsilon)$ and $v_i(x,\varepsilon)$ is a smooth one parameter family of vector fields that generate the diffeomorphisms on $\bar{g}_{ij}(\varepsilon)$ along the flow.

We assume the vacuum on the reference flat space is static so we may use the earlier relation (4.7). Further, we assume the spatial components of the stress tensor one-point function on flat space are simply determined by the homogeneous pressure p,

so

$$\langle T_{ij}\rangle_{\bar{g}} = p\,\bar{g}_{ij}(x;\varepsilon) \tag{4.12}$$

at the point ε in the flow. Note that if the one-point function is not renormalised, the UV divergence will be the same as in the earlier Equation (4.8) so $p = c_1\Lambda^3 + \mathcal{O}(\Lambda^0)$. Then using Equation (4.7) we have

$$\frac{\mathrm{d}\bar{F}}{\mathrm{d}\varepsilon} = -p\frac{\mathrm{d}}{\mathrm{d}\varepsilon}\mathrm{Vol}[\bar{g}(\varepsilon)], \tag{4.13}$$

where the volume functional is defined in terms of the metric $\bar{g}_{ij}(x,\varepsilon)$ as $\mathrm{Vol}[\bar{g}(\varepsilon)] = \int \mathrm{d}^2x\sqrt{\bar{g}(\varepsilon)}$. Now consider this (divergent) volume functional on the flat space $(\Sigma,\bar{g})$. In the compact case the volume is fixed for a given $(\Sigma,\bar{g})$ and cannot depend on the choice of coordinates. However, in this non-compact deformed flat-space setting it may not be fixed if 'large diffeomorphisms' are allowed. From its definition, we see that

$$\frac{\mathrm{d}}{\mathrm{d}\varepsilon}\mathrm{Vol}[\bar{g}(\varepsilon)] = \int \mathrm{d}^2x\sqrt{\bar{g}(\varepsilon)}\overline{\nabla}_i v^i = \int_{\partial_\infty\mathcal{M}} \mathrm{d}S_i v^i, \tag{4.14}$$

with $\mathrm{d}S_i$ the outward directed length element of the asymptotic boundary, $\partial_\infty\mathcal{M}$, which is understood as being defined via a suitable limit. Thus, if diffeomorphisms are allowed such that this boundary term does not vanish then the variation of $\mathrm{Vol}[\bar{g}(\varepsilon)]$ in the parameter ε may be finite and non-vanishing. One could disallow such diffeomorphisms, but this would put an unreasonably strong constraint on the allowed geometries (Σ, g). Hence, we learn that the reference flat space free energy we subtract in the non-compact case may have a coordinate dependence in ε, although this is *only* through the variation of volume due to large diffeomorphisms along the flow ε.

An explicit example may serve to illustrate this further. Consider the flat reference metric written in polar coordinates, $\bar{g}_{ij}(x)\mathrm{d}x^i\mathrm{d}x^j = \mathrm{d}r^2 + r^2\mathrm{d}\theta^2$. Then we may deform this along the flow by the large diffeomorphism

$$\rho^2 = r^2\left(\frac{1+2v(\varepsilon)r^2+r^4}{1+r^4}\right), \quad \bar{g}_{ij}(x,\varepsilon)\mathrm{d}x^i\mathrm{d}x^j = \left(\frac{\partial\rho(r,\varepsilon)}{\partial r}\right)^2\mathrm{d}r^2 + \rho(r,\varepsilon)^2\mathrm{d}\theta^2\,, \tag{4.15}$$

provided $v(\varepsilon) > -\frac{4}{3\sqrt{3}}$. This is still flat space. However, if we consider the variation of the volume in ε we find that

$$\frac{\mathrm{d}}{\mathrm{d}\varepsilon}\mathrm{Vol}(\bar{g},\varepsilon) = \frac{\mathrm{d}}{\mathrm{d}\varepsilon}\int_0^\infty \mathrm{d}r\int_0^{2\pi}\mathrm{d}\theta\rho(r,\varepsilon)\frac{\partial\rho(r,\varepsilon)}{\partial r} = 2\pi\int_0^\infty \mathrm{d}r\left(\frac{4r^3v'(\varepsilon)}{(1+r^4)^2}\right) = 2\pi v'(\varepsilon)\,. \tag{4.16}$$

Thus, the coordinate transformation $\rho^2 = r^2 + 2v(\varepsilon) + \mathcal{O}(\frac{1}{r})$ 'stretches' the space $(\Sigma,\bar{g})$

relative to the fixed coordinate chart. While the volume itself is infinite, its variation in ε is finite and non-vanishing.

Now, we may proceed as before to find the UV behaviour, but being careful to note in this non-compact case that the free energy functional evaluated on both $(\Sigma, g(\varepsilon))$ *and* the flat reference space depend on the flow parameter, ε i.e. $\beta F(\varepsilon) = -\ln Z[g(\varepsilon)]$ and $\beta \bar{F}(\varepsilon) = -\ln Z[\bar{g}(\varepsilon)]$ so that $\Delta F(\varepsilon) = F(\varepsilon) - \bar{F}(\varepsilon)$. We have the same expression as previously in Equation (4.9) for the UV divergence of $\mathrm{d}F(\varepsilon)/\mathrm{d}\varepsilon$, but now also have a similar expression for $\mathrm{d}\bar{F}(\varepsilon)/\mathrm{d}\varepsilon$ leading to

$$\frac{\mathrm{d}\Delta F}{\mathrm{d}\varepsilon} = -c_1 \Lambda^3 \left(\frac{\mathrm{d}}{\mathrm{d}\varepsilon} \mathrm{Vol}[g(\varepsilon)] - \frac{\mathrm{d}}{\mathrm{d}\varepsilon} \mathrm{Vol}[\bar{g}(\varepsilon)] \right) + \mathcal{O}(\Lambda^0) \,. \tag{4.17}$$

While the reference geometry is fixed to be flat space, we may choose 'large diffeomorphisms' to adjust the change in volume $\mathrm{dVol}[\bar{g}(\varepsilon)]/\mathrm{d}\varepsilon$ to equal that of the geometry of interest $\mathrm{dVol}[g(\varepsilon)]/\mathrm{d}\varepsilon$ — doing so then renders $\Delta F(\varepsilon)$ to be UV finite. Furthermore, since the variation of the reference free energy $\bar{F}(\varepsilon)$ only depends on the volume variation, as we saw in Equation (4.13), this completely fixes the finite part of the reference space subtraction too. We have seen in the explicit example above that, by an appropriate choice of the function $v(\varepsilon)$ in Equation (4.15), we may always solve this condition for flat space (at least in this example, we should be near enough to $\varepsilon = 0$ that $v(\varepsilon) > -\frac{4}{3\sqrt{3}}$ remains true, but, of course, one could use other choices of 'large diffeomorphism'). It may be interesting to explore this for other non-compact spaces.

Thus, while in the compact case we require the volume of (Σ, g) and $(\Sigma, \bar{g})$ to be equal to ensure a UV-finite free energy difference, the non-compact case is rather different. Due to 'large diffeomorphisms' there is no volume constraint on the geometry (Σ, g) — there could not be as the volumes of both (Σ, g) and $(\Sigma, \bar{g})$ are infinite and not well defined. The key point is that these 'large diffeomorphisms' may be used to subtract the 'correctly stretched' flat reference geometry, $(\Sigma, \bar{g})$, in order to ensure ΔF is UV finite. Note that had we not stretched the geometry $(\Sigma, \bar{g})$ appropriately, in order to have a UV-finite free energy difference we would have had to restrict to deformations such that $\mathrm{dVol}[g(\varepsilon)]/\mathrm{d}\varepsilon$ vanishes, which would be an unreasonably strong restriction on the allowed deformed geometries $g_{ij}(x, \varepsilon)$ given a starting flat reference geometry metric $\bar{g}_{ij}(x)$.

Perhaps another more physical way to say this is as follows. In the compact case one must compare a (Σ, g) and $(\Sigma, \bar{g})$ with the same volume, but there is always the freedom to scale one or the other to achieve this volume condition. Such freedom should also be present in the flat non-compact case. Since its volume is infinite, it does not make much sense to scale the space, but instead this freedom to 'match' the two spaces (Σ, g) and $(\Sigma, \bar{g})$ appropriately is implemented by these 'large diffeomorphisms' or 'stretching'.

In Chapter 3, we found in the free field case that $\Delta F \sim \mathcal{O}(\varepsilon^2)$ and hence is quadratic in the metric perturbation to flat space, rather than being linear which, naïvely,

one might have expected. We shall now show how to compute ΔF generally for perturbations of flat space from the variation of the stress tensor, and, in particular, we shall see why the variation is quadratic. We also treat the compact case, which we will see may also lead to the same quadratic behaviour.

Since the spatial geometry is two dimensional, we may choose coordinates so that we write the deformation of the geometry, $(\Sigma, g(\varepsilon))$, as a Weyl deformation of the reference geometry presented as $\bar{g}_{ij}(x)$, so

$$g_{ij}(x;\varepsilon) = \mathrm{e}^{2f(x;\varepsilon)}\bar{g}_{ij}(x), \tag{4.18}$$

where f is a one parameter family of smooth functions on Σ with $f(x;0) = 0$ so that $g(0) = \bar{g}$. We now expand about $\varepsilon = 0$ as

$$f(x) = \varepsilon\, f^{(1)}(x) + \varepsilon^2 f^{(2)}(x) + \mathcal{O}(\varepsilon^3)\,. \tag{4.19}$$

In response to this deformation, we write the perturbation to the VEV of the spatial part of the stress tensor due to this metric deformation as

$$\langle T_{ij}\rangle_{g(\varepsilon)} = \bar{\sigma}_{ij}(x) + \varepsilon\,\delta\sigma_{ij}(x) + \mathcal{O}(\varepsilon^2)\,. \tag{4.20}$$

Following the discussion above, one may take this one-point function to be either renormalised or not, as any divergent parts will cancel in the final result. We view $\delta\sigma_{ij}(x)$ as the linear response of the spatial stress tensor to the metric deformation. Thus, we think of $\delta\sigma_{ij}$ as a linear functional of $f^{(1)}$, while it is of course independent of the higher orders of the deformation, such as $f^{(2)}$. Again we assume the vacuum is static, in the sense that $\langle T_{ij}\rangle_{g(\varepsilon)}$ has only spatial dependence and no dependence on (Euclidean) time. Then we may use the earlier relation (4.7). We also assume that $(\Sigma, \bar{g})$ has a suitable translation invariance so that $\bar{\sigma}^i{}_i = \bar{\sigma}_{ij}\bar{g}^{ij} = \text{const}$. We would certainly expect this for $(\Sigma, \bar{g})$ being flat spacetime (when $\bar{\sigma}^i{}_i = 2p$) but also for other homogeneous (not necessarily isotropic) spaces such as tori and spheres. We note that this disallows 'striped' phases of vacuum (see for example [91]) although in the absence of sources for operators (other than a curved metric) one would not expect the homogeneous vacuum to spontaneously break this unless the theory possessed a tachyonic direction which would render it ill defined on flat spacetime (although perhaps valid on suitably small compact spaces). Following our assumptions, we use Equation (4.7) to write

$$\frac{\mathrm{d}F}{\mathrm{d}\varepsilon} = -\frac{1}{2}\bar{\sigma}^i_i\left(\frac{\mathrm{d}}{\mathrm{d}\varepsilon}\mathrm{Vol}[g(\varepsilon)]\right) + 2\varepsilon\int \mathrm{d}^2x\sqrt{\bar{g}}\left(\left(f^{(1)}\right)^2\bar{\sigma}^i{}_i - \frac{1}{2}f^{(1)}\,\delta\sigma^i{}_i\right) + \mathcal{O}\left(\varepsilon^2\right) \tag{4.21}$$

where indices are raised and lowered using the reference metric $\bar{g}_{ij}(x)$. In the compact case we choose the volume of $(\Sigma, g(\varepsilon))$ to equal that of $(\Sigma, \bar{g})$ to ensure UV finiteness, so

$\mathrm{dVol}[g(\varepsilon)]/\mathrm{d}\varepsilon = 0$, so we find

$$\Delta F(\varepsilon) = \varepsilon^2 \int \mathrm{d}^2x\sqrt{\bar{g}}\left(\left(f^{(1)}\right)^2 \bar{\sigma}^i{}_i - \frac{1}{2} f^{(1)}\,\delta\sigma^i{}_i\right) + \mathcal{O}\left(\varepsilon^3\right) . \tag{4.22}$$

However, following our discussion above we obtain precisely the same expression in the non-compact case for deformations of flat space, since for UV finiteness we choose appropriate 'large diffeomorphisms' for $\bar{g}_{ij}(x,\varepsilon)$ so that $\mathrm{dVol}[\bar{g}(\varepsilon)]/\mathrm{d}\varepsilon$ equals $\mathrm{dVol}[g(\varepsilon)]/\mathrm{d}\varepsilon$, and $\bar{F}(\varepsilon)$ evolves as in Equation (4.13). Hence, for deformations of both homogeneous compact spaces and flat space, where the vacuum of the undeformed space is static and has constant $\bar{\sigma}^i_i$, we arrive at a quadratic variation of our free energy difference. This is determined in terms of the linear deformation of the metric, $f^{(1)}$, both explicitly and implicitly through the response of the spatial stress components $\delta\sigma_{ij}$. If we chose to use the unrenormalised stress tensor one-point function, from earlier Equation (4.8) we would find that $\bar{\sigma}^i{}_i = 2c_1\Lambda^3 + \mathcal{O}(\Lambda^0)$ and $\delta\sigma^i{}_i = 4c_1\Lambda^3 f^{(1)} + \mathcal{O}(\Lambda^0)$, and hence the UV divergences will cancel between the two terms above, leaving only a UV-finite result as expected. Note that if we chose a reference geometry that was not homogeneous, and hence presumably $\bar{\sigma}^i_i$ would not be constant, then we would expect a linear variation in ε instead. It is the quadratic nature of the variation for homogeneous spaces that enables ΔF to potentially have a definite sign.

We now specialise to the case of the reference space $(\Sigma, \bar{g})$ being flat space, and choose natural coordinates so that $\bar{g}_{ij} = \delta_{ij}$. Then, we may decompose the leading metric perturbation as a Fourier transform

$$f^{(1)}(x) = \int \mathrm{d}^2k\, \mathrm{e}^{ik_i x^i}\, \tilde{f}(k_i), \tag{4.23}$$

where reality imposes $\tilde{f}(-k_i) = \tilde{f}(k_i)^\star$. On flat space the linear response of the trace of the spatial stress tensor, $\delta\sigma^i_i$, to the metric deformation is constrained by the rotational and translational invariance. For a deformation by a single Fourier mode the response will be proportional to that mode, with a coefficient depending on the wavevector k_i only through its magnitude, $k = \sqrt{k_i k_i}$. Hence, the response for a general perturbation will be

$$\delta\sigma^i_i(x) = \int \mathrm{d}^2k\, \mathrm{e}^{ik_i x^i}\, s(k)\tilde{f}(k_i) \tag{4.24}$$

and is characterised by the function $s(k)$. Then, we may write the quadratic variation of ΔF as,

$$\Delta F(\varepsilon) = -\varepsilon^2 \int \mathrm{d}^2k\, a(k) \left|\tilde{f}(k_i)\right|^2 + O\left(\varepsilon^3\right) \tag{4.25}$$

where the function $a(k) = (2\pi)^2\left(\frac{1}{2}s(k) - \bar{\sigma}^i_i\right)$ characterises the variation, and again only depends on the wavevector through its magnitude k. Note that as we have defined signs,

modes which have positive $a(k)$ give rise to a quadratic *decrease* in free energy relative to flat space.

4.2 Review: Finite Temperature Holographic CFTs and Hydrostatics

We now briefly review two calculations of the UV-finite free energy difference defined in Section 4.1: firstly, a computation of the leading-order response of the free energy to a small spatial deformation of a (2+1)-dimensional finite temperature holographic CFT on flat space and, following that, the leading long-wavelength variation for a general (2+1)-dimensional QFT that admits a hydrostatic description at finite temperature for weak deformations of the spatial geometry from flat space. These calculations were performed by my collaborators Krai Cheamsawat and Toby Wiseman [2].

Consider a (2+1)-dimensional holographic CFT on flat space. As explained in Section 1.2, these theories admit a description in terms of solutions to Einstein's equations with a negative cosmological constant. Under some reasonable assumptions, the bulk dual for a flat boundary at finite temperature T is planar AdS-Schwarzschild with metric

$$g^{(\mathrm{Sch})}_{AB}\mathrm{d}x^A\mathrm{d}x^B = \frac{\ell^2}{z^2}\left(\left(1-\left(\frac{z}{z_0}\right)^3\right)\mathrm{d}\tau^2 + \mathrm{d}x_i^2 + \frac{\mathrm{d}z^2}{1-\left(\frac{z}{z_0}\right)^3}\right), \tag{4.26}$$

where ℓ is the AdS length, z is the 'radial' coordinate, $\tau \sim \tau + T^{-1}$ is the Euclidean time coordinate, x^i are local coordinates on the conformal boundary at $z = 0$ — where the CFT is — and $z_0 = 3/(4\pi T)$ is the position of the horizon. By taking flat space to be the reference geometry with $\bar{g}_{ij} = \delta_{ij}$, considering Weyl perturbation,

$$g_{ij}(x;\varepsilon) = \mathrm{e}^{2f(x;\varepsilon)}\delta_{ij} = \left(1 + 2\varepsilon f^{(1)}(x)) + \mathcal{O}(\varepsilon^2)\right)\delta_{ij}, \tag{4.27}$$

to it, and finding the linear response of the bulk (and therefore the boundary stress tensor) to this change in boundary metric it is found that the characteristic function of ΔF (4.25) for a holographic CFT on flat space is

$$a(k,T) = \frac{\pi^4 c_T}{48}k^3\left(\frac{3k}{4\pi T}\right)^{-3} u_3\left(\frac{3k}{4\pi T}\right), \tag{4.28}$$

where u_3 is a dimensionless function determined by the $\xi \equiv z/z_0 \to 0^+$ asymptotics of a function $u(\xi)$,

$$u(\xi) \sim u_0 - \frac{\tilde{k}^2}{2}u_0\xi^2 + \frac{1}{6}u_3\xi^3 + \mathcal{O}(\xi^4), \tag{4.29}$$

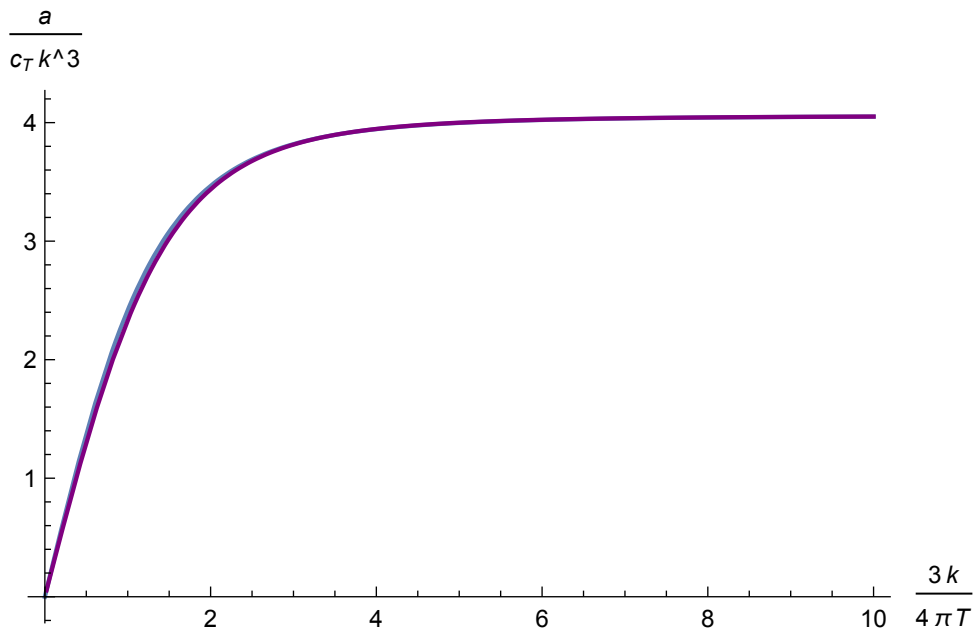

Figure 4.1: Graph of the function $a(k,T)$ which characterises the quadratic variation of the free energy difference from flat space, ΔF, normalised by the CFT central charge, c_T, and by k^3, against the dimensionless quantity $3k/(4\pi T)$ for both the holographic CFT (red curve) and free Dirac fermion CFT (blue curve).

that is given by solving the ODE

$$u''(\xi) - \left(\frac{16 - 24\xi^3 + 36\xi^6 - \xi^9}{8 - 6\xi^3 - 3\xi^6 + \xi^9}\right)\frac{u'(\xi)}{\xi} - \frac{\tilde{k}^2}{1-\xi^3}u(\xi) = 0, \tag{4.30}$$

where $\tilde{k} \equiv z_0 k$, subject to boundary conditions corresponding to regularity of the metric at the horizon and matching the boundary geometry of the CFT at $\xi = 0$. To determine u_3, and thus $a(k,T)$, the ODE (4.30) must be solved. This is possible analytically in the low-temperature regime $T \to 0^+$, giving that $u_3(\tilde{k}) \sim 2\tilde{k}^3$ and hence a characteristic function that agrees with the previous result for zero-temperature CFTs (1.69). Away from $T = 0$, (4.30) can be solved numerically to give a characteristic function as plotted in Figure 4.1.

The numerically determined $a(k,T)/(c_T k^3)$ for the holographic CFT is plotted as a function of $\tilde{k} = 3k/(4\pi T)$ in Figure 4.1. Plotted as well is the $a(k,T)/(c_T k^3)$ for the massless Dirac fermion as a function of $\tilde{k} = 3k/(4\pi T)$, determined by numerically integrating (3.34) with $I(k^2 t)$ given by (3.32b) and $c_T = c_{\mathrm{f}} = 3/(4\pi)^2$. As is expected, these two curves match in the low-temperature limit $\tilde{k} \to \infty$, where the universal CFT behaviour is observed. Two further interesting observations can also be made. Firstly, the characteristic function for the holographic CFT is positive for all $\tilde{k}$ and thus the quadratic variation of ΔF due to spatial perturbations is *negative* for all finite temperature strongly-coupled holographic CFTs on flat space — thereby extending the analogous result for free

theories shown in Chapter 3. Secondly, the two curves in Figure 4.1, and therefore ΔF for the Dirac fermion and a strong-coupled holographic CFT, are remarkably similar. They are so similar it is tempting to suggest that they are identical and that any difference between them is caused by numerical error. However, the $\tilde{k} \to 0$ behaviour of these curves can be deduced analytically (4.31) and doing so shows that the curves differ by a factor of 45/48 in this limit and so are indeed distinct. Nevertheless, the similarity is intriguing in itself. A priori, there is no reason to think these curves should be so similar — they arise from two theories that are qualitatively very different; one from a strongly-coupled field theory with a large number of degrees of freedom and the other from a free theory with a single degree of freedom. This similarity will be explored further in Chapter 6.

As with previous holographic results, these calculations suggest another avenue for progress. Much like the low-temperature limit, the defining ODE for u (4.30) admits an analytic solution order by order in $\tilde{k}$ as $\tilde{k} \to 0^+$. This corresponds to weak deformations of the spatial geometry i.e. where the curvature length scale is much larger than the thermal one. Solving the ODE (4.30) in this limit and taking $k/T \ll 1$ in the characteristic function for the free scalar and fermion[3] gives that

$$a(k,T) = \left\{ \begin{array}{cc} \frac{\pi}{60M}\left(1-10\xi+30\xi^2\right)\coth\left(\frac{M}{2T}\right)k^4, & \text{scalar} \\ \frac{\pi}{120M}\tanh\left(\frac{M}{2T}\right)k^4, & \text{massive fermion} \\ c_{\mathrm{f}}\frac{\pi^3}{45T}k^4, & \text{massless fermion} \\ c_T\frac{\pi^3}{48T}k^4, & \text{holographic CFT} \end{array} \right\} + \mathcal{O}(k^6). \quad (4.31)$$

Common to each of these theories is the fact that $a \sim k^4$. This suggests that in each case the non-trivial change to the stress tensor induced by the deformation involves four-derivative curvature corrections to a perfect fluid stress tensor. In the holographic case, this is the fluid/gravity limit of the correspondence in which it is known that theories admit a hydrostatic description, but this also suggests the same is true for the free scalar and fermion and possibly for a large class of theories. Assuming a hydrostatic description at weak curvatures, as is expected to be true for any ultrastatic (2+1)-dimensional QFT at finite temperature[4], and taking $(\Sigma, \bar{g})$ to be flat space and (Σ, g) to be a weakly-curved deformation of it, the spatial components the VEV of the stress tensor, in the absence of any (other) sources or currents, on a (2+1)-dimensional ultrastatic background simply

[3] More details on this can be found in Section 4.3.

[4] Hydrodynamic descriptions normally necessitate interactions so should not be expected to apply to free theories. Our systems are static and are kept at finite temperature by an external reservoir — thus always admit a fluid description

give

$$\langle T_{ij}\rangle_g = p(T)g_{ij} + b(T)\left(\nabla_i\nabla_j R - \nabla^2 R g_{ij} - \frac{1}{4}R^2 g_{ij}\right) + \mathcal{O}(\partial^6) \tag{4.32}$$

where R and ∇ are the Ricci scalar and Levi-Civita connection on (Σ, g), respectively, and the coefficients p and b are theory-dependent functions of T. After making a suitable 'stretch' of the reference space, this gives a free energy difference (4.7) that satisfies

$$\frac{\mathrm{d}\Delta F}{\mathrm{d}\varepsilon} = \frac{b(T)}{2}\int \mathrm{d}^2x\sqrt{g}\left(\nabla_i\nabla_j R - \nabla^2 R g_{ij} - \frac{1}{4}R^2 g_{ij}\right)\frac{\mathrm{d}g^{ij}}{\mathrm{d}\varepsilon} + \ldots, \tag{4.33}$$

which can be integrated up to give

$$\Delta F[g] = -\frac{b(T)}{4}\int_\Sigma \mathrm{d}^2x\sqrt{g}R^2 + \ldots. \tag{4.34}$$

The sign of the free energy difference is thus determined by the sign of $b(T)$. This function does not depend on the geometry, so it can be read off from the perturbative results in the long-wavelength limit. Doing so gives that the characteristic function (4.25) for ΔF is

$$a(k, T) = 4\pi^2 b(T)k^4 + \mathcal{O}(k^6). \tag{4.35}$$

Comparing this with the characteristic functions for the free scalar, free fermion and holographic CFT (4.31) gives that $b(T)$ is positive in each case and therefore that the negativity of ΔF extends to non-perturbative weak deformations of these theories.

4.3 Long-Wavelength Limit: Free Scalar and Fermion

We now return to my own work. Having inferred that the free scalar and fermion QFTs have a hydrostatic description from the behaviour $a(k, T) \sim k^4$, one might ask whether this can be derived directly. We shall now show this is indeed the case. Recall that the free energies of these theories can be evaluated as functional determinants of operators of the form (3.28) and thus in terms of heat kernels. So, for these theories, the free energy difference between (Σ, g) and an appropriately 'stretched' reference space, $(\Sigma, \bar{g})$, can be evaluated using differenced heat kernels, as in (3.8). Heat kernels admit an asymptotic expansion (2.15) from which it follows that the differenced heat kernels go as

$$\Delta K_L(t) \sim \sum_{m\geqslant 0}\Delta d_{2m}(L)t^{m-1}, \tag{4.36}$$

as $t \to 0^+$, where $d_{2m}(L)$ are the heat kernel coefficients, and in our two-dimensional context these are integrals of sums and products of the Ricci scalar and its derivatives so that $d_{2m}(L) \sim \ell^{2-2m}$, where ℓ is the characteristic length scale of the deformation.

Hence, this should be viewed as an expansion in the dimensionless quantity t/ℓ^2. In the hydrostatic regime discussed above we have low curvature compared to the thermal scale, so that $\ell T \gg 1$. Then, the integrand in Equation (3.8) is localised near $t = 0$ (where in the scalar case we also require a non-zero mass such that $\ell M \gg 1$) and using the heat kernel expansion gives,

$$\Delta F \simeq \frac{\sigma}{2} \sum_{m=0}^{\infty} \Delta d^{\mathrm{s,f}}_{2m+4} \frac{(-1)^m}{T^{2m+1}} J^{(m)}_{\mathrm{s,f}} \left(\frac{M^2}{T^2} \right) \tag{4.37}$$

where,

$$J_{\mathrm{s}}(x) = \frac{1}{\sqrt{x}} \coth\left(\frac{\sqrt{x}}{2} \right) , \quad J_{\mathrm{f}}(x) = \frac{1}{\sqrt{x}} \tanh\left(\frac{\sqrt{x}}{2} \right) \tag{4.38}$$

and we have used the fact that the first two heat kernel coefficients are proportional to the volume and Euler characteristic of (Σ, g), respectively, and cancel in the free energy difference when computed using the 'stretched' reference flat space metric, $\bar{g}_{ij}(x;\varepsilon)$, as detailed in Section 4.1. The first term in the expansion is then determined by the heat kernel coefficients (2.2):

$$\Delta d^{\mathrm{s}}_4 = \frac{1}{240\pi} \left(1 - 10\xi + 30\xi^2\right) \int \mathrm{d}^2x \sqrt{g} R^2 \Big|_{\Sigma} , \quad \Delta d^{\mathrm{f}}_4 = -\frac{1}{960\pi} \int \mathrm{d}^2x \sqrt{g} R^2 \Big|_{\Sigma} \tag{4.39}$$

for the two-dimensional scalar and Dirac operators, respectively. These give a leading contribution to ΔF that agrees precisely with the expressions obtained by using the form derived from hydrostatics in Equation (4.34), and the value of the coefficient $b(T)$ determined from the perturbative results (4.31).

4.4 Summary and Discussion

We have defined the free energy difference $\Delta F(\varepsilon) = F(\varepsilon) - \bar{F}(\varepsilon)$ where the free energy of a relativistic QFT on the product of time with a two-space $(\Sigma, g(\varepsilon))$ with metric $g_{ij}(x;\varepsilon) = \mathrm{e}^{2f(x;\varepsilon)}\bar{g}_{ij}(x)$ is differenced with that on a reference geometry $(\Sigma, \bar{g}(\varepsilon))$ at the same temperature. If the geometry is compact we require the reference geometry to have metric $\bar{g}_{ij}(x)$ and choose the deformation $f(x;\varepsilon)$ so that the volumes $\mathrm{Vol}[g(\varepsilon)]$, $\mathrm{Vol}[\bar{g}]$ are equal. In the non-compact case where $(\Sigma, g(\varepsilon))$ is a deformation of flat space, we subtract an appropriately 'stretched' reference flat space with spatial metric $\bar{g}_{ij}(x;\varepsilon)$ (in the same coordinates as for g_{ij}) given by an ε-dependent diffeomorphism of the flat reference metric $\bar{g}_{ij}(x)$, with the diffeomorphism chosen so that the volume variations $\mathrm{dVol}[g(\varepsilon)]/\mathrm{d}\varepsilon$ and $\mathrm{dVol}[\bar{g}(\varepsilon)]/\mathrm{d}\varepsilon$ are equal. For a (2+1)-dimensional QFT (although not for higher dimensions) this quantity $\Delta F(\varepsilon)$ is UV finite, and, hence, independent of

renormalisation ambiguity. We expect that for reasonable fall off of the perturbation this will also be IR finite on non-compact spaces.

We have shown that for deformations that are perturbations of flat space, then, under the assumption that for flat space the finite temperature spatial stress tensor is governed by a homogeneous isotropic pressure, the variation of $\Delta F(\varepsilon)$ is quadratic in the perturbation. We have also shown that the same holds for perturbations of homogeneous compact spaces, where for the unperturbed homogeneous space the trace of the spatial parts of the stress tensor, $\bar{\sigma}^i{}_i$, is constant — as, for example, we would expect on a sphere or torus. This explains why the variation of free energy found on a torus in Chapter 3 was quadratic.

We have reviewed a computation of this variation for holographic CFTs, showing that the quadratic variation is always negative at any temperature and for any perturbation, as was previously found for free scalars and fermions in Chapter 3. Furthermore, it is strikingly similar in functional form to that for the free massless Dirac fermion CFT (the theory on the worldvolume of graphene). We have also reviewed an argument that in any theory that has a hydrostatic limit for long-wavelength deformations of flat space (but now not necessarily small in amplitude) relative to the temperature scale, then ΔF is governed by a specific curvature correction to the stress tensor, and is negative for the free scalar and fermion theories, as well as the holographic CFT. In particular, the corrections to the free energy difference of the free scalar and fermion theories have been derived to all orders in inverse powers of the curvature scale.

The differenced free energy defined here is a physically relevant quantity in both the compact and non-compact cases. For example, for a compact two-dimensional membrane on which degrees of freedom live that are governed by a relativistic QFT on the curved ultrastatic geometry induced on the membrane, the compact $\Delta F(\varepsilon)$ precisely describes a quadratic (in membrane metric perturbations) free energy contribution as the membrane is perturbed, provided it is inextensible, or is deformed to preserve its area. In the non-compact case, the generic $a(k) \sim k^4$ behaviour observed for long wavelengths implies that the quadratic variation of ΔF is dominated by shorter wavelength deformations and suggests, therefore, that we may ultimately view our formal flat space quantity ΔF as giving the short-distance response of thermal vacuum energy on scales shorter than the characteristic curvature scale of the space that is perturbed[5]. The case for both of these claims — hence the utility of the free energy difference as measure free energy — will be presented more comprehensively for deformations of S^2 in the following chapter.

[5]Note that for temperature to be relevant in this limit, it must also be large compared to the curvature scale of the unperturbed space.

Chapter 5

Free Theories on S^2

The round shape of a soap bubble arises from competition between its intrinsic surface tension, which energetically prefers to collapse it, and a pressure differential between the air inside and outside of the bubble. More generally, the competition between various physical effects determines the shape of any physical membrane.

Of particular interest to us are membranes that support relativistic quantum degrees of freedom living on them. A fiducial example is that of a graphene monolayer, whose energetics in a Born-Oppenheimer-like approximation can be split into a sum of two contributions: one from the atomic background lattice and another from relativistic excitations that propagate on this background. At scales well above the lattice spacing, the lattice can be treated as a continuous membrane, and the free energy will depend on its geometry. The contribution to this free energy from the background, interpreted as a *classical* contribution $F_{\rm c}$, is then captured by a Landau free energy constructed from its embedding into an ambient flat space [84, 92, 93] (see [86] for a review). The effective relativistic excitations are four free massless Dirac fermions (with effective speed of light $c_{\rm eff}$ given by the Fermi velocity $\approx 10^6$ m/s), and their free energy — interpreted as a *quantum* contribution $F_{\rm q}$ that depends on the membrane's intrinsic geometry — is computed via an appropriate path integral. The classical contribution to the free energy is relatively well-understood thus our goal is to understand the contribution from the Dirac fermions.

While graphene is our motivating physical system, there are other more exotic examples of membranes supporting relativistic quantum fields, as mentioned in the Introduction. Further, the results presented in Chapters 1, 3 and 4 have raised some questions about general QFTs on these spaces. Consequently, in this chapter (based on [3]) our main objective is to study the free energy of more general classes of relativistic QFTs living on (2+1)-dimensional geometries, with the massless Dirac fermion corresponding to graphene as a special case[1].

The work presented in this thesis thus far has found that such relativistic quantum

[1]We note that studying the free energy on Euclidean three-dimensional geometries is also interesting and has fascinating links to quantum cosmology [94, 95].

fields tend to energetically prefer deformed geometries. To briefly summarise, let us assume that this field theory lives on $\mathbb{R} \times M$, where $M = (\Sigma, g)$ is a two-dimensional spatial manifold with metric g. Per the discussion above, F_{q} will depend on the intrinsic geometry of M, i.e. on g. Because F_{q} is a free energy, it is extensive, and therefore in order to sensibly discuss its dependence on the *shape* of M we should imagine keeping the volume of M (computed with respect to g) fixed as we vary g[2]. We therefore consider the 'background-subtracted' free energy $\Delta F_{\mathrm{q}} \equiv F_{\mathrm{q}}[g] - F_{\mathrm{q}}[\bar{g}]$, with $\bar{g}$ taken to be some fiducial reference metric which endows Σ with the same volume as g. With this understanding ΔF_{q} has been shown to be negative for many different theories when $\bar{g}$ is taken to be the round sphere or the flat plane, a result most well-established when the geometry on Σ is perturbatively close to $(\Sigma, \bar{g})$[3]. Note that ΔF_{q} remains non-zero even at zero temperature, when it can be interpreted as a Casimir energy.

These observations naturally lead to the following question: if the free energy F_{q} governs the equilibrium configuration of a membrane, does the fact that ΔF_{q} is always negative lead to an instability of the round sphere or flat space? If so, will a membrane settle down to some less-symmetric equilibrium configuration, or does this instability ultimately lead to a runaway process (which presumably breaks down once a UV scale is reached)? Answering this question will depend on how ΔF_{q} competes with other contributions to the free energy; returning to the case of graphene, in Chapter 3 we performed a parametric comparison of the competition between ΔF_{q} and the classical bending free energy ΔF_{c}, finding that the typical curvature scale l_{crit} at which the negative contribution of ΔF_{q} becomes dominant over the (positive) contribution of ΔF_{c} agrees with the 'rippling' length scale l_{rip} of graphene measured in experiments [44]. However, the order of magnitude of this scale is only slightly above that of the lattice spacing, where the effective Dirac fermion description breaks down, so the validity of our estimates for ΔF_{q} and ΔF_{c} in this regime is suspect.

Moreover, the order-of-magnitude analysis of Chapter 3 was made subtle for two reasons. Firstly, since Σ is a plane, its volume is infinite; hence one must be careful in defining precisely what is meant by the condition that the volumes computed from g and $\bar{g}$ match. Secondly, the leading perturbation to ΔF_{c} is quadratic in the height function amplitude ε (as shown in Equation(3.36)), while ΔF_{q} is quartic in ε; hence balancing these two contributions requires a careful accounting of various orders-of-limits.

The first purpose of this chapter is, therefore, to repeat the perturbative analysis of Chapter 3 — that is, the perturbative computation of ΔF_{q} for the non-minimally-coupled free scalar and the free Dirac fermion — in the case where Σ has sphere topology, rather

[2] In other words, of course one can always make F_{q} arbitrarily large or small by simply varying the volume of M arbitrarily, but this is a standard volume-dependence that can be eliminated by, say, a classical tension term in F_{c}.

[3] We note also that non-positivity results have also been obtained on related quantities for holographic theories for various (Σ, g), namely the local energy density [96] and the energy difference [97, 98].

than a plane. This modification will alleviate both of the issues just mentioned, since when Σ is a sphere it has finite volume and we will also find that the contributions ΔF_{c} and ΔF_{q} are both quadratic in ε. Again, we will find that the round sphere locally maximises F_{q}.

Our second purpose is then to investigate the questions posed above: namely, is the round sphere a *global* maximum of ΔF_{q}? Does ΔF_{q} eventually find some new equilibrium configuration after a sufficiently large deformation to the sphere, or can it decrease indefinitely? To address these questions, we will numerically compute ΔF_{q} for large (axisymmetric[4]) deformations of the round sphere using the heat kernel methods in Chapter 2. These numerical computations require highly-accurate estimates for the relevant spectra and this will be achieved using pseudo-spectral differencing — which we will review. We will find that ΔF_{q} is always negative, and in fact that it can be made arbitrarily negative as the geometry becomes singular. Our conclusion, therefore, is that the energetics of ΔF_{q} favour geometries that are *not* smooth. Surprisingly, we will also find that the behaviour of ΔF_{q} for such large deformations is remarkably similar for the scalar and the fermion when normalised by its perturbative expression.

In fact, our main result will be stronger: not only is ΔF_{q} always negative for the deformations we will study, but the heat kernel $\Delta K_L(t)$ which computes ΔF_{q} has definite sign for all t. The fact that $\Delta K_L(t)$ apparently has fixed sign for all t is therefore a non-trivial statement about the behaviour of the eigenvalues of L. The universality of this result leads us to conjecture that $\Delta K_L(t)$ has fixed sign for *any* free field theory and volume-preserving deformation of the sphere. This conjecture has already been made for a free scalar field [100] — here, we will provide a significant body of further evidence for this claim and the case for it to generalise to the Dirac and non-minimally-coupled scalar cases.

The order-of-magnitude analysis of the competition between ΔF_{c} and ΔF_{q} will be provided immediately below, in Section 5.1, for the sake of illustrating more clearly some of the concepts discussed so far. We will then establish our setup, conventions, and formalism in Section 5.2, focusing specifically on the computation of ΔF_{q} using heat kernels. We will then present the perturbative calculation of ΔF_{q} for the free non-minimally-coupled scalar and the free Dirac fermion in Section 5.3, along with some checks showing that our results reproduce the CFT result of Section 1.4 and the flat-space result of Chapter 3 in appropriate limits. Section 5.4 will review pseudo-spectral methods for numerically estimating the eigenvalues of a second-order linear differential operator. In particular, the case of a one-dimensional non-periodic compact domain will be studied. We will then present the numerical calculation of ΔF_{q} for large deformations of the sphere in

[4]For the scalar, preliminary follow-up numerical work in the non-axisymmetric case has thus far produced similar results to the axisymmetric case [99]: fixed sign differenced heat kernels that compute ΔF_{q}. Indeed, it appears that they give *lower* ΔF_{q} than their axisymmetric counterparts in the minimally-coupled case.

Section 5.5, focusing for simplicity on axisymmetric perturbations. Finding that F_{q} seems to decrease monotonically as the amplitude of the deformation is increased, in Section 5.6 we will analyse its behaviour on extremely deformed geometries, showing that approaching a conical singularity allows ΔF_{q} to become arbitrarily negative. Section 5.7 will round off the chapter with a summary of our main conclusions and unexpected results.

5.1 A Perturbative Example: Graphene

For illustrative purposes, let us now study in some more detail the competition between ΔF_{c} and ΔF_{q} for two-dimensional crystalline materials such as monolayer graphene, focusing on the case where (Σ, g) is a small deformation of a round sphere (for large deformations, this competition will be discussed in Section 5.6.4). We note there is considerable technological interest in producing *spherical* monolayer graphene (see for example [101]). As mentioned above, at scales much larger than the lattice spacing this crystal can be described as a smooth membrane, and the free energy will depend on the geometry of this membrane. For simplicity, we will further assume that this effective description is diffeomorphism invariant (although of course this is not expected to be the case for a crystalline material like graphene [86]).

For an order-of-magnitude estimate of perturbations to the round sphere, we also assume that the sphere minimises the classical bending contribution ΔF_{c} to the free energy. Keeping only up to second derivatives, we may then write the Landau free energy as

$$\Delta F_{\mathrm{c}} = \kappa \int \mathrm{d}^2x \, \sqrt{g} \left(K - \frac{2}{r_0} \right)^2 , \tag{5.1}$$

where K is the mean curvature of (Σ, g), κ is a bending rigidity, r_0 is the radius of the sphere that minimises ΔF_{c}, and no term containing the scalar curvature of g appears because such a term is topological. Working perturbatively around the sphere of radius r_0, we write the ambient flat space in the usual spherical coordinates

$$\mathrm{d}s^2_{\mathbb{R}^3} = \mathrm{d}r^2 + r^2 \left(\mathrm{d}\theta^2 + \sin^2\theta \, \mathrm{d}\phi^2 \right) \tag{5.2}$$

and take $\{\theta, \phi\}$ as coordinates on Σ and embed (Σ, g) as $r = r_0(1 + \varepsilon f(\theta, \phi))$, where ε is a dimensionless expansion parameter. To linear order in ε, the induced metric on (Σ, g) is in a gauge conformal to the round sphere,

$$\mathrm{d}s^2 = r_0^2 \left(1 + 2\varepsilon f\right) \left(\mathrm{d}\theta^2 + \sin^2\theta \, \mathrm{d}\phi^2 \right) + \mathcal{O}(\varepsilon^2), \tag{5.3}$$

while the free energy (5.1) becomes[5]

$$\Delta F_{\rm c} = \varepsilon^2 \kappa \int {\rm d}\theta \, {\rm d}\phi \, \sin\theta \left(2f + \overline{\nabla}^2 f\right)^2 + \mathcal{O}(\varepsilon^3), \tag{5.4}$$

where $\overline{\nabla}^2$ denotes the Laplacian on the round sphere of unit radius. We then decompose f in spherical harmonics as

$$f = \sum_{\ell,m} f_{\ell,m} Y_{\ell,m}, \tag{5.5}$$

with the condition that the volume of (Σ, g) remain unchanged imposing that $f_{0,0} = 0$. We thus obtain

$$\Delta F_{\rm c} = \varepsilon^2 \kappa \sum_{\ell,m} |f_{\ell,m}|^2 (\ell-1)^2 (\ell+2)^2 + \mathcal{O}(\varepsilon^3). \tag{5.6}$$

The general contribution of quantum scalar or Dirac fermionic fields to $\Delta F_{\rm q}$ is obtained in Section 5.3 below. To streamline the present analysis, let us take the relativistic quantum fields living on (Σ, g) to be a CFT; this is the case for graphene when it is slightly perturbed from a flat plane (additional gauge fields associated to the underlying lattice structure vanish when the the metric is in a conformally-flat form) [35–37, 42, 102]. Here we assume the effective CFT description remains valid for small perturbations of the round sphere. At zero temperature, the contribution of these degrees of freedom to $\Delta F_{\rm q}$ is as in Section 1.4:

$$\Delta F_{\rm q} = -\varepsilon^2 \frac{\pi^2 c_T \hbar c_{\rm eff}}{48 r_0} \sum_{\ell,m} |f_{\ell,m}|^2 \frac{(\ell^2-1)(\ell+2)}{\ell} \left(\frac{\Gamma\left(\frac{\ell+1}{2}\right)}{\Gamma\left(\frac{\ell}{2}\right)} \right)^2 + \mathcal{O}(\varepsilon^3), \tag{5.7}$$

where $c_{\rm eff}$ is the effective speed of light for these relativistic degrees of freedom and c_T is the central charge; in our conventions, the central charges of a conformally-coupled massless scalar field and of a massless Dirac fermion are $c_T = (3/2)/(4\pi)^2$ and $c_T = 3/(4\pi)^2$, respectively [95, 103]. Importantly, at large ℓ the coefficients in the sum grow like ℓ^3, indicating that this contribution is non-local: that is, unlike $\Delta F_{\rm c}$ it does not arise from some local geometric functional. Also note that while technically (5.7) is only valid at zero temperature, the leading corrections to it go like $\mathrm{e}^{-l_T^2/(2l)^2}$, where $l_T = \hbar c_{\rm eff}/(k_B T)$ is a thermal length scale and l is the typical length scale of the perturbation f; hence (5.7) holds for $l_T \gtrsim 2l$. (The corrections to the zero-temperature result will be discussed in Section 5.5.3.)

The combined contribution to the free energy from the classical and quantum

[5] Breaking diffeomorphism invariance would allow for more general coefficients in front of the f^2, $f\overline{\nabla}^2 f$, and $(\overline{\nabla}^2 f)^2$ terms.

contributions therefore goes like

$$\Delta F = \varepsilon^2 \frac{\kappa}{\bar{\beta}^2} \sum_{\ell,m} |f_{\ell,m}|^2 \left[A_\ell^{(\mathrm{c})} - \frac{\gamma}{r_0} A_\ell^{(\mathrm{q})} \right] + \mathcal{O}(\varepsilon^3), \tag{5.8}$$

where

$$\gamma \equiv \frac{\bar{\beta}^2 \pi^2 c_T \hbar c_{\mathrm{eff}}}{48\kappa} \tag{5.9}$$

is some characteristic length scale,

$$A_\ell^{(\mathrm{c})} \equiv (\ell-1)^2(\ell+2)^2, \qquad A_\ell^{(\mathrm{q})} \equiv \frac{(\ell^2-1)(\ell+2)}{\ell} \left(\frac{\Gamma\left(\frac{\ell+1}{2}\right)}{\Gamma\left(\frac{\ell}{2}\right)} \right)^2 \tag{5.10}$$

and we have introduced a factor of $\bar{\beta}$ to account for the fact that, for example, the Dirac fermions on graphene see a metric perturbation that is factor of $\bar{\beta} \approx 3.3$ larger than the true perturbation[6] [43]. We would like to investigate whether this combined expression can ever be *negative* in its regime of validity. This question can be investigated as follows: first note that at large ℓ, $A_\ell^{(\mathrm{c})}$ goes like ℓ^4 while $A_\ell^{(\mathrm{q})}$ only grows like ℓ^3, so the positive classical free energy will always dominate at sufficiently high angular momentum quantum number. We must, therefore, investigate the behaviour of the lowest modes[7]: $\ell = 0$ does not contribute since $f_{0,0} = 0$, while the contributions of $\ell = 1$ modes to both ΔF_{c} and ΔF_{q} vanish due to the fact that such deformations correspond to infinitesimal diffeomorphisms. However, since $A_\ell^{(\mathrm{c})}$ vanishes quadratically around $\ell = 1$ while $A_\ell^{(\mathrm{q})}$ only vanishes *linearly*, it is clear that for sufficiently small $\ell - 1 > 0$, $A_\ell^{(\mathrm{c})} - (\gamma/r_0) A_\ell^{(\mathrm{q})} < 0$. Since ℓ is an integer, making ΔF negative therefore requires this to be true a ll the way to $\ell = 2$, and hence

$$\gamma \geqslant \gamma_{\mathrm{crit}} \equiv \frac{A_{\ell=2}^{(\mathrm{c})}}{A_{\ell=2}^{(\mathrm{q})}} r_0 = \frac{32}{3\pi} r_0. \tag{5.12}$$

[6] We note that factor was (erroneously) omitted in [3] and we correct that here.

[7] We note that this is the opposite regime to the one we considered in the flat-space case. This is somewhat counterintuitive given that one expects the large-ℓ behaviour on a sphere to approach flat-space behaviour. The difference is owed to the fact that in the flat-space limit we must also take $r_0 \to \infty$ (while keeping ℓ/r_0 fixed). This limit eliminates the order ε^2 term considered here in ΔF_{q} i.e. this term is *not* present for deformations of the plane. Concretely, the flat-space embedding with height function $h(x,y)$ that decays to zero as $(x^2+y^2) \to \infty$ is obtained by setting $(x,y) = (r_0(\theta - \pi/2), r_0\phi)$, $f(\theta,\phi) = h(r_0(\theta-\pi/2), r_0\phi)/r_0$ and considering the limit in which $r_0/|h| \to \infty$ and $|\varepsilon| \ll 1$ with x and y fixed. In this limit, ΔF_{c} for the perturbed sphere (5.4) approaches that of the perturbed plane (3.36). In contrast, the leading correction to ΔF_{q} (5.7) is suppressed by a further factor of r_0^{-2} and so vanishes at order ε^2. Indeed, the (exact) induced metric due to an embedding of this form is

$$\mathrm{d}s^2 = r_0^2 \left(1 + 2\varepsilon f + \varepsilon^2 f^2\right) \left(\mathrm{d}\theta^2 + \sin^2\theta\, \mathrm{d}\phi^2\right) + r_0^2 \varepsilon^2 \partial_i f \partial_j f \mathrm{d}\theta^i \mathrm{d}\theta^j \to \left(\delta_{ij} + \varepsilon^2 \partial_i h \partial_j h\right) \mathrm{d}x^i \mathrm{d}x^j, \tag{5.11}$$

so the metric is perturbed at order ε^2 and thus ΔF_{q} is perturbed at order ε^4, matching the behaviour we saw when working directly in flat space. As well as being suppressed by a further factor of ε^2, this term grows faster at large-ℓ than its finite r_0 counterpart as its sourced by a metric perturbation that goes as $(\partial h)^2$ rather than h.

Since our analysis is only valid at scales well above the lattice spacing a, we also require $r_0 \gg a$, which implies $\gamma \gg a$.

For the particular case of graphene, typically the bending rigidity is taken as $\kappa \sim 1$ eV, $a \sim 2.5$ Å, $c_{\text{eff}} \sim 10^6$ m/s [87], and $c_T = 4 \times 3/(4\pi)^2$ (the factor of four coming from the four massless Dirac fermions that describe the effective electronic structure of graphene), from which one finds $\gamma/a \sim 0.4$ (note that the numerical prefactors matter: a purely-parametric estimate would give $\gamma/a \sim c_{\text{eff}}\hbar/a\kappa \sim 10$). Hence, for graphene it does not seem likely that the quantum effect we have identified can ever compete with the classical bending energy to render the round sphere unstable, even if one were to keep more careful track of the precise form of the Landau free energy. In the absense of fine-tuning, this result could have been expected: with no fine-tuning, the energy scale κ should be set by the lattice spacing and hence $\kappa \sim \hbar c_{\text{eff}}/a$, from which it would follow that γ/a is order unity[8]. We therefore interpret the condition $\gamma \gg a$ as the required fine-tuning of the membrane parameters (e.g. κ, c_{eff}) that makes it possible for ΔF_{q} to dominate over ΔF_{c}. Given the great current interest in monolayer graphene-like materials, conceivably such fine-tuned crystalline membranes could be engineered in a lab.

5.2 Setup

We consider thermal states of (2+1)-dimensional (unitary, relativistic) QFTs on the geometry $\mathbb{R} \times \Sigma$, where Σ is a two-dimensional manifold with spherical topology. The Euclidean continuation of this geometry is

$$\mathrm{d}s^2 = \mathrm{d}\tau^2 + g_{ij}(x)\mathrm{d}x^i\mathrm{d}x^j, \tag{5.13}$$

with the period of Euclidean time τ given by the inverse temperature $\beta = 1/T$, and we have made explicit the fact that the spatial metric $g_{ij}(x)$ on Σ is independent of τ. The free energy is thus a functional of g_{ij} and of β; to simplify notation, we will denote this free energy simply as $F[\beta, g]$ (i.e. without the subscript q as was used above).

5.2.1 Free Energy

In this chapter, our interest lies in the free energy of (2+1)-dimensional QFTs as a contribution to an effective action describing the geometry of its supporting membrane. This free energy, F, is determined by the Euclidean partition function Z, which will depend

[8] The large-ℓ scaling of $A_\ell^{(\text{q})}$, which is necessary for this argument to go through, can be inferred by noting that perturbations with large ℓ should be insensitive to the size of the sphere, and thus should behave as in flat space. Interpreting $k = \ell/r_0$ as a wave number for large ℓ, and knowing that ΔF_{q} is quadratic in the perturbation f, implies by dimensional analysis that ΔF_{q} must go like k^3.

on both β and the spatial geometry g_{ij}:

$$Z[\beta, g] = \int \mathcal{D}\Phi \, \mathrm{e}^{-S_{\mathrm{E}}[\beta,g,\Phi]} = \mathrm{e}^{-\beta F[\beta,g]}, \tag{5.14}$$

where S_{E} is the Euclidean action and Φ schematically stands for the QFT fields in the system. Of course, as written Z (and thus F) is UV divergent, so we must regulate it. Since we are only considering relativistic QFTs, any UV regulator (like, say, a lattice) cannot break diffeomorphism invariance in the IR, and hence for simplicity we may use a covariant UV regulator to ultimately compute UV-finite quantities. To that end, note that for a UV cutoff Λ, the most general covariant counterterms that can be added to the Euclidean action are

$$S_{\mathrm{CT}} = \int \mathrm{d}\tau \int \mathrm{d}^2x\sqrt{g} \, \left[c_1\Lambda^3 + c_2\mu\Lambda^2 + (c_3\mu^2 + c_4 R)\Lambda\right], \tag{5.15}$$

where μ schematically stands for any parameter in the QFT with dimensions of energy, if one exists (for instance, a mass), R is the Ricci scalar of g, and the theory-dependent coefficients c_i are dimensionless and independent of Λ and of the geometry. Hence, the most general divergence structure of the free energy takes the form

$$F[\beta, g] = \mathrm{Vol}[g](c_1\Lambda^3 + c_2\mu\Lambda^2 + c_3\mu^2\Lambda) + 4\pi c_4\chi(\Sigma)\Lambda + F_{\mathrm{fin}}[\beta, g], \tag{5.16}$$

where $\chi(\Sigma)$ is the Euler characteristic of Σ and $F_{\mathrm{fin}}[\beta, g]$ is finite as $\Lambda \to \infty$. Note in particular that the divergence structure depends on g only through the volume $\mathrm{Vol}[g]$ of Σ; in the context of two-dimensional crystalline lattices discussed at the beginning of this chapter one can think of these terms as contributing to some (UV-cutoff dependent) tension in the classical membrane action. In other words, we may interpret the volume-preservation condition as merely a convenient way of grouping the leading-order divergences in (5.16) with the couplings in the classical membrane action.

Physical information about the free energy is contained in the finite part F_{fin}, but this object is not uniquely defined by the expansion (5.16) (since a general change in the UV cutoff can induce a change in F_{fin}). However, the differenced free energy $\Delta F \equiv F[\beta, g] - F[\beta, \bar{g}]$ discussed in Sections 3.1 and 4.1 (in which $\bar{g}$ is a reference metric such that $\mathrm{Vol}[\bar{g}] = \mathrm{Vol}[g]$) *is* scheme-independent. This differenced free energy can be defined via

$$\mathrm{e}^{-\beta\Delta F} = \left\langle \mathrm{e}^{-\Delta S_{\mathrm{E}}} \right\rangle_{\bar{g}}, \tag{5.17}$$

where ΔS_{E} is the difference of the Euclidean actions constructed from g and $\bar{g}$ and the expectation value on the right-hand side is taken in the thermal vacuum state (of inverse temperature β) associated to the geometry $\bar{g}$. In short, the UV-finite differenced free energy defined in Section 4.22 is the appropriate physical measure of the free energy

contribution of relativistic quantum degrees of freedom on a membrane to its effective action.

5.2.2 Heat Kernels

Let us now restrict to the case where the QFT fields Φ are free. The free energy is then conveniently evaluated via heat kernel methods, as detailed in Section 3.1. The massive free scalar fields and Dirac fermions on which we focus have actions

$$S_{\mathrm{E}}[\phi] = \frac{1}{2}\int \mathrm{d}\tau \int \mathrm{d}^2x\sqrt{g}\,\phi(-\nabla^2 + \xi R + M^2)\phi, \tag{5.18a}$$

$$S_{\mathrm{E}}[\bar{\psi},\psi] = \int \mathrm{d}\tau \int \mathrm{d}^2x\sqrt{g}\,\bar{\psi}(i\not{D} - iM)\psi, \tag{5.18b}$$

where ξ is the curvature coupling of the scalar, M is a mass, and the spinor conventions are as in Chapter 3. As in Chapter 3, by performing the path integral on the geometry (5.13) one obtains

$$Z = (\det\mathcal{L})^{\sigma} \text{ with } \mathcal{L} = -\partial_\tau^2 + L + M^2, \tag{5.19}$$

where $\sigma = -1/2$ $(+1)$ for the scalar (fermion) and L is a differential operator on Σ. For the non-minimally-coupled scalar we have simply $L = -\nabla^2 + \xi R$, which acts on functions with spin weight zero. The case of the Dirac fermion is slightly more complicated and we will give the full expression for L in (5.35) below, but the key idea is that the square of the Dirac operator on the ultrastatic geometry (5.13) is diagonal in the spinor indices and L is one of these two diagonal components, which acts on functions of spin weight $1/2$.

Recall from Section 3.1, the differenced free energy can be obtained directly from the difference $\Delta K_{\mathcal{L}}(t)$ between heat kernels corresponding to the spatial geometries (Σ, g) and $(\Sigma, \bar{g})$:

$$\beta\Delta F = \sigma\int_0^\infty \frac{\mathrm{d}t}{t}\,\mathrm{e}^{-M^2t}\Theta_\sigma(T^2t)\Delta K_L(t), \tag{5.20}$$

and

$$\Theta_\sigma(\zeta) \equiv \sum_{n=-\infty}^{\infty} \mathrm{e}^{-(2\pi)^2(n-\sigma+1/2)^2\zeta}, \tag{5.21}$$

which arises from a sum over Matsubara frequencies on the thermal circle and that as long as (Σ, g) and $(\Sigma, \bar{g})$ have the same volume and topology, ΔF is UV finite. We will be concerned with the case where Σ is a topological sphere, in which case it is natural to take the reference metric $\bar{g}_{ij}$ to be that of a round sphere. Finally, we note that the heat kernel expansion (2.15) for $\Delta K_L(t)$ takes the form

$$\Delta K_L(t) \sim t\sum_{n=0}^{\infty}\Delta b_{2n+4}t^n, \tag{5.22}$$

where the Δb_{2n} are the differences of the heat kernel coefficients between the geometries (Σ, g) and $(\Sigma, \bar{g})$.

5.3 Perturbative Results

The expression (5.20) for the differenced free energy in terms of the heat kernel of L is convenient because it simply requires computing the variation in the spectrum of L as the spatial geometry g is varied:

$$\Delta K_L(t) = \mathrm{Tr}(\mathrm{e}^{-tL}) - \mathrm{Tr}(\mathrm{e}^{-t\overline{L}}) = \sum_I \left(\mathrm{e}^{-t\lambda_I} - \mathrm{e}^{-t\bar{\lambda}_I}\right), \tag{5.23}$$

where I indexes the eigenvalues of L and $\overline{L}$. An explicit computation of this perturbed heat kernel was performed for deformations of flat space in Chapter 3, with the key result being that for both the fermion and the scalar $\sigma\Delta K_L(t)$ is negative for all t to leading non-trivial order in the perturbation parameter (and hence ΔF is negative for all perturbations). In order to compare to our later results, we now repeat this calculation on the perturbed round sphere (5.24). We remind the reader that the reasons for working on the sphere are twofold: firstly, since the sphere is compact we do not have to deal with IR divergences; secondly, we will find that for small perturbations of the round sphere, the free energy of quantum fields is of the same order as the contribution from the classical membrane free energy, and hence the two can consistently be compared.

In this section, we will take the metric on Σ to be conformal to the round sphere, as in (5.3):

$$\mathrm{d}s^2 = \mathrm{e}^{2f}\left(\mathrm{d}\theta^2 + \sin^2\theta\,\mathrm{d}\phi^2\right), \tag{5.24}$$

where f is some scalar field on the sphere and we are using units in which $r_0 = 1$. We use the formulae derived in Section 3.2, from which we recall that we expand $f = \varepsilon f^{(1)} + \varepsilon^2 f^{(2)} + \mathcal{O}(\varepsilon^3)$, $L = \overline{L} + \varepsilon L^{(1)} + \varepsilon^2 L^{(2)} + \mathcal{O}(\varepsilon^3)$ and the perturbed heat kernel is

$$\Delta K_L(t) = \varepsilon\,\Delta K^{(1)}(t) + \varepsilon^2 \Delta K^{(2)}(t) + \mathcal{O}(\varepsilon^3). \tag{5.25}$$

The explicit expressions for $L^{(1)}$ and $L^{(2)}$ in terms of $f^{(1)}$ and $f^{(2)}$ are provided in Appendix A.5.

5.3.1 Scalar

For the scalar, the operator L for general f is

$$L = \mathrm{e}^{-2f}\left[-\overline{\nabla}^2 + 2\xi\left(1 - \overline{\nabla}^2 f\right)\right], \tag{5.26}$$

with $\overline{\nabla}$ the covariant derivative on the round sphere ($f = 0$). The unperturbed operator $\overline{L}$ is $-\overline{\nabla}^2 + 2\xi$ and has eigenvalues $\bar{\lambda}_\ell = \ell(\ell+1) + 2\xi$, with $\ell \in \{0, 1, 2, \ldots\}$ a non-negative integer. For the computation of the matrix elements $\widetilde{L}^{(n)}_{\ell,m,\ell',m'}$ (from Section 3.2), we may take the eigenfunctions $\tilde{h}_{\ell,m}$ to just be the usual spherical harmonics $Y_{\ell,m}$. Since the calculation is rather cumbersome and unilluminating, we relegate it to Appendix A.5; in short, expanding $f^{(1)}$ in spherical harmonics as

$$f^{(1)} = \sum_{\ell,m} f_{\ell,m} Y_{\ell,m}, \tag{5.27}$$

for the non-minimally-coupled scalar one ultimately obtains $\Delta K^{(1)} = 0$ and

$$\Delta K^{(2)}(t) = \sum_{\ell,m} a_\ell(t) |f_{\ell,m}|^2, \qquad a_\ell(t) \equiv t \sum_{\ell'=0}^{\infty} \mathrm{e}^{-\bar{\lambda}_{\ell'} t} \left(\alpha_{\ell,\ell'} + \beta_{\ell,\ell'} t\right), \tag{5.28}$$

with the general expressions for $\alpha_{\ell,\ell'}$ and $\beta_{\ell,\ell'}$ given in (A.52) and (A.55) in the Appendix. For the special case of odd ℓ, the expressions simplify substantially to[9]

$$\alpha_{\ell,\ell'} = \begin{cases} \dfrac{(2\ell'+1)(\bar{\lambda}_{\ell'} - \xi\ell(\ell+1))^2}{\pi\ell(\ell+1)} \dfrac{\left(\frac{2+\ell}{2}\right)_{\ell'} \left(\frac{\ell}{2}\right)_{-\ell'}}{\left(\frac{3+\ell}{2}\right)_{\ell'} \left(\frac{1+\ell}{2}\right)_{-\ell'}}, & \ell' < \dfrac{\ell}{2} \\ 0, & \ell' > \dfrac{\ell}{2} \end{cases}, \tag{5.29a}$$

$$\beta_{\ell,\ell'} = 0, \tag{5.29b}$$

where $(x)_n \equiv \Gamma(x+n)/\Gamma(x)$ are Pochhammer symbols. We will comment further on this expression in Section 5.3.5 below.

5.3.2 Dirac Fermion

For the benefit of the reader, let us briefly summarise how to obtain the operator L for the fermion; more details can be found in Appendix A.3. We first evaluate

$$(i\not{D} + iM)(i\not{D} - iM) = -D^2 + \frac{1}{4}R + M^2, \tag{5.30}$$

where $D_\mu = {}^{(3)}\nabla_\mu + \omega_{\mu ab} S^{ab}/2$ is the spinor covariant derivative, with ${}^{(3)}\nabla_\mu$ the usual Levi-Civita connection on the full (three-dimensional) Euclidean geometry, $\omega_{\mu ab}$ the spin connection, and S^{ab} the generators of the Lorentz group. Evaluating this object in the

[9] Technically this expression for $\alpha_{\ell,\ell'}$, as well as that given in (A.55) for general ℓ, was obtained by evaluating (A.54) (which expresses $\alpha_{\ell,\ell'}$ as a finite sum) for various values of ℓ, ℓ' and then inferring a closed-form formula by using built-in sequence finders in `Mathematica`. Although we have checked that the resulting formula is correct for all values of ℓ, ℓ' from zero to 100, we are unable to provide a general derivation.

ultrastatic geometry (5.13), one finds that it is diagonal in its spinor indices:

$$(i\not{D} + iM)(i\not{D} - iM) = \mathcal{L}P_{\mathrm{L}} + \mathcal{L}^* P_{\mathrm{R}}, \tag{5.31}$$

where $\mathcal{L}$ is the operator introduced in (5.19) and $P_{\mathrm{L,R}}$ are projectors onto left- and right-helicity Weyl spinors on the two-dimensional geometry (Σ, g); it is this decomposition that allows us to compute the fermion partition function from just the spectrum of the (non-spinorial) operator $\mathcal{L}$. The explicit form of the operator L defining $\mathcal{L}$ can be given most easily by working in conformally flat coordinates on (Σ, g),

$$\mathrm{d}s^2 = \mathrm{e}^{2\hat{f}} \left((\mathrm{d}x^1)^2 + (\mathrm{d}x^2)^2 \right), \tag{5.32}$$

in which case

$$L = -\nabla^2 + \frac{1}{4}R - i\varepsilon^{ij} \left(\partial_i \hat{f} \right) \partial_j + \frac{1}{4} \left(\nabla_i \hat{f} \right)^2. \tag{5.33}$$

The expression adapted to the spherical coordinates of (5.24) can be obtained easily by transforming from the conformally flat coordinates $\{x^1, x^2\}$ to the spherical coordinates $\{\theta, \phi\}$ via $\sin\theta = \operatorname{sech} x^1$, $\phi = x^2$; then since $\hat{f} = f + \ln\sin\theta$, in terms of the conformal factor f one ultimately obtains[10]

$$L = -\mathrm{e}^{-2f} \left[\overline{\nabla}^2 - \frac{1}{2} \left(1 - \overline{\nabla}^2 f \right) + i\bar{\varepsilon}^{ij} (\overline{\nabla}_i f) \overline{\nabla}_j + i \cot\theta \operatorname{cosec}\theta \, \partial_\phi \right.$$
$$\left. - \frac{1}{4} \left(\overline{\nabla}_i f \right)^2 - \frac{1}{2} \cot\theta \, \partial_\theta f - \frac{1}{4} \cot^2\theta \right], \tag{5.35}$$

where as before $\overline{\nabla}$ is the covariant derivative on the round sphere. L acts on functions with spin weight $1/2$, and hence the unperturbed eigenfunctions $\tilde{h}_{\ell,m}$ can be taken to be the spin-weighted spherical harmonics ${}_{1/2}Y_{\ell,m}$ of spin weight $1/2$, where $\ell \in \{1/2, 3/2, 5/2, \ldots\}$ is a positive half odd integer and as usual $m \in \{-\ell, -\ell+1, \ldots, \ell\}$. The corresponding unperturbed eigenvalues are $\bar{\lambda}_\ell = (\ell + 1/2)^2$.

Again, we relegate the details of the computation of the heat kernel to Appendix A.5; ultimately we obtain $\Delta K^{(1)} = 0$ and

$$\Delta K^{(2)}(t) = \sum_{\ell,m} a_\ell(t) |f_{\ell,m}|^2, \qquad a_\ell(t) \equiv t \sum_{\ell'=1/2}^{\infty} \mathrm{e}^{-\bar{\lambda}_{\ell'} t} \left(\alpha_{\ell,\ell'} + \beta_{\ell,\ell'} t \right), \tag{5.36}$$

with the expressions for $\alpha_{\ell,\ell'}$ and $\beta_{\ell,\ell'}$ given in (A.70). As for the scalar, taking ℓ to be

[10] A more covariant expression can be given by introducing the spin weight raising and lowering operators $\eth$, $\bar{\eth}$, in terms of which

$$L = -\mathrm{e}^{-2f} \left[\eth\bar{\eth} + \frac{1}{2} \left(\overline{\nabla}^2 f + (\bar{\eth} f)\eth - (\eth f)\bar{\eth} \right) - \frac{1}{4} (\overline{\nabla}_i f)^2 \right]; \tag{5.34}$$

more details are presented in Appendix A.5.

odd substantially simplifies them:

$$\alpha_{\ell,\ell'} = \begin{cases} -\dfrac{(2\ell'+1)^3}{16\pi} \dfrac{\left(\frac{2+\ell}{2}\right)_{\ell'+1/2}}{\left(\frac{1+\ell}{2}\right)_{\ell'+1/2}} \dfrac{\left(\frac{2+\ell}{2}\right)_{-(\ell'+1/2)}}{\left(\frac{1+\ell}{2}\right)_{-(\ell'+1/2)}}, & \ell' < \dfrac{\ell}{2} \\ 0, & \ell' \geqslant \dfrac{\ell}{2} \end{cases}, \tag{5.37a}$$

$$\beta_{\ell,\ell'} = 0. \tag{5.37b}$$

5.3.3 Check: Conformal Field Theories

As a simple check of our results, let us compare to the results of Section 1.4, which computed the zero-temperature perturbative energy difference $\Delta E^{(2)}$ for *any* unitary conformal field theory. There it was found that in any CFT, this leading-order energy difference is

$$\Delta E^{(2)}_{\text{CFT}} = -\sum_{\ell,m} A^{(\text{CFT})}_\ell |f_{\ell,m}|^2, \quad A^{(\text{CFT})}_\ell = \frac{\pi^2 c_T}{48} \frac{(\ell^2-1)(\ell+2)}{\ell} \left(\frac{\Gamma\left(\frac{\ell+1}{2}\right)}{\Gamma\left(\frac{\ell}{2}\right)} \right)^2, \tag{5.38}$$

with c_T the central charge.

We now show that our expressions (5.28) and (5.36) reproduce (5.38) with the correct central charges when the fields are conformal; we note that in this case, $\bar{\lambda}_{\ell'} = (\ell'+1/2)^2$ for both the scalar and the fermion (though the allowed values of ℓ' of course still differ). To do so, first note that the free energy difference is given by inserting (5.28) and (5.36) into (5.20); for simplicity we will restrict to perturbations $f_{\ell,m}$ with odd ℓ, so that we may use the more compact expressions (5.29) and (5.37). In the zero-temperature limit, the integral over t can be performed explicitly by noting that Poisson resummation gives (for both the scalar and the fermion)

$$\lim_{T\to 0} T\, \Theta_\sigma(T^2 t) = \frac{1}{\sqrt{4\pi t}} \tag{5.39}$$

for any $t > 0$; hence the zero-temperature perturbative energy difference for odd ℓ is

$$\Delta E^{(2)}|_{T=0} = -\sum_{\ell,m} A_\ell |f_{\ell,m}|^2, \tag{5.40}$$

where

$$A_\ell = -\frac{\sigma}{\sqrt{4\pi}} \int_0^\infty \frac{\mathrm{d}t}{t^{3/2}}\, a_\ell(t) = -\frac{\sigma}{2} \sum_{\ell'} \frac{\alpha_{\ell,\ell'}}{(\bar{\lambda}_{\ell'})^{1/2}}, \tag{5.41}$$

where we used the fact that the sum over ℓ' is finite to integrate term-by-term (it is understood that the sum over ℓ' runs over integers or half-integers depending on whether

we are considering the scalar or the fermion, with $\alpha_{\ell,\ell'}$ the corresponding expression; we also remind the reader that $\sigma = -1/2$ for the scalar and $\sigma = 1$ for the fermion). We therefore have

$$A_\ell^{(\text{scal})} = \frac{1}{2\pi} \sum_{\ell'=0}^{(\ell-1)/2} \frac{((\ell'+1/2)^2 - \ell(\ell+1)/8)^2}{\ell(\ell+1)} \frac{\left(\frac{2+\ell}{2}\right)_{\ell'} \left(\frac{\ell}{2}\right)_{-\ell'}}{\left(\frac{3+\ell}{2}\right)_{\ell'} \left(\frac{1+\ell}{2}\right)_{-\ell'}}, \tag{5.42}$$

$$A_\ell^{(\text{ferm})} = \frac{1}{4\pi} \sum_{\ell'=0}^{(\ell-1)/2} (\ell')^2 \frac{\left(\frac{2+\ell}{2}\right)_{\ell'} \left(\frac{2+\ell}{2}\right)_{-\ell'}}{\left(\frac{1+\ell}{2}\right)_{\ell'} \left(\frac{1+\ell}{2}\right)_{-\ell'}}, \tag{5.43}$$

where in the expression for $A_\ell^{(\text{ferm})}$ we shifted the index of summation by $1/2$. While we are unable to analytically show that these expressions reproduce the form (5.38) predicted by CFT perturbation theory, by computing these sums exactly we find that they do, with the correct central charges $c_T = (3/2)/(4\pi)^2$ and $c_T = 3/(4\pi)^2$ (we have checked up to $\ell = 1001$).

Interestingly, if ℓ is even then evaluating A_ℓ by integrating term-by-term produces a divergent sum, presumably due to the fact that the (now infinite) sum over ℓ' in $a_\ell(t)$ does not commute with the integration over t. Nevertheless, the behaviour of $a_\ell(t)$ for even ℓ makes clear that the integral is indeed finite when performed after the summation, and we have confirmed numerically that it reproduces (5.38) for a range of even ℓ.

5.3.4 Check: The Flat Space Limit

As a final check of our results, let us consider the limit in which the radius of the sphere is taken to be very large, and only modes with large ℓ, m are excited. In this limit, we expect the theory to be insensitive to the curvature of the sphere, and thus the heat kernel should reproduce its flat space behaviour. This behaviour was computed for both the scalar field and the Dirac fermion in Chapter 3, in which it was found that when the perturbed metric is in the conformally flat form $\mathrm{d}s^2 = \mathrm{e}^{2f}\delta_{ij}\mathrm{d}x^i\mathrm{d}x^j$, the perturbation to the heat kernel is

$$\Delta K^{(2)}(t) = t \int \mathrm{d}^2k\, k^4 \left|\tilde{f}(\mathbf{k})\right|^2 I(k^2 t), \tag{5.44}$$

where $\mathbf{k}$ is a wavevector defined by the Fourier decomposition of $f^{(1)}$ as

$$f^{(1)}(x) = \int \mathrm{d}^2k\, \tilde{f}(\mathbf{k}) \mathrm{e}^{i\mathbf{k}\cdot\mathbf{x}}, \tag{5.45}$$

$k = |\mathbf{k}|$ is its magnitude, and the functions $I(\zeta)$ are given for the scalar and fermion as

$$I(\zeta) = \begin{cases} -\frac{\pi}{4\zeta^2}\left[6 + \zeta(1-8\xi) \right. \\ \qquad \left. - \left(6 + 2\zeta(1-4\xi) + \frac{\zeta^2}{2}(1-4\xi)^2\right)\mathcal{F}\left(\frac{\sqrt{\zeta}}{2}\right)\right], & \text{scalar} \\ \frac{\pi}{4\zeta^2}\left[(6+\zeta)\,\mathcal{F}\left(\frac{\sqrt{\zeta}}{2}\right) - 6\right], & \text{fermion} \end{cases} \tag{5.46}$$

with $\mathcal{F}(\zeta) = \zeta^{-1}\mathrm{e}^{-\zeta^2}\int_0^\zeta \mathrm{d}\zeta'\,\mathrm{e}^{(\zeta')^2}$.

We now introduce an appropriate flat-space scaling limit in which our expressions for $\Delta K^{(2)}$ reproduce (5.44). To do so, let us explicitly reintroduce the radius r_0 of the sphere, so that the deformed sphere metric (5.24) becomes

$$\mathrm{d}s^2 = r_0^2\mathrm{e}^{2f}\left(\mathrm{d}\theta^2 + \sin^2\theta\,\mathrm{d}\phi^2\right). \tag{5.47}$$

The scaling limit is defined by "zooming in" on a point on the equator of the sphere by introducing new coordinates $x = r_0(\theta - \pi/2)$, $y = r_0\phi$ and then taking the limit $r_0 \to \infty$ with x, y held fixed. The resulting metric is in the desired conformally flat form,

$$\mathrm{d}s^2 \to \mathrm{e}^{2f}\left(\mathrm{d}x^2 + \mathrm{d}y^2\right), \tag{5.48}$$

with x and y having infinite range. Restoring r_0 to the expressions (5.28) and (5.36), we obtain

$$\Delta K^{(2)}(t) = \sum_{\ell,m} a_\ell(t)|f_{\ell,m}|^2, \qquad a_\ell(t) = \frac{t}{r_0^2}\sum_{\ell'}\mathrm{e}^{-\bar{\lambda}_{\ell'}t/r_0^2}\left(\alpha_{\ell,\ell'} + \beta_{\ell,\ell'}\frac{t}{r_0^2}\right), \tag{5.49}$$

with $\alpha_{\ell,\ell'}$ and $\beta_{\ell,\ell'}$ unchanged. Now let us again focus on the case where $f^{(1)}$ only contains modes with odd ℓ, so $\beta_{\ell,\ell'}$ vanishes and the sum over ℓ' runs to $\ell/2$. In order to consider modes with large ℓ, we define $k = \ell/r_0$ and $k' = \ell'/r_0$ and keep k and k' fixed as we take $r_0 \to \infty$. As we show in Appendix A.6, in this limit we find that

$$a_{r_0k}(t) \to \frac{r_0^2\,t}{4\pi^2}\,k^4 I(k^2t) \tag{5.50}$$

with $I(\zeta)$ precisely the functions given in (5.46); assuming $a_{r_0k}(t)$ is continuous in k in this scaling limit, we may now remove the restriction to modes with odd r_0k. We also find that as long as $f^{(1)}(x,y)$ vanishes at large (x,y) (i.e. $f^{(1)}(\theta,\phi)$ vanishes away from $(\theta = \pi/2, \phi = 0)$), $f_{\ell,m} = f_{r_0k,r_0k_y}$ becomes

$$f_{r_0k,r_0k_y} \to \frac{2\pi}{r_0^2}\frac{\sqrt{k}}{(k^2-k_y^2)^{1/4}}\left(\tilde{f}(\sqrt{k^2-k_y^2},k_y) \pm \tilde{f}(-\sqrt{k^2-k_y^2},k_y)\right), \tag{5.51}$$

where $\tilde{f}(k_x, k_y)$ is the Fourier transform of $f^{(1)}(x, y)$, the upper (lower) signs correspond to even (odd) $(k + k_y)r_0$, and we are neglecting an overall phase that will cancel out. Inserting these expressions into (5.49) and decomposing the sum over $\ell = kr_0$ into sums over even and odd kr_0, we finally obtain precisely the flat-space expression (5.44) given in Chapter 3:

$$\Delta K^{(2)} \to t \int \mathrm{d}^2k\, k^4 I(k^2 t) \left|\tilde{f}(\mathbf{k})\right|^2 . \tag{5.52}$$

We note this result supports the claim we made in Chapter 4 (based on the long-wavelength behaviour of free energy difference) that we may view the flat-space ΔF we defined there as giving the short-distance response of the thermal vacuum energy on scales that are small relative to the characterstic curvature scale of the space that has been deformed.

It is perhaps worth emphasising that computing the perturbation to the free energy of a perturbation of flat space is rather subtle due to the requirement that the perturbed and unperturbed geometries have the same volume: since the volume of flat space is infinite, an IR divergence is introduced, and the volume-preservation condition is interpreted as controlling this IR divergence to yield a finite differenced free energy. In Chapter 3, this problem was addressed by computing the heat kernel on a torus and then taking the limit in which the cycles of the torus go to infinity; this is analogous to the procedure performed here, where we computed the heat kernel on the sphere and then took a flat-space scaling limit. In these regularisation schemes, the 'extra' bits of the torus or the sphere that get sent to infinity in the flat space limit essentially deform in such a way as to ensure that the leading-order UV divergences in (5.16) cancel out between the deformed and undeformed geometries. It is, however, possible to ensure that the UV-divergent terms in (5.16) cancel out even without such a compactification: as shown in Chapter 4, one can introduce a one-parameter family of large diffeomorphisms on flat space (that is, diffeomorphisms that do not vanish in the asymptotic region) in order to ensure that the differenced free energy is UV and IR finite.

Though the final result obtained in the flat-space limit of both the torus and the sphere is the same, we note the interesting difference that on the finite-size torus, the Dirac fermion has a negative mode for which ΔK_L does *not* have fixed sign, and in fact even renders ΔF *positive*[11]; as we now discuss, this is not the case for the sphere.

[11] Explicitly, consider the deformed torus $\mathrm{d}s^2 = \mathrm{e}^{2f}[(\mathrm{d}x^1)^2 + (\mathrm{d}x^2)^2]$, where x^1 and x^2 both have periodicity Δx, and we take $f = \varepsilon \cos(2\pi x^1/\Delta x) + \mathcal{O}(\varepsilon^2)$. The perturbative heat kernel for the Dirac fermion on a deformed torus is computed in Chapter 3, and in this case comes out to be

$$\Delta K^{(2)} = -2t \left(\frac{2\pi}{\Delta x}\right)^2 \sum_{n_1, n_2 \in \mathbb{Z}} \mathrm{e}^{-(2\pi/\Delta x)^2 (n_1^2 + n_2^2) t} \left(\frac{(n_1^2 + n_2^2 - 1/4)^2 + n_2^2/4}{2n_1 - 1} + \frac{1}{16} \right). \tag{5.53}$$

This expression is positive for $t > t_*$ for some t_*, and with $T = 0$, $M = 0$ the differenced free energy (5.20) comes out positive as well.

5.3.5 Negativity of ΔK

Our results imply that for any non-trivial deformation of the round sphere, $\sigma\Delta K$ is strictly negative for all t to leading non-trivial order in ε (because $\sigma a_\ell(t)$ is) and thus ΔF is too. This is easiest to see when $f^{(1)}$ contains only modes with odd ℓ: in this case, it is clear from the expressions (5.29) and (5.37) that $\sigma\alpha_{\ell,\ell'}$ is negative when ℓ is odd and greater than one, and hence so too is $\sigma\Delta K^{(2)}(t)$ for all t (recall that $\sigma = -1/2$ for the scalar and $\sigma = 1$ for the fermion). When $\ell = 1$, $a_\ell(t) = 0$ for both the scalar and the fermion, and hence $\Delta K^{(2)}$ vanishes; this is due to the fact that $\ell = 1$ deformations generate infinitesimal diffeomorphisms of the sphere and therefore do not change its intrinsic geometry to leading order in ε. We will show this explicitly in Section 5.5.2.

The case of even ℓ is more subtle. For the scalar, it follows from the full expression (A.55) that $\sigma\alpha_{\ell,\ell'}$ can be *positive* for $\ell' \geqslant \ell/2$; likewise, for the fermion it follows from (A.70b) that $\sigma\beta_{\ell,\ell'}$ is positive. Hence, in both cases the sign of $a_\ell(t)$ is not immediately clear. However, note that the large-ℓ behaviour of $a_\ell(t)$ can be obtained in the flat-space scaling limit discussed above, and is given in (5.50); assuming $a_{r_0 k}(t)$ is continuous in k as $r_0 \to \infty$, we therefore conclude that for all large ℓ (whether even or odd), $\sigma a_\ell(t)$ is negative. We therefore need only investigate the sign of $\sigma a_\ell(t)$ for small even ℓ (i.e. before the transition to the flat-space behaviour). The result is shown in Figure 5.1, which verifies that $\sigma a_\ell(t) < 0$ for all t.

Thus $\sigma\Delta K_L^{(2)}(t)$ is indeed negative for all t. This implies, of course, that small, non-trivial deformations of the round sphere all lower the free energy of the scalar and of the fermion (for any mass, temperature, and curvature coupling), but it is in fact a much stronger result: negativity of ΔF *does not* require that the heat kernel $\Delta K_L(t)$ itself be everywhere negative. We now investigate whether this stronger result continues to hold even for large volume-preserving deformations of the sphere. To probe $\Delta K_L(t)$ at values of t that cannot be accessed analytically, it is essential we obtain highly-accurate estimates for the eigenvalues of L. This is made possible by pseudo-spectral methods, which we review in following section.

5.4 Review: Pseudo-Spectral Methods

Pseudo-spectral methods are a class of techniques for solving differential equations numerically. In contrast with finite difference methods, they are *global methods* — they use information about a function on the entirety of its domain to estimate its derivatives. Given that derivatives are determined by the local behaviour of a function, it seems counterintuitive to use function values from the whole domain to estimate them. Done in the right way, however, such methods can achieve far better global accuracy for a commensurate number of grid points. This global accuracy is key to our hope of numerically

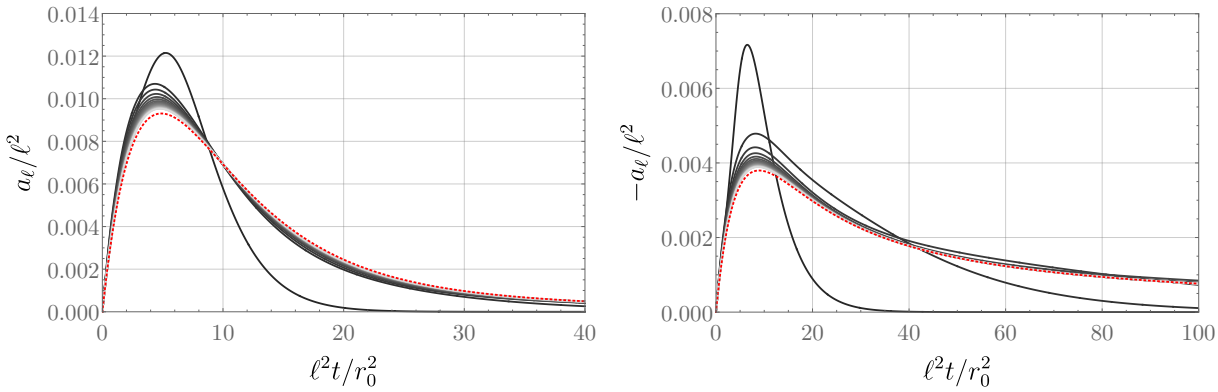

(a) Minimally-coupled scalar

(b) Fermion

Figure 5.1: The function $a_\ell(t)$ for even ℓ for the minimally-coupled scalar (left) and the Dirac fermion (right); from dark to light grey, the curves correspond to $\ell = 2$ to $\ell = 40$. The dashed red curve is the flat-space limit given by (5.50). The convergence of $a_\ell(t)$ to the flat-space limit for the non-minimally-coupled scalar is analogous.

approximating the heat kernels of free quantum field theories where it is essential that very accurate estimates of eigenvalues are used. In this section, we will detail how pseudo-spectral methods can be used to accurately estimate the eigenvalues of second-order linear ordinary differential operators subject to boundary conditions, using as an example the case of a compact non-periodic domain. The practical application of these methods are covered extensively in [104] and the particular case of Chebyshev interpolation on compact non-periodic domains we will review in this section will merely touch upon the content in [105, 106].

5.4.1 Interpolation

To numerically solve a differential equation on a continuous interval, some kind of discretisation procedure must be undertaken. In pseudo-spectral methods, functions are sampled at a finite number of points in their domains and that data alone is used to construct an appropriate approximating function. There are a variety of ways to do this. For example, for a function of a periodic domain one may take the approximating function to be the truncated Fourier series. Alternatively, one could instead work with the finite Fourier sum that interpolates the function i.e. with Fourier coefficients that are the discrete Fourier transform (DFT) of the function values. This function is then used to obtain globally accurate estimates for the function and its derivatives on the whole domain. Here we will work with an interpolating function. The optimal method of interpolation depends on a number of factors such as, for example, whether the domain is compact, whether the domain is periodic and any boundary conditions. We will consider a domain which is non-periodic and compact. Other cases include periodic domains that are best served by the DFT of the function sampled on a uniform grid [107].

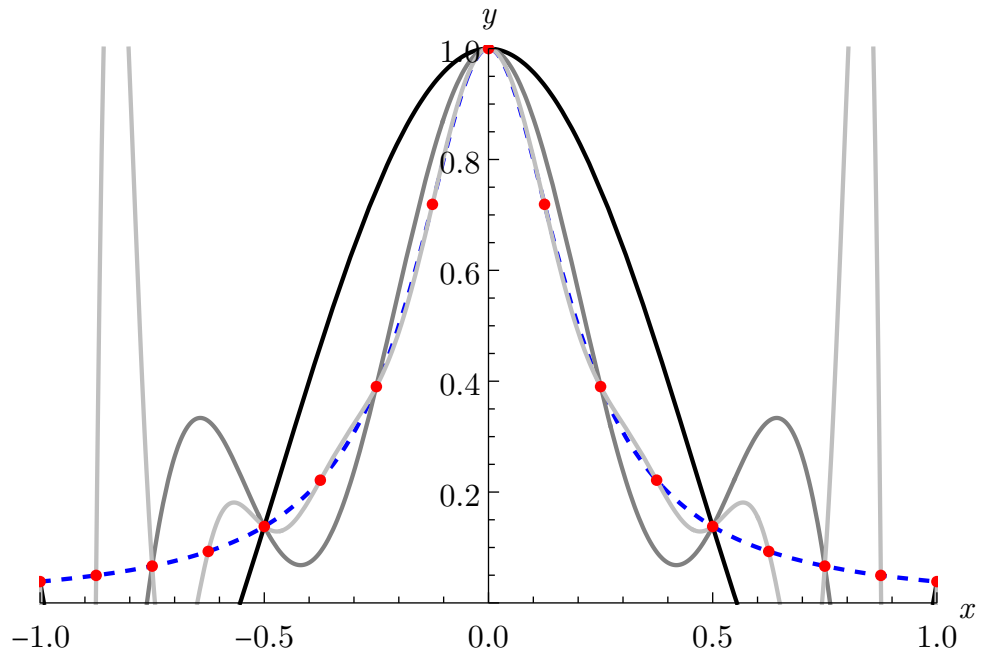

Figure 5.2: The plots of the Runge function (5.55) and its interpolants $p_4(x), p_8(x)$ and $p_{16}(x)$ (5.54) for uniform grid; from dark to light grey, the solid curves correspond to $N = 4, 8$ and 16. The dashed blue curve is $f(x)$ and the red dots are points on this curve for a uniform grid with 16 points.

Let $f : [-1, 1] \to \mathbb{R}$ be a smooth function. Suppose we wish to approximate this function using a polynomial. Given $N + 1$ distinct points $1 \geqslant x_0 > x_1 > \ldots > x_{N-1} > x_N \geqslant -1$ there is a unique degree N polynomial that interpolates $\{(x_i, f(x_i))\}_{i=0}^N$, namely

$$p_N(x) = \sum_{i=0}^{N} f(x_i) C_i(x) \tag{5.54}$$

where $C_i(x) \equiv \prod_{j \neq i} \frac{x - x_j}{x_i - x_j}$ is the degree N Cardinal polynomial satisfying $C_i(x_j) = \delta_{ij}$. This gives an efficient mapping between f and the data that determines its interpolant. Moreover, as long as we use the same basis functions, such as Cardinal polynomials for a non-periodic interval, the approximations of the derivatives of f at the grid can be expressed as a function independent linear map on the function values at the grid points. This gives a computationally efficient method for mapping a linear differential operator to a matrix equation. However, it remains to be seen whether these approximations are accurate. Indeed, if we were to use a uniform grid then we could encounter the *Runge Phenomenon*. We will illustrate this with an example. Consider the Runge function

$$f(x) = \frac{1}{1 + 25x^2}. \tag{5.55}$$

This function and its interpolants p_4, p_8 and p_{16} can be seen in Figure 5.2. Note that as the grid is refined the interpolating polynomials, while becoming better approximations

in the centre of the domain, begin to oscillate wildly near its boundaries and so become a very poor approximation to the function and its derivatives. This behaviour gets even worse as $N \to \infty$. It can be shown that, provided we select a uniform grid,

$$\lim_{N\to\infty} \|f(x) - p_N(x)\|_\infty = \infty, \tag{5.56}$$

where $\|\cdot\|_\infty$ is the uniform norm on $[-1,1]$ [108]. In order to compute the spectra of differential operators it is important that our approximations work well *globally*. To minimise the error, we turn to the Cauchy Error Theorem[12] which gives that

$$f(x) - p_N(x) = \frac{f^{(N+1)}(\xi(x))}{(N+1)!}\prod_{i=0}^{N}(x - x_i) \tag{5.58}$$

where $\xi(x) \in (-1,1)$ depends on f. From this, it is clear that the optimal grid is the one that minimises $\left\|\prod_{i=0}^{N}(x-x_i)\right\|_\infty$. It follows from Chebyshev's equioscillation theorem that a monic polynomial of degree $\leqslant N+1$ that minimises the uniform norm is $2^{-N}T_{N+1}(x)$ where $T_{N+1}(x)$ is the Chebyshev polynomial of the first kind. Thus, an optimal choice for the grid points are the roots of the Chebyshev polynomials of the first kind,

$$x_i = \cos\left(\frac{\pi(2i+1)}{2(N+1)}\right) \text{ where } i = 0, 1, \ldots, N. \tag{5.59}$$

For problems involving boundary conditions — like the one we wish to solve — it is helpful to choose a grid that includes the boundary points. Thus, for the rest of this section we will instead use the (closely-related) locations of the extrema of the Chebyshev polynomials: the Chebyshev-Gauss-Lobatto (CGL) points,

$$x_i = \cos\left(\frac{\pi i}{N}\right) \text{ where } i = 0, 1, \ldots, N. \tag{5.60}$$

In the following section, we will show how using them achieves *spectral accuracy*.

5.4.2 Spectral Accuracy

A key feature of pseudo-spectral methods is that they are very accurate, with their approximations converging to true values at an exponential rate as $N \to \infty$. We will show explicitly that this is the case for smooth functions on $[-1,1]$ when interpolating through

[12] This follows from (iteratively) applying Rolle's Theorem between the $N+2-k$ roots of the k^{th} derivative of the function

$$\Delta(x') \equiv f(x') - p_N(x') - c(x)\prod_{i=0}^{N}(x' - x_i) \tag{5.57}$$

for $k = 0, 1, \ldots, N$, where $x \in [-1,1] \setminus \{x_i\}$ and $c(x) = (f(x) - p_N(x))/\prod_{i=0}^{N}(x - x_i)$ is chosen so that $\Delta(x) = 0$, giving that there exists some $\xi(x) \in (-1,1)$ such that $\Delta^{(N+1)}(\xi(x)) = 0$, hence the result.

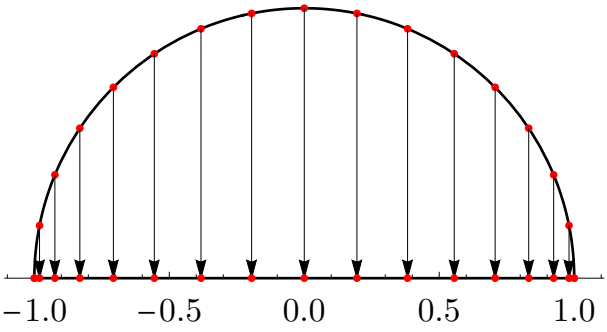

Figure 5.3: A diagram showing the distribution of Chebyshev-Gauss points (5.59) on the interval $[-1, 1]$ with $N = 16$.

CGL points, but the method and results are mirrored in other examples e.g. the discrete Fourier transform on a periodic domain.

Chebyshev polynomials of the first kind are a basis for Lipschitz continuous functions on $[-1, 1]$. Therefore, there exist unique $(\alpha_n)_{n=0}^{\infty}$ such that

$$f(x) = {\sum_{n=0}^{\infty}}' \alpha_n T_n(x). \tag{5.61}$$

where $\sum'$ denotes that the first term is halved. The coefficients $(\alpha_n)_{n=0}^{\infty}$ are given explicitly in terms of f by

$$\alpha_n = \frac{1}{\pi}(2 - \delta_{n,0}) \int_{-1}^{1} \frac{\mathrm{d}x}{\sqrt{1-x^2}} f(x) T_n(x). \tag{5.62}$$

The Chebyshev polynomials of degree $\leqslant N$ form a basis for polynomials of degree $\leqslant N$ so there exist unique $\{a_n\}_{n=0}^{N}$ satisfying

$$p_N(x) = {\sum_{n=0}^{N}}'' a_n T_n(x) \tag{5.63}$$

where $\sum''$ denotes that the first and last terms are halved. The two sets of coefficients are related by[13]

$$a_n = \alpha_n + \sum_{j=1}^{\infty} \left(\alpha_{n+2jN} + \alpha_{-n+2jN} \right). \tag{5.64}$$

Using also that $|T_n^{(k)}(x)| \leqslant n^{2k}$ for $0 < k < N/2$, it follows that p_N estimates f and its derivatives with error

$$\|f^{(k)} - p_N^{(k)}\|_{\infty} \leqslant 2 \sum_{n=N+1}^{\infty} |\alpha_n| n^{2k}. \tag{5.65}$$

Just as with Fourier transforms, the coefficients α_n decay very quickly for smooth functions. Indeed, by writing $x = \cos\theta$ and $F(\theta) \equiv f(\cos\theta)$ in (5.62) and integrating by

[13] This can be verified by evaluating p_N at each of the $N + 1$ CGL points and checking agreement with (5.61) using the fact that $T_{2jN \pm n}(\cos(\pi i/N)) = \cos(\pi n i/N) = T_n(\cos(\pi i/N))$.

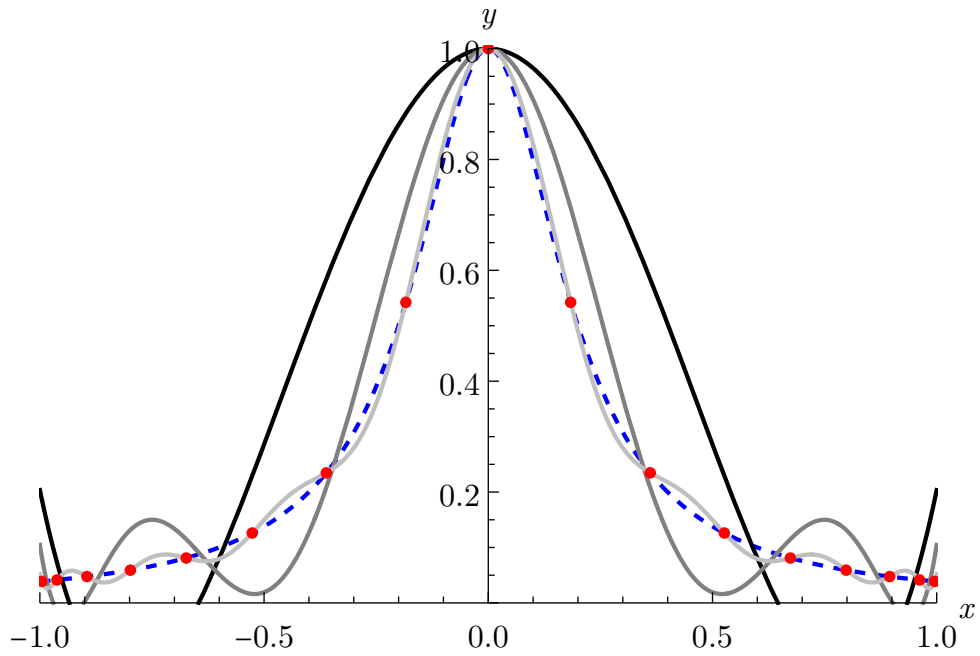

Figure 5.4: The plots of the Runge function (5.55) and its interpolants $p_4(x), p_8(x)$ and $p_{16}(x)$ (5.54) for a Chebyshev-Gauss grid ; from dark to light grey, the solid curves correspond to $N = 4, 8$ and 16. The dashed blue curve is $f(x)$ and the red dots are points on this curve for a Chebyshev-Gauss grid with 16 points.

parts m times gives that

$$\alpha_n = \frac{(-1)^m}{n^m}\frac{1}{\pi}(2-\delta_{n,0})\int_0^\pi \mathrm{d}\theta F^{(m)}(\theta)\begin{cases}\sin n\theta, \ m \text{ odd}\\ \cos n\theta, \ m \text{ even}\end{cases} \tag{5.66}$$

and therefore $\alpha_n = \mathcal{O}(n^{-m})$ for all $m \geqslant 0$ as $n \to \infty$. This gives that polynomial interpolation of a smooth function using $N+1$ CGL points yields an approximation that satisfies

$$\|f^{(k)} - p_N^{(k)}\|_\infty = \mathcal{O}(N^{-m}) \text{ for } k, m = 0, 1, 2, \ldots \tag{5.67}$$

This exceptionally fast *uniform* convergence of p_N and its derivatives to f is the real strength of spectral methods — allowing us to obtain *globally* accurate estimates with high accuracy. We will now turn our focus to numerical implementation.

5.4.3 Differentiation Matrices

Having shown that pseudo-spectral methods can accurately approximate the derivatives of smooth functions, we now show how to take advantage of this numerically to solve for eigenvalues of second-order linear differential operators.

We seek eigenvalues of a differential operator, $\mathcal{L} : \mathcal{C}^\infty([-1,1]) \to \mathcal{C}^\infty([-1,1])$, with

Robin boundary conditions:

$$\mathcal{L}u = p(x)\frac{\mathrm{d}^2u}{\mathrm{d}x^2} + q(x)\frac{\mathrm{d}u}{\mathrm{d}x} + r(x)u(x) \text{ with } \begin{array}{rl} a_{-1}u(-1) + b_{-1}u'(-1) & = 0 \\ a_1u(1) + b_1u'(1) & = 0. \end{array} \tag{5.68}$$

By working with a pseudo-spectal approximation to u, we can map this to a numerically tractable matrix eigenvalue problem. Firstly, we sample $u(x)$ at a set of appropriate grid points, in this case $N+2$ CGL points, and write them in a column vector[14]:

$$\bar{\mathbf{u}} = \begin{pmatrix} u_0 \\ u_1 \\ \vdots \\ u_{N+1} \end{pmatrix} \text{ where } u_I \equiv u(x_I) \tag{5.69}$$

For the remainder of the section upper-case Latin letters will be assumed to range from 0 to $N+1$ and lower-case Latin letters from 1 to N. Each component of the differential operator can then be expressed as a linear map on the vector $\bar{\mathbf{u}}$. The pointwise multiplication by a function $g(x)$ maps to matrix multiplication by $G_{IJ} = \delta_{IJ}g(x_J)$ (no sum). Derivatives are more subtle and depend on the grid chosen and the boundary conditions. In this case, the pseudo-spectral approximation to the derivative of u at the CGL points is $p_{N+1}(x)$ and so the differentiation matrix $\bar{D}$ is defined by

$$\sum_{j=0}^{N+1} \bar{D}_{IJ}u_J \equiv p'_N(x_I) = \sum_{J=0}^{N+1} u_J C'_J(x_I) \tag{5.70}$$

so that the derivative operator is represented by matrix multiplication by the differentiation matrix

$$\bar{D}_{IJ} = C'_J(x_I) = \sum_{M\neq J} \frac{1}{x_J - x_M} \prod_{K\neq M,J} \frac{x_I - x_K}{x_J - x_K} \text{ where } x_I = \cos\left(\frac{\pi I}{N+1}\right) \tag{5.71}$$

The boundary conditions are then used to eliminate u_0 and u_{N+1} as

$$(a_{-1} + b_{-1}\bar{D}_{0,0})u_0 + b_{-1}\bar{D}_{0,N+1}u_{N+1} = -\sum_{j=1}^{N} \bar{D}_{0,j}u_j \tag{5.72}$$

$$b_1\bar{D}_{N+1,0}u_0 + (a_1 + b_1\bar{D}_{N+1,N+1})u_{N+1} = -\sum_{j=1}^{N} \bar{D}_{N+1,j}u_j. \tag{5.73}$$

This degeneracy is then used to reduce this $(N+2)\times(N+2)$ matrix problem to an $N\times N$

[14]We will later wish to consider a reduced grid consisting of the N interior points of the grid given by the $N+2$ CGL points. To this end, we will denote quantities defined the extended grid with 'bars' to distinguish them from quantities defined only on the interior points.

one. Let $\mathbf{u} = (u_i)$. Solving the linear system to express u_0 and u_{N+1} as linear functions of $\mathbf{u}$ so that $u_I = A_{Ij}u_j$ for $I = 0, N+1$ and inserting that back into the derivative operator then gives a new $N \times N$ matrix which incorporates the boundary conditions. This new differentiation matrix is defined by $(D\mathbf{u})_{1\leqslant i\leqslant N} \equiv (\bar{D}\bar{\mathbf{u}})_{1\leqslant i\leqslant N}$ and given explicitly by

$$D_{ij} = \bar{D}_{ij} + \bar{D}_{i,0}A_{0,j} + \bar{D}_{i,N+1}A_{N+1,j} \tag{5.74}$$

where

$$A_{0,j} = \frac{b_{-1}\bar{D}_{0,N+1}\bar{D}_{N+1,j} - (a_1 + b_1\bar{D}_{N+1,N+1})\bar{D}_{0,j}}{(a_{-1} + b_{-1}\bar{D}_{0,0})(a_1 + b_1\bar{D}_{N+1,N+1}) - b_{-1}\bar{D}_{0,N+1}b_1\bar{D}_{N+1,0}} \tag{5.75}$$

$$A_{N+1,j} = \frac{b_1\bar{D}_{N+1,0}\bar{D}_{0,j} - (a_{-1} + b_{-1}\bar{D}_{0,0})\bar{D}_{N+1,j}}{(a_{-1} + b_{-1}\bar{D}_{0,0})(a_1 + b_1\bar{D}_{N+1,N+1}) - b_{-1}\bar{D}_{0,N+1}b_1\bar{D}_{N+1,0}}. \tag{5.76}$$

Similarly, the second derivative operator is given by

$$D^{(2)}_{ij} = \bar{D}^{(2)}_{ij} + \bar{D}^{(2)}_{i,0}A_{0,j} + \bar{D}^{(2)}_{i,N+1}A_{N+1,j} \tag{5.77}$$

where $\bar{D}^{(2)}_{IJ} = C''_J(x_I)$. Thus the eigenvalues of $\mathcal{L}$ with the associated boundary conditions (5.68) are approximated by the eigenvalues of the matrix

$$L = PD^{(2)} + QD + R \tag{5.78}$$

where P_{ij}, Q_{ij} and R_{ij} are given by $p(x_i)\delta_{ij}, q(x_i)\delta_{ij}$ and $r(x_i)\delta_{ij}$ (no sum), respectively. By using the formula

$$\bar{D}_{00} = \frac{2N^2+1}{6},\ \bar{D}_{NN} = -\frac{2N^2+1}{6}, \tag{5.79}$$

$$\bar{D}_{JJ} = -\frac{x_J}{2(1-x_J^2)},\ J = 1, \ldots, N-1, \tag{5.80}$$

$$\bar{D}_{IJ} = \frac{c_I}{c_J}\frac{(-1)^{I+J}}{(x_I - x_J)},\ I \neq J,\ I, J = 0, \ldots N \tag{5.81}$$

for the order $N+1$ Chebyshev differentiation matrix [109], where $c_I = 1 + \delta_{I,0} + \delta_{I,N}$, Chebyshev differentiation matrices and hence matrix approximations to differential operators can be generated efficiently. The differentiation matrices for arbitrary intervals can then be derived from $\bar{D}^{(n)}_{IJ}$ via a rescaling.

The same procedure can be used to derive the differentiation matrices for other pseudo-spectral approximation schemes. The differentiation matrices they derive are usually available within packages for most high-level programming languages. For example, the 'MATLAB Differentiation Suite' developed by Weideman and Reddy [110] consists of functions that output differentiation matrices for Fourier, Chebyshev and Hermite interpolation. The Chebyshev differencing found there and in `Mathematica` will prove an

essential tool for probing the differenced heat kernel beyond the perturbative regime considered thus far.

5.5 Non-perturbative Results

In Section 5.3, we found that small perturbations of the round sphere always yield a negative $\sigma\Delta K_L(t)$ (and hence also free energy ΔF) for both the scalar and fermion at any temperature, mass, or curvature coupling. This observation naturally prompts a question: is the free energy maximised *globally* by the round sphere, as it is for holographic CFTs at zero temperature, as detailed in Section 1.3? Or do there exist sufficiently large deformations of the round sphere at which the free energy eventually increases above its value on the round sphere? If the free energy is globally maximised, does the stronger result that the differenced heat kernel has fixed sign continue to hold? Our purpose now is to examine these questions. To do so, we will ultimately need to use numerics in order to evaluate the heat kernel (3.13) for large deformations of the round sphere. However, we will first examine the behaviour of $\Delta K_L(t)$ at large and small t, which is tractable analytically even for large deformations.

5.5.1 Heat Kernel Asymptotics

Recall that the small-t behaviour of the differenced heat kernel is given by the heat kernel expansion (5.22):

$$\Delta K_L(t) = t\,\Delta b_4 + \mathcal{O}(t^2). \tag{5.82}$$

The leading-order coefficient Δb_4 is given by (2.2)

$$\Delta b_4^{(\text{scal})} = \frac{1}{1440\pi}(5(6\xi-1)^2+1)\int \mathrm{d}^2x\left(\sqrt{g}\,R^2 - \sqrt{\bar{g}}\,\bar{R}^2\right), \tag{5.83a}$$

$$\Delta b_4^{(\text{ferm})} = -\frac{1}{960\pi}\int \mathrm{d}^2x\left(\sqrt{g}\,R^2 - \sqrt{\bar{g}}\,\bar{R}^2\right), \tag{5.83b}$$

where $\bar{R}$ is the Ricci scalar of the round sphere. But it follows from volume preservation, the Gauss-Bonnet theorem, and the fact that $\bar{R}$ is constant that

$$\int \mathrm{d}^2x\left(\sqrt{g}\,R^2 - \sqrt{\bar{g}}\,\bar{R}^2\right) = \int \mathrm{d}^2x\sqrt{g}(R-\bar{R})^2 \geqslant 0 \tag{5.84}$$

with equality if and only if $R=\bar{R}$, i.e. if g_{ij} is the metric of the round sphere. Hence for both the scalar and fermion, $\sigma\Delta K_L(t)$ is strictly *negative* at sufficiently small t for any non-trivial deformation of the sphere, regardless of the size of the deformation.

To inspect the large-t behaviour, we instead recall that the differenced heat kernel

can be expressed in terms of the eigenvalues λ_I, $\bar{\lambda}_I$ of the operators L and $\overline{L}$:

$$\Delta K_L(t) = \sum_I \left(\mathrm{e}^{-t\lambda_I} - \mathrm{e}^{-t\bar{\lambda}_I} \right). \tag{5.85}$$

The large-t behaviour of this expression — particularly its sign — is clearly dominated by the smallest eigenvalue of either L or $\overline{L}$, so we must compare the low-lying spectra of these two operators. For the scalar, this comparison can be performed by using a Rayleigh-Ritz formula for the lowest eigenvalue of L:

$$\lambda_{\min} = \inf_\phi J[\phi], \qquad J[\phi] \equiv \left[\int \mathrm{d}^2x \sqrt{g}\, \phi^2 \right]^{-1} \int \mathrm{d}^2x \sqrt{g}\, \phi(-\nabla^2 + \xi R)\phi, \tag{5.86}$$

with the infimum taken over all (square-integrable) test functions ϕ. Thus $\lambda_{\min}$ can be bounded from above by taking ϕ to be a constant function; then again using the Gauss-Bonnet theorem and volume preservation, we have

$$\lambda_{\min} \leqslant J[\text{const.}] = \frac{4\pi\xi\chi(\Sigma)}{\mathrm{Vol}[g]} = \bar{\lambda}_{\min} \tag{5.87}$$

with equality if and only if a constant function is an eigenfunction of L, which for $\xi \neq 0$ is only the case if R is a constant and thus g_{ij} is the metric of the round sphere. Hence for $\xi \neq 0$ and a non-trivial perturbation of the sphere, the lowest eigenvalue of L is always strictly less than any eigenvalue of $\overline{L}$, and $\Delta K_L(t)$ is positive at sufficiently large t. On the other hand, when $\xi = 0$ constant functions are always eigenfunctions of $L = -\nabla^2$, and hence the lowest eigenvalues of L and $\overline{L}$ are identical. The large-t behaviour of $\Delta K_L(t)$ is then controlled by the next-lowest eigenvalue λ_{next} of $-\nabla^2$, which is known to be bounded by [111]

$$\lambda_{\text{next}} \leqslant \frac{8\pi}{\mathrm{Vol}[g]} = \bar{\lambda}_{\text{next}}. \tag{5.88}$$

Hence, for the case $\xi = 0$ we again find that $\Delta K_L(t)$ is positive at sufficiently large t.

We come to a similar conclusion for the fermion by invoking a theorem from [112]: namely, given that Σ is a two-dimensional manifold of genus zero, all eigenvalues of the squared Dirac operator are bounded below by $4\pi/\mathrm{Vol}[g] = \bar{\lambda}_{\min}$, with equality only holding if g_{ij} is the metric of the round sphere. Hence we, again, conclude that at sufficiently large t, $\sigma\Delta K_L(t)$ is negative.

We have therefore established that $\sigma\Delta K_L(t)$ is always negative at sufficiently small or large t, regardless of the size of the perturbation to the sphere. To analyse the intermediate-t regime, and in particular to determine whether ΔF decreases arbitrarily as the size of the perturbation grows, we turn to numerics.

5.5.2 Numerical Results

The advantage of using heat kernels to evaluate the differenced free energy is that computing the (differenced) heat kernel (3.13) amounts to computing the spectrum of L. Moreover, only the smallest few eigenvalues of L are needed to obtain a good approximation for $\Delta K_L(t)$ everywhere except near $t = 0$ — but small t is precisely the region in which the heat kernel expansion gives a good approximation. The heat kernel expansion therefore provides both a check of the numerics as well as a tractable way of computing the differenced free energy (which requires the behaviour of $\Delta K_L(t)$ to be known for all t). In short, we compute $\Delta K_L(t)$ numerically to a sufficient accuracy that at sufficiently small t it agrees with the leading linear behaviour $\Delta b_4 t$ of the heat kernel expansion, and we then sew these two behaviours together to perform the integration over all t that gives ΔF. This requires a very high level of accuracy which is achieved through approximating the eigenvalues of L using the pseudo-spectral methods described in Section 5.4. We present more information on the numerical method used, as well as details of these checks, numerical errors, and computation of ΔF, in Appendix B.1. Here, we describe the setup and the results.

Firstly, note that on sufficiently deformed backgrounds the Ricci scalar will become negative somewhere, and hence the spectrum of L for the non-minimally-coupled scalar may become negative. If these eigenvalues are sufficiently larger in magnitude than M^2 (as will always occur if M is fixed and the sphere is deformed more and more extremely), their presence introduces tachyonic instabilities, implying that the theory becomes ill defined. Consequently, we will restrict to numerical analysis of only the *minimally-coupled* scalar ($\xi = 0$), that, as we showed in the previous section, always has a non-negative spectrum. No restriction is required on the fermion, since as mentioned above the spectrum of L for the fermion is always positive.

A numerical analysis can only by used to study a specific subset of deformations of the round sphere. Here, we will consider certain classes of axisymmetric deformations. We begin by considering deformed spheres embedded in $\mathbb{R}^3$ via $r = R(\theta)$, corresponding to the induced metric[15]

$$\mathrm{d}s^2 = R(\theta)^2 \left[\left(1 + \frac{R'(\theta)^2}{R(\theta)^2} \right) \mathrm{d}\theta^2 + \sin^2\theta \, \mathrm{d}\phi^2 \right] . \tag{5.89}$$

Specifically, we will take

$$R_{\ell,\varepsilon}(\theta) = c_{\ell,\varepsilon} \left(1 + \varepsilon \, Y_{\ell,0}(\theta, 0) \right) , \tag{5.90}$$

where $c_{\ell,\varepsilon}$ is a (positive) constant that ensures the volume of the sphere remains unchanged as ε is varied. It is straightforward to see that to linear order in ε, the metric (5.89) ob-

[15] Such an embedding restricts Σ to be star-shaped in the technical sense that any ray fired from $r = 0$ intersects Σ precisely once.

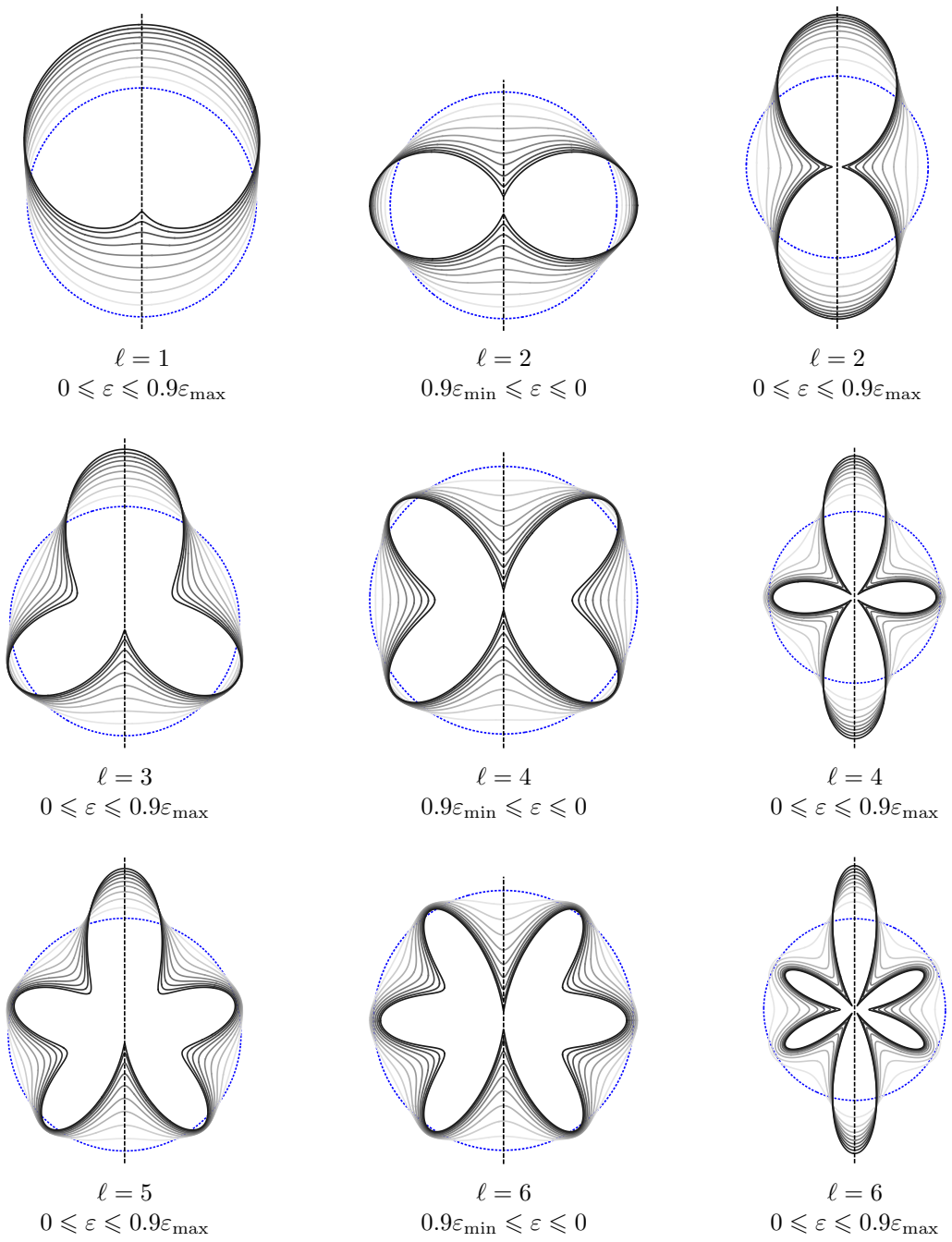

Figure 5.5: Cross-sections of the geometries we consider; these should be rotated around the dotted axis to generate the corresponding deformed sphere. The dotted blue circle is the unperturbed sphere; from light to dark grey, each curve corresponds to ε ranging in steps of $0.1\varepsilon_{\max}$ (or $0.1\varepsilon_{\min}$) from $0.1\varepsilon_{\max}$ ($0.1\varepsilon_{\min}$) to $0.9\varepsilon_{\max}$ ($0.9\varepsilon_{\min}$). For odd ℓ, negative ε is related to positive ε by a parity transformation which turns the cross-section "upside-down", leaving the geometry unchanged.

tained from these embedding functions is in the form (5.24) conformal to the round sphere, and hence the behaviour of $\Delta K_L(t)$ to leading non-trivial order in ε should be the same as that obtained in Section 5.3 (with $f^{(1)} = Y_{\ell,0}$). However, higher-order effects in ε break the conformal form of the metric. We will consider deformations (5.90) with $\ell = 1, 2, \ldots, 6$, while the range of $\varepsilon \in (\varepsilon_{\min}, \varepsilon_{\max})$ is fixed by the condition that $R_{\ell,\varepsilon} > 0$ everywhere; we show cross-sections of the embeddings of these surfaces into $\mathbb{R}^3$ in Figure 5.5. Note that for odd ℓ it suffices to consider only $\varepsilon > 0$, since positive and negative ε are related by a parity transformation: the transformation $(\theta, \phi) \to (\pi - \theta, \phi + \pi)$ sends $Y_{\ell,0} \to (-1)^\ell Y_{\ell,0} = -Y_{\ell,0}$, and thus since $Y_{\ell,0}$ always appears with a factor of ε, we find that $R_{\varepsilon,\ell} \to R_{-\varepsilon,\ell}$ for odd ℓ. It is also worth noting that the $\ell = 1$ embedding does not appear to change the shape of the sphere much at all until ε is relatively large; as mentioned above, this is because the $\ell = 1$ deformation is an infinitesimal diffeomorphism, and thus the deformation of the intrinsic geometry is trivial to linear order in ε. This can be seen explicitly by noting that since $Y_{1,0}(\theta) = p\cos\theta$ (with $p = \sqrt{3/4\pi}$), the induced metric (5.89) with $R = R_{1,\varepsilon}$ becomes

$$\mathrm{d}s^2 = c_{1,\varepsilon}^2 (1 + p\varepsilon\cos\theta)^2 \left[(1 + p^2\varepsilon^2 \sin^2\theta)\mathrm{d}\theta^2 + \sin^2\theta\,\mathrm{d}\phi^2\right] + \mathcal{O}(\varepsilon^3); \tag{5.91}$$

converting to a new coordinate ϑ defined by $\theta = \vartheta - p\varepsilon\sin\vartheta + p^2\varepsilon^2\sin\vartheta\cos\vartheta + \mathcal{O}(\varepsilon^3)$, we get

$$\mathrm{d}s^2 = \left(1 - \frac{\varepsilon^2}{\sqrt{20\pi}} Y_{2,0}(\vartheta)\right)\left[\mathrm{d}\vartheta^2 + \sin^2\vartheta\,\mathrm{d}\phi^2\right] + \mathcal{O}(\varepsilon^3), \tag{5.92}$$

so the induced metric to linear order in ε is diffeomorphic to the round sphere, as claimed. The non-trivial perturbation comes in at order ε^2 and takes the form of those considered in Section 5.3 with $f^{(1)} = -Y_{2,0}/\sqrt{20\pi}$; the differenced heat kernel should thus be $\mathcal{O}(\varepsilon^4)$.

In Figures 5.6 and 5.7, we show the differenced heat kernels $\Delta K_L(t)$ for the minimally-coupled scalar and for the Dirac fermion normalised by ε^2 (or by ε^4 in the case of $\ell = 1$) along with the perturbative results derived in Section 5.3. Note that we only plot ΔK_L down to $t = 0.0005$; this is because in the small-t regime more and more eigenvalues of L contribute to ΔK_L leading to difficulty in controlling the numerics. But as discussed above, the small-t regime is controlled by the heat kernel expansion, which guarantees the sign of $\sigma\Delta K_L$ to be negative there. We therefore see that $\sigma\Delta K_L(t)$ is negative for all t even for large deformations of the sphere. Interestingly, $\Delta K_L(t)$ appears to *grow* with ε at sufficiently small fixed values of t; this is due to the fact that as the geometry becomes more singular, its Ricci curvature grows, causing the heat kernel coefficient Δb_4 defined in (5.83) to grow as well. This growth is especially pronounced in the deformations with odd ℓ and those with even ℓ and $\varepsilon < 0$; comparing to Figure 5.5, these deformations all limit towards a connected geometry with a cusp-like defect (the geometries with even ℓ and $\varepsilon > 0$, on the other hand, pinch off into separate disconnected components as $\varepsilon \to \varepsilon_{\max}$). This growth of ΔK_L at small t should lead to a corresponding

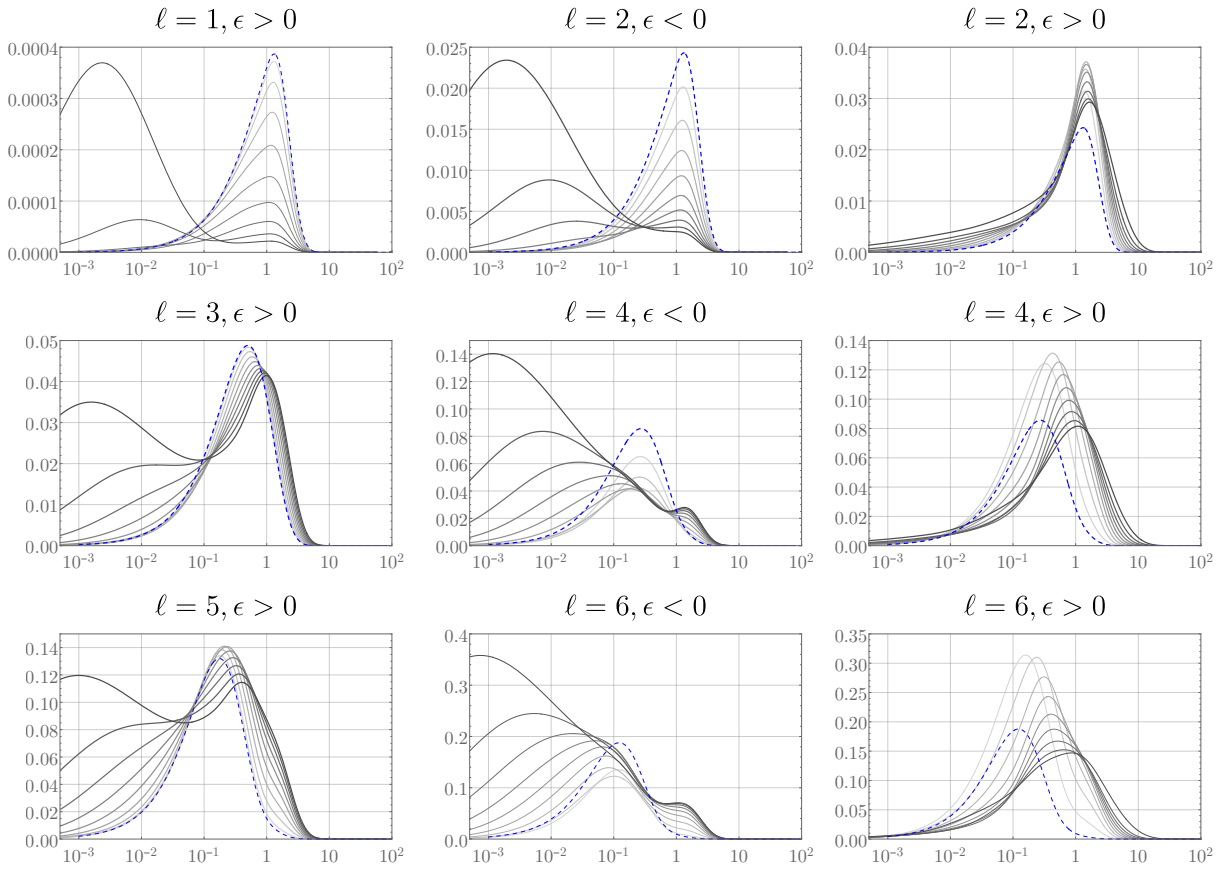

Figure 5.6: The differenced heat kernel $\Delta K_L(t)$ as a function of t for the minimally-coupled scalar on the deformed spheres given by (5.90). Each plot shows the rescaled heat kernel $-\sigma\Delta K_L/\varepsilon^2$ (except for $\ell = 1$, which shows $-\sigma\Delta K_L/\varepsilon^4$), with the dashed blue line corresponding to the perturbative result (5.28) and the grey lines to the numerical results for the deformations shown in Figure 5.5 (hence light to dark grey corresponds to increasing $|\varepsilon|$, with $\varepsilon \in [0.9\varepsilon_{\min}, 0.9\varepsilon_{\max}]$).

growth in the free energy ΔF; we now investigate this free energy, and then more carefully investigate the divergence structure associated to the limiting singular geometries.

5.5.3 Behaviour of the Free Energy

At zero mass and temperature, the differenced free energy $\Delta F_{T=0} = \Delta E$ may be computed by using (5.39) and then integrating the heat kernel with (5.20); more details on the computation can be found in Appendix B.1. In Figure 5.8 we show ΔE for the deformations described above, normalised by the perturbative result ΔE_{pert}. As expected, $|\Delta E|$ grows monotonically with increasing $|\varepsilon|$, though this may not be apparent from Figure 5.8 as the curves are normalised by a factor of ε^2 (or ε^4 for $\ell = 1$) contained in ΔE_{pert}. This is shown more clearly by the non-normalised ΔE plots shown in Figure 5.9. Due to the growth of ΔK at small t as ε approaches $\varepsilon_{\min}$ or $\varepsilon_{\max}$, we only show ΔE for a range of ε within which the error in ΔE is no greater than a few percent (this corresponds to ε up to $0.8\varepsilon_{\max}$ for $\ell = 1$ and up to $0.5\varepsilon_{\max}$ for $\ell = 6$). Nevertheless, the growth in

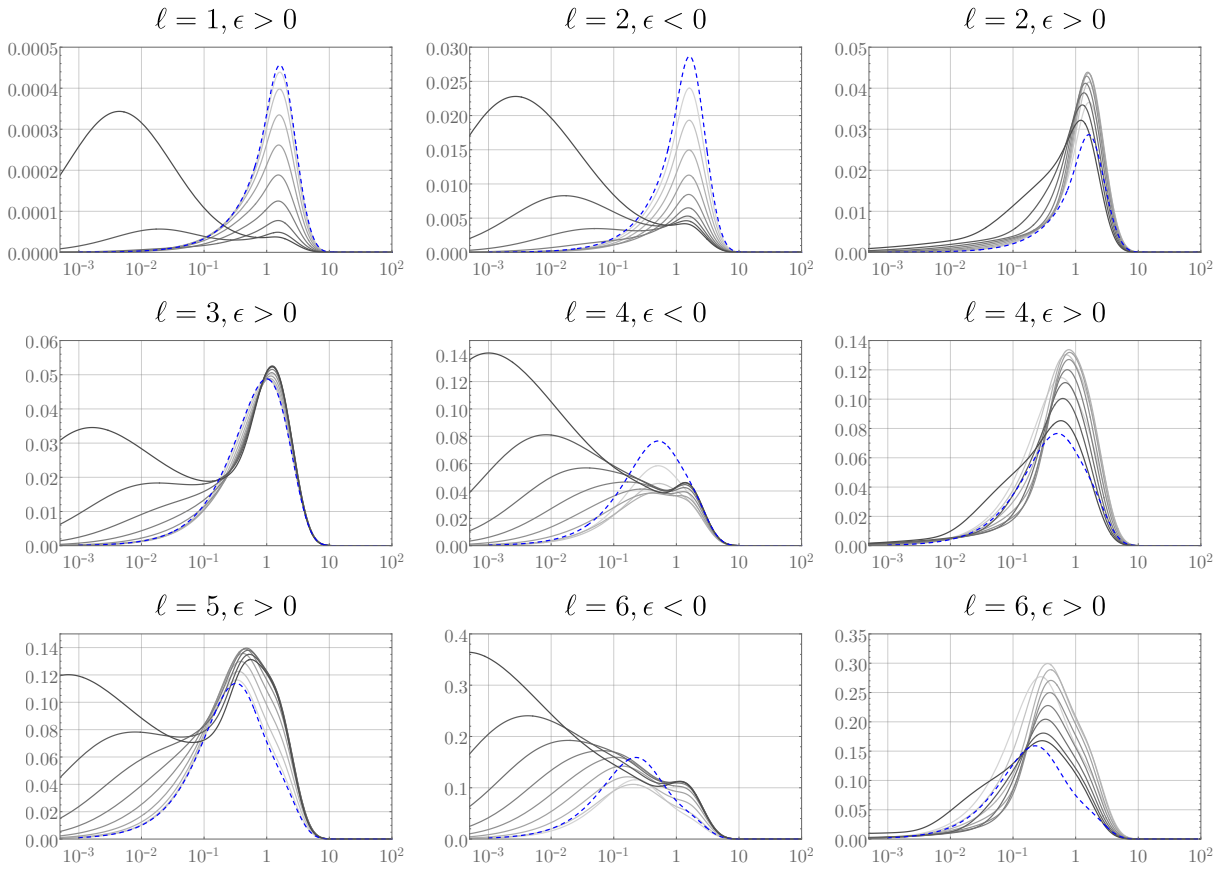

Figure 5.7: The differenced heat kernel $\Delta K_L(t)$ as a function of t for the Dirac fermion on the deformed spheres given by (5.90). Each plot shows the rescaled heat kernel $-\sigma\Delta K_L/\varepsilon^2$ (except for $\ell = 1$, which shows $-\sigma\Delta K_L/\varepsilon^4$), with the dashed blue line corresponding to the perturbative result (5.36) and the grey lines to the numerical results for the deformations shown in Figure 5.5 (hence light to dark grey corresponds to increasing $|\varepsilon|$, with $\varepsilon \in [0.9\varepsilon_{\text{min}}, 0.9\varepsilon_{\text{max}}]$).

the small-t behaviour of the heat kernel makes clear that ΔE should continue to grow as the geometry is successively deformed; we will investigate this growth in more detail in the following section. For now, let us note the remarkable feature that $\Delta E/\Delta E_{\text{pert}}$ looks extremely similar for both the scalar and fermion, despite the fact that the corresponding heat kernels in Figures 5.6 and 5.7 are more substantially different. It therefore appears that the theory-dependence of ΔE is contained almost completely in the perturbative contribution ΔE_{pert}: the ratio $\Delta E/\Delta E_{\text{pert}}$ is almost entirely theory-independent (we highlight *almost*: the difference between the curves is larger than numerical error, so they are genuinely different). This feature is interestingly reminiscent of the results of [95], which study the free energy of the massless Dirac fermion, the conformally-coupled scalar, and holographic CFTs on a squashed Euclidean three-sphere; they found that for small and modest squashings, the free energies of all of these theories agree more closely than should be expected from CFT considerations alone. Indeed, there is a conjecture and good evidence that the subleading term in the perturbative expansion of the free energy

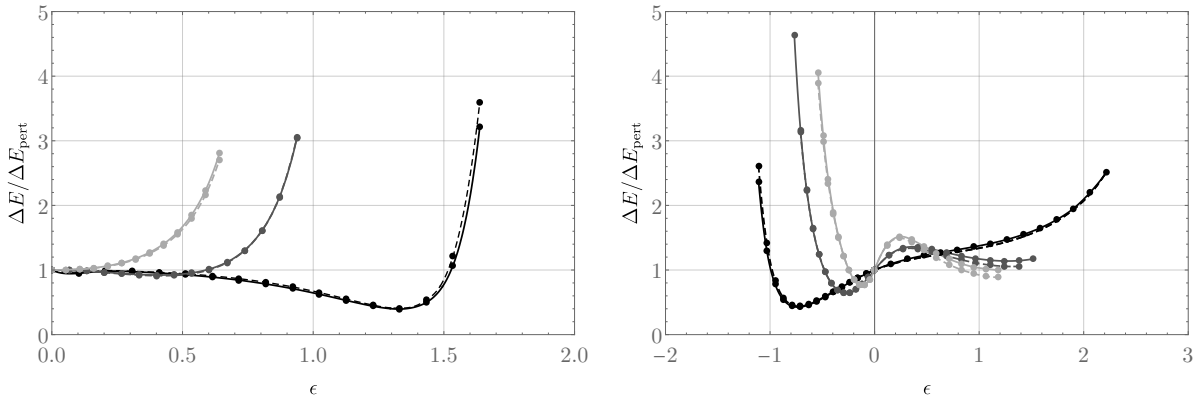

(a) Odd ℓ (b) Even ℓ

Figure 5.8: The zero-temperature differenced energy ΔE normalised by its perturbative behaviour ΔE_{pert} on the deformed spheres given by (5.89) and (5.90). Solid lines show results for the massless Dirac fermion, while dashed lines are for the massless minimally-coupled scalar (points are numerical data; the curves are drawn to guide the eye). From black to light grey, the curves corresponds to $\ell = 1, 3, 5$ (left) and $\ell = 2, 4, 6$ (right). It is striking that the Dirac fermion and scalar give very similar curves.

in the squashing parameter, determined by the three-point function of the stress tensor, is surprisingly universal for all three-dimensional CFTs [113, 114]. This link will be explored in more detail in Chapter 6 where the behaviour of $\Delta E/\Delta E_{\text{pert}}$ for the massless Dirac fermion, the conformally-coupled scalar, and holographic CFTs (the three-dimensional CFTs considered in [95, 113]) on a product of time with static deformation of a two-sphere will be calculated, allowing for a more direct comparison with these results in Section 6.4.

In fact, this theory independence becomes exact in a long-wavelength limit. Specifically, let l be the typical curvature scale of the deformed geometry; then the heat kernel coefficient Δb_{2n} scales like l^{-2n} for $n \geqslant 2$. The heat kernel expansion (5.22) then implies that for $l \gg T^{-1}, M^{-1}$, the free energy (5.20) can be expressed as an expansion in powers of $1/(Tl)$ or $1/(Ml)$[16]. Indeed, for general M, T we can derive (as we did for flat space in Section 4.3) that

$$\Delta F = \sigma \sum_{n=0}^{\infty} (-1)^n \frac{\Delta b_{2n+4}}{T^{2n+1}} J^{(n)}\left(\frac{M^2}{T^2}\right), \tag{5.93}$$

where $J^{(n)}$ is the nth derivative of the function given by

$$J(\zeta) = \frac{1}{2\sqrt{\zeta}} \begin{cases} \coth\left(\frac{\sqrt{\zeta}}{2}\right), & \text{scalar,} \\ \tanh\left(\frac{\sqrt{\zeta}}{2}\right), & \text{fermion.} \end{cases} \tag{5.94}$$

[16] In fact, for the scalar such an expansion necessarily requires $lM \gg 1$, whereas for the fermion it is sufficient for *either* Ml *or* Tl to be large. This is due to the fact that at large T, $\Theta_\sigma(T^2 t)$ falls off exponentially for the fermion but approaches a non-zero constant for the scalar.

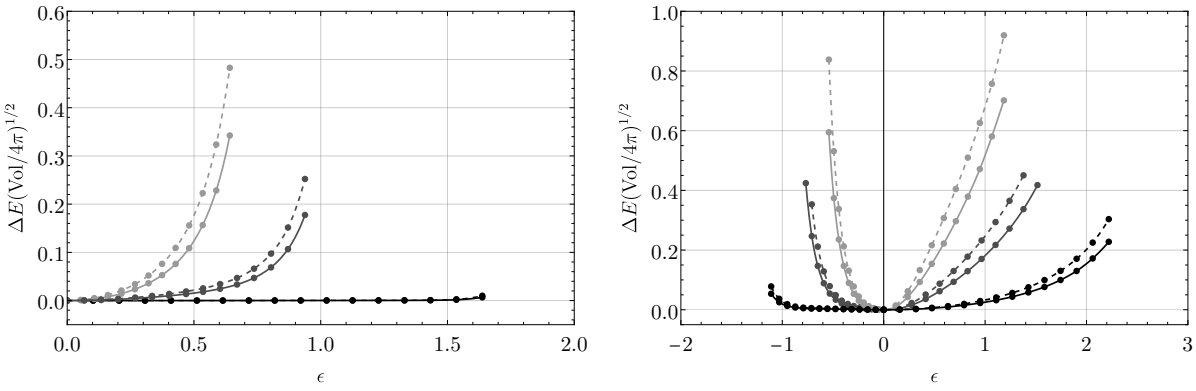

(a) Odd ℓ (b) Even ℓ

Figure 5.9: The zero-temperature differenced energy ΔE (in units of one over the radius of the reference round sphere) on the deformed spheres given by (5.89) and (5.90). Solid lines show results for the massless Dirac fermion, while dashed lines are for the massless minimally-coupled scalar (points are numerical data; the curves are drawn to guide the eye). From black to light grey, the curves corresponds to $\ell = 1, 3, 5$ (left) and $\ell = 2, 4, 6$ (right).

For $M \sim T$, (5.93) is clearly an expansion in $1/(Tl)^2$. For $M \gg T$, it instead becomes

$$\Delta F = \frac{\sigma}{\sqrt{4\pi}\, M} \sum_{n=0}^{\infty} \frac{\Delta b_{2n+4}}{M^{2n}} \Gamma\left(n + \frac{1}{2}\right) \left[1 + \mathcal{O}\left(\mathrm{e}^{-M/T}\right)\right], \tag{5.95}$$

which is an expansion in $1/(Ml)^2$. On the other hand, for $M \ll T$ we have

$$\Delta F = \sigma \sum_{n=0}^{\infty} \Delta b_{2n+4} \begin{Bmatrix} \dfrac{T}{M^2} \dfrac{n!}{M^{2n}}, & \text{scalar} \\ \dfrac{(-1)^n J^{(n)}(0)}{T^{2n+1}}, & \text{fermion} \end{Bmatrix} \left[1 + \mathcal{O}\left(M^2/T^2\right)\right], \tag{5.96}$$

which is an expansion in $1/(Ml)^2$ for the scalar and $1/(Tl)^2$ for the fermion.

The point is that as long as $l \gg T^{-1}, M^{-1}$, the leading-order behaviour of the differenced free energy is governed by the lowest heat kernel coefficient Δb_4:

$$\Delta F = \sigma \frac{\Delta b_4}{T} J\left(\frac{M^2}{T^2}\right) + \cdots, \tag{5.97}$$

where $\cdots$ denotes subleading terms. The theory dependence of ΔF can be seen by expanding

$$\Delta b_4 = \Delta b_4^{(2)} \varepsilon^2 + \mathcal{O}(\varepsilon^3), \tag{5.98}$$

from which we have

$$\frac{\Delta F}{\Delta F_{\mathrm{pert}}} = \frac{\Delta b_4}{\Delta b_4^{(2)} \varepsilon^2} + \cdots. \tag{5.99}$$

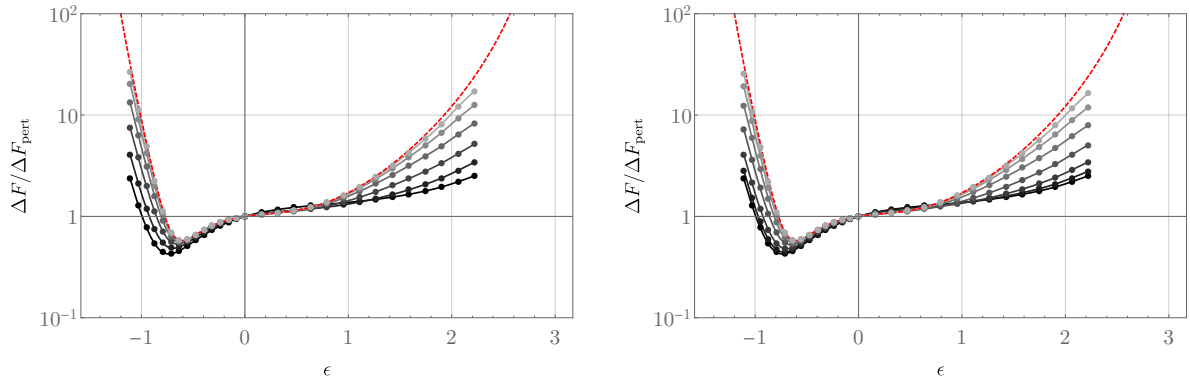

(a) $M = 0$, varying T (b) $T = 0$, varying M

Figure 5.10: The ratio $\Delta F/\Delta F_{\text{pert}}$ at various temperatures and masses for the Dirac fermion on the deformed spheres given by (5.90), for the representative case $\ell = 2$. In both figures, the black curves correspond to the massless, zero-temperature result, while the dashed red line is the long-wavelength behaviour given by (5.99). From black to light grey, the left figure shows temperatures $T = 0$, 0.5, 1, 2, 4, and 8, while the right figure shows masses $M = 0$, 0.5, 1, 2, 4, 8 and 16 (points are numerical data; the curves are drawn to guide the eye). The range of the x-axis goes from ε_{min} to ε_{max}; the data shown here takes $|\varepsilon|$ sufficiently small that the numerical error in ΔF is no greater than one percent.

But from (5.83), the ratio $\Delta b_4/\Delta b_4^{(2)}$ is the same for the fermion and the scalar, so to leading order $\Delta F/\Delta F_{\text{pert}}$ is independent of the theory (as well as of the mass and temperature).

At intermediate masses and temperatures, ΔF interpolates between the massless zero-temperature behaviour shown in Figure 5.8 and the behaviour given by (5.97). As a representative example, we show this interpolation in Figure 5.10 for the case of the fermion and the deformed spheres (5.90) with $\ell = 2$ (results for the scalar and higher ℓ are analogous). We also show the non-normalised ΔF for the same deformations in Figure 5.11 to exhibit more clearly the monotonic dependence on $|\varepsilon|$. The takeaway is that for any mass and temperature, large deformations of the sphere appear to decrease ΔF arbitrarily. The deformations considered here tend to 'pinch off' the sphere somewhere, and hence to better understand the behaviour of ΔF under such extreme deformations, we now examine more closely the behaviour of the heat kernel near these transitions.

5.6 Towards Singular Geometries

As remarked above, the deformations shown in Figure 5.5 fall into roughly two classes: the left two columns (corresponding to odd ℓ and even ℓ with $\varepsilon < 0$) limit to a connected geometry that 'pinches' somewhere, while the geometries shown in the right column (corresponding to even ℓ with $\varepsilon > 0$) tend to disconnect as $\varepsilon \to \varepsilon_{\text{max}}$, with the individual connected pieces each potentially having a defect near the transition. In both classes,

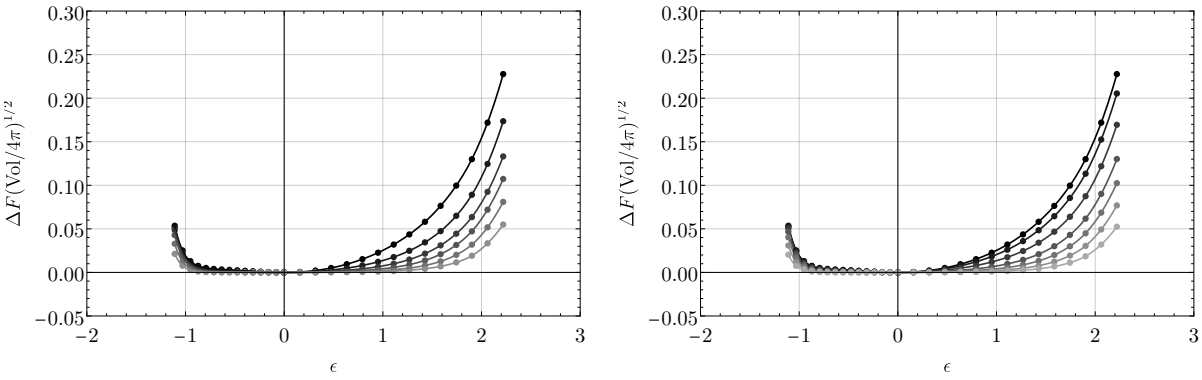

(a) $M = 0$, varying T (b) $T = 0$, varying M

Figure 5.11: The differenced free energy ΔF (in units of one over the radius of the reference round sphere) at various temperatures and masses for the Dirac fermion on the deformed spheres given by (5.90), for the representative case $\ell = 2$. From black to light grey, the left figure shows temperatures $T = 0$, 0.5, 1, 2, 4, and 8, while the right figure shows masses $M = 0$, 0.5, 1, 2, 4, 8 and 16 (points are numerical data; the curves are drawn to guide the eye). The range of the x-axis goes from $\varepsilon_{\min}$ to $\varepsilon_{\max}$; the data shown here takes $|\varepsilon|$ sufficiently small that the numerical error in ΔF is no greater than one percent.

we expect the gradient of ΔK_L to diverge at $t = 0$ as $\varepsilon \to \varepsilon_{\min,\max}$ because the heat kernel coefficient Δb_4 diverges as the geometry becomes singular due to the Ricci scalar becoming unbounded near the pinch-off[17]. However, the behaviour of ΔK_L at small *non-zero* t differs between these two classes. The class with even ℓ and $\varepsilon > 0$ is perhaps most intuitive: the case $\ell = 2$ looks like a change in topology from one sphere to two, while for $\ell \geqslant 4$ the singular geometry also exhibits conical defects near the transition (in addition to the divergence of the Ricci scalar there). An isolated conical defect (with no curvature singularity) can be studied analytically, so we begin with a discussion of the associated divergences.

5.6.1 Conical Defects

In the vicinity of a conical defect on some manifold Σ, the geometry takes the form

$$\mathrm{d}s^2 = \left[\mathrm{d}r^2 + r^2\mathrm{d}\phi^2\right]\left(1 + \mathcal{O}(r)\right) \tag{5.100}$$

where ϕ has periodicity α (with $\alpha = 2\pi$ corresponding to a smooth geometry). Recall that a conical deficit (corresponding to $\alpha < 2\pi$) can be embedded in $\mathbb{R}^3$, while an excess (corresponding to $\alpha > 2\pi$) cannot. The differenced free energy, of course, depends only on

[17]This unboundedness of the Ricci scalar renders the asymptotic series (5.20) no longer valid. The heat kernel may still admit a Frobenius expansion around $t = 0$ when $\varepsilon = \varepsilon_{\min,\max}$, but the coefficients in this expansion cannot be given by integrals of successively higher-derivative curvature invariants, because these diverge.

the intrinsic geometry, so we may still analyse its behaviour regardless of the existence of any embedding. In the presence of such a defect, the corresponding heat kernel expansion exhibits an additional constant term associated to it [80]:

$$\sigma K_L(t) = \frac{\sigma \mathrm{Vol}[g]}{4\pi t} - \frac{\chi(\Sigma)}{12} - \frac{(2\pi-\alpha)^2}{48\pi\alpha} + \mathcal{O}(t). \tag{5.101}$$

The differenced heat kernel thus satisfies

$$\sigma \Delta K_L(t) = -\frac{(2\pi-\alpha)^2}{48\pi\alpha} + \mathcal{O}(t), \tag{5.102}$$

which clearly leads to a UV divergence in ΔF. Importantly, note that this divergence has fixed sign: it always contributes negatively to $\sigma\Delta K_L(t)$, and hence to ΔF.

Interestingly, for a cone (that is, the geometry (5.100) with vanishing subleading corrections), the sign of the divergence of the energy depends on whether the defect corresponds to a conical excess or deficit. For example, in the case of a conformally-coupled scalar at zero temperature, the energy density of a cone is [115]

$$\rho \equiv \langle T_{00} \rangle = \frac{G(\alpha)}{r^3}, \tag{5.103}$$

where $G(\alpha) < 0$ for $\alpha < 2\pi$ and $G(\alpha) > 0$ for $\alpha > 2\pi$. Hence the differenced free energy between a cone and a planar geometry with no conical defect is negatively UV divergent[18] when $\alpha < 2\pi$, and *positively* divergent when $\alpha > 2\pi$. One might have naïvely expected the behaviour (5.103) to have been universal near conical defects (at least for QFTs with UV fixed points, which are CFTs in the UV), but the heat kernel expansion (5.101) shows that the behaviour of the stress tensor near such defects must be sensitive to the global properties of (Σ, g) (and in particular, if Σ is compact, it follows from (5.102) that the difference ΔF is always negatively UV divergent, whether the defect is an excess or a deficit).

To manifestly illustrate such deformations, as well as to connect to the deformations considered in Section 5.5, consider a one-parameter family of spatial geometries that interpolates from a smooth geometry to one with a conical defect at a pole. An explicit axisymmetric example of such a family is given by the embedding

$$R_\varepsilon(\theta) = c_\varepsilon \left(1 + \frac{1}{4}\sqrt{1 + 40\sin^2\left(\theta/2\right)} - \frac{1}{4}\sqrt{(1-\varepsilon)^2 + 50\sin^2\left(\theta/2\right)}\right)^2, \tag{5.104}$$

where c_ε is a volume-preserving constant that fixes the volume to 4π, i.e. the volume of the round unit sphere. For any $\varepsilon < 1$, this geometry is everywhere smooth, and for $\varepsilon = 1$, it exhibits a conical defect at $\theta = 0$ with angle $\alpha = 2\pi/\sqrt{3}$ and a Ricci scalar which is

[18] We are ignoring potential IR divergences associated with the fact that a cone is not compact.

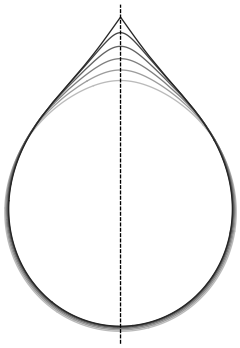

Figure 5.12: Cross-sections of the geometries described by the embedding function (5.104); these should be rotated around the dotted axis to generate the corresponding deformed spheres. From grey to black, we show $\varepsilon = 0$ to 1 in intervals of 0.2; the $\varepsilon = 1$ embedding exhibits a conical defect at the pole.

bounded everywhere excluding the defect; see Figure 5.12. For $\varepsilon < 1$ we may therefore numerically compute the heat kernel as described in the previous section; we show these in Figure 5.13. As expected, the differenced heat kernel vanishes linearly at small t for any $\varepsilon < 1$, but its gradient there diverges as $\varepsilon \to 1$. In the limit $\varepsilon \to 1$, the heat kernel clearly approaches a function that goes to a *non-zero* value at $t = 0$, consistent with the expectation from (5.102):

$$\lim_{t\to 0^+} \lim_{\varepsilon \to 1^-} \sigma \Delta K_L(t) = -\frac{2\sqrt{3} - 3}{36}, \tag{5.105}$$

with the right-hand side just the $\alpha = 2\pi/\sqrt{3}$ case of (5.102).

We can investigate a conical excess analogously by specifying the deformed sphere geometry directly rather than considering an embedding. To that end, consider the family of deformed spheres given by

$$\mathrm{d}s^2 = c_\varepsilon \left(\mathrm{d}\theta^2 + \mathrm{e}^{2f_\varepsilon} \sin^2\theta \, \mathrm{d}\phi^2 \right), \text{ with } f_\varepsilon(\theta) = \frac{\ln(\alpha/2\pi)}{\sec^2(\theta/2) + (1-\varepsilon)^2 \mathrm{cosec}^2(\theta/2)}, \tag{5.106}$$

where c_ε is again a volume-preserving constant. For $\varepsilon < 1$, these geometries are smooth, while the $\varepsilon = 1$ geometry exhibits a conical defect of angle α at the pole $\theta = 0$ and a Ricci scalar which is bounded everywhere excluding this pole. The small-t behaviour of the differenced heat kernels for $\alpha = 3\pi$ is shown in Figure 5.14; note that in the limit $\varepsilon \to 1$, these too approach the $t = 0$ value expected from (5.102). Moreover, one again finds $\sigma \Delta K_L$ appears positive for all t. In particular, these results confirm that on a topological sphere with a conical defect, both a deficit *and* an excess contribute *negatively* to the free energy, in contrast with the expectation from (5.103) for planar geometries.

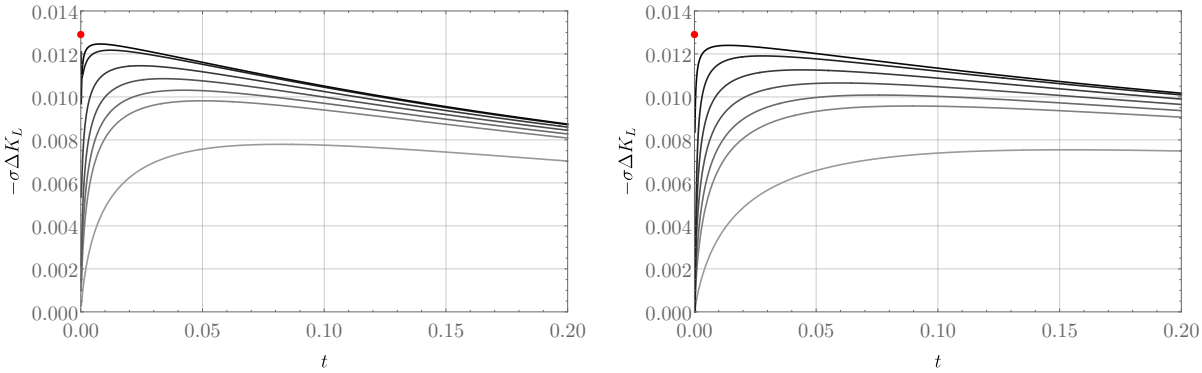

(a) Minimally-coupled scalar

(b) Fermion

Figure 5.13: The small-t behaviour of ΔK_L for the minimally-coupled scalar (left) and the Dirac fermion (right) on the geometries described by the embedding (5.104). From lightest to darkest, the curves correspond to $\varepsilon = 0.9, 0.95, 0.96, 0.97, 0.98, 0.99$, and 0.995. The red dot indicates the $t = 0$ value (5.105) expected on the conical defect geometry corresponding to $\varepsilon = 1$.

5.6.2 Even ℓ, $\varepsilon > 0$

Let us now return to the case of the deformed spheres shown in the right-hand column of Figure 5.5. As a representative example, in Figure 5.15 we show the small-t behaviour of ΔK for the $\ell = 2$ deformation (5.90) near $\varepsilon = \varepsilon_{\text{max}}$. As expected, the heat kernel always vanishes linearly at $t = 0$ for any $\varepsilon < \varepsilon_{\text{max}}$ but its gradient there diverges as $\varepsilon \to \varepsilon_{\text{max}}$. More interestingly, ΔK appears to stabilise to a function that approaches a finite non-zero value at $t = 0$. This behaviour is quite evident in the case of the fermion, though it is a bit less obvious for the scalar as the successive change in ΔK_L appears to grow with each successive step in ε.

We might hope to understand this behaviour by using the heat kernel expansion, but as mentioned above, for $\varepsilon = \varepsilon_{\text{max}}$ this expansion breaks down due to the unbounded Ricci scalar near the pinch-off point. We therefore should not expect the expansion (5.101) to capture quantitative details of the small-t behaviour near the transition. However, it is interesting to note that it does capture some qualitative features; for instance, the differenced heat kernel appears to be approaching a function that limits to a non-zero constant at $t = 0$, similarly to the hear kernels shown in Figures 5.13 and 5.14. Moreover, note that the $\ell = 2$, $\varepsilon = \varepsilon_{\text{max}}$ geometry does not have a conical defect and can be thought of as a transition from one to two topological spheres. This transition doubles the Euler characteristic from $\chi = 2$ to $\chi = 4$, which from the heat kernel expansion would correspond to a differenced heat kernel of

$$\sigma\Delta K_L(t) = -\frac{1}{6} + \mathcal{O}(t); \tag{5.107}$$

this limiting value of $-1/6$ is surprisingly very close to the limiting behaviour for the

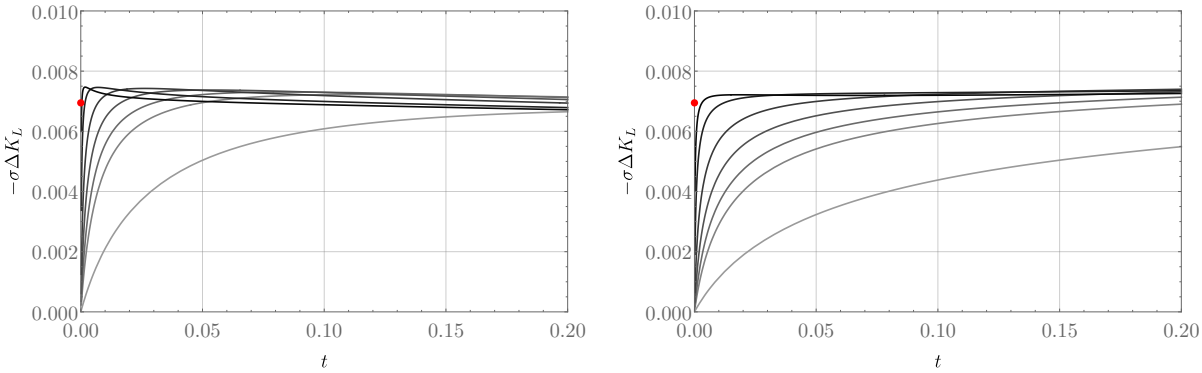

(a) Minimally-coupled scalar (b) Fermion

Figure 5.14: The small-t behaviour of ΔK_L for the minimally-coupled scalar (left) and the Dirac fermion (right) on the geometries (5.106) with $\alpha = 3\pi$. From lightest to darkest, the curves correspond to $\varepsilon = 0.9, 0.95, 0.96, 0.97, 0.98, 0.99$, and 0.995. The red dot indicates the $t = 0$ value $-1/144$ expected on the conical defect geometry with $\varepsilon = 1$.

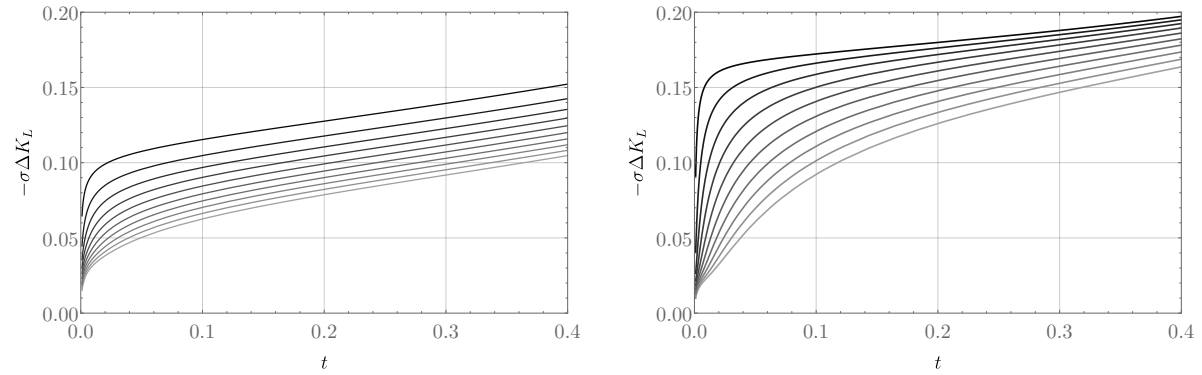

(a) Minimally-coupled scalar (b) Fermion

Figure 5.15: The behaviour of ΔK_L at small t for $\ell = 2$ and $\varepsilon > 0$ for the minimally-coupled scalar (left) and the Dirac fermion (right). From lightest to darkest, the curves correspond to $\varepsilon/\varepsilon_{\max} = 0.9$ to 0.99 in intervals of 0.01.

fermion shown in Figure 5.15b, even though a priori the heat kernel expansion should not be applicable (the scalar heat kernel in Figure 5.15a, on the other hand, does not appear to approach this limiting value of $-1/6$, though this is more difficult to verify conclusively because the scalar heat kernel does not appear to be growing linearly in ε near $\varepsilon = \varepsilon_{\max}$).

5.6.3 Odd ℓ and Even ℓ, $\varepsilon < 0$

For odd ℓ and even ℓ with $\varepsilon < 0$, the limiting geometry instead has a cusp. The corresponding behaviour of the differenced heat kernels (for $\ell = 2$) is shown in Figure 5.16; note that now the heat kernel itself, rather than just its gradient, appears to grow at small t as the geometry becomes singular. As shown in Figure 5.17, at intermediate values of t this growth appears to go roughly like $t^{-1/2}$, but does not appear to be maintained to arbitrarily small t. Indeed, the difficulty in inferring the limiting small-t behaviour is

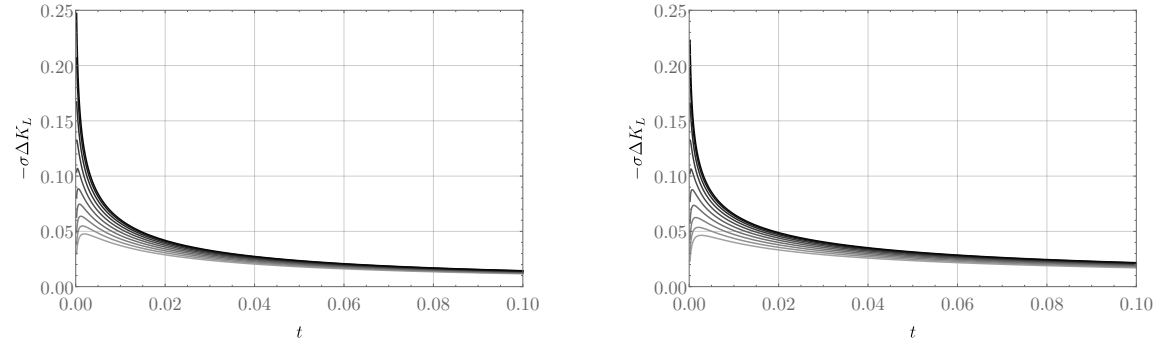

(a) Minimally-coupled scalar (b) Fermion

Figure 5.16: The behaviour of ΔK_L at small t for $\ell = 2$ and $\varepsilon < 0$ for the minimally-coupled scalar (left) and the Dirac fermion (right). From lightest to darkest, the curves correspond to $\varepsilon/\varepsilon_{\text{min}} = 0.9$ to 0.99 in intervals of 0.01.

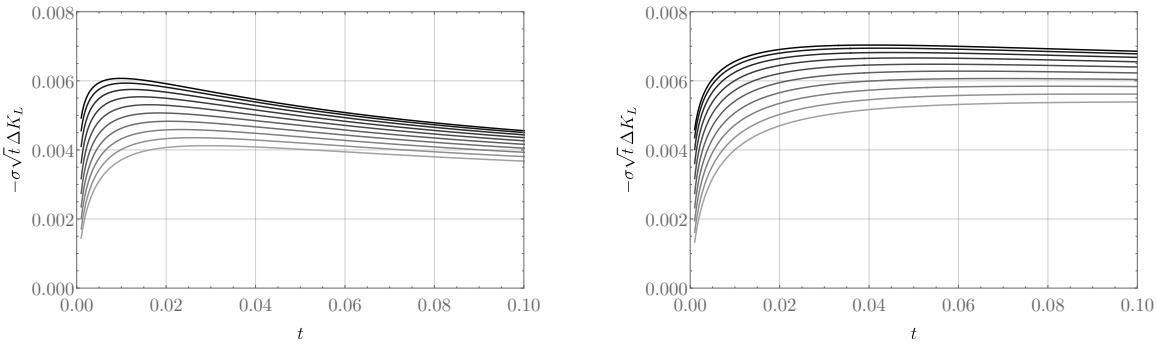

(a) Minimally-coupled scalar (b) Fermion

Figure 5.17: The same as Figure 5.16, normalised by a factor of $\sqrt{t}$. At small-but-not-too-small t, ΔK_L appears to go like $t^{-1/2}$. It is unclear what happens at much smaller t due to lack of numerical precision there.

presumably due to the breakdown of the heat kernel expansion in the singular limit — that is, it is unclear whether or not $\sqrt{t}\,\Delta K_L$ vanishes at $t = 0$ in the singular limit, and therefore whether ΔK_L actually approaches a finite non-zero constant at $t = 0$ like it does for the cone or whether ΔK_L genuinely diverges there. Nevertheless, we note that the scaling as $t^{-1/2}$ is interesting as such a scaling of the heat kernel is expected on manifolds with boundary (2.19). This behaviour suggests that perhaps the cusp can be interpreted as a sort of boundary.

5.6.4 Implications for Graphene-Like Materials

The fact that $\Delta K_L(t)$ approaches a non-zero constant at small t could have interesting consequences for materials like graphene, that, as discussed at the beginning of this chapter, may exhibit a competition between a classical membrane free energy ΔF_{c} and the contribution ΔF_{q} from effective QFT degrees of freedom. Indeed, note that (5.20) implies

that on a geometry with a conical defect, ΔF_{q} has a linear UV divergence:

$$\Delta F_{\mathrm{q}} = -B\rho^{-1} + \mathcal{O}(\rho^0), \tag{5.108}$$

where ρ is a short-distance cutoff that resolves the conical singularity (imposed by restricting to $t > \rho^2$) and B is a positive constant. On the other hand, the Landau free energy ΔF_{c} given in (5.1) merely has a logarithmic divergence that is due to its scale-invariance: near $\theta = 0$ the mean curvature of the embedding (5.104) with $\varepsilon = 1$ diverges as θ^{-1}, and hence

$$\Delta F_{\mathrm{c}} = \widetilde{B} \ln \rho^{-1} + \mathcal{O}(\rho^0), \tag{5.109}$$

with $\widetilde{B}$ a positive constant. Interpreting $(1 - \varepsilon) \sim \rho$ as the resolution parameter of the cone, it therefore follows that ΔF_{c} must grow more slowly with ε than ΔF_{q}, and hence a deformation with ε sufficiently close to 1 will have $\Delta F_{\mathrm{c}} + \Delta F_{\mathrm{q}} < 0$. This argument will fail, of course, once ε is so close to 1 that UV effects from the 'tip' of the cone — that presumably are how the divergences in (5.108) and (5.109) are resolved — change the relative growth of ΔF_{c} and ΔF_{q} with ε.

On the other hand, per the analysis of Section 5.1, for graphene we have that at small ε, $\Delta F_{\mathrm{c}} + \Delta F_{\mathrm{q}} > 0$. So although competition between ΔF_{c} and ΔF_{q} does not render the round sphere locally unstable, it appears that sufficiently large deformations of the round sphere may be preferred to the round sphere itself, even after accounting for the Landau free energy of the membrane. Whether this is actually the case will depend on the details of when our analysis breaks down.

5.7 Summary and Discussion

We have provided evidence that for a (minimally- or non-minimally-coupled) free scalar field and for a Dirac fermion living on $(\mathbb{R} \times \Sigma, -\mathrm{d}t^2 + g)$, with Σ a two-dimensional manifold with sphere topology and endowed with metric g, the free energy is *maximised* when g is the metric of the round sphere. This observation applies to any mass and at any temperature. We demonstrated this result perturbatively around the round sphere for *any* non-trivial perturbation to the geometry, while for non-perturbative deformations we focused on a class of axisymmetric deformations. We found, in fact, not just that the free energy difference ΔF is negative, but that the (differenced) heat kernel $\Delta K_L(t)$ itself has fixed sign — a much stronger result than merely negativity of ΔF. We have also shown that the free energy difference ΔF between an arbitrary g and the round sphere metric is unbounded below, diverging as g develops a conical defect. This property implies that any dynamics of the membrane driven by this free energy will tend to drive the membrane to a singular geometry (that presumably gets regulated by UV effects).

As an application of our results, we have also briefly investigated their relevance

to (2+1)-dimensional crystalline systems like graphene, in which there are several contributions to the free energy. Specifically, in a Born-Oppenheimer approximation, the free energy we have calculated is that of the low-energy effective field theory of *quantum* excitations propagating on a fixed background determined by the atomic lattice; it simply corresponds to studying QFT on a curved background. The contribution to the free energy from this background is governed by a *classical* Landau free energy, and in this approximation it is the sum of these two that gives the total free energy of the membrane configuration. Consequently, understanding whether the negative free energy of QFTs on the membrane is sufficient to render the geometry singular depends on how well this quantum effect can compete with the Landau free energy of the underlying lattice. In the case of graphene at sufficiently low temperatures, we performed an analysis of this competition and found that with the simplifying assumption of a diffeomorphism-invariant Landau free energy, the membrane energy dominates for small perturbations of the round sphere, rendering the round sphere stable. However, in Section 5.1 we provided a more general diagnostic (5.12) for when the QFT free energy can make the round sphere unstable. This constraint depends on parameters like the bending rigidity, lattice spacing, and details of the effective QFT fields living on the membrane. Since these parameters are presumably experimentally tuneable from one type of crystalline membrane to another, it is plausible that a system can be engineered in which the QFT free energy *does* dominate that of the Landau free energy, and hence one should be able to experimentally observe the preference of such a membrane to deform to a singular effective geometry. Even without such engineering, the fact that integrating out the QFT fields gives a *non-local* contribution to the free energy (as opposed to the classical contribution from the geometric membrane action, which is local) suggests that perhaps the QFT contribution could be experimentally teased out from the classical piece, even if it never actually dominates the free energy.

More importantly, for *large* deformations of the sphere, we have shown that both ΔF_{q} and ΔF_{c} can be made arbitrarily large as the geometry becomes singular, with ΔF_{q} negative and growing faster than ΔF_{c}. Hence, it is conceivable that even if the round sphere is *locally* stable, it is not *globally* stable, and large deformations are preferred. Verifying whether this is indeed the case requires understanding, for instance, how large ε must be in the one-parameter family (5.104) before our analysis breaks down due to UV effects.

One unanswered question from this chapter concerns the quantitative behaviour of ΔF: what underlying mechanism is responsible for the similarity of ΔF between the minimally-coupled scalar and the Dirac fermion at small deformation parameter? As discussed in Section 5.5.3, this mechanism can be understood well in a long-wavelength limit, but we do not yet understand why the zero-temperature curves shown in Figure 5.8 are remarkably similar. In turns out that, in addition to the sign of ΔF, its behaviour as a functional of the deformation exhibits rather striking *universal* behaviour, not only for

free theories, but also for holographic CFTs. This will be explored further in Chapter 6.

Chapter 6

A Surprising Similarity Between Holographic CFTs and a Free Fermion

Holography in the form of AdS/CFT (as described in Section 1.2) is a very powerful tool for probing features of certain strongly-coupled field theories that would otherwise be intractable using conventional field-theoretic methods — as exhibited, for example, by the holographic results presented in Section 1.2 to which the intuition for the subject matter of this thesis is owed. While, in principle, the dual gravitational description of such holographic field theories always exists as a full quantum theory of gravity, in practice holography can only give insights into the field theory when the gravitational theory is in a semiclassical regime. This regime corresponds to a small Planck length in the bulk, and hence a large number of degrees of freedom in the field theory. While the 'real' field theories in which we might typically be interested do not have arbitrarily many degrees of freedom (nor necessarily even a holographic dual description), there has nevertheless been a large effort in using holography to describe physics for theories with relatively few degrees of freedom, or even in theories without holographic duals. An example of such an application is to heavy ion physics motivated by the resemblance between QCD and certain Yang-Mills theories which do possess (at least conventional) dual gravitational descriptions, and under the assumption that three colours in QCD is 'close' to large N in Yang-Mills for the purposes of computing observables of interest (see e.g. [116] for a review).

When pushing holography beyond its obvious regime of validity, a phenomenological question then arises: how similar is the behaviour of holographic field theories to conventional ones? In this chapter (based on [4]), we will explore this question in the context of the computation of vacuum energies of (2+1)-dimensional CFTs on ultrastatic backgrounds. Specifically, we will compare the vacuum energy of two free CFTs — the massless Dirac fermion and the conformally-coupled scalar — to that of a holographic CFT as a functional of their spatial geometries. As in Chapter 5, we will take the CFTs to live on a product of time with a topological two-sphere.

While simple, this setting is of physical interest — recall that the free massless fermion is an effective description of the behaviour of electrons in monolayer graphene (and generalisations thereof) near Dirac points, with the geometry on which the fermion lives given by (a slight modification of) the geometry of the monolayer [35–37, 43]. The behaviour of the vacuum energy of the free Dirac fermion on these geometries may therefore be relevant to technological applications. From a different perspective, various statements about the vacuum energy and energy density in the holographic theory in this setting can be proved using elegant geometric arguments — for example, for deformations of the two-sphere for which there exists an infilling bulk geometry, the vacuum energy is globally maximised by the round sphere, as demonstrated in Section 1.3. In Section 5.5, we presented evidence this may also be true for free field theories, suggesting this might be a universal behaviour among a large class of field theories, even beyond CFTs.

For a (2+1)-dimensional CFTs (as all the theories we will consider in this chapter are), the energy on the round two-sphere vanishes, and one is naturally led to ask how the energy varies as the sphere is deformed. Since the dependence of the free energy on the volume of the deformed sphere is trivial, we will restrict to perturbations that leave this volume unchanged. For small such deformations, we noted in Section 1.4 that the vacuum energy is universal for all CFTs, depending only on the theories through their central charge. For large deformations, one would instead naïvely expect different behaviours for different theories. However, in the previous chapter we observed that for fixed-volume deformations, the vacuum energies of the minimally-coupled scalar (which is *not* a CFT) and of the Dirac fermion actually were not only always negative relative to the round sphere, but also qualitatively very similar. Perhaps this is not too surprising — the scalar and fermion are both free theories, after all. Our purpose in this chapter is to compare the free-field results to those of a holographic CFT, which on the other hand is strongly coupled.

We will find that the behaviours of the vacuum energies of the scalar, fermion, and holographic CFTs are all qualitatively very similar. In fact, our comparison of these energies yields a surprise: for a wide range of non-perturbative deformations of the sphere (with its volume held fixed), the vacuum energy of the holographic theory is remarkably *quantitatively* close to that of the free fermion. While they are not identical, the surprising closeness of these energies is somewhat of a mystery and perhaps suggests the presence of some underlying mechanism responsible for this fine-tuning. Moreover, such a close agreement between the fermion and the holographic CFT has also been exhibited in entropic computations like the entanglement entropy corner function [117, 118] and the ratio c_s/c_T, where c_s is the coefficient in the thermal entropy density of a CFT in flat space: $s = c_s T^2$ [119]. We do note, however, that this similarity in the vacuum energy does not extend to other closely-related deformations. For instance, if we were to turn on a finite temperature, the confining nature of the holographic CFT would lead to a temperature-

independent free energy at sufficiently-low temperature with a corresponding first-order deconfinement transition [120], whereas the free theories would exhibit free energies with a non-trivial and smooth temperature dependence, as demonstrated in Chapter 5. Likewise, in Euclidean signature the analogue of the free energy is the partition function, which was computed in [95] for these three CFTs on the Euclidean squashed (Berger) three-sphere (which does not have a Lorentzian interpretation). In that case the fermion and holographic CFT yield different behaviours of the partition function, and in fact even the partition functions of the scalar and of the fermion are qualitatively different (for example, for large enough perturbations of the three-sphere, the partition function of the fermion is larger than that of the unsquashed sphere, while that of the scalar is always smaller). These observations naturally prompt the question of why the fermion, scalar, and holographic CFT vacuum energies are all so similar for the classes of deformations we will study in this chapter.

A plan for the chapter is as follows. Firstly, in Section 6.1 we will introduce the physical setup and the fixed-volume sphere deformations we will consider. In Section 6.2 we will review the harmonic approach to numerically constructing static solutions to the (Euclidean) Einstein equation with a non-positive cosmological constant [121–123], the approach used by my collaborators to construct the bulk geometries of interest in this chapter. We will also review their novel method for extracting the vacuum energy much more accurately than the entire vacuum stress tensor itself. In Section 6.3 we will then compare the vacuum energies of the various deformations we will consider and briefly conclude in Section 6.4.

6.1 Physical Setting

As remarked above, we take our (2+1)-dimensional CFTs to be in vacuum on the space-time with manifold $\mathbb{R} \times \Sigma$ and metric

$$\mathrm{d}s^2 = -\mathrm{d}t^2 + h_{ij}\mathrm{d}y^i\,\mathrm{d}y^j, \tag{6.1}$$

where (Σ, h) is a (time-independent) two-dimensional Riemannian manifold with spherical topology. We do not turn on any other sources for local CFT operators. Consequently, the vacuum energy $E[h]$ is a functional only of the geometry h. Note that because we are considering the vacuum state of CFTs, all dimensionful scales are set by the geometry; therefore a rigid rescaling $h \to \lambda^2 h$ (for some constant λ) causes the vacuum energy to scale trivially as $E[h] \to \lambda^{-1}E[h]$. Hence, WLOG we fix the volume of (Σ, h) to be that of the unit round two-sphere: $\mathrm{Vol}[h] = 4\pi$.

On the ultrastatic geometry (6.1), the vacuum energy $E[h]$ can be defined as the integral over (Σ, h) of the energy density $\langle T_{tt}\rangle$, where $\langle T_{\mu\nu}\rangle$ is the VEV of the stress tensor.

For a general QFT there are counterterm ambiguities when renormalising the stress tensor on curved spacetime, but for a three-dimensional CFT the counterterms required by power counting — corresponding to a cosmological constant and an Einstein-Hilbert term in the action — both must vanish as they are not Weyl invariant. Hence, $E[h]$ is an unambiguous physical quantity. We further note that the vacuum energy vanishes when (Σ, h) is the round sphere (S^2, Ω), which can be seen most easily by noting that the corresponding Euclidean spacetime $\mathbb{R} \times S^2$[1] is conformally equivalent to Euclidean flat space $\mathbb{R}^3$ on which the vacuum stress tensor vanishes. The lack of any conformal anomaly means that the same must be true on the original geometry $\mathbb{R} \times S^2$, and hence $E[\Omega] = 0$[2].

We will consider three CFTs: a conformally-coupled scalar, a free Dirac fermion, and a holographic CFT in the regime in which its geometric dual is classical Einstein gravity (i.e. the limit of large central charge and strong coupling). These have central charges $c_\mathrm{s} = 3/(4\pi)^2$, $c_\mathrm{f} = (3/2)/(4\pi)^2$, and $48c_\mathrm{h}/\pi^2$, respectively, and we recall that $c_\mathrm{h} = \ell^2/(16\pi G)$ with ℓ and G the dual AdS length and Newton's constant. Because we are turning on no sources besides the metric, for the holographic CFT we will take the dual gravity theory to be four-dimensional pure gravity with negative cosmological constant, whose solutions may be embedded in various top-down models in explicit cases such as e.g. the ABJM theory [124]. In principle, there could be situations in which bulk matter fields spontaneously condense. However, we will not consider such situations here.

Now, when (Σ, h) is a small deformation of the round sphere, we may write its metric in a form conformal to the round sphere as

$$h = \left(1 + 2\varepsilon f(\theta, \phi)\right) \left(\mathrm{d}\theta^2 + \sin^2\theta \, \mathrm{d}\phi^2\right), \tag{6.2}$$

with $|\varepsilon| \ll 1$. Recall that the leading-order behaviour of the vacuum energy in ε is, decomposing f in spherical harmonics as $f = \sum_{l,m} f_{l,m} Y_{l,m}(\theta, \phi)$, from Section 1.4, is

$$E[h] = -\varepsilon^2 \frac{\pi^2 c_T}{48} \sum_{l,m} |f_{l,m}|^2 \frac{(l^2-1)(l+2)}{l} \left(\frac{\Gamma\left(\frac{l+1}{2}\right)}{\Gamma\left(\frac{l}{2}\right)} \right)^2 + \mathcal{O}(\varepsilon^3), \tag{6.3}$$

with c_T the central charge of the theory, as given above. To compute the vacuum energy for general h we must instead use numerical computations. To make this more tractable we restrict to the case where (Σ, h) is axisymmetric; hence we take the metric to be

$$h = b(\theta)\mathrm{d}\theta^2 + s(\theta) \sin^2\theta \, \mathrm{d}\phi^2 \tag{6.4}$$

[1] With standard metrics.

[2] Thus, alternatively, we may view $E[h]$ as a differenced free energy, as defined in Chapter 4, between the vacuum energy on (Σ, h) and the vacuum energy on the unit round sphere — which we have shown to be UV-finite and unambiguous, and therefore physically meaningful.

(with the usual identification $\phi \sim \phi + 2\pi$) with smoothness at the poles $\theta = 0, \pi$ requiring that the functions $b(\theta)$ and $s(\theta)$ be smooth in θ there, as well as $b(0) = s(0)$ and $b(\pi) = s(\pi)$.

An appropriate transformation of θ allows us to write (6.4) in a form conformal to the round sphere; hence the space of axisymmetric geometries in which we are interested is parametrised by a single function of θ. This space is impossible to comprehensively explore numerically; we will therefore be satisfied with considering various one-parameter families of geometries that smoothly deform from the round sphere at $\varepsilon = 0$ to a singular geometry at some $\varepsilon \neq 0$. We will focus on two classes of such geometries:

Type 1 Geometries are embedded in $\mathbb{R}^3$ as surfaces of revolution given by an embedding function $r = R_\varepsilon(\theta)$ in the usual (r, θ, ϕ) spherical coordinates. These embeddings lead to the metric

$$h = (R_\varepsilon(\theta)^2 + R'_\varepsilon(\theta)^2)\mathrm{d}\theta^2 + R_\varepsilon^2(\theta)\sin^2\theta\,\mathrm{d}\phi^2. \tag{6.5}$$

Specifically, we will consider the one-parameter families of embedding functions given by

$$R_\varepsilon(\theta) = a_{l,\varepsilon}\left(1 + \varepsilon Y_{l,0}(\theta)\right) \tag{6.6}$$

for various l, with $a_{l,\varepsilon}$ a constant chosen to keep the volume fixed to 4π. As we will briefly discuss in Section 6.2, restricting to parity-symmetric geometries allows us to reach greater accuracy in the holographic CFT computations. Therefore, we will make this restriction from now on, corresponding to considering only even l. For each l, the range of ε is bounded as $\varepsilon_{\min} < \varepsilon < \varepsilon_{\max}$ (arising from the requirement that $R_\varepsilon(\theta) > 0$ for all θ); as $\varepsilon \to \varepsilon_{\min}$ the geometry remains connected but develops a cusp-like singularity, while as $\varepsilon \to \varepsilon_{\max}$ the geometry pinches off into disconnected components. In Figure 6.1 we plot these embeddings for the range of ε for which we will present numerical results in Section 6.3.

Type 2 Geometries are given by

$$h = \tilde{a}_{n,\varepsilon}\left(\mathrm{d}\theta^2 + H_{n,\varepsilon}(\theta)\sin^2\theta\,\mathrm{d}\phi^2\right), \tag{6.7}$$

where now

$$H_{n,\varepsilon}(\theta) = 1 + \varepsilon\sin^2(n\theta) \tag{6.8}$$

for various n, and again $\tilde{a}_{n,\varepsilon}$ is chosen to fix the volume to be 4π. These have even parity for $n \in \mathbb{Z}$, and now $\varepsilon \in (-1, \infty)$. Note that these geometries are not embeddable in $\mathbb{R}^3$ for all n and ε; in Figure 6.2 we show those that are. As $\varepsilon \to -1$ the geometry tends to pinch off into disconnected components, while as $\varepsilon \to \infty$ it remains connected but develops a cusp-like singularity.

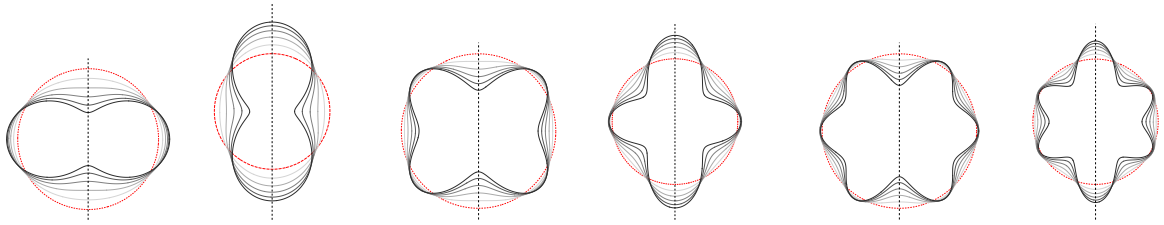

$l = 2$ $-0.51 < x < 0$ | $l = 2$ $0 < x < 0.6$ | $l = 4$ $-0.34 < x < 0$ | $l = 4$ $0 < x < 0.37$ | $l = 6$ $-0.28 < x < 0$ | $l = 6$ $0 < x < 0.3$

Figure 6.1: Embeddings of the geometries (6.5) in $\mathbb{R}^3$ for $l = 2$, 4, and 6; the full geometries are surfaces of revolution obtained by rotating about the dotted vertical line. The red dotted circle represents the undeformed round sphere, while from light grey to black the other curves show even spacings in x for the labeled range with x related to ε as in (6.9). The black curves, corresponding to the extremal values of x for each l, show the largest values of x for which we will present results in Section 6.3.

The Type 1 geometries (6.5) are those previously explored in Section 5.5 for the free scalar field and Dirac fermion. Here, we are limited by the accuracy of the holographic calculations so the deformations considered are less extreme than those in Section 5.5. We also consider the Type 2 geometries (6.7) partly for variety, but also partly to ensure that the phenomena we see are not specifically tied to considering geometries that are embeddable in $\mathbb{R}^3$. Moreover, the numerical methods perform slightly better on the Type 2 geometries than on Type 1 due to the simpler form of the metric functions. We also note that for both types of geometry, it will be useful to introduce a modified deformation parameter

$$x = \frac{\varepsilon}{A\varepsilon + B}, \tag{6.9}$$

with A and B chosen so that $x \in (-1, 1)$[3].

Our primary purpose in this chapter is to compare the vacuum energy of a holographic CFT for these classes of geometries, with the results obtained for the conformally-coupled scalar and the massless free Dirac fermion. These latter two CFTs have Euclidean actions given by

$$S_{\mathrm{E}}[\phi] = \frac{1}{2}\int \mathrm{d}^3x\sqrt{g}\,\phi\left(-\nabla^2 + \frac{1}{8}R\right)\phi, \tag{6.10a}$$

$$S_{\mathrm{E}}[\bar{\psi}, \psi] = i\int \mathrm{d}^3x\sqrt{g}\,\bar{\psi}\not{D}\psi; \tag{6.10b}$$

the reader is once again referred to Appendix A.3 for more on our conventions. The computation of the vacuum energy of these free theories is as described in the previous chapter. In short, the vacuum energy can be expressed in terms of the heat kernel defined by the spatial part of the equations of motion of the actions (6.10). Evaluating this

[3]Explicitly, for the Type 1 geometries we take $A = (\varepsilon_{\max} + \varepsilon_{\min})/(\varepsilon_{\max} - \varepsilon_{\min})$, $B = -2\varepsilon_{\min}\varepsilon_{\max}/(\varepsilon_{\max} - \varepsilon_{\min})$, while for the Type 2 geometries we take $A = 1$, $B = 2$.

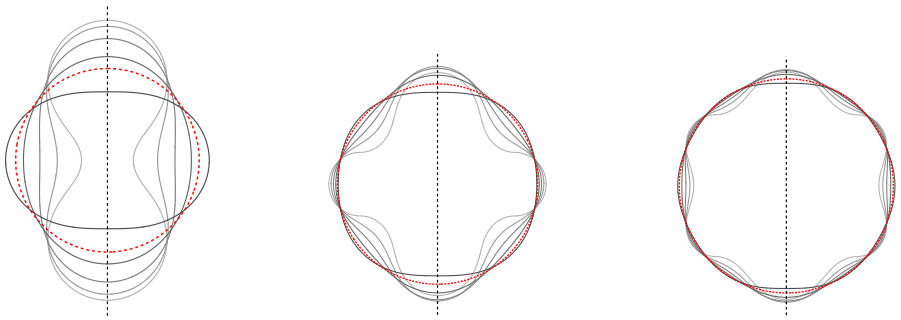

$n = 1$
$-0.905 \leqslant x \leqslant 1/7$

$n = 2$
$-0.422 \leqslant x \leqslant 1/25$

$n = 3$
$-0.178 \leqslant x \leqslant 1/55$

Figure 6.2: Axisymmetric embeddings of the geometries (6.7) in $\mathbb{R}^3$ for $n = 1$, 2, and 3 for the range of x for which embeddings exist; the full geometries are surfaces of revolution obtained by rotating about the dotted vertical line. The red dotted circle represents the round sphere $x = 0$, while the other curves show even spacings in x; lines go from light to dark with increasing x, with only the black lines corresponding to positive x. At positive x, embeddings fail to exist for $x > 1/(1 + 6n^2)$, corresponding to the Ricci curvature becoming negative at the poles (no axisymmetric embedding can have negative curvature at the poles). For negative x, corresponding to the lighter grey lines, the smallest values of x for which embeddings exist is determined numerically, except for the case $n = 1$ for which embeddings exist all the way to $x = -1$ when the sphere pinches off into two pieces (the lowest value $x = -0.905$ shown here is the smallest value of x reached in the numerics discussed in Section 6.3).

heat kernel amounts to computing the spectrum of the spatial part of the equations of motion, which can be done numerically using the pseudo-spectral methods described in Section 5.4. An improvement on the approximations used to calculate the vacuum energies in Chapter 5 is made possible by the restriction to zero temperature here. For more details on these computations, we refer the reader to Appendix B.4 where we give some details on the implementation and quantify its accuracy. Our focus now turns to the evaluation of the vacuum energy of the holographic CFT. This was carried out by my collaborators.

6.2 Holographic Gravity Solutions

Because we are considering CFTs dual to pure gravity, obtaining bulk solutions requires us to solve the vacuum Einstein equation with negative cosmological constant,

$$R_{AB} = -\frac{3}{\ell^2} g_{AB}, \tag{6.11}$$

for a static locally asymptotically AdS metric whose conformal boundary matches (6.4). Note that when the boundary sphere is deformed in an axisymmetric manner, we expect the static bulk to inherit this axisymmetry [125], so we will restrict to axisymmetric bulk solutions. For convenience, we also now choose units in which the AdS length $\ell = 1$.

In numerically constructing the bulk solutions, the harmonic approach of [121–123]

was followed. We will briefly summarise this here.

6.2.1 The Einstein DeTurck Equation

Suppose we seek static solutions to the Euclidean Einstein equations (6.11). We would expect such equations to be elliptic. However, when considered as a differential operator acting on metric perturbations the static Euclidean Einstein equations eliminate pure-gauge modes (i.e diffeomorphisms) and thus fail to be elliptic. Ellipticity is restored, however, when they are restricted to only act on physical degrees of freedom. This causes issues when attempting to numerically solve these equations using standard techniques for elliptic PDEs, most of which are relaxation methods. These start from an initial guess in configuration space and from there move in a (method dependent) direction that reduces the residual error. This step is then iterated until a sufficiently small error is achieved. To implement this numerically the metric components must be approximated by functions on a lattice — an approximation that is *only* accurate for functions which are smooth on the scale of the lattice spacing. As far as the relaxation method is concerned there is no cost to 'enhancing' a guess by short-wavelength gauge modes so they are not damped. They do, however, increase the discretisation error. These errors then accumulate and squander any hope of convergence. Therefore, the gauge freedom must be removed. The harmonic approach gives a covariant method for lifting the gauge freedom in the Einstein equations for static geometries giving an elliptic PDE. It proceeds as follows in the non-positive cosmological constant case.

To lift the gauge invariance we require a gauge-fixing condition. Let $\bar{g}$ be smooth (static) fiducial metric and $\Gamma^A_{BC}[\bar{g}]$ its Levi-Civita connection. Then $\xi^A = 0$, where

$$\xi^A \equiv g^{BC}\left(\Gamma^A_{BC}[g] - \Gamma^A_{BC}[\bar{g}]\right) \tag{6.12}$$

is the DeTurck vector, is a valid gauge fixing constraint [121]. The challenge then is to solve this constraint simultaneously with the Einstein equations. This can be done by solving the related Einstein DeTurck equation,

$$R_{AB} - \Lambda g_{AB} = \nabla_{(A}\xi_{B)}, \tag{6.13}$$

where Λ is a non-positive constant, provided an appropriate choice of $\bar{g}$ is made. By contracting the free index of the contracted Bianchi identity with ξ^A it follows that any solution to (6.13) satisfies the elliptic inequality

$$\nabla^2\xi^2 + \xi^A\nabla_A\xi^2 = \nabla_A\xi_B\nabla^A\xi^B - 2\Lambda\xi^2 \geqslant 0. \tag{6.14}$$

Thus, ξ^2 is subject to a maximum principle that guarantees ξ^2 can only attain max-

ima on a boundary of its domain and its outward normal derivatives, $\partial_n \xi^2$, at these maxima are strictly positive. So as long as $\xi^2 = 0$ or $\partial_n \xi^2 = 0$ on each boundary then $\xi^2 = 0$ everywhere. Choosing a $\bar{g}$ that obeys the same boundary conditions as g ensures that $\xi^2 = 0$ or $\partial_n \xi^2 = 0$ on each boundary [122] and thus that any solution to the Einstein DeTurck equations (6.13) is also a solution to the Einstein equations (6.11) subject to the constraint $\xi^A = 0$. Crucially, the Einstein DeTurck equations have principal part $-\frac{1}{2} g^{CD} \partial_C \partial_D g_{AB}$ and so are elliptic on static geometries and thus amenable to standard numerical methods for elliptic PDEs. My collaborators Krai Cheamsawat and Toby Wiseman used these to solve the Einstein DeTurck equations to find the bulk duals of the boundary geometries described in Section 6.1, finding the metric functions with a pointwise accuracy of one part in 10^6 or better. More details on these numerics can be found in [4].

Having found the bulk solutions, these can then be used to deduce the vacuum energy of the boundary CFTs. The most direct route the CFT energy is via integrating the boundary stress tensor (1.39) over the boundary. However, using this method compromises accuracy on two counts. Firstly, computing the boundary stress tensor requires third-order derivatives of the metric and, secondly, because this integral involves a lot of cancellation. This is evident from the perturbative case in Section 1.4 where we have seen that despite the stress tensor being perturbed at linear order the vacuum energy only varies quadratically. For these reasons, my collaborators extracted the energy via an alternative method, by using Equation (1.48):

$$E = -\frac{c_{\mathrm{h}}}{2} \int_{\mathcal{M}} \mathrm{d}^3 x \sqrt{\tilde{g}} \left| \tilde{R}_{IJ} - \frac{1}{3} \tilde{R}\, \tilde{g}_{IJ} \right|^2 , \tag{6.15}$$

where $(\mathcal{M}, \tilde{g})$ is the optical geometry $\tilde{R}_{IJ}$ and $\tilde{R}$ is the Ricci curvature of the optical metric, as defined in Section 1.4. The integrand here is at most second order in derivatives of the bulk metric, avoiding the need to compute third derivatives, and manifestly non-negative, bypassing the cancellation that occurs in computing (1.39). This formula, therefore, can be used to make much more accurate estimates of the holographic CFT energies.

6.3 Results

We now compare the vacuum energy of the holographic CFT, computed from numerical solutions using (6.15), to that of the conformally-coupled scalar and of the free Dirac fermion. Because the bulk geometries become more difficult to obtain as the boundary spheres approach becoming singular, we only present results for which we are confident in the holographic CFT calculation to about 0.01% or better (the accuracy of the results we present is limited by the holographic computations; the vacuum energies of the free fields can be obtained comfortably to larger deformations, as was done in Chapter 5).

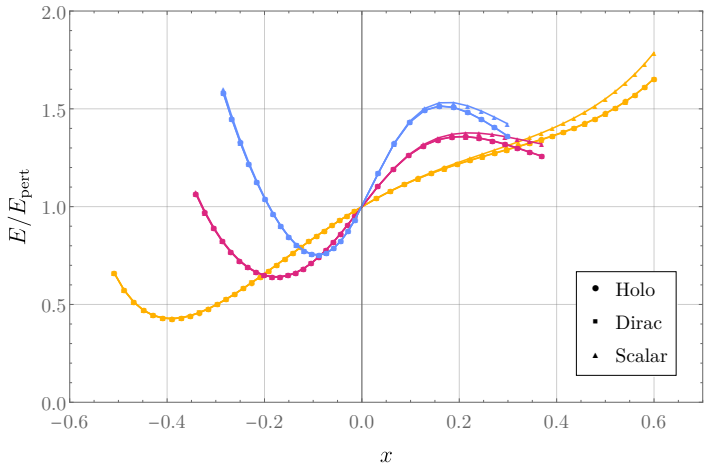

Figure 6.3: The vacuum energy for the conformal scalar, Dirac fermion, and holographic CFT on the Type 1 geometries (6.5); orange, magenta, and blue correspond to $l = 2$, 4, and 6, respectively. The energies are normalised by the perturbative behaviour (6.3), hence all the curves cross through 1 at $x = 0$ by design. Note that the data for the holographic CFT and the fermion cannot be distinguished by eye on this plot. Also note that for visual clarity we show only the restricted domain $x \in (-0.6, 0.7)$ (all other plots in this chapter show the full domain $x \in (-1, 1)$).

In Figure 6.3 we show the vacuum energy of the Type 1 deformations for $l = 2$, 4, and 6, normalised by the perturbative expectation (6.3). Outside the range of x for which we show data, either the gravity solutions have significant numerical error at the maximum resolutions used, it was not possible to find solutions at all. It is thought, however, that these do solution do in fact exist and the failure to find them is due to limitations of the numerics. Likewise, in Figure 6.4 we show the vacuum energy of the Type 2 deformations for $n = 1$, 2, and 3, again normalised by the perturbative expectation (6.3). Note that in this case larger values of x are reached than those shown in Figure 6.3; in part this is simply because the Type 2 deformations grow more slowly with x than the Type 1 ones. To illustrate this more explicitly, in Figure 6.5 we show the difference $(R_{\text{max}} - R_{\text{min}})/R_0$ between the maximum and minimum Ricci scalar of the boundary geometries (6.5) and (6.7), normalised by the value $R_0 = 2$ for the round sphere. An important feature to note is that over the range of x shown in Figures 6.3 and 6.4, the Ricci scalar varies by about two orders of magnitude, so these deformations are far from the perturbative regime[4].

It is worth noting that for large deformations, the conformal scalar may develop a negative eigenvalue of $-\nabla^2 + R/8$, that renders the theory ill defined. For the ranges of x shown here this occurs for the positive-x Type 2 geometries. Indeed, in Figure 6.4 the scalar energies extend to smaller (positive) values of x than those of the Dirac and

[4]That our most extreme deformations are well outside the perturbative regime can also be seen more intuitively but more qualitatively by noting that the embeddings shown in Figure 6.1 simply look like large deformations of the round sphere.

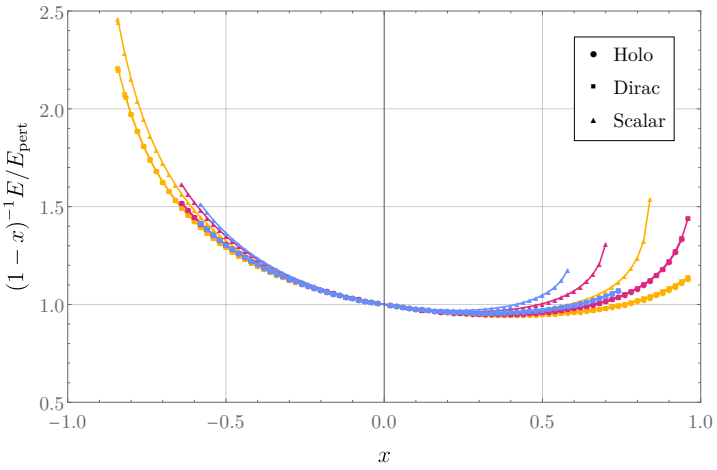

Figure 6.4: The vacuum energy for the conformal scalar, Dirac fermion, and holographic CFT on the Type 2 geometries (6.7); orange, magenta, and blue correspond to $n = 1$, 2, and 3, respectively. The energies are normalised by the perturbative behaviour (6.3), hence all the curves cross through 1 at $x = 0$ by design; note also an additional normalisation factor of $(1 - x)^{-1}$, introduced to clarify the behaviour near $x = 1$. We emphasise that the data for the holographic CFT and the fermion cannot be distinguished by eye on this plot. We note that the scalar theory has less extent in the positive x sense than the other theories as it ceases to exist when the conformal Laplacian $-\nabla^2 + R/8$ fails to be positive.

holographic theories for precisely this reason. An interesting point is that the results of [126][5] show that when the conformal Laplacian $-\nabla^2 + R/8$ has a negative eigenvalue, there does not exist a Weyl rescaling of the full (2+1)-dimensional spacetime to another static spacetime with positive Ricci scalar. But, as far as we are aware, the only arguments for the existence of bulk gravity solutions in our setting require a static Weyl frame with positive boundary scalar curvature [125]. Since my collaborators were able to construct holographic bulk solutions beyond the regime in which the conformal scalar is well defined, their results show that bulk solutions apparently continue to exist even when there is no conformal frame where the boundary metric has positive curvature.

Returning to the vacuum energies, the first striking feature of Figures 6.3 and 6.4 is how similar the behaviour of the vacuum energy is between the three theories. This similarity had already been observed in Chapter 5 between the fermion and the minimal scalar, even at non-zero temperature and mass (at high temperature, the similarity can be explained by a hydrodynamic expansion). Here, we see that the similarity extends to the conformal scalar and to the holographic CFT. Perhaps more striking is the fact that the Dirac fermion and the holographic CFT almost perfectly coincide: in Figures 6.6a and 6.7a we show the ratio $c_{\text{f}}^{-1}E_{\text{Dirac}}/c_{\text{h}}^{-1}E_{\text{holo}}$ of the vacuum energies of the Dirac fermion and the

[5] In fact, the proof of the result as it stated in [126] is not quite correct for the (2+1)-dimensional case we are interested in. However, following some minor modifications to arguments used there, the result can be shown in this case. This argument is detailed in Appendix C.

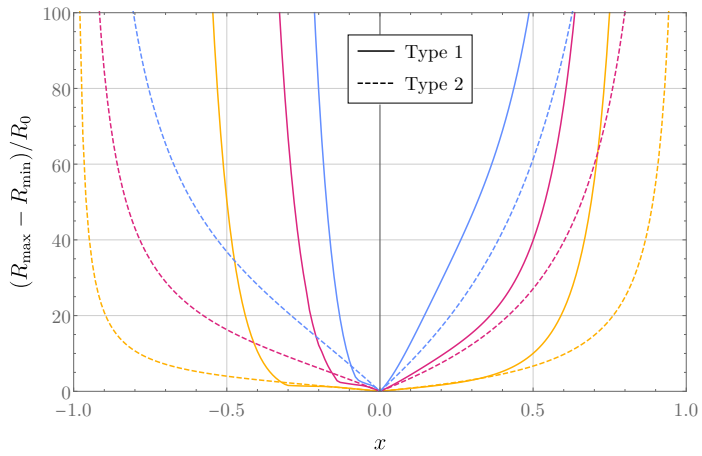

Figure 6.5: The difference $(R_{\max} - R_{\min})/R_0$ between the maximum and minimum values of the Ricci scalar on the geometries (6.5) and (6.7), normalised by the value on the round sphere $R_0 = 2$; solid orange, magenta, and blue correspond to the $l = 2$, 4, and 6 Type 1 geometries, while dashed orange, magenta, and blue correspond to the $n = 1$, 2, and 3 Type 2 geometries.

holographic CFT normalised by their central charges, noting that they agree to $\sim 0.1\%$ for most of the deformations, and still to better than 1% for the entire range we are able to accurately construct; this is reminiscent of the similarity seen in Chapter 4 between the Dirac fermion and holographic CFTs on deformations of flat space, that persisted to non-zero temperatures. Importantly, the difference shown in Figures 6.6a and 6.7a is substantially larger than any of our numerical uncertainties (which recall we restricted to be no larger than roughly 0.01%), indicating that despite the close quantitative agreement, the fermion and the holographic CFT do not coincide *exactly*. We do not know of an explanation for this behaviour; a putative explanation may well require some kind of fine-tuning. We also note that while we fix the volume of the deformations to that of the undeformed sphere, this is irrelevant for the ratio of energies plotted in Figures 6.6a and 6.7a, due to the scale invariance of the theories.

For comparison, in Figures 6.6b and 6.7b we also show the ratio $c_{\rm s}^{-1}E_{\rm scalar}/c_{\rm h}^{-1}E_{\rm holo}$ of the vacuum energies of the conformally-coupled scalar and the holographic CFT normalised by their central charges; this ratio is much larger than that with the fermion. Notably, for the Type 2 deformations shown in Figure 6.7b this ratio becomes quite large for the most extreme deformations at positive x, indicating a substantial deviation between the behaviour of the scalar field and the holographic CFT — this deviation is presumably related to the aforementioned fact that at large x, the conformal scalar becomes ill defined due to $-\nabla^2 + R/8$ acquiring a negative eigenvalue.

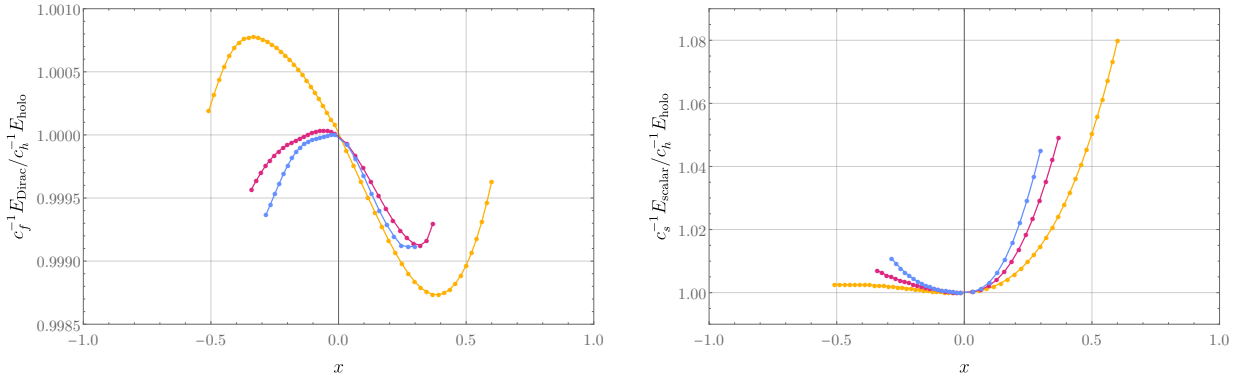

(a) Fermion

(b) Scalar

Figure 6.6: The ratio between the vacuum energy of the holographic CFT and the free fields on the geometries (6.5); orange, magenta, and blue correspond to $l = 2$, 4, and 6, respectively. Note that the variation between the Dirac fermion and the holographic CFT is less than $\sim 0.1\%$ for all the deformations shown here, while the variation between the scalar and the holographic CFT reaches up to $\sim 8\%$.

6.4 Discussion

We have numerically computed the vacuum energy of two types of CFTs, the massless Dirac fermion and conformally-coupled scalar, whose spatial geometries are given by the deformed spheres (6.5) and (6.7), and we have seen that even for large deformations of the sphere the behaviour of the vacuum energy is remarkably qualitatively similar, both to each other and to that of a holographic CFT. This similarity is perhaps even more surprising given that the scalar and Dirac fields are free theories, while the holographic theory is strongly coupled. Moreover, the agreement between the Dirac fermion and the holographic CFT is generally better than 0.1%, and everywhere better than 1% for the deformations that were constructed and over which there was good numerical control. The strongest deviations are found for the most singular geometries where it becomes challenging to construct the gravity solutions, and also preserve good accuracy for the free theories. This close agreement between a free theory and a strongly-coupled one deserves a better understanding, especially in light of related results showing that the free massless fermion and the holographic CFT dual to Einstein gravity show close agreement in other ways, e.g. in the entanglement entropy corner function [117, 118] and in the ratio c_s/c_T [119].

One natural guess is that conformal invariance somehow enforces the behaviour of the vacuum energy to be universal beyond the leading perturbative order (6.3). This is clearly not consistent with our results: the subleading behaviour of the vacuum energy of perturbations of the round sphere is captured by the behaviour of Figures 6.6 and 6.7 around $x = 0$, and the non-zero slope there indicates that the vacuum energies of the three theories do not agree exactly beyond leading order. Nevertheless, it is worth noting

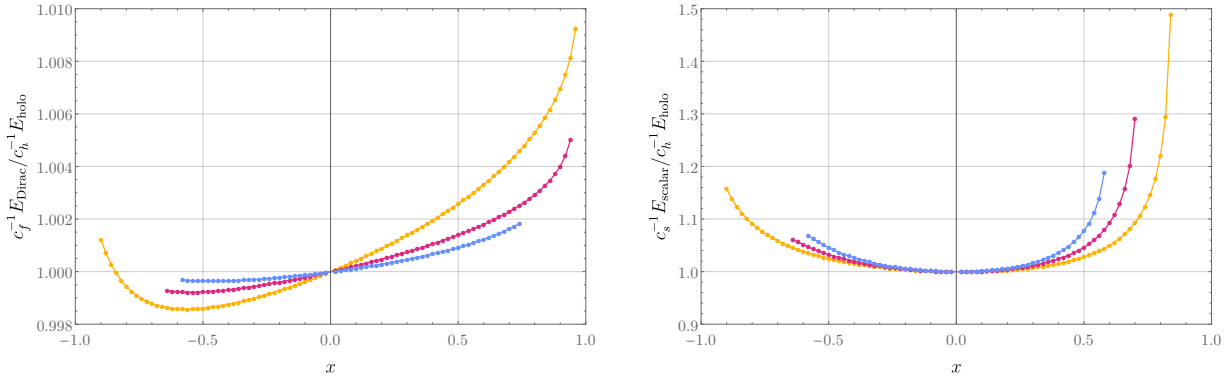

(a) Fermion (b) Scalar

Figure 6.7: The ratio between the vacuum energy of the holographic CFT and the free fields on the geometries (6.7); orange, magenta, and blue correspond to $n = 1$, 2, and 3, respectively. Note that the variation between the Dirac fermion and the holographic CFT is less than $\sim 1\%$ for all the deformations shown here, while the variation between the scalar and the holographic CFT reaches up to $\sim 50\%$ for the most extreme deformations.

that in certain contexts there can be close agreement between the free fermion, conformal scalar, and holographic CFTs dual to pure Einstein gravity beyond leading perturbative order. Indeed, the partition function of CFTs on the squashed Euclidean three-sphere S^3_α has been studied in e.g. [95, 113, 114, 127]:

$$\ln Z[S^3_\alpha] - \ln Z[S^3_{\alpha=0}] = c\left(a_2\alpha^2 + a_3\alpha^3\right) + \mathcal{O}(\alpha^4), \tag{6.16}$$

where α is a squashing parameter, c is the central charge, a_2 is theory-independent due to conformal invariance, and a_3 is constructed from the three-point function of the stress tensor on the round sphere. In fact, for a large class of holographic CFTs a_3 is proportional to the three-point function charge t_4 (defined in [128]; see also [59]), while numerical results suggest that this proportionality also holds for the massless Dirac fermion and the conformal scalar [114]. For holographic CFTs dual to Einstein gravity, a_3 vanishes, while for the massless fermion and the conformal scalar it is non-zero but of order 10^{-3}. Hence, the subleading behaviour of the squashed sphere partition function (6.16) almost agrees for all three of these theories, reminiscent of the small but non-zero difference between the free energies of the holographic CFT and of the fermion shown in Figures 6.6a and 6.7a.

However, the results of [95] on the squashed three-sphere merely exhibited a surprising similarity between the partition functions of the scalar, fermion, and holographic CFT for *small* squashings; for non-perturbatively large squashings, the fermion behaves very differently from the holographic CFT (in fact, the fermion partition function can even change sign relative to that of the unperturbed sphere, whereas that of the holographic CFT always has fixed sign). Hence, the close quantitative agreement between the Dirac fermion and the holographic CFT we have seen here must somehow rely on

the particular structure of the deformations we have considered. One might therefore conclude that perhaps our results are merely an odd coincidence, potentially due to the symmetries we have imposed to make the computations numerically tractable; namely: ultrastaticity, axisymmetry, and parity.

In any case, we note the behaviour of the vacuum energy exhibited by non-perturbative Type 2 deformations of the two-sphere in this chapter provides further evidence that QFTs on (2+1)-dimensional ultrastatic backgrounds universally disfavour maximally-symmetric spatial geometries. In the following chapter, we will begin to make steps towards finding out *why* this vacuum energy negativity appears to hold so broadly.

Chapter 7

Power-Counting-Renormalisable Theories on Flat Space

The vacuum energy of (2+1)-dimensional QFTs as a functional of their spatial geometries is maximised locally by symmetric spaces — for flat and spherical topologies — for a broad selection of theories. This universal behaviour is exhibited by a diverse range of theories, from non-interacting massive particles to strongly-coupled CFTs with a large number of degrees of freedom. Because of the differences between them, the optimal approach for calculating the vacuum energy has been different for each type of theory — our treatment of free theories appealed to heat kernel methods while all holographic results have relied on constructing solutions to classical gravity equations. While the qualitative diversity of the theories we have considered is interesting — it suggests that vacuum energy non-positivity may hold rather generally — it could be said that the ad-hoc approach to calculating the vacuum energy, though necessary to probe the global aspects of the vacuum energy functional that are intractable for a generic theory, has not been conducive to revealing the fundamental reason *why* vacuum energy negativity seems to hold so broadly. A less theory-dependent approach could help to gain insight into this issue. Our purpose, therefore, is to adopt a new theory-independent approach to computing the vacuum energy and gain some insight into the seemingly universal vacuum energy non-positivity of (2+1)-dimensional QFTs on ultrastatic geometries.

In this chapter (based on work done in collaboration with Andrew Tolley and Toby Wiseman), we will adopt a new approach to computing vacuum energy in (2+1)-dimensional QFT which will then used to show vacuum energy non-positivity for *all* power-counting-renormalisable relativistic QFTs with a mass gap on a product of time with a small deformation of flat $\mathbb{R}^2$. This set of theories include the massive free scalar and fermion theories studied in Chapter 3 and also many other interacting theories, such as Yang-Mills, but are, of course, disjoint from CFTs (that have already been accounted for by the results of Section 1.4). As such, we further extend the set of (2+1)-dimensional QFTs whose vacuum energy we know is maximised locally by flat space.

In contrast to previous chapters, our analysis will be carried out using canonical methods. As noted in Chapter 4, the response of the vacuum energy on a d-dimensional space with metric g, $E[g]$, due to a change in g is determined by the VEV of the stress tensor on that space. When perturbing flat space, it turns out that the leading-order non-local contribution to the variation of $E[g]$ is given in terms of the time-ordered two-point function of the stress tensor on flat space. Provided the theory is Lorentz invariant, we will find that the two-point function of stress tensors on flat space makes a universal contribution to the vacuum energy, with all the theory dependence captured by two spectral densities. Further, we will find that the positive definiteness of Hilbert Space norms necessitates that these functions are non-negative and, therefore, that the time-ordered two-point function makes a negative non-local contribution to the variation of $E[g]$ for all non-trivial perturbations to g. In the special case of $d = 2$ this is sufficient to deduce that the vacuum energy is negative since, after appropriate regularisation, $E[g]$ is a finite and unambiguous — i.e. it is insensitive to renormalisation-scheme ambiguities that are usually associated with local terms — measure of vacuum energy. This work assumes very little about the theories in question and, in doing so, highlights a property that potentially plays a key role in the negativity of $E[g]$: the Poincaré invariance of flat spacetime.

The plan for this chapter is as follows. The setup of the problem will be established in Section 7.1 with particular attention paid to the definition of the vacuum energy and the geometries for which a finite and unambiguous measure of the vacuum energy can be obtained. Section 7.2 will set out the steps to calculate the perturbative variation of the vacuum energy due to spatial metric perturbations around flat space — including the case of non-diffeomorphism-invariant regulation. The spectral decomposition of the two-point function of the stress tensor for power-counting-renormalisable theories on flat space with a mass gap will be illustrated in Section 7.3 with explicit examples given in the case of free massive scalars with curvature coupling and Dirac fermions. In Section 7.4, the implications of this decomposition for the variation of the vacuum energy will be discussed. The chapter will then conclude with a summary in Section 7.5.

7.1 Setup

We consider a QFT on an $n = (d+1)$-dimensional Lorentzian manifold that is a product of time with a static d-space, (Σ, g),

$$\mathrm{d}s^2 = \hat{g}_{\mu\nu}\mathrm{d}x^\mu \mathrm{d}x^\nu = -\mathrm{d}t^2 + g_{ij}\mathrm{d}x^i \mathrm{d}x^j, \tag{7.1}$$

in its vacuum state. For a theory with matter fields Φ and action $S[g, \Phi]$, the energy of the theory in the vacuum state is the integral of the energy density over a spatial slice of

the background,

$$E[g] = \int \mathrm{d}^d x \sqrt{g} \langle T_{tt}(t,x) \rangle_g, \tag{7.2}$$

where the stress tensor is defined by $T_{\mu\nu}(t,x) \equiv -(2/\sqrt{|\hat{g}|})(\delta S/\delta \hat{g}^{\mu\nu}(t,x))$ and correlation functions are defined with respect the path integral $Z[g] \equiv \int \mathcal{D}\Phi \mathrm{e}^{iS[g,\Phi]}$, so that, in particular,

$$\langle T_{\mu\nu}(t,x) \rangle_g = \frac{1}{Z[g]} \int \mathcal{D}\Phi \, T_{\mu\nu}(t,x) \mathrm{e}^{iS[g,\Phi]}. \tag{7.3}$$

We note that, due to time translation invariance, the VEV of $T_{\mu\nu}$ and therefore $E[g]$ are time independent. As ever, it is key that we consider a quantity that is finite and unambiguous. In Chapter 3, we showed that with a diffeomorphism-invariant regulator, $\Delta E[g] = E[g] - E[\bar{g}]$ is such a quantity in (2+1) dimensions — provided that $\bar{g}$ endows Σ with a volume matching that of g. Here, we also treat regulation that is not diffeomorphism invariant. Along with the counterterms required to renormalise the flat-space theory[1], renormalising the theory on a general curved space (Σ, g) involves local geometric counterterms[2],

$$S_{\mathrm{CT}} = \int^{\Lambda} \mathrm{d}^n x \sqrt{|\hat{g}|} \left(a_0 + a_2 R + \ldots + a_{\lfloor n/2 \rfloor} R^{\lfloor n/2 \rfloor} \right), \tag{7.4}$$

and also *non*-diffeomorphism-invariant counterterms whose finite parts are fixed by the requirement that the renormalised stress tensor is finite and conserved i.e.

$$\langle \chi | T_{\mu\nu} | \psi \rangle \text{ is finite and } \nabla^\mu \langle \chi | T_{\mu\nu} | \psi \rangle = 0 \tag{7.5}$$

for all $|\chi\rangle$ and $|\psi\rangle$. These conditions do not determine the finite parts of the a_{2i} coefficients. This is as much progress as we can make without any further assumptions the dimension d. Our case of interest is when Σ is topologically $\mathbb{R}^2$. It is conventional to renormalise the VEV of the stress tensor to vanish on flat space[3] so that $E[\delta] = 0$. This fixes the value of a_0 as the regulator is removed. Further, a_2 is the coefficient of the (vanishing) Euler characteristic for two-dimensional Σ, and thus a_2 makes no contribution. Power counting in $d = 2$ rules out contributions from further relevant local geometric counterterms and thus the vacuum energy, $E[g]$, as defined by (7.2) is finite, unambiguous and corresponds to the physical energy difference from flat space considered in Chapter 4 provided we renormalise as set out above. For $d > 2$ this quantity is ambiguous — not only is the Einstein-Hilbert term no longer topological but there are finite ambiguities coming from the coefficients of the further relevant higher-derivative terms.

[1] As before, no sources other than the metric will be varied here.

[2] Here $R^{\lfloor n/2 \rfloor}$ schematically represents $2\lfloor n/2 \rfloor$ derivative higher curvature terms.

[3] This is possible because homogeneity and isotropy imply that $\langle T_{\mu\nu} \rangle_g \propto (\text{const.}) \hat{g}_{\mu\nu}$ and thus the constant can be tuned to zero by a_0.

7.2 Perturbation Theory

We are interested in the local behaviour of $E[g]$ near $(\mathbb{R}^2, \delta)$. We consider perturbations about flat space, $(\Sigma, \bar{g})$, so that

$$g^{ij}(\varepsilon) = \bar{g}^{ij} - \varepsilon h^{ij}, \;\; g_{ij}(\varepsilon) = \bar{g}_{ij} + \varepsilon h_{ij} + \varepsilon^2 h_{ik} h^k{}_j + \mathcal{O}(\varepsilon^3) \tag{7.6}$$

where $|\varepsilon| \ll 1$, $h_{ij}(x)$ is a time independent metric perturbation and indices are raised and lowered with respect to the reference metric $\bar{g}$. We work perturbatively in ε. For deformations of this form with $\bar{g}_{ij} = \delta_{ij}$, the counterterms are of the form

$$S^{\text{tot}}_{\text{CT}}[g] = \int^{\Lambda} \mathrm{d}^n x \left(b^{(0)} + \varepsilon b^{(1)}_{ij} h^{ij} + \varepsilon^2 h^{ij} b^{(2)}_{ij,k\ell} h^{k\ell} + \mathcal{O}(\varepsilon^3) \right) \tag{7.7}$$

where $b^{(0)}$ is a constant and $b^{(1)}_{ij}$ and $b^{(2)}_{ij,kl}$ are differential operators that depend on the regulator and the physical parameters. They will include both contributions from geometric counterterms, such as the cosmological term

$$\int^{\Lambda} \mathrm{d}^n x \, \sqrt{g} a_0 = a_0 \int \mathrm{d}^n x \left(1 + \varepsilon \frac{1}{2} \delta_{ij} h^{ij} + \varepsilon^2 \frac{1}{8} h^{ij} \left[\delta_{ij}\delta_{k\ell} + \delta_{ik}\delta_{j\ell} + \delta_{i\ell}\delta_{jk} \right] h^{k\ell} + \mathcal{O}(\varepsilon^3) \right) \tag{7.8}$$

and the Einstein-Hilbert term

$$\begin{aligned} \int \mathrm{d}^n x \sqrt{g} a_2 R = a_2 \varepsilon^2 \int \mathrm{d}^n x \Big(& h^{ij} \Big[\left\{ \delta_{k(i}\delta_{j)\ell} - \delta_{ij}\delta_{k\ell} \right\} \partial^2 \\ & - \delta_{k(i}\partial_{j)}\partial_\ell - \delta_{\ell(i}\partial_{j)}\partial_k + \delta_{ij}\partial_k\partial_\ell + \delta_{k\ell}\partial_i\partial_j \Big] h^{k\ell} + \mathcal{O}(\varepsilon^3) \Big) , \end{aligned} \tag{7.9}$$

and the counterterms required to impose diffeomorphism invariance. Recall from Equation (4.7) that under such a deformation the vacuum energy varies as

$$\frac{\mathrm{d}E}{\mathrm{d}\varepsilon} = -\frac{1}{2} \int \mathrm{d}^2 x \sqrt{g(\varepsilon)} \langle T_{ij}(0,x) \rangle_{g(\varepsilon)} h^{ij}(x) \, . \tag{7.10}$$

Thus, the variation of the vacuum energy is determined by the VEV of the stress tensor on (Σ, g). Under a deformation to the geometry (7.6) the stress tensor varies as

$$\sqrt{g(x)} T_{ij}(t,x) = \sqrt{\bar{g}(x)} \, \overline{T}_{ij}(t,x) + \varepsilon \sqrt{\bar{g}(x)} \, O_{ij,k\ell}(t,x) h^{k\ell}(x) + \mathcal{O}(\varepsilon^2) \tag{7.11}$$

and the action is deformed from $S[\bar{g}, \Phi] \mapsto S[g(\varepsilon), \Phi]$ so that it is the sum of the reference space action and a correction, $S[g(\varepsilon), \Phi] = S[\bar{g}, \Phi] + \Delta S[\varepsilon, \Phi]$, that is given explicitly by

$$\Delta S[\varepsilon, \Phi] = \frac{1}{2} \varepsilon \int \mathrm{d}^n x \sqrt{\bar{g}(x)} h^{ij}(x) \overline{T}_{ij}(t,x) + \mathcal{O}(\varepsilon^2) \tag{7.12}$$

where $\overline{T}_{\mu\nu}(t,x)$ is the renormalised stress tensor of the flat-space theory, i.e. it satisfies (7.5), and $O_{\mu\nu,\rho\sigma}$ is a local[4] flat-space operator satisfying $O_{\mu\nu,\rho\sigma} = O_{(\mu\nu),\rho\sigma} = O_{\rho\sigma,\mu\nu}$. These operators contain the counterterms that renormalise the theory, both for $g = \bar{g}$ and deformations of it, as described in Section 7.1. The $b^{(1)}_{ij}$ and $b^{(2)}_{ij,k\ell}$ terms in Equation (7.7) are part of the $\overline{T}_{ij}$ and $O_{ij,k\ell}$ operators in ΔS, respectively ($b^{(0)}$ is part of $S[\bar{g},\Phi]$). In particular, the $\mathcal{O}(\varepsilon)$ term in Equation (7.8) is part of the $\overline{T}_{ij}$ term in Equation (7.12) and the $\mathcal{O}(\varepsilon^2)$ terms are part of $O_{ij,k\ell}$ (and the $\mathcal{O}(\varepsilon^0)$ term is part of $S[\bar{g},\Phi]$). Since $(\Sigma,\bar{g})$ is maximally symmetric i.e. is both homogeneous and isotropic, we can tune a_0 so that $\langle\overline{T}_{ij}(t,x)\rangle_{\bar{g}} = 0$ (which, we note, also sets $\langle\overline{T}_{tt}(t,x)\rangle_{\bar{g}} = 0$). We can then express the VEV of the stress tensor on (Σ,g) in terms of flat space theory quantities by expanding the action and the stress tensor in Equation (7.3) about $\varepsilon = 0$:

$$\begin{aligned}\langle T_{ij}(0,x)\rangle_{g(\varepsilon)} = &\left(\int \mathcal{D}\Phi\, \mathrm{e}^{iS[\bar{g},\Phi]}\left[1+\frac{i\varepsilon}{2}\int \mathrm{d}t\,\mathrm{d}^d y\sqrt{\bar{g}(y)}h^{k\ell}(y)\overline{T}_{k\ell}(t,y)+\mathcal{O}(\varepsilon^2)\right]\right.\\ &\left.\left[\overline{T}_{ij}(0,x)-\frac{1}{2}\varepsilon h^{kk}(x)\overline{T}_{ij}(0,x)+\varepsilon O_{ij,k\ell}(0,x)h^{k\ell}(x)+\mathcal{O}(\varepsilon^2)\right]\right)\\ &\left(\int \mathcal{D}\Phi\, \mathrm{e}^{iS[\bar{g},\Phi]}\left[1+\frac{i\varepsilon}{2}\int \mathrm{d}t\,\mathrm{d}^d y\sqrt{\bar{g}(y)}h^{k\ell}(y)\overline{T}_{k\ell}(t,y)+\mathcal{O}(\varepsilon^2)\right]\right)^{-1}\end{aligned} \tag{7.13}$$

which, after using that the VEV of the stress tensor vanishes on flat space, gives

$$\langle T_{ij}(0,x)\rangle_{g(\varepsilon)} = \frac{i\varepsilon}{2}\int \mathrm{d}t\,\mathrm{d}^d y\sqrt{\bar{g}(y)}\langle\mathcal{T}\overline{T}_{ij}(0,x)\overline{T}_{k\ell}(t,y)\rangle_{\bar{g}}h^{k\ell}(y)+\varepsilon\langle O_{ij,k\ell}(0,x)\rangle_{\bar{g}}h^{k\ell}(x)+\mathcal{O}(\varepsilon^2). \tag{7.14}$$

where $\mathcal{T}$ is the time-ordering operator. Inserting this expression for $\langle T_{ij}(0,x)\rangle_{g(\varepsilon)}$ into Equation (7.10) and integrating term by term in ε gives

$$\begin{aligned}E[g] = -\frac{i\varepsilon^2}{8}\int \mathrm{d}t\,\mathrm{d}^d x\mathrm{d}^d y\sqrt{\bar{g}(x)}\sqrt{\bar{g}(y)}h^{ij}(x)\langle\mathcal{T}\overline{T}_{ij}(0,x)\overline{T}_{k\ell}(t,y)\rangle_{\bar{g}}h^{k\ell}(y)\\ -\frac{\varepsilon^2}{4}\int \mathrm{d}^d x\sqrt{\bar{g}(x)}\,h^{ij}(x)\langle O_{ij,k\ell}(0,x)\rangle_{\bar{g}}h^{k\ell}(x)+\mathcal{O}(\varepsilon^3)\end{aligned} \tag{7.15}$$

or

$$E[g] = -\frac{\varepsilon}{4}\int \mathrm{d}^d x\sqrt{\bar{g}(x)}\langle T_{ij}(0,x)\rangle_{g(\varepsilon)}h^{ij}(x)+\mathcal{O}(\varepsilon^3), \tag{7.16}$$

where we note the difference in prefactor with the similar looking relation in Equation (7.10). This is due to the fact that $\langle T_{ij}\rangle_{\bar{g}} = 0$ so that $\langle T_{ij}(0,x)\rangle_{g(\varepsilon)}$ is $\mathcal{O}(\varepsilon)$ and has been integrated up, giving a result that is, critically, correct up to $\mathcal{O}(\varepsilon^3)$.

In order for $E[g]$ to be diffeomorphism invariant we must have that the VEV of the stress tensor on (Σ,g) is conserved and therefore that the combination of the time-ordered

[4] We assume that when the theory is deformed from flat the curved-space stress tensor (and therefore $O_{\mu\nu,\rho\sigma}$) remains local.

two-point function of the stress tensor on flat space and the VEV of $O_{ijk\ell}$ on flat space as written in (7.14) must be too. The two-point function written here consists of a finite part but also local divergences that will be canceled by the counterterms that have been absorbed into the $O_{ij,k\ell}$ operator. Having renormalised so that $E[g]$ is diffeomorphism invariant, we, in particular, wish to extract the part of this two-point function that is finite and conserved. We will use a canonical approach here: the Hilbert Space of the theory will be central to our treatment and make manifest the positivity of the spectral densities that are essential to demonstrating the negative-definite nature of this two-point function. In this formulation the time-ordering operator is given by

$$\mathcal{T}\overline{T}_{\mu\nu}(x)\overline{T}_{\rho\sigma}(y) \equiv \Theta(x^0 - y^0)\overline{T}_{\mu\nu}(x)\overline{T}_{\rho\sigma}(y) + \Theta(y^0 - x^0)\overline{T}_{\rho\sigma}(y)\overline{T}_{\mu\nu}(x). \tag{7.17}$$

and does not, for example, give rise to time-ordered stress tensor two-point functions that are conserved a priori. This differs from the covariant time-ordering, $\mathcal{T}^\star$, that emerges from a path integral approach with covariant regulation, but only by local contact terms which parametrise renormalisation-scheme ambiguity [129]. For CFTs, we note that conformal symmetry eliminates all VEVs and constrains the form of the time-ordered two-point function to be (the analytic continuation to Lorentzian time of) Equation (1.57) which, when appropriately UV regulated as in [30], recovers the CFT negativity result of Section 1.4 via Equation (7.15). Here, we consider theories with a mass gap.

7.3 Spectral Decomposition

Our goal is to show that the static two-point function of flat space stress tensors make a negative contribution to the vacuum energy of deformed spaces when $d = 2$. Since we will only consider theories on flat space, the bars that had previously been used to denote flat space stress tensor will be dropped. This section will keep the dimension general, with discussion of the particular case of $d = 2$ restricted to matters of renormalisation[5]. The positivity properties of two-point functions are best seen via their Källén-Lehmann spectral representation [130, 131], which we will derive here. We will consider theories with a mass gap. Consider the Wightman function in momentum space

$$\widetilde{\mathcal{W}}_{\mu\nu\rho\sigma}(p) \equiv \int \mathrm{d}^{d+1}x\, \mathrm{e}^{-ip\cdot x}\langle 0|T_{\mu\nu}(x)T_{\rho\sigma}(0)|0\rangle. \tag{7.18}$$

where $|0\rangle$ is the unit-norm vacuum state. Since our theories are invariant under the Poincaré group $\mathrm{ISO}(d,1)$, we may choose the Hilbert Space basis to consist of states with

[5] We have already established that ambiguities are present for $d > 2$ in Section 7.1.

definite rest mass m_λ, d-momentum $\mathbf{p}$ and spin s[6] so that:

$$\mathbb{1} = |0\rangle\langle 0| + \sum_{\lambda,s} \int \frac{\mathrm{d}^d p}{(2\pi)^d} \frac{1}{2E_\lambda(\mathbf{p})} |\lambda, \mathbf{p}, s\rangle\langle \lambda, \mathbf{p}, s| \tag{7.19}$$

where $E_\lambda(\mathbf{p}) = \sqrt{m_\lambda^2 + \mathbf{p}^2}$ and, in particular, $|\lambda, 0, s\rangle$ form a unitary representation of the compact group $\mathrm{SO}(d)$ and so, by the Peter-Weyl Theorem, can be arranged into irreducible finite-dimensional unitary representations of $\mathrm{SO}(d)$. Assuming we have renormalised the VEV of $T_{\mu\nu}$ to zero, inserting this complete set of states gives that

$$\widetilde{\mathcal{W}}_{\mu\nu\rho\sigma}(p) \equiv \sum_{\lambda,s} \frac{(2\pi)\delta(p^0 - E_\lambda(\mathbf{p}))}{2E_\lambda(\mathbf{p})} \langle 0|T_{\mu\nu}(0)|\lambda, \mathbf{p}, s\rangle\langle \lambda, \mathbf{p}, s|T_{\rho\sigma}(0)|0\rangle, \tag{7.20}$$

from which it is evident that $\widetilde{\mathcal{W}}_{\mu\nu\rho\sigma}(p)$ only has support for timelike p with $p^0 > 0$. For these p, we can choose to work in the frame with $\mathbf{p} = 0$. By translation invariance $\langle 0|T_{\mu\nu}(x)|\lambda, \mathbf{p}, s\rangle = \langle 0|T_{\mu\nu}(0)\mathrm{e}^{ip\cdot x}|\lambda, \mathbf{p}, s\rangle$ so it follows from the conservation of the stress tensor that $\langle 0|T_{0\nu}(0)|\lambda, 0, s\rangle = 0$ and thus that the only non-zero components of the Wightman function in the rest frame are

$$\widetilde{\mathcal{W}}_{ijk\ell}(p^0, 0) \equiv \sum_{\lambda,s} \frac{(2\pi)\delta(p^0 - m_\lambda)}{2m_\lambda} \langle 0|T_{ij}(0)|\lambda, 0, s\rangle\langle \lambda, 0, s|T_{k\ell}(0)|0\rangle. \tag{7.21}$$

The stress tensor has only spin-0, T_{ii}, and spin-2, $\hat{T}_{ij} \equiv T_{ij} - T_{kk}\delta_{ij}/d$ parts, so only spin-0 and spin-2 states contribute. The spin-0 states give a contribution proportional to $\delta_{ij}\delta_{kl}$. The spin-2 representation spaces are traced over thus

$$\sum_{\lambda} \frac{(2\pi)\delta(p^0 - m_\lambda)}{2m_\lambda} \langle 0|\hat{T}_{ij}(0)|\lambda, 0, 2\rangle\langle \lambda, 0, 2|\hat{T}_{k\ell}(0)|0\rangle \tag{7.22}$$

is an isotropic $\mathrm{SO}(d)$ tensor of rank 4 that is symmetric in its first and last pairs of indices. This determines the tensorial structure of the spin-2 contributions[7] to be, along with the spin-0 terms,

$$\sum_{\lambda} \frac{(2\pi)\delta(p^0 - m_\lambda)}{2m_\lambda} \langle 0|T_{ij}(0)|\lambda, 0, 0\rangle\langle \lambda, 0, 0|T_{k\ell}(0)|0\rangle = \alpha^{(0)}(p_0) p_0^4 \left(\delta_{ij}\delta_{kl}\right), \tag{7.23a}$$

$$\sum_{\lambda} \frac{(2\pi)\delta(p^0 - m_\lambda)}{2m_\lambda} \langle 0|\hat{T}_{ij}(0)|\lambda, 0, 2\rangle\langle \lambda, 0, 2|\hat{T}_{k\ell}(0)|0\rangle = \alpha^{(2)}(p_0) p_0^4 \left(\delta_{i(k}\delta_{l)j} - \frac{1}{d}\delta_{ij}\delta_{kl}\right), \tag{7.23b}$$

[6] The spin here corresponds the eigenvalue under the operator $J^2 = J_{ab}J_{ab}/2$ where J_{ab}, $1 \leqslant a \neq b \leqslant d$, are the rotation operators i.e. we say a (rest frame) state $|\psi\rangle$ has spin s if $J^2|\psi\rangle = s(s+d-2)|\psi\rangle$.

[7] Also using that $\hat{T}_{ij}$ is trace free.

for some functions $\alpha^{(0)}$ and $\alpha^{(2)}$. These expressions can be written in an explicitly Lorentz covariant form by introducing projectors onto the spin-0 and spin-2 parts of $(2,0)$ tensors,

$$\Pi^{(0)}_{\mu\nu\rho\sigma}(p) \equiv S_{\mu\nu}S_{\rho\sigma} \text{ and } \Pi^{(2)}_{\mu\nu\rho\sigma}(p) \equiv S_{\mu(\rho}S_{\sigma)\nu} - \frac{1}{d}S_{\mu\nu}S_{\rho\sigma} \tag{7.24}$$

where $S_{\mu\nu} = p_\mu p_\nu - p^2\eta_{\mu\nu}$ (and hence satisfies $p^\mu S_{\mu\nu} = 0$), respectively. In the rest frame all the time components of $\widetilde{\mathcal{W}}_{\mu\nu\rho\sigma}(p^0, 0)$ vanish, $S_{ij} = p_0^2\delta_{ij}$ and $S_{\mu 0} = 0$ so the covariant form of the Wightman function on positive energy timelike p is

$$\widetilde{\mathcal{W}}_{\mu\nu\rho\sigma}(p) = \alpha^{(0)}(\sqrt{-p^2})\Pi^{(0)}_{\mu\nu\rho\sigma}(p) + \alpha^{(2)}(\sqrt{-p^2})\Pi^{(2)}_{\mu\nu\rho\sigma}(p). \tag{7.25}$$

This can be written as an expression that is valid for all p by using the fact that $\widetilde{\mathcal{W}}_{\mu\nu\rho\sigma}(p)$ is only non-zero for positive energy timelike p to write

$$\alpha^{(0/2)}(\sqrt{-p^2}) = \int_0^\infty \mathrm{d}\mu\, c^{(0/2)}(\mu)\tilde{D}(p;\mu) \text{ where } \tilde{D}(p;\mu) \equiv \frac{(2\pi)\delta(p^0 - E_\mu(\mathbf{p}))}{2E_\mu(\mathbf{p})}, \tag{7.26}$$

is the momentum space Wightman function and $c^{(0/2)}(\mu) \equiv \mu\alpha^{(0/2)}(\mu)/\pi$ for $\mu > 0$, and thus obtain the spectral representation of $\widetilde{\mathcal{W}}_{\mu\nu\rho\sigma}$:

$$\widetilde{\mathcal{W}}_{\mu\nu\rho\sigma}(p) = \int_0^\infty \mathrm{d}\mu \left(c^{(0)}(\mu)\Pi^{(0)}_{\mu\nu\rho\sigma}(p) + c^{(2)}(\mu)\Pi^{(2)}_{\mu\nu\rho\sigma}(p)\right)\tilde{D}(p;\mu) \tag{7.27}$$

where the spectral densities are given by the expressions[8]

$$c^{(0)}(\mu) = \frac{1}{d^2\mu^4}\sum_\lambda \delta(\mu - m_\lambda)|\langle 0|T_{ii}(0)|\lambda, 0\rangle|^2 \text{ and} \tag{7.28a}$$

$$c^{(2)}(\mu) = \frac{2}{(d+2)(d-1)\mu^4}\sum_\lambda \delta(\mu - m_\lambda)|\langle 0|\hat{T}_{ij}(0)|\lambda, 0\rangle|^2. \tag{7.28b}$$

Crucially, for a given μ the states being summed over have fixed energy and so these expressions have no UV divergences. Thus, the expressions (7.28) are finite implying that the spectral functions $c^{(0/2)}(\mu)$ are real and non-negative. Having a completeness relation of the form (7.19) was key to obtaining the universal expression (7.27) for the two-point function in terms of these two non-negative univariate functions. We owe this relation to two fundamental properties of our theories: (i) their symmetry under the Poincaré group and (ii) the positivity of their Hilbert Space norms. Utilising the representation theory of $\mathrm{ISO}(d,1)$ was key to deriving the functional form of the two-point function and the non-negativity of the spectral densities is owed to the positivity of Hilbert Space element norms.

The spectral densities have dimension $d-2$ so $c^{(0/2)}(\mu)/\mu^{d-2}$ are dimensionless

[8] In the following expressions we have absorbed the spin labels into λ.

functions of μ/M_i, where M_i are the physical mass parameters of the theory. Having renormalised the theory, we know that in the limit $\mu \to \infty$ the spectral densities must be insensitive to the precise values of the M_i and thus $c^{(0/2)}(\mu)$ are at most $\mathcal{O}(\mu^{d-2})$ as $\mu \to \infty$.

From here we may derive the spectral representation of the finite and conserved part of the time-ordered two-point function on flat space,

$$G^{\mathrm{F}}_{\mu\nu\rho\sigma}(p) \equiv i \int \mathrm{d}^{d+1}x\, \mathrm{e}^{-ip\cdot x} \langle 0|\mathcal{T} T_{\mu\nu}(x) T_{\rho\sigma}(0)|0\rangle, \tag{7.29}$$

that, due to the time-ordering, is *not* conserved, i.e. $p^\mu G^{\mathrm{F}}_{\mu\nu\rho\sigma}(p) =$ local terms $\neq 0$. Note that we may obtain this by replacing the Wightman function in Equation (7.27) with the Feynman propagator,

$$\tilde{D}(p;\mu) \to \tilde{D}_{\mathrm{F}}(p;\mu) = -\frac{i}{p^2 + \mu^2 - i\varepsilon}, \tag{7.30}$$

(and a similar replacement yields the Euclidean correlator [132]) and that this representation is indeed finite and conserved when $d = 2$. This, however, obscures the regularisation steps taken along the way thus we will set out the calculation here in full.

From the definition of the time-ordering operator (7.17), we see that $G^{\mathrm{F}}_{\mu\nu\rho\sigma}(p)$ is the sum of two convolutions and therefore

$$G^{\mathrm{F}}_{\mu\nu\rho\sigma}(p) = -\int_{-\infty}^{\infty} \frac{\mathrm{d}\xi}{(2\pi)} \left[\frac{1}{p^0 - \xi + i\varepsilon} \widetilde{\mathcal{W}}_{\mu\nu\rho\sigma}(\xi, \mathbf{p}) + \frac{1}{-p^0 + \xi + i\varepsilon} \widetilde{\mathcal{W}}_{\mu\nu\rho\sigma}(-\xi, -\mathbf{p}) \right], \tag{7.31}$$

which can then be simplified using the spectral representation of the Wightman functions (7.27). The spin-0 and spin-2 projectors are invariant under $p \mapsto -p$, $\Pi^{(0/2)}_{\mu\nu\rho\sigma}(-p) = \Pi^{(0/2)}_{\mu\nu\rho\sigma}(p)$, and the δ-function in $\tilde{D}(p;\mu)$ can be used to perform the integrals over ξ. This requires interchanging order of the $\int \mathrm{d}\mu$ and $\int \mathrm{d}\xi$ integrals and, although this is operation is not strictly valid, the resulting expression differs only by local terms, so it has the same non-local part that we are interested in. In swapping the order of integration we implicitly neglect local divergences present in (7.31) that, in any case, cancel with terms in $O_{ij,k\ell}$ in Equation (7.15). Having quantised in a non-covariant way, we obtained a time-ordered two-point function on flat space that was not conserved. To extract the part that is finite and conserved — and thus appropriate for deducing the diffeomorphism-invariant observable $E[g]$ — it is necessary to separate out non-conserved divergent terms. These have finite parts and are fixed by the requirement that the renormalised two-point function is conserved. This gives that the time-ordered two-point function in momentum space is

given by

$$G^{\mathrm{F}}_{\mu\nu\rho\sigma}(p) = -\int_0^\infty \mathrm{d}\mu \left(c^{(0)}(\mu)\Pi^{(0)}_{\mu\nu\rho\sigma}(p) + c^{(2)}(\mu)\Pi^{(2)}_{\mu\nu\rho\sigma}(p)\right) \frac{1}{2E_\mu(\mathbf{p})}\left(\frac{1}{p^0 - E_\mu(\mathbf{p}) + i\varepsilon} - \frac{1}{p^0 + E_\mu(\mathbf{p}) - i\varepsilon}\right) + 2\tilde{I}_{\mu\nu\rho\sigma}(p) \quad (7.32)$$

or

$$G^{\mathrm{F}}_{\mu\nu\rho\sigma}(p) = \int_0^\infty \mathrm{d}\mu \left(c^{(0)}(\mu)\Pi^{(0)}_{\mu\nu\rho\sigma}(p) + c^{(2)}(\mu)\Pi^{(2)}_{\mu\nu\rho\sigma}(p)\right) \frac{1}{p^2 + \mu^2 - i\varepsilon} + 2\tilde{I}_{\mu\nu\rho\sigma}(p). \quad (7.33)$$

where $\tilde{I}_{\mu\nu\rho\sigma}(p)$ are non-conserved local divergences. Recall that $c^{(0/2)}(\mu) = \mathcal{O}(\mu^{d-2})$, so for $d = 2$ this integral in Equation (7.33) is finite and conserved. Further details on the renormalisation of this two-point function, including an explicit expression for the divergences when $d = 2$, are given in Appendix A.7. We note that for $d > 2$, this integral is conserved but *not* finite and crucially, unlike $d = 2$, requires the introduction of local geometric covariant counterterms (with scheme-dependent finite parts) to render it so.

7.3.1 Example: Scalar Field

A scalar field with mass m and curvature coupling ξ has stress tensor

$$T_{\mu\nu} = \partial_\mu\phi\partial_\nu\phi - \frac{1}{2}\eta_{\mu\nu}\left((\partial\phi)^2 + m^2\phi^2\right) + \xi\left(\eta_{\mu\nu}\partial^2 - \partial_\mu\partial_\nu\right)(\phi^2). \quad (7.34)$$

For this theory, we can choose the complete set of states to consist of states with definite particle number. The only such states that have non-zero overlap with $T_{\mu\nu}|0\rangle$ are two-particle states — the projector onto them is given by

$$\mathbb{1}_2 = \frac{1}{2}\int \frac{\mathrm{d}^2u}{(2\pi)^2 2E(\mathbf{u})}\frac{\mathrm{d}^2v}{(2\pi)^2 2E(\mathbf{v})}|\mathbf{u},\mathbf{v}\rangle\langle\mathbf{u},\mathbf{v}| \quad (7.35)$$

where $|\mathbf{u},\mathbf{v}\rangle$ is the relativistically normalised two-particle state with particles of momentum $\mathbf{u}$ and $\mathbf{v}$ and $E(\mathbf{u}) = \sqrt{\mathbf{u}^2 + m^2}$. For comparison with the sum over states used to compute the spectral densities (7.28) we make a change of variables, choosing instead to label two-particle states in terms of their total momentum, $\mathbf{p} = \mathbf{u}+\mathbf{v}$, the rest mass of the state, μ, and the direction of one of the particles in the centre of mass (COM) frame, θ. This induces a change of measure

$$\frac{1}{2}\int \frac{\mathrm{d}^2u}{(2\pi)^2 2E(\mathbf{u})}\frac{\mathrm{d}^2v}{(2\pi)^2 2E(\mathbf{v})} = \frac{1}{4(2\pi)^2}\int_0^\infty \mathrm{d}\mu \int_0^{2\pi}\mathrm{d}\theta \int \frac{\mathrm{d}^2p}{(2\pi)^2 2E(\mathbf{p})}. \quad (7.36)$$

So the sum over the zero momentum states required to compute the spectral densities has measure

$$\sum_{\lambda} = \frac{1}{4(2\pi)^2}\int_0^\infty \mathrm{d}\mu \int_0^{2\pi} \mathrm{d}\theta. \tag{7.37}$$

We choose to normal order the stress tensor $T_{\mu\nu}$ so that its VEV vanishes in flat space (thus excluding the need for a cosmological counterterm). When acting on zero momentum two-particle states, the normal-ordered stress tensor gives

$$\langle 0|\, :T_{ij}(0):\, |\mathbf{q},-\mathbf{q}\rangle = (E(\mathbf{q})^2(8\xi-1)-m^2)\delta_{ij} + (2q_iq_j - \delta_{ij}\mathbf{q}^2). \tag{7.38}$$

when decomposed into spin-0 and spin-2 parts. In COM frame variables $\hat{\mathbf{q}} = (\cos\theta, \sin\theta)$ and $\mu = 2E(\mathbf{q})$ so the matrix elements (7.38) can be plugged into (7.28) to give the spectral functions for a free scalar of mass m with curvature coupling ξ:

$$c_{\mathrm{s}}^{(0)}(\mu) = \frac{1}{64(2\pi)}\Theta(\mu-2m)\left(1-8\xi+\frac{4m^2}{\mu^2}\right)^2 \text{ and} \tag{7.39}$$

$$c_{\mathrm{s}}^{(2)}(\mu) = \frac{1}{64(2\pi)}\Theta(\mu-2m)\left(1-\frac{4m^2}{\mu^2}\right)^2, \tag{7.40}$$

which are — as expected — finite, non-negative and $\mathcal{O}(\mu^0)$ as $\mu\to\infty$. We note also that limit $\xi \to 1/8$, $m\to 0$, in which a CFT is recovered, the spin-0 density vanishes and the spin-2 is a constant.

7.3.2 Example: Dirac Fermion

For a Dirac fermion, the two-particle states also consist of a two particles with spatial momenta that are equal in magnitude and opposite directions. In this case, they must be a particle-antiparticle pair and each of the particles also has a spin state. Thus

$$\sum_{\lambda} = \frac{1}{2(2\pi)^2}\int_0^\infty \mathrm{d}\mu \int_0^{2\pi} \mathrm{d}\theta \sum_{r,s} \tag{7.41}$$

where μ and θ are as before and r, s index the spins of the particles. As in the scalar case, we normal order the stress tensor. The calculations here are an exercise in spinor manipulation, the details of which are covered in Appendix A.8. The key difference with the scalar case is the sum over spin states which yields

$$\sum_{r,s}\langle 0|\, :T_{ij}(0,\mathbf{0}):\, |\mathbf{q},s,r,\mathbf{p}\rangle_2\langle 0|\, :T_{k\ell}(0,\mathbf{0}):\, |\mathbf{q},s,r,\mathbf{p}\rangle_2^\star$$
$$= \frac{1}{2}(u-v)_{(i}(\mathbf{u}\mathbf{v}^{\mathrm{T}} + \mathbf{v}\mathbf{u}^{\mathrm{T}} + 2E(\mathbf{q})^2\delta_{j)(\ell})(u-v)_{k)} \tag{7.42}$$

where $|\mathbf{q}, s, r, \mathbf{p}\rangle$ is the state with a particle and an antiparticle with spins s and r, respectively, total momentum $\mathbf{p}$, and where the particle has momentum $\mathbf{q}$ in the rest frame and u and v are the momenta of the particle and antiparticle, respectively. Now putting $\mathbf{p} = 0$; then $u^\mu = (E(\mathbf{q}), \mathbf{q})$ and $v^\mu = (E(\mathbf{q}), -\mathbf{q})$ and writing $\mu = 2E(\mathbf{q})$ for the rest mass of the states we can use this result to deduce that

$$\sum_{r,s} |\langle 0| :T_{ii}(0): |\mathbf{q}, s, r, 0\rangle_2|^2 = m^2\mu^2 \left(1 - \frac{4m^2}{\mu^2}\right) \text{ and} \tag{7.43a}$$

$$\sum_{r,s} |\langle 0| :\hat{T}_{ij}(0): |\mathbf{q}, s, r, 0\rangle_2|^2 = \frac{\mu^4}{8} \left(1 - \frac{4m^2}{\mu^2}\right) \left(1 + \frac{4m^2}{\mu^2}\right). \tag{7.43b}$$

from which it follows that spectral functions for a free Dirac fermion on mass m are

$$c_{\mathrm{f}}^{(0)}(\mu) = \frac{1}{8(2\pi)} \Theta(\mu - 2m) \frac{m^2}{\mu^2} \left(1 - \frac{4m^2}{\mu^2}\right) \tag{7.44}$$

$$c_{\mathrm{f}}^{(2)}(\mu) = \frac{1}{32(2\pi)} \Theta(\mu - 2m) \left(1 - \frac{4m^2}{\mu^2}\right) \left(1 + \frac{4m^2}{\mu^2}\right) \tag{7.45}$$

which are — as expected — finite, non-negative and $\mathcal{O}(\mu^0)$ as $\mu \to \infty$. We note also that in the limit $m \to 0$ in which a CFT is recovered, the spin-0 density vanishes and the spin-2 is a constant.

7.4 Non-positivity of Vacuum Energy

The time-ordered two-point function of the stress tensor on flat space enters the vacuum energy $E[g]$ (7.15) as the static propagator, which in momentum space is $-iG^{\mathrm{F}}_{ijk\ell}(0, \mathbf{p})$. Plugging this into the perturbative expression for $E[g]$ (7.15) gives

$$\begin{aligned} E[g] = &-\frac{\varepsilon^2}{4} \int \mathrm{d}^2x\, h^{ij}(\mathbf{x}) \langle 0| O_{ij,k\ell}(0, \mathbf{x}) + I_{ijk\ell}(\partial) |0\rangle h^{k\ell}(\mathbf{x}) \\ &- \frac{\varepsilon^2\pi^2}{2} \int \mathrm{d}^2p\, \tilde{h}^{ij}(\mathbf{p}) \tilde{h}^{k\ell}(\mathbf{p})^\star \int_0^\infty \frac{\mathrm{d}\mu}{\mathbf{p}^2 + \mu^2} \left(c^{(0)}(\mu) \Pi^{(0)}_{ijk\ell}(0, \mathbf{p}) + c^{(2)}(\mu) \Pi^{(2)}_{ijk\ell}(0, \mathbf{p})\right) + \mathcal{O}(\varepsilon^3), \end{aligned} \tag{7.46}$$

where

$$h^{ij}(\mathbf{x}) = \int \mathrm{d}^2p\, \mathrm{e}^{-i\mathbf{p}\cdot\mathbf{x}} \tilde{h}^{ij}(\mathbf{p}) \text{ and } \delta(\mathbf{x}) I_{ijk\ell}(\partial) \equiv \int \frac{\mathrm{d}^2p}{(2\pi)^2}\, \mathrm{e}^{-i\mathbf{p}\cdot\mathbf{x}} \tilde{I}_{ijk\ell}(0, \mathbf{p}). \tag{7.47}$$

Index symmetries, homogeneity and isotropy constrain the VEV of the term involving $O_{ij,k\ell}$ to satisfy

$$\langle 0|O_{ij,k\ell}(0,\mathbf{x}) + I_{ijk\ell}(\partial)|0\rangle = c_1\delta_{i(k}\delta_{\ell)j} + c_2\delta_{ij}\delta_{k\ell} \tag{7.48}$$

where c_1 and c_2 are some renormalised (possibly differential operator) coefficients. Diffeomorphisms must leave $E[g]$ invariant. These take the form $\tilde{h}_{ij}(\mathbf{p}) = p_{(i}\tilde{v}_{j)}(\mathbf{p})$ for some vector field $\tilde{v}$ and thus eliminate the transverse projectors which characterise the non-local contribution to (7.46), leaving a local contribution that vanishes if and only if $c_1 = c_2 = 0$. Further, using the fact that in two spatial dimensions $2\Pi^{(0)}_{ijk\ell}(0,\mathbf{p}) = \Pi^{(2)}_{ijk\ell}(0,\mathbf{p})$, the leading-order perturbation to the vacuum energy of a renormalisable QFT on (2+1)-dimensional flat space under a deformation $g^{ij} \mapsto \delta^{ij} - \varepsilon h^{ij}$ can be written as

$$E[g] = -\frac{\varepsilon^2\pi^2}{2}\int \mathrm{d}^2p\,|\tilde{h}^{ij}(\mathbf{p})S_{ij}(0,\mathbf{p})|^2\int_0^\infty \frac{\mathrm{d}\mu}{\mathbf{p}^2+\mu^2}\left(c^{(0)}(\mu) + \frac{1}{2}c^{(2)}(\mu)\right) + \mathcal{O}(\varepsilon^3). \tag{7.49}$$

This expression is finite and manifestly negative for any non-trivial perturbation provided the spectral functions are non-negative, non-zero somewhere and finite in the limit $\mu \to \infty$. These requirements are fulfilled by the non-negativity of Hilbert Space norms, non-emptiness and renormalisability of the theory, respectively. A quick consistency check of this formula is provided by the fact that the spectral densities (7.39) and (7.44) reproduce the vacuum energies derived in Chapter 3 for the free the scalar and Dirac fermion, respectively.

It is clear from this expression for the vacuum energy that the non-negativity of the spectral densities and thus the non-negativity of Hilbert Space norms of the flat-space theory are key to negativity. Indeed, the corresponding expression derived for CFTs (1.69) in Chapter 1 supports this hypothesis — the result there shows that CFTs that have (sufficiently many) negative-norm states, and therefore possibly *negative* central charge, can have positive vacuum energy.

7.5 Summary and Discussion

We have shown that for all (2+1)-dimensional power-counting-renormalisable Poincaré invariant QFTs on flat space the vacuum energy is *lowered* when the spatial geometry is deformed (perturbatively) away from being flat — thereby extending the result that was shown to hold for CFTs, in Section 1.4, and free theories, in Chapter 3. Further, showing this provided some insight into the — thus far elusive — question of *why* so many of the vacuum energies considered in this thesis are negative, with the proof leaning on two properties of the theory: dimensionality and Lorentz invariance.

Such observations were a facilitated by using a canonical approach to calculate the

vacuum energy. The vacuum energy on a d-dimensional spatial geometry (Σ, g), $E[g]$, was defined as the integral of the energy density over a spatial slice of the background. It was noted that provided the theory is renormalised so that $E[\delta] = 0$ and observables are diffeomorphism invariant then $E[g]$ is a UV-finite and unambiguous measure of vacuum energy when $d = 2$, matching the free energy difference defined in Chapter 4. For $d > 2$, these conditions are not sufficient to remove all ambiguities, thus highlighting the importance of the two-dimensionality of the spatial geometry. By writing the action and the stress tensor as expansions about their flat space values, the VEV of the stress tensor on d-dimensional (Σ, g), and thus the variation of $E[g]$, was expressed in terms of the Hilbert Space and operators of the QFT on a flat reference space $(\Sigma, \bar{g})$. Small deformations of this space induce a leading-order perturbation to the vacuum energy that is characterised by the time-ordered two-point function of the stress tensor on $(\Sigma, \bar{g})$. The Poincaré invariance enjoyed by the QFT on $(\Sigma, \bar{g})$ permits a universal spectral representation of this two-point function that *only* depends on the theory through two functions that count the number of degrees of freedom that couple to the stress tensor at a given energy scale — the spectral densities, functions that are non-negative thanks to the positivity of Hilbert Space norms. For $d = 2$ this representation gave rise to a scheme-independent conserved finite time-ordered two-point function and, in turn, an unambiguous diffeomorphism-invariant UV-finite vacuum energy that is characterised entirely by a negative-definite combination of the spectral functions. Requiring that the time-ordered two-point function is conserved is not sufficient to remove all its scheme dependence when $d > 2$.

While the arguments presented in this chapter are only valid for theories with a mass gap, the fact that identical results hold for CFTs rule this out as being necessary for vacuum energy negativity. We do know, however, that for many (2+1)-dimensional QFTs on spaces that are not topologically flat, the vacuum energy is maximised locally by (Σ, g) that do *not* benefit from Poincaré invariance. In particular, for Σ that are deformed spheres we have seen in Chapters 1 and 5 that this is the case for a free scalar with a curvature coupling, a free Dirac fermion and all CFTs (with positive central charge) — all theories whose vacuum energies are maximised by round two-spheres. This raises the question of whether the arguments of this chapter can be adapted to show perturbative vacuum energy negativity for round-sphere backgrounds. It follows from the arguments in Section 7.1 (as in Chapter 4 for diffeomorphism-invariant regulation) that a UV-finite and unambiguous vacuum energy can be obtained for theories on compact (Σ, g) (topological spheres and tori) by considering the differenced vacuum energy with a reference space of the same volume and topology (for which natural choices are the round sphere and flat torus). The question then is: what can be said about the time-ordered two-point function without the symmetry of the whole Poincaré group? Our treatment explicitly used boost covariance which no longer applies here. Hilbert Space axioms ensure that — *before* renormalisation — the two-point function is positive definite, but the fact that

there are perturbations of the flat torus that *raise* the vacuum energy of the Dirac fermion — shown in Equation (5.53) — suggests that some amount of symmetry is necessary to yield a positive-definite static propagator after renormalisation. Indeed, it is possible the isometry group of (the product of time with) the two-sphere is sufficient, especially given that the time-ordered two-point function contributes to the vacuum energy through the static propagator on spatial legs — an object that manifestly breaks Lorentz invariance in the flat-space case. This promising direction for future research could also help show vacuum energy negativity for perturbations of flat space theories at finite temperature, for which there is also a commensurate body of evidence and a smaller (but significant) symmetry group.

Closing Remarks

The vacuum energy — or free energy at finite temperature — of ultrastatic (2+1)-dimensional QFTs has proven to be an intriguing investigation topic. Within the realm of vacuum energy in curved space QFT, it is special. We found that, subject to appropriate regularisation, there is an unambiguous UV-finite measure of (2+1)-dimensional free energy as a functional of spatial geometry: the free energy difference, ΔF. It does not suffer renormalisation-scheme ambiguities that are generically present in vacuum energy calculations and is thus a well-defined observable of the QFT. Motivated by extant holographic results on the negativity of this vacuum energy, we calculated the free energy for a variety of QFTs on a range of deformations to maximally-symmetric spatial geometries, the results of which are summarised in Table 7.1. In parallel, analogous results were derived for holographic theories [2, 97, 98]. The key takeaway from this being that ΔF is *lowered* by *all* volume-preserving deformations to maximally-symmetric two-spaces (namely the plane and the round sphere) for all the theories we have considered. This quantity is exists both at finite temperature and at zero temperature, where it is *purely* quantum. Further, ΔF was shown to be even more negative the more the space is deformed. In short, (2+1)-dimensional relativistic quantum degrees of freedom seem to *disfavour* smooth spatial geometries: a somewhat unexpected result. For the free theories, we computed the free energy using heat kernel methods. By computing the eigenvalues of a positive definite second-order linear differential operator, we were able to evaluate ΔF both analytically for perturbative deformations, by finding the perturbative corrections to the eigenvalues, and numerically for large deformations, by adopting a novel numerical approach that uses pseudo-spectral methods to obtain highly accurate estimates of the eigenvalues. ΔF is a meaningful physical quantity, parametrising a *non-local* contribution to the free energy of a physical membrane that, due to relativistic degrees of freedom on them, seeks to crumple them. Using our novel numerical methods, we observed an unexpected quantitative similarity between a free massless Dirac fermion and a holographic CFT. In summary, the exploration of (2+1)-dimensional vacuum energy has led to a number of surprising results with interesting physical implications and a new technique for computing vacuum energy, a generically difficult computation, that works for a range of geometries. It is hoped that the work in this thesis can provide both a technical and motivational platform for further progress in this area.

Theory	(Σ, g)	Temp.	Result	Ref.
Unitary CFT	$(S^2, \bar{g}+\varepsilon h)$ or $(\mathbb{R}^2, \bar{g}+\varepsilon h)$	$T=0$	$\Delta F_{\mathrm{q}} \leqslant 0$	Section 1.4
Free scalar or fermion	$(\mathbb{R}^2, \bar{g}+\varepsilon h)$	$T \geqslant 0$	$\Delta F_{\mathrm{q}} \leqslant 0$	Chapter 3
Free scalar or fermion	$(\mathbb{R}^2, \text{long wavelength})$	$T \geqslant 0$	$\Delta F_{\mathrm{q}} \leqslant 0$	Chapter 4
Free scalar or fermion	$(S^2, \bar{g}+\varepsilon h)$	$T \geqslant 0$	$\Delta F_{\mathrm{q}} \leqslant 0$	Chapter 5
Free scalar or fermion	$(S^2, g)^*$	$T \geqslant 0$	$\Delta F_{\mathrm{q}} \leqslant 0$	Chapter 5
Free scalar or fermion	$(S^2, \text{long wavelength})$	$T \geqslant 0$	$\Delta F_{\mathrm{q}} \leqslant 0$	Chapter 5
Renormalisable	$(\mathbb{R}^2, \bar{g}+\varepsilon h)$	$T=0$	$\Delta F_{\mathrm{q}} \leqslant 0$	Chapter 7

Table 7.1: A summary of new results presented in this thesis for the free energy F_{q} for various types QFTs at various temperatures. The scalar refers to a scalar field of any mass and curvature coupling; and the fermion refers to a Dirac fermion of any mass. $\bar{g}$ is always taken to be the maximally-symmetric geometry on the manifold Σ (so $\bar{g}$ is the round sphere metric when $\Sigma = S^2$ and the flat metric when $\Sigma = \mathbb{R}^2$), and when we write $\bar{g}+\varepsilon h$ it is understood that the result holds to leading non-trivial order in the perturbative expansion parameter ε. 'Long wavelength' refers to metrics whose curvature is small compared to the temperature and/or mass of the field. 'Renormalisable' here is short for power-counting renormalisable. All inequalities on ΔF_{q} are saturated if and only if $g = \bar{g}$. * indicates conjecture based on a significant amount of numerical evidence in the case of axisymmetric deformations.

We conclude with a summary of some of the open questions posed by the work presented here, of which there two distinct categories. On the one hand, there are many theoretical problems that are yet to be understood. Firstly, does the differenced heat kernel of *any* free field theory on a deformed sphere always have fixed sign? This is essentially a purely geometric inquiry, as one can define a heat kernel associated to *any* elliptic differential operator L. Presumably arguments like the ones we used in Section 5.5.1 to show that $\sigma\Delta K_L$ is negative at sufficiently small and large t could be used to gain control over the asymptotics of ΔK_L for general L, but we do not know how to extend that analysis to intermediate values of t even in the case of the Dirac fermion and scalar studied here (though we note that renormalised determinants of free field operators are rigorously studied in mathematics [133]). Nevertheless, we conjecture that (under the condition that the spectrum of L is positive, to ensure that the free field theory defined by L is stable) the differenced heat kernel does indeed always have a fixed sign. For the Laplacian, this conjecture has already been made in mathematical literature [100] solely based on the small- and large-t arguments given in Section 5.5.1. Here, we have presented a significant amount of evidence in its favour and, given that a similar body of evidence exists for the Dirac operator, have sufficient reason to believe it may hold in the more general case. Secondly, is the differenced free energy ΔF of *any* unitary, relativistic QFT on a deformed maximally-symmetric two-space negative? As shown in Table 7.1, this differenced free energy has been shown to be negative for a large range of theories, providing tantalising evidence that perhaps it is some universal feature of general QFTs. The generality of this picture suggests that there must be a universal underlying mechanism;

it would be extremely interesting to uncover what this mechanism must be. It is possible hints may lie within extending the perturbative flat-space proof of Chapter 7 — that only assumed power-counting renormalisability and Lorentz invariance of the flat-space theory — to the sphere, which would also be an interesting problem in itself. Perhaps the answer is related to the F-theorem, that requires ΔF on the Euclidean three-sphere to decrease under RG flow induced by spin-zero operators. A potential connection between the present results and the F-theorem is not obvious, however, both for the simple reason that the topologies we considered are not deformed three-spheres, but also because the free energy need not behave monotonically under deformations of the three-sphere's geometry (corresponding to spin-two deformations), as found in [95]. Further, the fact there is a (small) deformation of the torus that renders the vacuum energy of the free massless Dirac fermion *positive* remains a curious footnote to this story that could yet provide some insight. Lastly, a number of unanswered questions remain about the remarkably close quantitative agreement shown between the (appropriately normalised) vacuum energies of the free Dirac fermion and a holographic CFT considered in Chapter 6. The closeness is suggestive of some underlying reason for the universality: what is it? This is but one of an growing list of unexplained similarities in observables between these two very different theories [117–119]. Improving the numerical methods to allow an accurate determination of the vacuum energies closer to the singular limits of the geometries, where the biggest differences occur, may be enlightening. Further, the results of [95] confirm that breaking ultrastaticity, as the Euclidean three-sphere does, is enough to break the close matching between the fermion and the holographic CFT. Why? And what happens under the breaking of parity symmetry or axisymmetry? It would be informative to check whether such deformations exhibit vacuum energies with similar behaviour.

On the other hand, the behaviour of ΔF is suggestive of some phenomenological implications for the geometry of physical membranes that support relativistic quantum degrees of freedom. These certainly merit further exploration. Our analysis in Chapter 5 concluded that ΔF, while too small to imply the existence of a crumpled equilibrium configuration for graphene, nevertheless gave rise to an important non-local contribution that should be factored into any quantum simulations that hope to understand the energetics of monolayer graphene, and could influence the equilibrium geometry of an appropriately finely-tuned material. How feasible would it be to engineer materials that actually exhibit this negative ΔF, either as a genuine instability of the round sphere, or as a non-local contribution to an effective description of a membrane's dynamics? Failing that, the possibility remains that optical lattices — given their capacity to be finely tuned — offer a route to engineering a setup in which the effects of ΔF are observable. As such, it is a distinct possibility that the peculiar properties of (2+1)-dimensional vacuum energy exhibited in this work become one of the very few effects of QFT on curved space to be realisable in the lab.

Bibliography

[1] Sebastian Fischetti, Lucas Wallis, and Toby Wiseman. "What Spatial Geometries do (2+1)-Dimensional Quantum Field Theory Vacua Prefer?" In: *Phys. Rev. Lett.* 120.26 (2018), p. 261601. DOI: 10.1103/PhysRevLett.120.261601. arXiv: 1803.04414 [hep-th].

[2] Krai Cheamsawat, Lucas Wallis, and Toby Wiseman. "Free energy dependence on spatial geometry for (2+1)-dimensional QFTs". In: *Class. Quant. Grav.* 36.19 (2019), p. 195011. DOI: 10.1088/1361-6382/ab353d. arXiv: 1811.05995 [hep-th].

[3] Sebastian Fischetti, Lucas Wallis, and Toby Wiseman. "Does the Round Sphere Maximize the Free Energy of (2+1)-Dimensional QFTs?" In: *JHEP* 10 (2020), p. 078. DOI: 10.1007/JHEP10(2020)078. arXiv: 2003.09428 [hep-th].

[4] Krai Cheamsawat, Sebastian Fischetti, Lucas Wallis, and Toby Wiseman. "A surprising similarity between holographic CFTs and a free fermion in (2 + 1) dimensions". In: *JHEP* 05 (2021), p. 246. DOI: 10.1007/JHEP05(2021)246. arXiv: 2012.14437 [hep-th].

[5] A. Einstein. "Zur Elektrodynamik bewegter Körper [AdP 17, 891 (1905)]". In: *Annalen der Physik* 14.S1 (Feb. 2005), pp. 194–224. DOI: 10.1002/andp.200590006.

[6] H. B. G. Casimir and D. Polder. "The Influence of retardation on the London-van der Waals forces". In: *Phys. Rev.* 73 (1948), pp. 360–372. DOI: 10.1103/PhysRev.73.360.

[7] Kimball A. Milton. *Casimir Effect, The: Physical Manifestations of Zero-Point Energy*. WORLD SCIENTIFIC PUB CO INC, Oct. 2001. 320 pp. ISBN: 9810243979. URL: https://www.ebook.de/de/product/3669504/kimball_a_milton_casimir_effect_the_physical_manifestations_of_zero_point_energy.html.

[8] H. B. G. Casimir. "On the Attraction Between Two Perfectly Conducting Plates". In: *Indag. Math.* 10 (1948), pp. 261–263.

[9] S. K. Lamoreaux. "Demonstration of the Casimir force in the 0.6 to 6 micrometers range". In: *Phys. Rev. Lett.* 78 (1997). [Erratum: Phys.Rev.Lett. 81, 5475–5476 (1998)], pp. 5–8. DOI: 10.1103/PhysRevLett.78.5.

[10] Michael Bordag, U. Mohideen, and V. M. Mostepanenko. "New developments in the Casimir effect". In: *Phys. Rept.* 353 (2001), pp. 1–205. DOI: 10.1016/S0370-1573(01)00015-1. arXiv: quant-ph/0106045.

[11] Andrew R. Liddle. "An introduction to modern cosmology". In: 1999.

[12] Adam G. Riess et al. "Observational Evidence from Supernovae for an Accelerating Universe and a Cosmological Constant". In: *The Astronomical Journal* 116.3 (Sept. 1998), pp. 1009–1038. DOI: 10.1086/300499.

[13] S. Perlmutter et al. "Measurements of Ω and Λ from 42 high redshift supernovae". In: *Astrophys. J.* 517 (1999), pp. 565–586. DOI: 10.1086/307221. arXiv: astro-ph/9812133.

[14] and N. Aghanim et al. "Planck 2018 results". In: *Astronomy & Astrophysics* 641 (Sept. 2020), A6. DOI: 10.1051/0004-6361/201833910.

[15] Juan Martin Maldacena and Liat Maoz. "Wormholes in AdS". In: *JHEP* 02 (2004), p. 053. DOI: 10.1088/1126-6708/2004/02/053. arXiv: hep-th/0401024.

[16] G. J. Galloway, K. Schleich, D. M. Witt, and E. Woolgar. "Topological censorship and higher genus black holes". In: *Phys. Rev. D* 60 (1999), p. 104039. DOI: 10.1103/PhysRevD.60.104039. arXiv: gr-qc/9902061.

[17] G. J. Galloway, K. Schleich, D. Witt, and E. Woolgar. "The AdS / CFT correspondence conjecture and topological censorship". In: *Phys. Lett. B* 505 (2001), pp. 255–262. DOI: 10.1016/S0370-2693(01)00335-5. arXiv: hep-th/9912119.

[18] Edward Witten. "Light rays, singularities, and all that". In: *Reviews of Modern Physics* 92.4 (Nov. 2020), p. 045004. DOI: 10.1103/revmodphys.92.045004.

[19] Juan Maldacena, Alexey Milekhin, and Fedor Popov. "Traversable wormholes in four dimensions". In: (July 2018). arXiv: 1807.04726 [hep-th].

[20] Juan Maldacena and Alexey Milekhin. "Humanly traversable wormholes". In: *Phys. Rev. D* 103.6 (2021), p. 066007. DOI: 10.1103/PhysRevD.103.066007. arXiv: 2008.06618 [hep-th].

[21] Roger Penrose. "Gravitational Collapse and Space-Time Singularities". In: *Physical Review Letters* 14.3 (1965), pp. 57–59. DOI: 10.1103/PhysRevLett.14.57.

[22] S. W. Hawking. "Chronology protection conjecture". In: *Physical Review D* 46.2 (1992), pp. 603–611. DOI: 10.1103/PhysRevD.46.603.

[23] Nima Arkani-Hamed, Savas Dimopoulos, and G. R. Dvali. "The Hierarchy problem and new dimensions at a millimeter". In: *Phys. Lett.* B429 (1998), pp. 263–272. DOI: 10.1016/S0370-2693(98)00466-3. arXiv: hep-ph/9803315 [hep-ph].

[24] Lisa Randall and Raman Sundrum. "A Large mass hierarchy from a small extra dimension". In: *Phys. Rev. Lett.* 83 (1999), pp. 3370–3373. DOI: 10.1103/PhysRevLett.83.3370. arXiv: hep-ph/9905221 [hep-ph].

[25] T. Vachaspati. *Kinks and domain walls*. Cambridge: CUP, 2006.

[26] Juan Martin Maldacena. "The Large N limit of superconformal field theories and supergravity". In: *Int. J. Theor. Phys.* 38 (1999), pp. 1113–1133. DOI: 10.1023/A:1026654312961. arXiv: hep-th/9711200.

[27] S.S. Gubser, Igor R. Klebanov, and Alexander M. Polyakov. "Gauge theory correlators from noncritical string theory". In: *Phys. Lett. B* 428 (1998), pp. 105–114. DOI: 10.1016/S0370-2693(98)00377-3. arXiv: hep-th/9802109.

[28] Edward Witten. "Anti-de Sitter space and holography". In: *Adv. Theor. Math. Phys.* 2 (1998), pp. 253–291. DOI: 10.4310/ATMP.1998.v2.n2.a2. arXiv: hep-th/9802150.

[29] Andrew Hickling and Toby Wiseman. "Vacuum energy is non-positive for (2 + 1)-dimensional holographic CFTs". In: *Class. Quant. Grav.* 33.4 (2016), p. 045009. DOI: 10.1088/0264-9381/33/4/045009. arXiv: 1508.04460 [hep-th].

[30] Sebastian Fischetti and Toby Wiseman. "On universality of holographic results for (2 + 1)-dimensional CFTs on curved spacetimes". In: *JHEP* 12 (2017), p. 133. DOI: 10.1007/JHEP12(2017)133. arXiv: 1707.03825 [hep-th].

[31] K. S. Novoselov. "Electric Field Effect in Atomically Thin Carbon Films". In: *Science* 306.5696 (Oct. 2004), pp. 666–669. DOI: 10.1126/science.1102896.

[32] Antonio Castro Neto, Francisco Guinea, and Nuno Miguel Peres. "Drawing conclusions from graphene". In: *Physics World* 19.11 (Nov. 2006), pp. 33–37. DOI: 10.1088/2058-7058/19/11/34.

[33] A. K. Geim and K. S. Novoselov. "The rise of graphene". In: *Nature Materials* 6.3 (Mar. 2007), pp. 183–191. DOI: 10.1038/nmat1849.

[34] Brahim Aïssa, Nasir K. Memon, Adnan Ali, and Marwan K. Khraisheh. "Recent Progress in the Growth and Applications of Graphene as a Smart Material: A Review". In: *Frontiers in Materials* 2 (Sept. 2015). DOI: 10.3389/fmats.2015.00058.

[35] K. Novoselov, A. Geim, S. Morozov, D. Jiang, Y. Zhang, S. Dubonos, I. Grigorieva and A. Firsov. "Electric field effect in atomically thin carbon films". In: *Science* 306 (2004), pp. 666–669.

[36] K. Novoselov et al. "Two-dimensional gas of massless Dirac fermions in graphene". In: *Nature* 438 (2005), pp. 197–200.

[37] Y. Zhang, J. Tan, H. Stormer and P. Kim. "Experimental observation of the quantum Hall effect and Berry's phase in graphene". In: *Nature* 438 (2005), pp. 201–204.

[38] P. R. Wallace. "The Band Theory of Graphite". In: *Physical Review* 71.9 (May 1947), pp. 622–634. DOI: 10.1103/physrev.71.622.

[39] Gordon W. Semenoff. "Condensed-Matter Simulation of a Three-Dimensional Anomaly". In: *Physical Review Letters* 53.26 (Dec. 1984), pp. 2449–2452. DOI: 10.1103/physrevlett.53.2449.

[40] A. H. Castro Neto et al. "The electronic properties of graphene". In: *Rev. Mod. Phys.* 81 (2009), pp. 109–162. DOI: 10.1103/RevModPhys.81.109. arXiv: 0709.1163 [cond-mat.other].

[41] Fernando de Juan, Mauricio Sturla, and María A. H. Vozmediano. "Space Dependent Fermi Velocity in Strained Graphene". In: *Phys. Rev. Lett.* 108.22 (22 May 2012), p. 227205. DOI: 10.1103/PhysRevLett.108.227205. URL: https://link.aps.org/doi/10.1103/PhysRevLett.108.227205.

[42] Matthew M. Roberts and Toby Wiseman. "Does elastically deformed monolayer graphene have a curved space Dirac description?" In: (Dec. 2021). eprint: 2112.09144. URL: https://arxiv.org/pdf/2112.09144.pdf.

[43] R M Ribeiro et al. "Strained graphene: tight-binding and density functional calculations". In: *New Journal of Physics* 11.11 (Nov. 2009), p. 115002. DOI: 10.1088/1367-2630/11/11/115002. URL: https://doi.org/10.1088%2F1367-2630%2F11%2F11%2F115002.

[44] Jannik C. Meyer et al. "The structure of suspended graphene sheets". In: *Nature* 446.7131 (Mar. 2007), pp. 60–63. DOI: 10.1038/nature05545.

[45] Alfredo Iorio and Gaetano Lambiase. "Quantum field theory in curved graphene spacetimes, Lobachevsky geometry, Weyl symmetry, Hawking effect, and all that". In: *Physical Review D 90, 025006 (2014)* (Aug. 2013). DOI: 10.1103/PhysRevD.90.025006. arXiv: 1308.0265 [hep-th].

[46] F. Bemani, R. Roknizadeh, and M.H. Naderi. "Quantum simulation of discrete curved spacetime by the Bose–Hubbard model: From analog acoustic black hole to quantum phase transition". In: *Annals of Physics* 388 (Jan. 2018), pp. 186–196. DOI: 10.1016/j.aop.2017.11.010.

[47] S. W. Hawking. "Zeta Function Regularization of Path Integrals in Curved Space-Time". In: *Commun. Math. Phys.* 55 (1977), p. 133. DOI: 10.1007/BF01626516.

[48] J. S. Dowker and Raymond Critchley. "Effective Lagrangian and energy-momentum tensor in de Sitter space". In: *Physical Review D* 13.12 (June 1976), pp. 3224–3232. DOI: 10.1103/physrevd.13.3224.

[49] David R. Morrison and M. Ronen Plesser. "Nonspherical horizons. 1." In: *Adv. Theor. Math. Phys.* 3 (1999), pp. 1–81. DOI: 10.4310/ATMP.1999.v3.n1.a1. arXiv: hep-th/9810201.

[50] James Sparks. "Sasaki-Einstein Manifolds". In: *Surveys Diff. Geom.* 16 (2011), pp. 265–324. DOI: 10.4310/SDG.2011.v16.n1.a6. arXiv: 1004.2461 [math.DG].

[51] Vijay Balasubramanian and Per Kraus. "A Stress tensor for Anti-de Sitter gravity". In: *Commun. Math. Phys.* 208 (1999), pp. 413–428. DOI: 10.1007/s002200050764. arXiv: hep-th/9902121.

[52] M. Henningson and K. Skenderis. "The Holographic Weyl anomaly". In: *JHEP* 07 (1998), p. 023. DOI: 10.1088/1126-6708/1998/07/023. arXiv: hep-th/9806087 [hep-th].

[53] Sebastian de Haro, Sergey N. Solodukhin, and Kostas Skenderis. "Holographic reconstruction of space-time and renormalization in the AdS / CFT correspondence". In: *Commun. Math. Phys.* 217 (2001), pp. 595–622. DOI: 10.1007/s002200100381. arXiv: hep-th/0002230.

[54] J. David Brown and James W. York Jr. "Quasilocal energy and conserved charges derived from the gravitational action". In: *Phys. Rev. D* 47 (1993), pp. 1407–1419. DOI: 10.1103/PhysRevD.47.1407. arXiv: gr-qc/9209012.

[55] Charles Fefferman, C. Robin Graham, and Collectif. "Conformal invariants". en. In: Astérisque S131 (1985). URL: http://www.numdam.org/item/AST_1985__S131__95_0/.

[56] Kostas Skenderis. "Lecture notes on holographic renormalization". In: *Class. Quant. Grav.* 19 (2002), pp. 5849–5876. DOI: 10.1088/0264-9381/19/22/306. arXiv: hep-th/0209067 [hep-th].

[57] Steven S. Gubser. "Curvature singularities: The Good, the bad, and the naked". In: *Adv. Theor. Math. Phys.* 4 (2000), pp. 679–745. DOI: 10.4310/ATMP.2000.v4.n3.a6. arXiv: hep-th/0002160.

[58] M. A. Abramowicz, B. Carter, and J. P. Lasota. "Optical reference geometry for stationary and static dynamics". In: *General Relativity and Gravitation* 20.11 (Nov. 1988), pp. 1173–1183. DOI: 10.1007/bf00758937.

[59] H. Osborn and A.C. Petkou. "Implications of conformal invariance in field theories for general dimensions". In: *Annals Phys.* 231 (1994), pp. 311–362. DOI: 10.1006/aphy.1994.1045. arXiv: hep-th/9307010.

[60] M. F. Atiyah and I. M. Singer. "The index of elliptic operators on compact manifolds". In: *Bulletin of the American Mathematical Society* 69.3 (1963), pp. 422–433. DOI: bams/1183525276. URL: https://doi.org/.

[61] Peter B Gilkey. "Curvature and the eigenvalues of the Laplacian for elliptic complexes". In: 10.3 (June 1973), pp. 344–382. DOI: 10.1016/0001-8708(73)90119-9.

[62] M. Atiyah, R. Bott, and V. K. Patodi. "On the heat equation and the index theorem". In: 19.4 (Dec. 1973), pp. 279–330. DOI: 10.1007/bf01425417.

[63] V. Fock. "Proper time in classical and quantum mechanics". In: *Phys. Z. Sowjetunion* 12 (1937), pp. 404–425.

[64] Julian Schwinger. "On Gauge Invariance and Vacuum Polarization". In: *Physical Review* 82.5 (June 1951), pp. 664–679. DOI: 10.1103/physrev.82.664.

[65] Bryce S. DeWitt. "Dynamical theory of groups and fields". In: *Conf. Proc. C* 630701 (1964). Ed. by C. DeWitt and B. DeWitt, pp. 585–820.

[66] Bryce S. DeWitt. "Quantum Theory of Gravity. 1. The Canonical Theory". In: *Phys. Rev.* 160 (1967). Ed. by Li-Zhi Fang and R. Ruffini, pp. 1113–1148. DOI: 10.1103/PhysRev.160.1113.

[67] Bryce S. DeWitt. "Quantum Theory of Gravity. 2. The Manifestly Covariant Theory". In: *Phys. Rev.* 162 (1967). Ed. by Jong-Ping Hsu and D. Fine, pp. 1195–1239. DOI: 10.1103/PhysRev.162.1195.

[68] Bryce S. DeWitt. "Quantum Theory of Gravity. 3. Applications of the Covariant Theory". In: *Phys. Rev.* 162 (1967). Ed. by Jong-Ping Hsu and D. Fine, pp. 1239–1256. DOI: 10.1103/PhysRev.162.1239.

[69] Curtis Callan and Frank Wilczek. "On geometric entropy". In: *Physics Letters B* 333.1-2 (July 1994), pp. 55–61. DOI: 10.1016/0370-2693(94)91007-3. arXiv: hep-th/9401072.

[70] R.D. Ball. "Chiral gauge theory". In: *Physics Reports* 182.1-2 (Oct. 1989), pp. 1–186. DOI: 10.1016/0370-1573(89)90027-6.

[71] S. A. Fulling. "Systematics of the relationship between vacuum energy calculations and heat kernel coefficients". In: *J. Phys. A* 36 (2003), pp. 6857–6873. DOI: 10.1088/0305-4470/36/24/320. arXiv: quant-ph/0302117.

[72] R. T. Seeley. "Singular Integrals and Boundary Value Problems". In: *American Journal of Mathematics* 88.4 (Oct. 1966), p. 781. DOI: 10.2307/2373078.

[73] R. Seeley. "The Resolvent of an Elliptic Boundary Problem". In: *American Journal of Mathematics* 91.4 (Oct. 1969), p. 889. DOI: 10.2307/2373309.

[74] D. V. Vassilevich. "Heat kernel expansion: User's manual". In: *Phys. Rept.* 388 (2003), pp. 279–360. DOI: 10.1016/j.physrep.2003.09.002. arXiv: hep-th/0306138 [hep-th].

[75] Michael E. Peskin and Daniel V. Schroeder. *An Introduction to quantum field theory*. Reading, USA: Addison-Wesley, 1995. ISBN: 978-0-201-50397-5.

[76] Peter B. Gilkey. "Invariance theory, the heat equation and the Atiyah-Singer index theorem". In: (1995).

[77] David J. Gross. "Asymptotically Free Gauge Theories. I". In: *Physical Review D* 8.10 (1973), pp. 3633–3652. DOI: 10.1103/PhysRevD.8.3633.

[78] H. David Politzer. "Reliable Perturbative Results for Strong Interactions?" In: *Phys. Rev. Lett.* 30 (1973). Ed. by J. C. Taylor, pp. 1346–1349. DOI: 10.1103/PhysRevLett.30.1346.

[79] M. Hortaçsu, K. D. Rothe, and B. Schroer. "Generalized two-dimensional QED and functional determinants". In: *Physical Review D* 20.12 (Dec. 1979), pp. 3203–3212. DOI: 10.1103/physrevd.20.3203.

[80] Dmitri V. Fursaev and Gennaro Miele. "Cones, spins and heat kernels". In: *Nucl. Phys.* B484 (1997), pp. 697–723. DOI: 10.1016/S0550-3213(96)00631-1. arXiv: hep-th/9605153 [hep-th].

[81] Peter B. Gilkey, Klaus Kirsten, and Dmitri V. Vassilevich. "Heat trace asymptotics with transmittal boundary conditions and quantum brane-world scenario". In: *Nuclear Physics B* 601.1-2 (May 2001), pp. 125–148. DOI: 10.1016/s0550-3213(01)00083-9.

[82] Peter B. Gilkey. "The spectral geometry of the higher order Laplacian". In: *Duke Mathematical Journal* 47.3 (Sept. 1980). DOI: 10.1215/s0012-7094-80-04731-6.

[83] V.P. Gusynin. "Seeley-Gilkey coefficients for fourth-order operators on a riemannian manifold". In: *Nuclear Physics B* 333.1 (Mar. 1990), pp. 296–316. DOI: 10.1016/0550-3213(90)90233-4.

[84] Nelson, D.R. and Peliti, L. "Fluctuations in membranes with crystalline and hexatic order". In: *J. Phys. France* 48.7 (1987), pp. 1085–1092. DOI: 10.1051/jphys:019870048070108500. URL: https://doi.org/10.1051/jphys:019870048070108500.

[85] D. Nelson, T. Piran and S. Weinberg. *Statistical Mechanics of Membranes and Surfaces*. Singapore: World Scientific, 2004.

[86] M. Bowick, A. Travesset. "The statistical mechanics of membranes". In: *Phys. Rept.* 344 (2001), pp. 255–308.

[87] A. Fasolino, J. Los, and M. Katsnelson. "Intrinsic ripples in graphene". In: *Nature Materials* 6 (2007), pp. 858–861. arXiv: 0704.1793 [cond-mat].

[88] Ignat V. Fialkovsky and Dmitri V. Vassilevich. "Graphene through the looking glass of QFT". In: *Mod. Phys. Lett.* A31.40 (2016), p. 1630047. DOI: 10.1142/S0217732316300470. arXiv: 1608.03261 [hep-th].

[89] Rudolf Baier et al. "Relativistic viscous hydrodynamics, conformal invariance, and holography". In: *JHEP* 04 (2008), p. 100. DOI: 10.1088/1126-6708/2008/04/100. arXiv: 0712.2451 [hep-th].

[90] Sayantani Bhattacharyya, Veronika E Hubeny, Shiraz Minwalla, and Mukund Rangamani. "Nonlinear Fluid Dynamics from Gravity". In: *JHEP* 02 (2008), p. 045. DOI: 10.1088/1126-6708/2008/02/045. arXiv: 0712.2456 [hep-th].

[91] Aristomenis Donos and Jerome P. Gauntlett. "Holographic striped phases". In: *JHEP* 08 (2011), p. 140. DOI: 10.1007/JHEP08(2011)140. arXiv: 1106.2004 [hep-th].

[92] Maya Paczuski, Mehran Kardar, and David R. Nelson. "Landau Theory of the Crumpling Transition". In: *Phys. Rev. Lett.* 60 (25 1988), pp. 2638–2640. DOI: 10.1103/PhysRevLett.60.2638. URL: https://link.aps.org/doi/10.1103/PhysRevLett.60.2638.

[93] D. Nelson, T. Piran, S. Weinberg, ed. *Statistical Mechanics of Membranes and Surfaces* (Singapore). World Scientific, 1989. ISBN: 9971507226.

[94] Dionysios Anninos, Frederik Denef, and Daniel Harlow. "Wave function of Vasiliev's universe: A few slices thereof". In: 88.8 (Oct. 2013), p. 084049. DOI: 10.1103/physrevd.88.084049.

[95] Nikolay Bobev, Pablo Bueno, and Yannick Vreys. "Comments on Squashed-sphere Partition Functions". In: *JHEP* 07 (2017), p. 093. DOI: 10.1007/JHEP07(2017)093. arXiv: 1705.00292 [hep-th].

[96] Sebastian Fischetti, Andrew Hickling, and Toby Wiseman. "Bounds on the local energy density of holographic CFTs from bulk geometry". In: *Class. Quant. Grav.* 33.22 (2016), p. 225003. DOI: 10.1088/0264-9381/33/22/225003. arXiv: 1605.00007 [hep-th].

[97] Krai Cheamsawat. "A new energy bound for Einstein-Scalar theory in $AlAdS_4$ and holographic bound for deformed CFT_3". In: (2020). arXiv: 2002.11741 [hep-th].

[98] Krai Cheamsawat, Gary Gibbons, and Toby Wiseman. "A new energy upper bound for AdS black holes inspired by free field theory". In: (2019). arXiv: 1906.07192 [hep-th].

[99] Emanuele Panella. "Numerical Investigations of the Free Energy for a Scalar Field Theory on Deformed Spheres". MA thesis. Imperial College London, 2021. URL: https://www.imperial.ac.uk/media/imperial-college/research-centres-and-groups/theoretical-physics/msc/dissertations/Emanuele-Panella-Dissertation.pdf.

[100] Ahmad El Soufi and Saïd Ilias. "Critical metrics of the trace of the heat kernel on a compact manifold". In: 81 (2002), pp. 1053–1070. ISSN: 0021-7824. DOI: 10.1016/s0021-7824(02)01271-0.

[101] Cao et al. "Hollow graphene spheres self-assembled from graphene oxide sheets by a one-step hydrothermal process". In: *Carbon* 56 (2013), pp. 389–391.

[102] Glenn Wagner, Fernando de Juan, and Dung X. Nguyen. "Quantum Hall effect in curved space realized in strained graphene". In: (2019). arXiv: 1911.02028 [cond-mat.str-el].

[103] Andrea Cappelli and Antoine Coste. "On the stress tensor of conformal field theories in higher dimensions". In: *Nuclear Physics B* 314.3 (1989), pp. 707–740. ISSN: 0550-3213. DOI: https://doi.org/10.1016/0550-3213(89)90414-8. URL: http://www.sciencedirect.com/science/article/pii/0550321389904148.

[104] Lloyd N Trefethen. *Spectral methods in MATLAB*. Vol. 10. Siam, 2000.

[105] J.C. Mason and David C. Handscomb. *Chebyshev Polynomials*. Chapman and Hall/CRC, Sept. 2002. DOI: 10.1201/9781420036114. URL: https://doi.org/10.1201%2F9781420036114.

[106] T.J. Rivlin. *Chebyshev Polynomials*. Dover Books on Mathematics. Dover Publications, 2020. ISBN: 9780486842332. URL: https://books.google.co.uk/books?id=rPLwDwAAQBAJ.

[107] Lloyd N. Trefethen. *Finite Difference and Spectral Methods for Ordinary and Partial Differential Equations*. unpublished text, 1996. URL: http://people.maths.ox.ac.uk/trefethen/pdetext.html.

[108] James F Epperson. "On the Runge example". In: *The American Mathematical Monthly* 94.4 (1987), pp. 329–341.

[109] D. Gottlieb, M. Hussaini, and S. Orszag. "Theory and applications of spectral methods". In: 1984.

[110] J. A. Weideman and S. C. Reddy. "A MATLAB differentiation matrix suite". In: *ACM Transactions on Mathematical Software* 26.4 (Dec. 2000), pp. 465–519. DOI: 10.1145/365723.365727.

[111] Paul C. Yang and Shing-Tung Yau. "Eigenvalues of the laplacian of compact Riemann surfaces and minimal submanifolds". en. In: *Annali della Scuola Normale Superiore di Pisa - Classe di Scienze* Ser. 4, 7.1 (1980), pp. 55–63. URL: http://www.numdam.org/item/ASNSP_1980_4_7_1_55_0.

[112] Christian Bär. "Lower eigenvalue estimates for Dirac operators". In: *Mathematische Annalen* 293.1 (1992), pp. 39–46.

[113] Pablo Bueno, Pablo A. Cano, Robie A. Hennigar, and Robert B. Mann. "Universality of Squashed-Sphere Partition Functions". In: *Phys. Rev. Lett.* 122.7 (2019), p. 071602. DOI: 10.1103/PhysRevLett.122.071602. arXiv: 1808.02052 [hep-th].

[114] Pablo Bueno et al. "Partition functions on slightly squashed spheres and flux parameters". In: *JHEP* 04 (2020), p. 123. DOI: 10.1007/JHEP04(2020)123. arXiv: 2001.10020 [hep-th].

[115] J. S. Dowker. "Casimir Effect Around a Cone". In: *Phys. Rev.* D36 (1987), p. 3095. DOI: 10.1103/PhysRevD.36.3095.

[116] Jorge Casalderrey-Solana et al. *Gauge/String Duality, Hot QCD and Heavy Ion Collisions*. Cambridge University Press, 2014. ISBN: 978-1-139-13674-7. DOI: 10.1017/CBO9781139136747. arXiv: 1101.0618 [hep-th].

[117] Pablo Bueno, Robert C. Myers, and William Witczak-Krempa. "Universality of corner entanglement in conformal field theories". In: *Phys. Rev. Lett.* 115 (2015), p. 021602. DOI: 10.1103/PhysRevLett.115.021602. arXiv: 1505.04804 [hep-th].

[118] Pablo Bueno and Robert C. Myers. "Corner contributions to holographic entanglement entropy". In: *JHEP* 08 (2015), p. 068. DOI: 10.1007/JHEP08(2015)068. arXiv: 1505.07842 [hep-th].

[119] Pablo Bueno, Robert C. Myers, and William Witczak-Krempa. "Universal corner entanglement from twist operators". In: *JHEP* 09 (2015), p. 091. DOI: 10.1007/JHEP09(2015)091. arXiv: 1507.06997 [hep-th].

[120] Edward Witten. "Anti-de Sitter space, thermal phase transition, and confinement in gauge theories". In: *Adv. Theor. Math. Phys.* 2 (1998). Ed. by L. Bergstrom and U. Lindstrom, pp. 505–532. DOI: 10.4310/ATMP.1998.v2.n3.a3. arXiv: hep-th/9803131.

[121] Matthew Headrick, Sam Kitchen, and Toby Wiseman. "A New approach to static numerical relativity, and its application to Kaluza-Klein black holes". In: *Class. Quant. Grav.* 27 (2010), p. 035002. DOI: 10.1088/0264-9381/27/3/035002. arXiv: 0905.1822 [gr-qc].

[122] Pau Figueras, James Lucietti, and Toby Wiseman. "Ricci solitons, Ricci flow, and strongly coupled CFT in the Schwarzschild Unruh or Boulware vacua". In: *Class. Quant. Grav.* 28 (2011), p. 215018. DOI: 10.1088/0264-9381/28/21/215018. arXiv: 1104.4489 [hep-th].

[123] Toby Wiseman. "Numerical construction of static and stationary black holes". In: *Black holes in higher dimensions*. Ed. by Gary T. Horowitz. 2012, pp. 233–270. arXiv: 1107.5513 [gr-qc].

[124] Ofer Aharony, Oren Bergman, Daniel Louis Jafferis, and Juan Maldacena. "$\mathcal{N}$ = 6 superconformal Chern-Simons-matter theories, M2-branes and their gravity duals". In: *Journal of High Energy Physics* 2008.10 (Oct. 2008), pp. 091–091. DOI: 10.1088/1126-6708/2008/10/091. URL: https://doi.org/10.1088/1126-6708/2008/10/091.

[125] Michael T. Anderson, Piotr T. Chrusciel, and Erwann Delay. "Nontrivial, static, geodesically complete, vacuum space-times with a negative cosmological constant". In: *JHEP* 10.10 (Oct. 2002), p. 063. DOI: 10.1088/1126-6708/2002/10/063. arXiv: gr-qc/0211006.

[126] Nicolas Ginoux. "About the Lorentzian Yamabe problem". In: *Geometriae Dedicata* 174.1 (Oct. 2014), pp. 287–309. DOI: 10.1007/s10711-014-0018-8.

[127] Pablo Bueno, Pablo A. Cano, and Alejandro Ruipérez. "Holographic studies of Einsteinian cubic gravity". In: *JHEP* 03 (2018), p. 150. DOI: 10.1007/JHEP03(2018)150. arXiv: 1802.00018 [hep-th].

[128] Diego M. Hofman and Juan Maldacena. "Conformal collider physics: Energy and charge correlations". In: *JHEP* 05 (2008), p. 012. DOI: 10.1088/1126-6708/2008/05/012. arXiv: 0803.1467 [hep-th].

[129] Luke Keltner and Andrew J. Tolley. "UV properties of Galileons: Spectral Densities". In: (Feb. 2015). arXiv: 1502.05706 [hep-th].

[130] Gunnar Kallen. "On the definition of the Renormalization Constants in Quantum Electrodynamics". In: *Helv. Phys. Acta* 25.4 (1952). Ed. by Cecilia Jarlskog, p. 417. DOI: 10.1007/978-3-319-00627-7_90.

[131] H. Lehmann. "On the Properties of propagation functions and renormalization contants of quantized fields". In: *Nuovo Cim.* 11 (1954), pp. 342–357. DOI: 10.1007/BF02783624.

[132] Andrea Cappelli, Daniel Friedan, and Jose I. Latorre. "C theorem and spectral representation". In: *Nucl. Phys. B* 352 (1991), pp. 616–670. DOI: 10.1016/0550-3213(91)90102-4.

[133] K. Okikiolu. "Critical Metrics for the Determinant of the Laplacian in Odd Dimensions". In: 153.2 (Mar. 2001), p. 471. DOI: 10.2307/2661347.

[134] A. Zee. *Quantum field theory in a nutshell*. 2003. ISBN: 978-0-691-14034-6.

[135] Daniel Z. Freedman and Antoine Van Proeyen. *Supergravity*. Cambridge University Press, 2012.

[136] C. Wetterich. "Spinors in euclidean field theory, complex structures and discrete symmetries". In: *Nucl. Phys.* B852 (2011), pp. 174–234. DOI: 10.1016/j.nuclphysb.2011.06.013. arXiv: 1002.3556 [hep-th].

[137] Robert J. Downes, Michael Levitin, and Dmitri Vassiliev. "Spectral asymmetry of the massless Dirac operator on a 3-torus". In: *J. Math. Phys.* 54 (2013), p. 111503. DOI: 10.1063/1.4828858. arXiv: 1306.5689 [math.SP].

[138] G. De Berredo-Peixoto. "A Note on the heat kernel method applied to fermions". In: *Mod. Phys. Lett.* A16 (2001), pp. 2463–2468. DOI: 10.1142/S0217732301005965. arXiv: hep-th/0108223 [hep-th].

[139] E. T. Newman and R. Penrose. "Note on the Bondi-Metzner-Sachs Group". In: *Journal of Mathematical Physics* 7.5 (1966), pp. 863–870. DOI: 10.1063/1.1931221. URL: https://doi.org/10.1063/1.1931221.

[140] J. N. Goldberg et al. "Spin-s Spherical Harmonics and $\eth$". In: *Journal of Mathematical Physics* 8.11 (1967), pp. 2155–2161. DOI: 10.1063/1.1705135. URL: https://doi.org/10.1063/1.1705135.

[141] A. R. Edmonds. *Angular Momentum in Quantum Mechanics*. Princeton: Princeton University Press, 1974.

[142] William J. Thompson. *Angular Momentum: An Illustrated Guide to Rotational Symmetries for Physical Systems*. New York: John Wiley and Sons, Inc., 1994.

[143] Hidehiko Yamabe. "On a deformation of Riemannian structures on compact manifolds". In: *Osaka Math. J.* 12.1 (1960), pp. 21–37. URL: https://projecteuclid.org:443/euclid.ojm/1200689814.

[144] John M. Lee and Thomas H. Parker. "The Yamabe problem". In: *Bull. Amer. Math. Soc. (N.S.)* 17.1 (July 1987), pp. 37–91. URL: https://projecteuclid.org:443/euclid.bams/1183553962.

[145] John M. Lee and Thomas H. Parker. "The Yamabe problem". In: *Bulletin of the American Mathematical Society* 17.1 (1987), pp. 37–91. DOI: 10.1090/s0273-0979-1987-15514-5. URL: https://doi.org/10.1090%2Fs0273-0979-1987-15514-5.

Appendix A

Analytic Work

A.1 Thermal Field Theory in Curved Spacetime

In this section, we sketch the argument that static Lorentzian QFTs at finite temperature have Euclidean QFT duals, more on which can be found in, for example, [134].

Consider a Lorentzian Quantum Field Theory at temperature β^{-1} with Hamiltonian $H[\phi]$ on a $(d+1)$-dimensional manifold $\mathbb{R}\times\mathcal{M}$. Statistical Mechanics tells us that the partition function for this system is

$$Z = \mathrm{Tr}\left(\mathrm{e}^{-\beta H}\right). \tag{A.1}$$

This can be written in terms of field eigenstates, $|\varphi\rangle$[1], as

$$Z = \int \mathcal{D}\varphi\, \langle(-)^F\varphi|\mathrm{e}^{-\beta H}|\varphi\rangle. \tag{A.2}$$

where $F = 0/1$ for a bosonic/fermionic field, whose integrand can be re-written suggestively as $\langle(-)^F\varphi|\mathrm{e}^{-i(-i\beta)H}|\varphi\rangle$. This amplitude looks a lot like the transition amplitude from the state φ back to itself in a time $-i\beta$. In path integral language, this amplitude is

$$\langle(-)^F\varphi|\mathrm{e}^{-i(-i\beta)H}|\varphi\rangle = \int_{M_\varphi}\mathcal{D}\phi\exp\left(-i\int_0^{-i\beta}\mathrm{d}t\int_{\mathcal{M}}\mathcal{L}(\phi)\right) \tag{A.3}$$

where $\mathcal{L}$ is the Lagrangian density and M_φ denotes the space of all (analytically continued) field configurations which satisfy $\phi(0,x) = (-)^F\phi(i\beta,x) = \varphi(x)$. So transforming to imaginary time, $\tau = it$,

$$\langle(-)^F\varphi|\mathrm{e}^{-i(-i\beta)H}|\varphi\rangle = \int_{M_\varphi}\mathcal{D}\phi_{\mathrm{E}}\,\mathrm{e}^{-\int_0^\beta\mathrm{d}\tau\int_{\mathcal{M}}\mathcal{L}_{\mathrm{E}}(\phi_{\mathrm{E}})} = \int_{M_\varphi}\mathcal{D}\phi_{\mathrm{E}}\,\mathrm{e}^{-S_{\mathrm{E}}[\phi_{\mathrm{E}}]} \tag{A.4}$$

[1] These are time independent as we are in thermodynamic equilibrium.

where

$$S_{\mathrm{E}}[\phi] = \int_0^\beta \mathrm{d}\tau \int_{\mathcal{M}} \mathcal{L}_{\mathrm{E}}(\phi_{\mathrm{E}}) \tag{A.5}$$

is the action of this new Euclidean theory. When the amplitude, in this form, is inserted back into the partition function, the integral over the eigenstates then softens the restriction on the ϕ_{E} integral to field configurations which satisfy $\phi_{\mathrm{E}}(x,0) = (-)^F \phi_{\mathrm{E}}(x,\beta)$, so the partition function is

$$Z = \int \mathcal{D}\phi_{\mathrm{E}}\, \mathrm{e}^{-S_{\mathrm{E}}[\phi_{\mathrm{E}}]} \tag{A.6}$$

which matches that of a Euclidean QFT with action S_{E} on a background $S^1 \times \mathcal{M}$ with periodic time coordinate $0 \leqslant \tau < \beta$ and fields satisfying (anti)periodic boundary conditions in τ for a (fermionic) bosonic field. This allows you the freedom to use any techniques you know for analysing Euclidean QFTs to calculate quantities which can then be analytically continued back to Lorentzian time in order the probe Lorentzian QFT at finite temperature.

A.2 One-Loop Effective Action

In this section, we detail the derivation of the one-loop effective action in terms of a functional determinant for relativistic quantum degrees of freedom in the presence of background fields as seen in, for example, [75]. For this section, $\hbar$ will be reinstated.

Consider a field theory with an action, $S[\phi,\psi]$ on a Riemannian manifold $(\mathcal{M}, g)$ of dimension n, where ϕ is some quantum field and ψ is all other fields. If we wish to do quantum field theory with this action, we integrate over all field configurations weighted by $\mathrm{e}^{-S/\hbar}$ to obtain the path integral

$$\int \mathcal{D}\psi\mathcal{D}\phi\, \mathrm{e}^{-S[\phi,\psi]/\hbar}. \tag{A.7}$$

While, in theory, it is possible to deduce anything you would want to know about this theory simply working with this object, there are more practical objects for certain applications. For example, we may be interested in the behaviour of the geometry of some membrane which has ϕ living on it. It is not important precisely what ϕ is doing, so, for our purposes, it is sufficient to integrate it out. Its effect will then be represented as a self interaction term for the out of plane displacements. This can be done by working with the quantum effective action. This is defined as the Legendre Transform of the energy functional $W[J,\psi] = -\hbar \ln Z[J,\psi]$, where $Z[J,\psi]$ is obtained by adding a source to the

action,

$$Z[J,\psi] = \int \mathcal{D}\phi \, \mathrm{e}^{-\left(S[\phi,\psi]+(J,\phi)\right)/\hbar} \tag{A.8}$$

where $(\cdot\,,\cdot)$ is an inner product on the vector bundle in which ϕ lives,

$$(\phi_1,\phi_2) = \int \mathrm{d}^n x \sqrt{g}\overline{\phi}_1\phi_2 \tag{A.9}$$

and $\overline{\phi}$ is a conjugation that makes the integrand a scalar. Thus the effective action $\Gamma[\Phi,\psi]$ is

$$\Gamma[\Phi,\psi] = W[J(\Phi,\psi)] - \big(J(\Phi,\psi),\Phi\big) \tag{A.10}$$

where $J(\Phi,\psi)$ is defined implicitly by the equation

$$\Phi(x) \equiv \frac{1}{\sqrt{g(x)}}\frac{\delta W}{\delta J(x)} \tag{A.11}$$

From here on, all dependence on ψ will be suppressed. The effective action has all the loop corrections built in — thus it is fully quantum corrected. Whereas the action S is a purely classical object, the effective action takes quantum effects into account, thus may be used to probe purely quantum effects such as anomalies and energy due to vacuum fluctuations. Generically, it is not possible to solve analytically for J in terms of Φ, however, progress can be made by expanding ϕ in powers of $\hbar$ and solving iteratively, order by order. In the limit $\hbar \to 0$, $Z[J]$ is dominated by the field configuration which minimises the exponent in the integrand i.e. where the classical equations of motion for ϕ,

$$\frac{\delta S}{\delta\phi(x)} = -\sqrt{g(x)}J(x) \tag{A.12}$$

are satisfied. We denote this solution as ϕ_{cl}. This means that in the limit $\hbar \to 0$,

$$\frac{1}{\sqrt{g(x)}}\frac{\delta W}{\delta J(x)} \to \phi_{\mathrm{cl}} \tag{A.13}$$

so $\Phi(x)$ and ϕ_{cl} coincide (as functions of J) to leading order in $\hbar$. Now change variables in the path integral $\phi = \phi_{\mathrm{cl}} + \eta$,

$$W[J] = S[\phi_{\mathrm{cl}}] + (J,\phi_{\mathrm{cl}}) - \hbar \ln\left(\int \mathcal{D}\eta \exp\left[-(\eta,D\eta)/\hbar + O(\hbar^{-1}\eta^3)\right]\right) \tag{A.14}$$

where the operator D is

$$D = \frac{1}{2\sqrt{g(x)}} \int \mathrm{d}^n y \frac{\delta^2 S}{\delta\phi(x)\delta\phi(y)}. \tag{A.15}$$

This is a second order differential operator that is self-adjoint with respect to $(\cdot\,,\cdot)$. From before, we know the integral in (A.14) is dominated by the region where η is small. In particular, the region where $\eta = O(\hbar^{1/2})$, thus ignore the $O(\eta^3\hbar^{-1})$ terms so

$$W[J] = S[\phi_{\mathrm{cl}}] + (J, \phi_{\mathrm{cl}}) - \sigma\hbar \ln\det D. \tag{A.16}$$

where σ is some number that depends on the vector bundle the field ϕ lives in. Then,

$$\Gamma[\Phi] = S[\phi_{\mathrm{cl}}] - \sigma\hbar \ln\det D + (J, \phi_{\mathrm{cl}}) - (J, \Phi). \tag{A.17}$$

J was introduced as a tool for doing the calculation, but in the end we can set J to 0 since we are not interested in the dynamics of field we have just integrated out. At $J = 0$, ϕ_{cl} is the solution to the unsourced equations of motion for ϕ and so the one-loop effective action is (reinserting ψ dependence)

$$\Gamma[\Phi, \psi] = S[\phi_{\mathrm{cl}}, \psi] - \sigma\hbar \ln\det D[\phi_{\mathrm{cl}}, \psi]. \tag{A.18}$$

for $\Phi - \phi_{\mathrm{cl}} = O(\hbar)$. Thus, the computation of the one-loop effective action has been reduced to calculating $\ln\det D$ which can be expressed in terms of a heat kernel.

While the derivation above shows that $-\sigma\hbar \ln\det D$ is the one-loop correction to the effective action, for any free theory i.e. theory quadratic in the field ϕ, it is the full correction, as there are no contributions from higher orders.

A.3 Fermion Partition Function

In this section, we set out the conventions for and details on the Euclidean Dirac fermion calculations in Chapters 3, 5 and 6, closely following the treatment in [1].

We will follow the Clifford algebra conventions of [135]: in Euclidean signature, the Clifford algebra is

$$\{\gamma^a, \gamma^b\} = 2\delta^{ab}, \tag{A.19}$$

which allows us to take the γ^a to be Hermitian. With such conventions, a natural choice of representation of the gamma matrices in three dimensions is $\gamma^a = \sigma^a$ with σ^a the Pauli matrices, though we note that none of our statements will depend on such a choice. Scalars are formed from spinors χ, ψ as the bilinears $\bar{\chi}\psi$ with $\bar{\chi} = \chi^\dagger$, and the massive

Euclidean Dirac action on a curved space with metric $g_{\mu\nu}$ is

$$S_{\mathrm{E}}[\bar{\psi},\psi] = \int \mathrm{d}^3x\sqrt{g}\,\bar{\psi}(i\not{D} - iM)\psi, \tag{A.20}$$

where $\not{D} = \gamma^a(e_a)^\mu D_\mu$ with $\{(e_a)^\mu\}$ for $a = 1, 2, 3$ a vielbein,

$$D_\mu = \nabla_\mu + \frac{1}{2}\omega_{\mu ab}S^{ab}, \tag{A.21}$$

∇_μ the usual Levi-Civita connection compatible with $g_{\mu\nu}$, $S^{ab} = [\gamma^a,\gamma^b]/4$ the generators of the Lorentz group, and $\omega_{\mu ab} = (e_a)^\nu\nabla_\mu(e_b)_\nu$ the spin connection. Note that the operator $i\not{D}$ is self adjoint, but the i in the mass term renders the Euclidean action non-Hermitian. This factor of i is necessary to ensure that the action obeys the Osterwalder-Schrader positivity conditions; see e.g. [136] for a discussion of such subtleties associated with spinors in Euclidean space.

The Dirac fermion path integral has solvable a path integral (as noted in Section 2.1):

$$Z = \int \mathcal{D}\bar{\psi}\,\mathcal{D}\psi\,\mathrm{e}^{-S_E[\bar{\psi},\psi]} = \det(i\not{D} - iM). \tag{A.22}$$

$i\not{D}$ is self adjoint and thus has real eigenvalues. Moreover, in the direct-product geometry (3.1), eigenspinors of $i\not{D}$ can be decomposed into Fourier modes $\psi = \mathrm{e}^{-i\Omega_n\tau}\psi_\Sigma$, with ψ_Σ a spinor on Σ and $\Omega_n = (2n+1)\pi/\beta$ a Matsubara frequency (with $n \in \mathbb{Z}$). It is then straightforward to show that if $\mathrm{e}^{-i\Omega_n\tau}\psi_\Sigma$ is an eigenspinor of $i\not{D}$ with eigenvalue λ, then $\mathrm{e}^{i\Omega_n\tau}\gamma^\tau\psi_\Sigma$ is an eigenspinor with eigenvalue $-\lambda$. Hence, the spectrum of $i\not{D}$ on the background (3.1) is symmetric about zero[2], allowing us to write

$$Z^2 = \det(i\not{D} - iM)\det(-i\not{D} - iM) = \det(\not{D}^2 - M^2). \tag{A.23}$$

(See e.g. [138] for more on this trick in $d = 4$.) By expressing the metric on (Σ, g) in the conformally flat form (3.10), we may evaluate $\not{D}^2 - M^2$. Noting that there is only one generator $S^{12} = (i/2)\gamma^\tau$ of rotations in two dimensions, we obtain

$$\not{D}^2 - M^2 = -\mathcal{L}P_{\mathrm{L}} - \mathcal{L}^*P_{\mathrm{R}}, \tag{A.24}$$

where $P_{\mathrm{L,R}} = (1 \pm \gamma^\tau)/2$ are left and right Weyl projectors on (Σ, g) and $\mathcal{L}$ is as given in (3.5). Decomposing $\psi = \mathrm{e}^{-i\Omega_n\tau}\psi_\Sigma$, we see that $\mathcal{L}$ and $\mathcal{L}^*$ act only on left- and right-helicity Weyl spinors $P_{\mathrm{L}}\psi_\Sigma$, $P_{\mathrm{R}}\psi_\Sigma$, respectively. As these spinors only have one component each, we may interpret $\mathcal{L}$ and $\mathcal{L}^*$ as acting only on complex functions (albeit with an-

[2]Note that the direct product structure of (3.1) was crucial; in a general odd-dimensional geometry the spectrum of $i\not{D}$ need not be symmetric [137].

tiperiodic boundary conditions on the thermal circle). This therefore allows us to write

$$\det(-\mathcal{L}P_{\mathrm{L}} - \mathcal{L}^* P_{\mathrm{R}}) = \det(-\mathcal{L})\det(-\mathcal{L}^*) = (\det\mathcal{L})^2, \tag{A.25}$$

where in the second expression we take the determinants only over the space of functions on which $\mathcal{L}$ and $\mathcal{L}^*$ act, and in the last equality we noted that because $\mathcal{L}$ is self adjoint (with respect to the usual L_2 norm), $\mathcal{L}$ and $\mathcal{L}^*$ have the same spectrum (and thus determinant). Hence, the partition function for the fermion can be evaluated by taking the functional determinant of a scalar differential operator acting on complex functions, thus aligning it with more closely with the scalar case.

A.4 Finite-d Heat Kernels on the Torus

In this section, we provide more details on the computation of the heat kernel at finite d for Section 3.3, closely following the treatment in [1]. Firstly, in order to deal with the issue of eigenfunction degeneracy, it is convenient to take r^2 irrational (which limits the degeneracy of each eigenvalue $\bar{\lambda}_I$ to be less than or equal to four) and choose the label I to consist of $\{\mathbf{N}^+, \mathbf{S}\}$, where $\mathbf{N}^+ = \{n_1^+, n_2^+\}$ is a pair of non-negative integers and $\mathbf{S} = \{s_1, s_2\}$ is a pair of signs, with $s_i = \pm 1$ if $n_i^+ \neq 0$ and $s_i = 0$ if $n_i^+ = 0$. The eigenspaces of $-\overline{\nabla}^2$ have eigenvalues $\bar{\lambda}_{\mathbf{N}^+} = (2\pi/d)^2((n_1^+)^2 + (n_2^+)^2/r^2)$ (and are thus labelled by $\mathbf{N}^+$) and the values of $\mathbf{S}$ index these degenerate subspaces, each of which have degeneracy $b_{\mathbf{N}^+} = (2 - \delta_{n_1^+,0})(2 - \delta_{n_2^+,0})$ and the eigenfunctions are written as

$$\bar{h}_{\mathbf{N}^+,\mathbf{S}}(x) = \frac{1}{\sqrt{r}\,d} \sum_{\mathbf{S}'} c_{\mathbf{S}\mathbf{S}'}^{(\mathbf{N}^+)} \mathrm{e}^{2\pi i \sum_{j=1}^2 s'_j n_j^+ x^j/d_j}, \tag{A.26}$$

where the sum runs over all $b_{\mathbf{N}^+}$ possible choices of $\mathbf{S}'$ and for fixed $\mathbf{N}^+$, $c_{\mathbf{S}\mathbf{S}'}^{(\mathbf{N}^+)}$ is an arbitrary $b_{\mathbf{N}^+} \times b_{\mathbf{N}^+}$ unitary matrix. In other words, for given $\mathbf{N}^+$ the $\bar{h}_{\mathbf{N}^+,\mathbf{S}}$ form an arbitrary orthonormal basis of the degenerate subspace of $-\overline{\nabla}^2$ with eigenvalue $\bar{\lambda}_{\mathbf{N}^+}$; the freedom to choose this basis is what allows us to satisfy the perturbation theory consistency conditions on $\bar{h}_{\mathbf{N}^+,\mathbf{S}}$.

Using this formalism, we may compute the second-order corrections to the heat kernels at finite d using (3.20) which, after some rearrangement, are found to be

$$\Delta K_{\mathrm{s}}^{(2)}(t) = t\frac{4(2\pi)^4}{(d_1 d_2)^2}\left[\frac{t}{2}\sum_{\mathbf{N}^+} \mathrm{e}^{-\bar{\lambda}_{\mathbf{N}^+}t} \sum_{\mathbf{S},\mathbf{S}',\mathbf{S}'\neq\mathbf{S}} \left|\tilde{f}^{(1)}_{\Delta\mathbf{S}\mathbf{N}^+}\right|^2 \left(\bar{\lambda}_{\mathbf{N}^+} - \xi\bar{\lambda}_{\Delta\mathbf{S}\mathbf{N}^+}\right)^2\right.$$
$$\left. + \sum_{\mathbf{N},\mathbf{N}'} \left|\tilde{f}^{(1)}_{\mathbf{N}}\right|^2 \mathrm{e}^{-\bar{\lambda}_{\mathbf{N}'}t} \left(\bar{\lambda}_{\mathbf{N}'} - \xi\bar{\lambda}_{\mathbf{N}}\right)\left(-\delta_{\bar{\lambda}_{\mathbf{N}'},\bar{\lambda}_{\mathbf{N}-\mathbf{N}'}} + \delta_{\bar{\lambda}_{\mathbf{N}'}\neq\bar{\lambda}_{\mathbf{N}-\mathbf{N}'}} \frac{\bar{\lambda}_{\mathbf{N}'} - \xi\bar{\lambda}_{\mathbf{N}}}{\bar{\lambda}_{\mathbf{N}-\mathbf{N}'} - \bar{\lambda}_{\mathbf{N}'}}\right)\right], \tag{A.27a}$$

$$\Delta K_{\mathrm{f}}^{(2)}(t) = t\,\frac{4(2\pi)^4}{(d_1 d_2)^2}\left[\frac{t}{2}\sum_{\mathbf{N}^+}\mathrm{e}^{-\bar{\lambda}_{\mathbf{N}^+}t}\sum_{\mathbf{S},\mathbf{S}',\mathbf{S}'\neq\mathbf{S}}\left|\tilde{f}^{(1)}_{\Delta\mathbf{S}\mathbf{N}^+}\right|^2\left(\left(\bar{\lambda}_{\mathbf{N}^+}-\frac{1}{4}\bar{\lambda}_{\Delta\mathbf{S}\mathbf{N}^+}\right)^2 - D^2_{\mathbf{S}\mathbf{N}^+,\mathbf{S}'\mathbf{N}^+}\right)\right.$$
$$+\sum_{\mathbf{N},\mathbf{N}'}\left|\tilde{f}^{(1)}_{\mathbf{N}}\right|^2\mathrm{e}^{-\bar{\lambda}_{\mathbf{N}'}t}\left(\frac{3}{16}\bar{\lambda}_{\mathbf{N}}-\bar{\lambda}_{\mathbf{N}'}\right.$$
$$\left.\left.+\delta_{\bar{\lambda}_{\mathbf{N}'}\neq\bar{\lambda}_{\mathbf{N}-\mathbf{N}'}}\frac{\left(\bar{\lambda}_{\mathbf{N}'}-\bar{\lambda}_{\mathbf{N}}/4+D_{\mathbf{N},\mathbf{N}'}\right)\left(\bar{\lambda}_{\mathbf{N}-\mathbf{N}'}-\bar{\lambda}_{\mathbf{N}}/4-D_{\mathbf{N},\mathbf{N}'}\right)}{\bar{\lambda}_{\mathbf{N}-\mathbf{N}'}-\bar{\lambda}_{\mathbf{N}'}}\right)\right], \quad \text{(A.27b)}$$

where we defined $\mathbf{S}\mathbf{N}^+ \equiv \{s_1 n_1^+, s_2 n_2^+\}$, $\Delta\mathbf{S}\mathbf{N}^+ \equiv (\mathbf{S}-\mathbf{S}')\mathbf{N}^+$, $D_{\mathbf{N},\mathbf{N}'} = i(2\pi)^2\left(n_1 n_2' - n_1' n_2\right)/(2d_1 d_2)$, and $\delta_{\bar{\lambda}_{\mathbf{N}'}\neq\bar{\lambda}_{\mathbf{N}-\mathbf{N}'}} = 1$ if $\bar{\lambda}_{\mathbf{N}'} \neq \bar{\lambda}_{\mathbf{N}-\mathbf{N}'}$ and 0 otherwise. Note that the precise form of the matrices $c^{(\mathbf{N}^+)}_{\mathbf{S}\mathbf{S}'}$ does not matter since they cancel out in traces (as seen in Section 3.2), but the presence of the sums over degenerate subspaces in the first terms in the above expressions is an artefact of needing to treat the degenerate subspaces properly.

We now take the limit $d \to \infty$. The first term in each expression above vanishes in this limit (essentially because $d^{-4}\sum_{\mathbf{N}} \to d^{-2}\int \mathrm{d}^2k \to 0$); for the same reason, the terms containing $\delta_{\bar{\lambda}_{\mathbf{N}'},\bar{\lambda}_{\mathbf{N}-\mathbf{N}'}}$ also vanish. This results in Equation (3.31) with

$$I_{\mathrm{s}}(k^2 t) = \frac{4}{k^4}\,\mathcal{P}\int \mathrm{d}^2q\,\mathrm{e}^{-q^2 t}\,\frac{(q^2-\xi k^2)^2}{k^2-2\mathbf{q}\cdot\mathbf{k}}, \quad \text{(A.28a)}$$

$$I_{\mathrm{f}}(k^2 t) = \frac{4}{k^4}\,\mathcal{P}\int \mathrm{d}^2q\,\mathrm{e}^{-q^2 t}\left(-\frac{1}{16}k^2 + \frac{(q^2-k^2/4)^2+(\mathbf{k}\times\mathbf{q})^2/4}{k^2-2\mathbf{q}\cdot\mathbf{k}}\right), \quad \text{(A.28b)}$$

where $q = |\mathbf{q}|$, $k = |\mathbf{k}|$, $\mathbf{k}\times\mathbf{q} = k_1 q_2 - k_2 q_1$, and $\mathcal{P}$ denotes a Cauchy principal value (that comes about since terms in which the denominator vanishes are excluded in the discrete sums). These integrals may then be performed analytically, yielding the expressions (3.32a) and (3.32b).

A.5 Details on the Perturbative Results for the Sphere

In this section we present the details on the perturbative calculation of the heat kernel for the scalar and the fermion in Chapter 5, closely following the treatment in [3].

A.5.1 Spin-Weighted Spherical Harmonics

In what follows, we will make use of the spin-weighted spherical harmonics ${}_sY_{\ell,m}$. We refer to the original papers [139, 140] for more details and explicit formulae; here we merely list the properties of these functions needed to make this section self-contained. Essentially, a function η associated to a tensorial structure on the sphere is said to have spin weight s if under a local rotation of orthonormal frame by angle ψ, η transforms like $\eta \to \mathrm{e}^{is\psi}\eta$. Scalar

fields of course are not tensorial and have spin weight zero, while the components of the Dirac spinor have spin weight 1/2. The spin-weighted spherical harmonics ${}_sY_{\ell,m}$ constitute an orthonormal basis for the space of spin weight-s functions on the sphere (hence the usual spherical harmonics are just the special case of spin weight zero: $Y_{\ell,m} = {}_0Y_{\ell,m}$). The index ℓ takes values $\ell \in \{|s|, |s|+1, |s|+2, \ldots\}$ with s an integer or half-integer, and $m \in \{-\ell, -\ell+1, \ldots, \ell\}$. We also note that they obey ${}_sY^*_{\ell,m} = (-1)^{s+m}\,{}_{-s}Y_{\ell,-m}$ as well as the addition theorem

$$\sum_{m=-\ell}^{\ell} {}_sY^*_{\ell,m}\,{}_sY_{\ell,m} = \frac{2\ell+1}{4\pi}. \tag{A.29}$$

It will be convenient for later to introduce the spin weight raising and lowering operators $\eth$ and $\bar{\eth}$, which act on a function η with spin weight s as

$$\eth\eta = -\sin^s\theta\left(\partial_\theta + i\mathrm{cosec}\theta\,\partial_\phi\right)\left(\sin^{-s}\theta\,\eta\right), \tag{A.30a}$$

$$\bar{\eth}\eta = -\sin^{-s}\theta\left(\partial_\theta - i\mathrm{cosec}\theta\,\partial_\phi\right)\left(\sin^{s}\theta\,\eta\right); \tag{A.30b}$$

$\eth\eta$ then has spin weight $s+1$ and $\bar{\eth}\eta$ has spin weight $s-1$. These operators obey the Leibniz rule (even on products of functions of different spin weights) and hence are bona fide derivative operators, and are also total derivatives in the sense that when $\eth\eta$ or $\bar{\eth}\eta$ has spin weight zero, its integral over the round sphere vanishes. Moreover, they relate spin-weighted spherical harmonics of different spin weight to each other:

$$\eth\,{}_sY_{\ell,m} = \sqrt{(\ell-s)(\ell+s+1)}\,{}_{s+1}Y_{\ell,m}, \tag{A.31a}$$

$$\bar{\eth}\,{}_sY_{\ell,m} = -\sqrt{(\ell+s)(\ell-s+1)}\,{}_{s-1}Y_{\ell,m}. \tag{A.31b}$$

(It then follows that the spin-weighted spherical harmonics with integer s can be generated from the ordinary spherical harmonics $Y_{\ell,m}$ by successive applications of $\eth$.)

The triple overlap of spin-weighted spherical harmonics can be expressed in terms of $3j$ symbols (see e.g. [141, 142][3]):

$$\int_{S^2} {}_{s_1}Y_{\ell_1,m_1}\,{}_{s_2}Y_{\ell_2,m_2}\,{}_{s_3}Y_{\ell_3,m_3} = \sqrt{\frac{(2\ell_1+1)(2\ell_2+1)(2\ell_3+1)}{4\pi}}\begin{pmatrix}\ell_1 & \ell_2 & \ell_3\\ -s_1 & -s_2 & -s_3\end{pmatrix}\begin{pmatrix}\ell_1 & \ell_2 & \ell_3\\ m_1 & m_2 & m_3\end{pmatrix}, \tag{A.32}$$

where here and in what follows we will leave the volume element $\sin\theta\,\mathrm{d}\theta\,\mathrm{d}\phi$ in integrals implied. The $3j$ symbol $\begin{pmatrix}\ell_1 & \ell_2 & \ell_3\\ m_1 & m_2 & m_3\end{pmatrix}$ vanishes unless the usual rules for angular

[3]Technically [141, 142] only give expressions for the triple integral of Wigner D-matrix elements, but the ${}_sY_{\ell,m}$ are precisely proportional to these matrix elements [140].

momentum addition are satisfied: that is, $m_i \in \{-\ell_i, -\ell_i+1, \cdots, \ell_i\}$ for each i, $m_1 + m_2 + m_3 = 0$, the ℓ_i obey the triangle condition $|\ell_1 - \ell_2| \leqslant \ell_3 \leqslant \ell_1 + \ell_2$, and finally $\ell_1+\ell_2+\ell_3$ must be an integer (in fact an even integer if all the m_i vanish). Moreover, the $3j$ symbols have the following properties:

$$\sum_m (-1)^{\ell-m} \begin{pmatrix} \ell & \ell & \ell' \\ m & -m & 0 \end{pmatrix} = \sqrt{2\ell+1}\,\delta_{\ell',0}, \tag{A.33}$$

$$\sum_{m_1,m_2} \begin{pmatrix} \ell_1 & \ell_2 & \ell_3 \\ m_1 & m_2 & m_3 \end{pmatrix} \begin{pmatrix} \ell_1 & \ell_2 & \ell_3' \\ m_1 & m_2 & m_3' \end{pmatrix} = \frac{1}{2\ell_3+1}\,\delta_{\ell_3,\ell_3'}\delta_{m_3,m_3'}\{\ell_1 \quad \ell_2 \quad \ell_3\}, \tag{A.34}$$

$$\sum_{\ell_1,m_1} (2\ell_1+1) \begin{pmatrix} \ell_1 & \ell_2 & \ell_3 \\ m_1 & m_2 & m_3 \end{pmatrix} \begin{pmatrix} \ell_1 & \ell_2 & \ell_3 \\ m_1 & m_2' & m_3' \end{pmatrix} = \delta_{m_2,m_2'}\delta_{m_3,m_3'}, \tag{A.35}$$

$$\begin{pmatrix} \ell_2 & \ell_1 & \ell_3 \\ m_2 & m_1 & m_3 \end{pmatrix} = \begin{pmatrix} \ell_1 & \ell_2 & \ell_3 \\ -m_1 & -m_2 & -m_3 \end{pmatrix} = (-1)^{\ell_1+\ell_2+\ell_3} \begin{pmatrix} \ell_1 & \ell_2 & \ell_3 \\ m_1 & m_2 & m_3 \end{pmatrix} \tag{A.36}$$

where $\{\ell_1 \quad \ell_2 \quad \ell_3\} = 1$ if the ℓ_i obey the triangle condition and zero otherwise, every sum over m_i is understood to run from $-\ell_i$ to ℓ_i, and (A.36) holds for any other odd permutation of the columns. Finally, integrating $\eth({}_{s_1}Y_{\ell_1,m_1}\,{}_{s_2}Y_{\ell_2,m_2}\,{}_{s_3}Y_{\ell_3,m_3})$ and $\bar{\eth}({}_{s_1}Y_{\ell_1,m_1}\,{}_{s_2}Y_{\ell_2,m_2}\,{}_{s_3}Y_{\ell_3,m_3})$ and using the relations (A.31) and the integration formula (A.32) gives the recursion relations

$$\begin{aligned} 0 = {} & \sqrt{(\ell_1 \mp s_1)(\ell_1 \pm s_1 + 1)} \begin{pmatrix} \ell_1 & \ell_2 & \ell_3 \\ s_1 \pm 1 & s_2 & s_3 \end{pmatrix} \\ & + \sqrt{(\ell_2 \mp s_2)(\ell_2 \pm s_2 + 1)} \begin{pmatrix} \ell_1 & \ell_2 & \ell_3 \\ s_1 & s_2 \pm 1 & s_3 \end{pmatrix} \\ & + \sqrt{(\ell_3 \mp s_3)(\ell_3 \pm s_3 + 1)} \begin{pmatrix} \ell_1 & \ell_2 & \ell_3 \\ s_1 & s_2 & s_3 \pm 1 \end{pmatrix}. \end{aligned} \tag{A.37}$$

A.5.2 Scalar

For the non-minimally-coupled scalar, the operator L was given in (5.26), which we repeat here:

$$L = \mathrm{e}^{-2f}\left[-\overline{\nabla}^2 + 2\xi\left(1 - \overline{\nabla}^2 f\right)\right]; \tag{A.38}$$

hence the operators $L^{(n)}$ introduced in (3.16) are

$$L^{(1)} = 2f^{(1)}\overline{\nabla}^2 - 2\xi\left(2f^{(1)} + \overline{\nabla}^2 f^{(1)}\right), \tag{A.39}$$

$$L^{(2)} = 2\left(f^{(2)} - (f^{(1)})^2\right)\overline{\nabla}^2 - 2\xi\left[2\left(f^{(2)} - (f^{(1)})^2\right) - 2f^{(1)}\overline{\nabla}^2 f^{(1)} + \overline{\nabla}^2 f^{(2)}\right]. \tag{A.40}$$

Decomposing $f^{(1)}$ in spherical harmonics as in (5.27), reality of $f^{(1)}$ requires that $f^*_{\ell,m} = (-1)^m f_{\ell,-m}$, while the volume-preservation condition (3.15) requires that $f_{0,0} = 0$. Then the matrix elements $\widetilde{L}^{(1)}_{\ell,m,\ell',m'}$ are given by

$$\widetilde{L}^{(1)}_{\ell,m,\ell',m'} = \int_{S^2} Y^*_{\ell,m} L^{(1)} Y_{\ell',m'} \tag{A.41}$$

$$= -2 \sum_{\ell'',m''} f_{\ell'',m''} \left(\bar{\lambda}_{\ell'} - \xi C_{\ell''}\right) \int_{S^2} Y_{\ell'',m''} Y^*_{\ell,m} Y_{\ell',m'}, \tag{A.42}$$

where $C_\ell = \ell(\ell+1)$ are the eigenvalues of $-\overline{\nabla}^2$ (and the eigenvalues of $\overline{L}$ are $\bar{\lambda}_\ell = \ell(\ell+1) + 2\xi$). Using (A.32), we thus find

$$\widetilde{L}^{(1)}_{\ell,m,\ell',m'} = -2(-1)^m \sum_{\ell'',m''} f_{\ell'',m''} \left(\bar{\lambda}_{\ell'} - \xi C_{\ell''}\right) \times \sqrt{\frac{(2\ell+1)(2\ell'+1)(2\ell''+1)}{4\pi}} \begin{pmatrix} \ell & \ell' & \ell'' \\ 0 & 0 & 0 \end{pmatrix} \begin{pmatrix} \ell & \ell' & \ell'' \\ m & -m' & m'' \end{pmatrix}. \tag{A.43}$$

From (A.33) and the fact that $f_{0,0} = 0$, it then follows that $\mathrm{Tr}\widetilde{\boldsymbol{L}}^{(1)}_{\ell,\ell}$ vanishes, and hence so does the linear correction to the heat kernel: $\Delta K^{(1)} = 0$.

To compute the second-order correction, we need the traces $\mathrm{Tr}\widetilde{\boldsymbol{L}}^{(2)}_{\ell,\ell}$ and $\mathrm{Tr}\left(\widetilde{\boldsymbol{L}}^{(1)}_{\ell,\ell'}\widetilde{\boldsymbol{L}}^{(1)}_{\ell',\ell}\right)$. To compute the former, we use the addition theorem (A.29), and hence

$$\mathrm{Tr}\widetilde{\boldsymbol{L}}^{(2)}_{\ell,\ell} = \frac{2\ell+1}{2\pi} \int_{S^2} \left[-\left(f^{(2)} - (f^{(1)})^2\right) C_\ell - \xi \left(2\left(f^{(2)} - (f^{(1)})^2\right) - 2 f^{(1)} \overline{\nabla}^2 f^{(1)}\right)\right], \tag{A.44}$$

$$= \frac{2\ell+1}{\pi} \int_{S^2} \left(\bar{\lambda}_\ell (f^{(1)})^2 + \xi f^{(1)} \overline{\nabla}^2 f^{(1)}\right), \tag{A.45}$$

$$= \frac{2\ell+1}{\pi} \sum_{\ell',m'} |f_{\ell',m'}|^2 (\bar{\lambda}_\ell - \xi C_{\ell'}), \tag{A.46}$$

where in the first line the Laplacian $\overline{\nabla}^2 f^{(2)}$ vanishes since it is a total divergence, in the second line we used the volume-preservation condition (3.15) to replace the remaining $f^{(2)}$,

and in the final line we used (5.27). To compute $\mathrm{Tr}\left(\widetilde{\boldsymbol{L}}^{(1)}_{\ell,\ell'}\widetilde{\boldsymbol{L}}^{(1)}_{\ell',\ell}\right)$, we use (A.43):

$$\mathrm{Tr}\left(\widetilde{\boldsymbol{L}}^{(1)}_{\ell,\ell'}\widetilde{\boldsymbol{L}}^{(1)}_{\ell',\ell}\right) = \sum_{m,m'} \widetilde{L}^{(1)}_{\ell,m,\ell',m'}\widetilde{L}^{(1)}_{\ell',m',\ell,m}, \tag{A.47}$$

$$\begin{aligned} &= \frac{(2\ell+1)(2\ell'+1)}{\pi}\sum_{\ell_1,m_1,\ell_2,m_2} f_{\ell_1,m_1}f_{\ell_2,m_2} \\ &\quad\times\sqrt{(2\ell_1+1)(2\ell_2+1)}\,(\bar{\lambda}_{\ell'}-\xi C_{\ell_1})(\bar{\lambda}_{\ell}-\xi C_{\ell_2})\begin{pmatrix}\ell & \ell' & \ell_1\\ 0 & 0 & 0\end{pmatrix}\begin{pmatrix}\ell' & \ell & \ell_2\\ 0 & 0 & 0\end{pmatrix} \\ &\quad\times\sum_{m,m'}(-1)^{m+m'}\begin{pmatrix}\ell & \ell' & \ell_1\\ m & -m' & m_1\end{pmatrix}\begin{pmatrix}\ell & \ell' & \ell_2\\ m & -m' & -m_2\end{pmatrix}, \end{aligned} \tag{A.48}$$

where we used (A.36). Now, because the $3j$ symbols vanish unless the sum of the m quantum numbers is zero, m and m' must be related by $m' = m+m_1$. We may therefore replace the phase $(-1)^{m+m'}$ with $(-1)^{m_1}$, which we may combine with f_{ℓ_1,m_1} to give $f^*_{\ell_1,-m_1}$. Then using the orthogonality relation (A.34) to evaluate the final sum, we obtain

$$\begin{aligned} \mathrm{Tr}\left(\widetilde{\boldsymbol{L}}^{(1)}_{\ell,\ell'}\widetilde{\boldsymbol{L}}^{(1)}_{\ell',\ell}\right) &= \frac{(2\ell+1)(2\ell'+1)}{\pi}\sum_{\ell_1,m_1}|f_{\ell_1,m_1}|^2 \\ &\quad\times(\bar{\lambda}_{\ell'}-\xi C_{\ell_1})(\bar{\lambda}_{\ell}-\xi C_{\ell_1})\begin{pmatrix}\ell & \ell' & \ell_1\\ 0 & 0 & 0\end{pmatrix}^2; \end{aligned} \tag{A.49}$$

the diagonal part of this result gives

$$\mathrm{Tr}\left((\widetilde{\boldsymbol{L}}^{(1)}_{\ell,\ell})^2\right) = \frac{(2\ell+1)^2}{\pi}\sum_{\ell_1,m_1}|f_{\ell_1,m_1}|^2(\bar{\lambda}_{\ell}-\xi C_{\ell_1})^2\begin{pmatrix}\ell & \ell & \ell_1\\ 0 & 0 & 0\end{pmatrix}^2. \tag{A.50}$$

We may now insert (A.46), (A.49), and (A.50) into (3.27) to obtain the second-order correction to the heat kernel; one obtains the expression (5.28) given in the main text with

$$\alpha_{\ell,\ell'} = -\frac{(2\ell'+1)(\bar{\lambda}_{\ell'}-\xi C_{\ell})}{\pi}\left[1+\sum_{\ell_1,\ell_1\neq\ell'}\frac{(2\ell_1+1)(\bar{\lambda}_{\ell_1}-\xi C_{\ell})}{\bar{\lambda}_{\ell'}-\bar{\lambda}_{\ell_1}}\begin{pmatrix}\ell & \ell' & \ell_1\\ 0 & 0 & 0\end{pmatrix}^2\right], \tag{A.51}$$

$$\beta_{\ell,\ell'} = \frac{(2\ell'+1)^2(\bar{\lambda}_{\ell'}-\xi C_{\ell})^2}{2\pi}\begin{pmatrix}\ell & \ell' & \ell'\\ 0 & 0 & 0\end{pmatrix}^2. \tag{A.52}$$

The sum in the expression for $\alpha_{\ell,\ell'}$ can be simplified slightly by noting that by (A.35),

$$1 = \sum_{\ell_1,m_1}(2\ell_1+1)\begin{pmatrix}\ell & \ell' & \ell_1\\ 0 & 0 & m_1\end{pmatrix}^2 = \sum_{\ell_1}(2\ell_1+1)\begin{pmatrix}\ell & \ell' & \ell_1\\ 0 & 0 & 0\end{pmatrix}^2, \tag{A.53}$$

and hence one can write

$$\alpha_{\ell,\ell'} = -\frac{(2\ell'+1)(\bar{\lambda}_{\ell'} - \xi C_\ell)}{\pi}\left[(2\ell'+1)\begin{pmatrix}\ell & \ell' & \ell'\\ 0 & 0 & 0\end{pmatrix}^2 + (\bar{\lambda}_{\ell'} - \xi C_\ell)\sum_{\ell_1,\ell_1\neq\ell'}\frac{2\ell_1+1}{\bar{\lambda}_{\ell'} - \bar{\lambda}_{\ell_1}}\begin{pmatrix}\ell & \ell' & \ell_1\\ 0 & 0 & 0\end{pmatrix}^2\right]. \quad \text{(A.54)}$$

The sum over ℓ_1 in $\alpha_{\ell,\ell'}$ is a finite sum due to the triangle condition $|\ell - \ell'| \leqslant \ell_1 \leqslant \ell + \ell'$; by calculating this sum exactly for several values of ℓ, ℓ' and using some sequence-finding functions in `Mathematica`, we are able to infer the closed-form expression

$$\alpha_{\ell,\ell'} = \begin{cases} \dfrac{(2\ell'+1)(\bar{\lambda}_{\ell'} - \xi C_\ell)^2}{\pi C_\ell}\dfrac{\left(\frac{2+\ell}{2}\right)_{\ell'}\left(\frac{\ell}{2}\right)_{-\ell'}}{\left(\frac{3+\ell}{2}\right)_{\ell'}\left(\frac{1+\ell}{2}\right)_{-\ell'}}, & \ell' < \dfrac{\ell}{2} \\ \left[\dfrac{(2\ell'+1)(\bar{\lambda}_{\ell'} - \xi C_\ell)^2}{2\pi}\left(H_{\ell'-\frac{\ell}{2}} - H_{\ell'+\frac{\ell}{2}} + H_{\ell'+\frac{\ell+1}{2}} - H_{\ell'-\frac{\ell+1}{2}} - \dfrac{2}{2\ell'+1}\right) - \dfrac{(2\ell'+1)^2(\bar{\lambda}_{\ell'} - \xi C_\ell)}{\pi}\right]\begin{pmatrix}\ell & \ell' & \ell'\\ 0 & 0 & 0\end{pmatrix}^2, & \ell' \geqslant \dfrac{\ell}{2} \end{cases} \quad \text{(A.55)}$$

where $(x)_n \equiv \Gamma(x+n)/\Gamma(x)$ are Pochhammer symbols and H_n are harmonic numbers. Though we are unable to provide a general derivation, we have verified that this result agrees with (A.54) for all values of ℓ and ℓ' from zero to 100.

Finally, note that the $3j$ symbols in the expressions (A.52) and (A.55) are only non-vanishing if $\ell + 2\ell'$ is an even integer, implying that whenever ℓ is odd, $\beta_{\ell,\ell'}$ vanishes for all ℓ' and $\alpha_{\ell,\ell'}$ vanishes for all $\ell' > \ell/2$. Thus the case of odd ℓ reproduces the expressions (5.29) given in the main text.

A.5.3 Dirac Fermion

For the fermion, we obtain the $L^{(n)}$ by expanding L given in (5.35). In fact, having introduced the spin weight raising and lowering operators $\eth$, $\bar{\eth}$ in (A.30) above, it is now natural to re-express L in terms of them using the fact that f has spin weight zero and L acts on the space of functions with spin weight $1/2$. We ultimately obtain

$$L = -\mathrm{e}^{-2f}\left[\eth\bar{\eth} + \frac{1}{2}\left(\overline{\nabla}^2 f + (\bar{\eth}f)\eth - (\eth f)\bar{\eth}\right) - \frac{1}{4}(\overline{\nabla}_i f)^2\right] \quad \text{(A.56)}$$

(we could also write $\overline{\nabla}^2 f = \eth\bar{\eth} f$ and $(\overline{\nabla}_i f)^2 = (\eth f)(\bar{\eth} f)$, but this rewriting will not be needed), and hence the unperturbed operator and the corrections $L^{(n)}$ are

$$\overline{L} = -\eth\bar{\eth}, \tag{A.57}$$

$$L^{(1)} = 2f^{(1)}\eth\bar{\eth} - \frac{1}{2}\left(\overline{\nabla}^2 f^{(1)} + (\bar{\eth} f^{(1)})\eth - (\eth f^{(1)})\bar{\eth}\right), \tag{A.58}$$

$$L^{(2)} = 2\left(f^{(2)} + (f^{(1)})^2\right)\eth\bar{\eth} - 2f^{(1)}L^{(1)} + \frac{1}{4}(\overline{\nabla}_i f^{(1)})^2, \tag{A.59}$$

where to simplify $L^{(2)}$ we took $f^{(2)}$ to be a constant; there is no loss of generality in this simplification, since the purpose of $f^{(2)}$ is only to ensure that the volume-preservation condition (3.15) can be satisfied for non-trivial $f^{(1)}$.

From (A.31), it follows that ${}_sY_{\ell,m}$ is an eigenfunction of $\eth\bar{\eth}$:

$$\eth\bar{\eth}\,{}_sY_{\ell,m} = -(\ell+s)(\ell-s+1)\,{}_sY_{\ell,m}. \tag{A.60}$$

Hence since $\overline{L}$ acts on the space of functions with spin weight $1/2$, the ${}_{1/2}Y_{\ell,m}$ form a basis of eigenfunctions of $\overline{L}$ with eigenvalues $\bar{\lambda}_\ell = (\ell+1/2)^2$, and we may compute the matrix elements $\widetilde{L}^{(n)}_{\ell,m,\ell',m'}$ by taking the unperturbed eigenfunctions to be $\tilde{h}_{\ell,m} = {}_{1/2}Y_{\ell,m}$. Proceeding in this manner, first we obtain (again by expanding $f^{(1)}$ in spherical harmonics as in (5.27))[4]

$$\widetilde{L}^{(1)}_{\ell,m,\ell',m'} = \sum_{\ell'',m''} f_{\ell'',m''}\left[\left(-2\bar{\lambda}_{\ell'} + \frac{1}{2}C_{\ell''}\right)\int_{S^2} {}_{1/2}Y^*_{\ell,m}\,Y_{\ell'',m''}\,{}_{1/2}Y_{\ell',m'}\right.$$
$$\left. -\frac{1}{2}\int_{S^2} {}_{1/2}Y^*_{\ell,m}\left((\bar{\eth}Y_{\ell'',m''})(\eth\,{}_{1/2}Y_{\ell',m'}) - (\eth Y_{\ell'',m''})(\bar{\eth}\,{}_{1/2}Y_{\ell',m'})\right)\right]. \tag{A.61}$$

We may then use the rules (A.31) to replace the derivatives of the spherical harmonics with spherical harmonics of different spin weights, and finally (using ${}_sY^*_{\ell,m} = (-1)^{s+m}\,{}_{-s}Y_{\ell,-m}$) we may use (A.32) to perform the remaining integrals, thereby obtaining

$$\widetilde{L}^{(1)}_{\ell,m,\ell',m'} = \frac{1}{2}\sum_{\ell'',m''} f_{\ell'',m''}(-1)^{m+1/2}\sqrt{\frac{(2\ell+1)(2\ell'+1)(2\ell''+1)}{4\pi}}$$
$$\times \begin{pmatrix} \ell & \ell' & \ell'' \\ -m & m' & m'' \end{pmatrix} A_{\ell,\ell',\ell''}, \tag{A.62}$$

[4]Technically for the fermion we should be careful to denote the limits of summation, since the index ℓ can either range over all non-negative integers, as it does for the decomposition of $f^{(1)}$ in terms of spin weight-zero spherical harmonics, or over positive half-odd integers $1/2, 3/2, \ldots$, as for the eigenfunctions $\tilde{h}_{\ell,m}$. We assume it is clear from context what the appropriate limits of each summation should be.

where to slightly compactify notation we have defined

$$A_{\ell,\ell',\ell''} \equiv \sqrt{(\bar{\lambda}_{\ell'}-1)C_{\ell''}}\begin{pmatrix}\ell & \ell' & \ell''\\ 1/2 & -3/2 & 1\end{pmatrix} - \sqrt{\bar{\lambda}_{\ell'}C_{\ell''}}\begin{pmatrix}\ell & \ell' & \ell''\\ 1/2 & 1/2 & -1\end{pmatrix} + \left(-4\bar{\lambda}_{\ell'}+C_{\ell''}\right)\begin{pmatrix}\ell & \ell' & \ell''\\ 1/2 & -1/2 & 0\end{pmatrix}, \tag{A.63}$$

$$= \left(\bar{\lambda}_{\ell}-3\bar{\lambda}_{\ell'}+2(-1)^{\ell+\ell'+\ell''}\sqrt{\bar{\lambda}_{\ell}\bar{\lambda}_{\ell'}}\right)\begin{pmatrix}\ell & \ell' & \ell''\\ 1/2 & -1/2 & 0\end{pmatrix}, \tag{A.64}$$

with the second expression obtained from the first by using (A.37) and (A.36).

As for the scalar, it follows immediately from (A.33) and the fact that $f_{0,0}=0$ that $\mathrm{Tr}\widetilde{\boldsymbol{L}}^{(1)}_{\ell,\ell}=0$, and hence $\Delta K^{(1)}=0$ as well. To get the second order term, we first compute

$$\mathrm{Tr}\widetilde{\boldsymbol{L}}^{(2)}_{\ell,\ell} = \frac{2\ell+1}{16\pi}\int_{S^2}(\overline{\nabla}_i f^{(1)})^2 - 2\sum_m \int_{S^2} {}_{1/2}Y^*_{\ell,m} f^{(1)} L^{(1)}\, {}_{1/2}Y_{\ell,m}, \tag{A.65}$$

$$= \frac{2\ell+1}{16\pi}\sum_{\ell'',m''} C_{\ell''}|f_{\ell'',m''}|^2 - 2\sum_{m,\ell',m'} \widetilde{L}^{(1)}_{\ell',m',\ell,m}\int_{S^2} {}_{1/2}Y^*_{\ell,m} f^{(1)}\, {}_{1/2}Y_{\ell',m'}, \tag{A.66}$$

where to get the first line we used the addition formula (A.29) and the volume-preservation condition (3.15), and to get to the second line we integrated by parts in the first integral and inserted a resolution of the identity in terms of the ${}_{1/2}Y_{\ell',m'}$ in the second. The remaining integral can be performed using (A.32), followed by using the expression (A.62) and the orthogonality relations (A.34) and (A.35) to collapse most of the sums (note that the orthogonality relation (A.35) is implemented most directly by writing $A_{\ell,\ell',\ell''}$ in the longer form (A.63)); the final result is

$$\mathrm{Tr}\widetilde{\boldsymbol{L}}^{(2)}_{\ell,\ell} = \frac{2\ell+1}{16\pi}\sum_{\ell'',m''}|f_{\ell'',m''}|^2\left(16\bar{\lambda}_\ell - 3C_{\ell''}\right). \tag{A.67}$$

The same manipulations, again using (A.62), also yield

$$\mathrm{Tr}\left(\widetilde{\boldsymbol{L}}^{(1)}_{\ell,\ell'}\widetilde{\boldsymbol{L}}^{(1)}_{\ell',\ell}\right) = \frac{(2\ell+1)(2\ell'+1)}{16\pi}\sum_{\ell'',m''}|f_{\ell'',m''}|^2 A_{\ell,\ell',\ell''}A_{\ell',\ell,\ell''}, \tag{A.68}$$

and hence also

$$\mathrm{Tr}\left((\widetilde{\boldsymbol{L}}^{(1)}_{\ell,\ell})^2\right) = \frac{(2\ell+1)^2}{16\pi}\sum_{\ell'',m''}|f_{\ell'',m''}|^2 A^2_{\ell,\ell,\ell''}. \tag{A.69}$$

Inserting these into the expression for the second-order correction to the heat kernel and

using (A.64), we thus obtain (5.36) with

$$\alpha_{\ell,\ell'} = -\frac{2\ell'+1}{16\pi}\Bigg[16\bar{\lambda}_{\ell'} - 3C_\ell + \sum_{\ell'',\ell''\neq\ell'} \frac{2\ell''+1}{\bar{\lambda}_{\ell'}-\bar{\lambda}_{\ell''}}\left(\bar{\lambda}_{\ell'} - 3\bar{\lambda}_{\ell''} + 2(-1)^{\ell+\ell'+\ell''}\sqrt{\bar{\lambda}_{\ell'}\bar{\lambda}_{\ell''}}\right) \times \left(\bar{\lambda}_{\ell''} - 3\bar{\lambda}_{\ell'} + 2(-1)^{\ell+\ell'+\ell''}\sqrt{\bar{\lambda}_{\ell'}\bar{\lambda}_{\ell''}}\right)\begin{pmatrix}\ell & \ell' & \ell''\\ 0 & 1/2 & -1/2\end{pmatrix}^2\Bigg], \tag{A.70a}$$

$$\beta_{\ell,\ell'} = \frac{(2\ell'+1)^2\bar{\lambda}_{\ell'}^2}{4\pi}\left(1+(-1)^\ell\right)\begin{pmatrix}\ell & \ell' & \ell'\\ 0 & 1/2 & -1/2\end{pmatrix}^2. \tag{A.70b}$$

Note that as for the scalar, $\beta_{\ell,\ell'}$ vanishes whenever ℓ is odd. The sum in $\alpha_{\ell,\ell'}$ is again a finite sum since the $3j$ symbol vanishes unless $|\ell-\ell'| \leqslant \ell'' \leqslant \ell+\ell'$; by evaluating the sum exactly for various values of ℓ, ℓ' we are able to infer the expression

$$\alpha_{\ell,\ell'} = \begin{cases} -\dfrac{(2\ell'+1)^3}{16\pi}\dfrac{\left(\frac{2+\ell}{2}\right)_{\ell'+1/2}\left(\frac{2+\ell}{2}\right)_{-(\ell'+1/2)}}{\left(\frac{1+\ell}{2}\right)_{\ell'+1/2}\left(\frac{1+\ell}{2}\right)_{-(\ell'+1/2)}}, & \ell' < \dfrac{\ell}{2} \\ -\dfrac{(1+2\ell')\,\Gamma\left(\frac{1+\ell}{2}\right)^2(1+(-1)^\ell)}{32\pi^2\,\Gamma\left(\frac{2+\ell}{2}\right)^2}\Bigg[16\ell'(\ell'+1)-\ell(\ell+1) & \\ \quad +4+\dfrac{16}{\pi}\displaystyle\sum_{\ell''=0}^{\frac{\ell-2}{2}}\dfrac{\left(\ell''+\frac12\right)^4\left(\frac{\ell}{2}-\ell''\right)_{1/2}\left(\frac{2+\ell}{2}+\ell''\right)_{1/2}}{\left(\left(\ell'+\frac12\right)^2-\left(\ell''+\frac12\right)^2\right)^2}\Bigg], & \ell' \geqslant \dfrac{\ell}{2} \end{cases} \tag{A.71}$$

which for odd ℓ reproduces the result (5.37) given in the main text. Though we are not able to give a derivation of this result, we have checked its agreement with (A.70a) for all values of ℓ up to 100 and all values of ℓ' up to 201/2.

A.6 Flat-Space Scaling Limit

Here we provide some more details on the flat-space scaling limit performed in Section 5.3.4. Firstly, to obtain the limiting behaviour (5.50), note that for odd $r_0 k$ we have from (5.49)

$$a_{r_0 k}(t) = \frac{t}{r_0^2}\sum_{k'}^{k/2} \mathrm{e}^{-(k')^2 t}\alpha_{r_0 k, r_0 k'} = r_0^2\, t\int_0^{k/2}\mathrm{d}k'\,\mathrm{e}^{-(k')^2 t}H(k,k') + \mathcal{O}(r_0), \tag{A.72}$$

where we have defined $H(k,k') = \lim_{r_0\to\infty} \alpha_{r_0 k, r_0 k'}/r_0^3$ and re-expressed the sum as an integral in the $r_0 \to \infty$ limit. The function $H(k,k')$ can be obtained from the closed-form expressions (5.29) and (5.37) by using the fact that for $x > 0$,

$$\frac{\Gamma(x+1/2)}{\Gamma(x)} = \sqrt{x} + \mathcal{O}(x^{-1/2}), \tag{A.73}$$

from which we find

$$H(k,k') = \begin{cases} \dfrac{2k'((k')^2 - \xi k^2)^2}{\pi k\sqrt{k^2 - 4(k')^2}}, & \text{scalar} \\ -\dfrac{(k')^3\sqrt{k^2-4(k')^2}}{2\pi k}, & \text{fermion} \end{cases} \tag{A.74}$$

Using these expressions to perform the integral in (A.72), we recover (5.50) as promised. We now remove the restriction that $r_0 k$ be odd.

Next, to obtain (5.51), we must keep track of how the mode decomposition of $f^{(1)}$ in spherical harmonics behaves in the $r_0 \to \infty$ scaling limit. To this end, we need the appropriate scaling behaviour of the spherical harmonics; to obtain it, first define as above $k = \ell/r_0$ and in addition $k_y = m/r_0$. Expressing the spherical harmonics in terms of Legendre polynomials $P_\ell^m(x)$, we immediately have

$$Y_{kr_0,k_y r_0}\left(\frac{\pi}{2} + \frac{x}{r_0}, \frac{y}{r_0}\right) \to N_{kr_0,k_y r_0} P_{r_0 k}^{r_0 k_y}\left(\frac{x}{r_0}\right) \mathrm{e}^{ik_y y}, \tag{A.75}$$

where $N_{kr_0,k_y r_0}$ is a normalisation constant. The functional form of $P_{r_0 k}^{r_0 k_y}$ as $r_0 \to \infty$ can be inferred from the scaling limit of Legendre's differential equation (as well as from the symmetry properties of $P_\ell^m(x)$ about $x = 0$), from which we then find that

$$Y_{kr_0,k_y r_0}\left(\frac{\pi}{2} + \frac{x}{r_0}, \frac{y}{r_0}\right) \to \widetilde{N}_{kr_0,k_y r_0} \cos\left(\sqrt{k^2 - k_y^2}\, x\right) \mathrm{e}^{ik_y y} \tag{A.76}$$

for even $(k+k_y)r_0$, and the same expression with a sine (instead of a cosine) for odd $(k+k_y)r_0$. Here $\widetilde{N}_{kr_0,k_y r_0}$ is some new constant, which can be obtained up to an overall phase by the normalisation condition

$$1 = \sum_{\ell',m'} \int Y^*_{\ell',m'}(\theta,\phi) Y_{\ell,m}(\phi,\theta) \sin\theta \,\mathrm{d}\theta \,\mathrm{d}\phi \tag{A.77}$$

$$\to \int_0^\infty \mathrm{d}k' \int_{-k'}^{k'} \mathrm{d}k'_y \, \widetilde{N}^*_{k' r_0, k'_y r_0} \widetilde{N}_{kr_0,k_y r_0} \tag{A.78}$$

$$\times \int_{-\infty}^{\infty} \mathrm{d}x \,\mathrm{d}y \, \cos\left(\sqrt{(k')^2 - (k'_y)^2}\, x\right) \cos\left(\sqrt{k^2 - k_y^2}\, x\right) \mathrm{e}^{i(k_y - k'_y)y}$$

for any $\ell = kr_0$ and $m = k_y r_0$, where the domain of integration in k' and k'_y comes from

the restriction that $\ell' > 0$ and $-\ell' \leqslant m' \leqslant \ell'$. Performing the integrals finally gives that up to an overall phase,

$$Y_{r_0 k, r_0 k_y}\left(\frac{\pi}{2} + \frac{x}{r_0}, \frac{y}{r_0}\right) \to \frac{1}{\pi} \frac{\sqrt{k}}{(k^2 - k_y^2)^{1/4}} \cos\left(\sqrt{k^2 - k_y^2}\, x\right) \mathrm{e}^{i k_y y} \tag{A.79}$$

for even $(k + k_y)r_0$ and the same expression with a sine for odd $(k + k_y)r_0$.

Hence in the $r_0 \to \infty$ scaling limit, the coefficients $f_{\ell,m}$ give the desired expression (5.51):

$$\begin{aligned} f_{r_0 k, r_0 k_y} &= \int Y^*_{r_0 k, r_0 k_y}(\theta, \phi) f(\theta, \phi) \sin\theta \, \mathrm{d}\theta \, \mathrm{d}\phi, && \text{(A.80)} \\ &= \frac{1}{r_0^2} \int Y^*_{r_0 k, r_0 k_y}\left(\frac{\pi}{2} + \frac{x}{r_0}, \frac{y}{r_0}\right) f(x, y) \sin\left(\frac{\pi}{2} + \frac{x}{r_0}\right) \mathrm{d}x \, \mathrm{d}y, && \text{(A.81)} \\ &\to \frac{1}{2\pi r_0^2} \frac{\sqrt{k}}{(k^2 - k_y^2)^{1/4}} \int \mathrm{d}x \, \mathrm{d}y \left(\mathrm{e}^{i\sqrt{k^2 - k_y^2}\, x} \pm \mathrm{e}^{-i\sqrt{k^2 - k_y^2}\, x}\right) \mathrm{e}^{-i k_y y} f(x, y), && \text{(A.82)} \\ &= \frac{2\pi}{r_0^2} \frac{\sqrt{k}}{(k^2 - k_y^2)^{1/4}} \left(\tilde{f}(\sqrt{k^2 - k_y^2}, k_y) \pm \tilde{f}(-\sqrt{k^2 - k_y^2}, k_y)\right), && \text{(A.83)} \end{aligned}$$

with the upper (lower) sign for even (odd) $(k + k_y)r_0$ (and we are neglecting an overall phase that will cancel out). We remind the reader that $\tilde{f}(k_x, k_y)$ is the Fourier transform of $f^{(1)}(x, y)$, and the assumption that $f^{(1)}(x, y)$ vanishes at large (x, y) (i.e. $f^{(1)}(\theta, \phi)$ vanishes away from $(\theta = \pi/2, \phi = 0)$) is what allows us to take the scaling limit of the integrand before evaluating the integral.

Finally, decomposing $\Delta K^{(2)}$ into contributions based on the parity of $(k + k_y)r_0$ as

$$\Delta K^{(2)} \to \Delta K^{(2)}_{\text{even}} + K^{(2)}_{\text{odd}}, \tag{A.84}$$

we have

$$\Delta K^{(2)}_{\text{even,odd}} = \frac{t}{r_0^2} \sum_{\substack{k, k_y \\ \text{even,odd } (k + k_y) r_0}} \frac{k^5 I(k^2 t)}{\sqrt{k^2 - k_y^2}} \left|\tilde{f}(\sqrt{k^2 - k_y^2}, k_y) \pm \tilde{f}(-\sqrt{k^2 - k_y^2}, k_y)\right|^2, \tag{A.85}$$

$$\to \frac{t}{2} \int_0^\infty \mathrm{d}k \int_{-k}^{k} \mathrm{d}k_y \, \frac{k^5 I(k^2 t)}{\sqrt{k^2 - k_y^2}} \left|\tilde{f}(\sqrt{k^2 - k_y^2}, k_y) \pm \tilde{f}(-\sqrt{k^2 - k_y^2}, k_y)\right|^2 \tag{A.86}$$

with the upper (lower) sign for $\Delta K^{(2)}_{\text{even}}$ ($\Delta K^{(2)}_{\text{odd}}$). Note that the factor of $1/2$ comes from the fact that for fixed kr_0, we are only summing over $k_y r_0$ with a given parity, and thus the spacing in k_y is $2/r_0$. We now first switch the integrals around by taking the range of the k_y integral to be $(-\infty, \infty)$ and the range of the k integral to be $(|k_y|, \infty)$, after which we change to a new variable $k_x = \sqrt{k^2 - k_y^2}$ which has range $(0, \infty)$. Since $\mathrm{d}k_x = (k/k_x)\mathrm{d}k$,

we thus have

$$\Delta K^{(2)}_{\text{even,odd}} \to \frac{t}{2}\int_{-\infty}^{\infty} \mathrm{d}k_y \int_0^{\infty} \mathrm{d}k_x\, k^4 I(k^2 t)\left|\tilde{f}(k_x,k_y) \pm \tilde{f}(-k_x,k_y)\right|^2, \tag{A.87}$$

$$= \frac{t}{2}\int \mathrm{d}^2k\, k^4 I(k^2t)\left(\left|\tilde{f}(\mathbf{k})\right|^2 \pm \tilde{f}^*(-k_x,k_y)\tilde{f}(k_x,k_y)\right), \tag{A.88}$$

with the latter expression obtained by expanding out the square and redefining $k_x \to -k_x$ as appropriate. Hence adding $\Delta K^{(2)}_{\text{even}}$ and $\Delta K^{(2)}_{\text{odd}}$ we obtain the flat-space expression (5.52).

A.7 Details on the Renormalisation of the Time-Ordered Two-Point Function of the Stress Tensor on Flat Space

In this section, we examine the precise divergence structure of the momentum space time-ordered two-point function of the stress tensor on flat space considered in Section 7.3. We will explicitly compute the necessary counterterms for its spatial legs. A similar calculation can be performed for the other components but since they do not contribute to our vacuum energy calculation we will not consider them here. Let Λ be a UV cutoff. We wish probe the large Λ asymptotics of

$$G^{\mathrm{F}}_{ijk\ell}(p) = -\int_{\xi<|\Lambda|}\frac{\mathrm{d}\xi}{(2\pi)}\left[\frac{1}{p^0-\xi+i\varepsilon}\widetilde{\mathcal{W}}_{ijk\ell}(\xi,\mathbf{p}) + \frac{1}{-p^0+\xi+i\varepsilon}\widetilde{\mathcal{W}}_{ijk\ell}(-\xi,-\mathbf{p})\right]. \tag{A.89}$$

The spatial legs of $\mathcal{W}_{ijk\ell}(\xi,\mathbf{p})$ are even in $\mathbf{p}$ so making the change of variables $\xi \to -\xi$ in the second term and noting that $\mathcal{W}_{ijk\ell}(\xi,\mathbf{p})$ is only non-zero for positive energy timelike arguments gives that

$$G^{\mathrm{F}}_{ijk\ell}(p) = -\int_0^{\Lambda}\frac{\mathrm{d}\xi}{(2\pi)}\left[\frac{1}{p^0-\xi+i\varepsilon} - \frac{1}{p^0+\xi-i\varepsilon}\right]\widetilde{\mathcal{W}}_{ijk\ell}(\xi,\mathbf{p}). \tag{A.90}$$

The $i\varepsilon$ terms do not influence the divergences so we take $\varepsilon \to 0$ and we can then write

$$G^{\mathrm{F}}_{ijk\ell}(p) = -\int_0^{\Lambda}\frac{\mathrm{d}\xi}{(2\pi)}\left[\frac{2\xi}{(p^0)^2-\xi^2}\right]\widetilde{\mathcal{W}}_{ijk\ell}(\xi,\mathbf{p}). \tag{A.91}$$

The divergences are given the large ξ behaviour of $\widetilde{\mathcal{W}}_{ijk\ell}(\xi,\mathbf{p})$ which is determined by the asymptotics of the spectral densities and the dependence of the spin-0 and spin-2 projectors on ξ. The spatial legs on the projector are

$$\Pi^{(0)}_{ijk\ell}(\xi,\mathbf{p}) = \xi^4\delta_{ij}\delta_{k\ell} + \xi^2\left[S_{ij}(\mathbf{p})\delta_{k\ell} + S_{k\ell}(\mathbf{p})\delta_{ij}\right] + \mathcal{O}(\xi^0) \text{ and} \tag{A.92a}$$

$$\Pi^{(2)}_{ijk\ell}(\xi,\mathbf{p}) = \frac{1}{2}\xi^4(\delta_{ik}\delta_{j\ell}+\delta_{i\ell}\delta_{kj}-\delta_{ij}\delta_{k\ell}) + \frac{1}{2}\xi^2\left[S_{ik}(\mathbf{p})\delta_{j\ell}+S_{j\ell}(\mathbf{p})\delta_{ik}+S_{i\ell}(\mathbf{p})\delta_{jk}+S_{jk}(\mathbf{p})\delta_{i\ell}\right]+\mathcal{O}(\xi^0) \quad \text{(A.92b)}$$

where $S_{ij}(\mathbf{p}) \equiv p_i p_j - \delta_{ij}\mathbf{p}^2$, so for spectral densities (7.28) with asymptotics

$$c^{(s)}(\mu) \sim \mu^{d-2}\left(c_0^{(s)} + \frac{c_2^{(s)}}{\mu^2} + \mathcal{O}\left(\frac{1}{\mu^4}\right)\right) \quad \text{(A.93)}$$

the $\Lambda\to\infty$ asymptotics of $G^{\mathrm{F}}_{ijk\ell}(p)$ when $d=2$ are

$$\begin{aligned} G^{\mathrm{F}}_{ijk\ell}(p) \sim{}& -\frac{\Lambda^3}{6}\left\{2c_0^{(0)}\delta_{ij}\delta_{k\ell}+c_0^{(2)}(\delta_{ik}\delta_{j\ell}+\delta_{i\ell}\delta_{kj}-\delta_{ij}\delta_{k\ell})\right\} \\ &-\frac{\Lambda}{2}\left\{[2c_2^{(0)}+c_0^{(0)}(2p_0^2+\mathbf{p}^2)]\delta_{ij}\delta_{k\ell}+[c_2^{(2)}+c_0^{(2)}(p_0^2+\mathbf{p}^2/2)](\delta_{ik}\delta_{j\ell}+\delta_{i\ell}\delta_{kj}-\delta_{ij}\delta_{k\ell})\right. \\ &\left.+2c_0^{(0)}\left[S_{ij}(\mathbf{p})\delta_{k\ell}+S_{k\ell}(\mathbf{p})\delta_{ij}\right]+c_0^{(2)}\left[S_{ik}(\mathbf{p})\delta_{j\ell}+S_{j\ell}(\mathbf{p})\delta_{ik}+S_{i\ell}(\mathbf{p})\delta_{jk}+S_{jk}(\mathbf{p})\delta_{i\ell}\right]\right\}+\mathcal{O}(\Lambda^0). \end{aligned} \quad \text{(A.94)}$$

To cancel these divergences non-covariant counterterms are required (a necessary condition for covariance is that $p^i G^{\mathrm{F}}_{ijk\ell}(0,\mathbf{p})=0$) so the finite parts of the counterterms needed to recover a conserved $G^{\mathrm{F}}_{\mu\nu\rho\sigma}(p)$ are determined and thus is there is no ambiguity associated with the conserved time-ordered two-point function of the stress tensor when $d=2$ here. Practically, the conserved and finite part of the two-point function, $\tilde{G}^{\mathrm{F}}_{\mu\nu\rho\sigma}(p)$, is obtained via dimensional regularisation. For $\Re(d)<-3$ the expression

$$\tilde{G}^{\mathrm{F}}_{\mu\nu\rho\sigma}(p) = -\int_{\xi<|\Lambda|}\frac{\mathrm{d}\xi}{(2\pi)}\left[\frac{1}{p^0-\xi+i\varepsilon}\widetilde{\mathcal{W}}_{\mu\nu\rho\sigma}(\xi,\mathbf{p})+\frac{1}{-p^0+\xi+i\varepsilon}\widetilde{\mathcal{W}}_{\mu\nu\rho\sigma}(-\xi,-\mathbf{p})\right]. \quad \text{(A.95)}$$

is finite in the limit $\Lambda\to\infty$. Further, after taking this limit and writing $\widetilde{\mathcal{W}}_{\mu\nu\rho\sigma}$ in its spectral representation (7.27) the swap in integration order $\int\mathrm{d}\xi \leftrightarrow \int\mathrm{d}\mu$ is valid. Using the δ-function to evaluate the ξ integral gives

$$\tilde{G}^{\mathrm{F}}_{\mu\nu\rho\sigma}(p) = \int_0^\infty \mathrm{d}\mu\left(c^{(0)}(\mu)\Pi^{(0)}_{\mu\nu\rho\sigma}(p)+c^{(2)}(\mu)\Pi^{(2)}_{\mu\nu\rho\sigma}(p)\right)\frac{1}{p^2+\mu^2-i\varepsilon}, \quad \text{(A.96)}$$

which can then be analytically continued to $d=2$.

A.8 The Fermion

In this section, we provide the details behind the calculation of the spectral densities for a free Dirac fermion of mass m for Chapter 7.

Firstly, we derive the stress tensor for a massive Dirac fermion on a $(d+1)$-

dimensional curved ultrastatic Lorentzian spacetime. On a space with vielbeins $\{e^{\mu}{}_{a}\}$, $\mu, a = 1, \ldots, d+1$ satisfying $e^{\mu}{}_{a}e^{\nu}{}_{b}\eta^{ab} = g^{\mu\nu}$, this theory has action

$$S = \int \mathrm{d}^{d+1}x(\det e)\bar{\psi}\left(i\gamma^{a}e^{\mu}_{a}D_{\mu} - m\right)\psi \tag{A.97}$$

where $\det e \equiv \det e_{\mu}{}^{a}$, D is the spin connection which acts on spinors as

$$D_{\mu}\psi = \partial_{\mu}\psi + \frac{1}{2}\omega_{\mu ab}S^{ab}\psi, \tag{A.98}$$

$\omega_{\mu}^{ab} = e^{\nu a}\nabla_{\mu}e_{\nu}{}^{b}$ is the spin connection, $S^{ab} = [\gamma^{a}, \gamma^{b}]/4$ and $\{\gamma^{a}\}$ are $N \times N$ matrices satisfying

$$\{\gamma^{a}, \gamma^{b}\} = -2\eta^{ab}\mathbb{1}_{N} \text{ and } \gamma^{a\dagger} = \gamma^{0}\gamma^{a}\gamma^{0} \tag{A.99}$$

where $N = 2^{\lfloor (d+1)/2 \rfloor}$. This has momentum conjugates given by

$$\pi(x) = \frac{\delta S}{\delta \dot{\psi}} = i\sqrt{g}\psi^{\dagger}, \tag{A.100}$$

so the Hamiltonian is

$$H = \int \mathrm{d}^{d}x\sqrt{g}\bar{\psi}(-i\gamma^{i}\partial_{i} + m)\psi. \tag{A.101}$$

This action depends explicitly on the vielbeins so need to express the stress tensor as variations with respect to them. Let $A_{\mu}{}^{a} = (\det e)^{-1}\,\delta S/\delta e^{\mu}{}_{a}$. Since $\delta g^{\rho\sigma} = (\delta^{\rho}_{\mu}e^{\sigma a} + \delta^{\sigma}_{\mu}e^{\rho a})\delta e^{\mu}{}_{a}$, then

$$A_{\mu}{}^{a} = (\det e)^{-1}\frac{\delta S}{\delta e^{\mu}{}_{a}} \tag{A.102}$$

$$= \frac{1}{\sqrt{g}}\frac{\delta S}{\delta g^{\rho\sigma}}\frac{\partial g^{\rho\sigma}}{\partial e^{\mu}{}_{a}} \tag{A.103}$$

$$= \frac{1}{2}T_{\mu}{}^{a} + \frac{1}{2}T^{a}{}_{\mu}. \tag{A.104}$$

Taking

$$T_{\mu\nu} = A_{\mu}{}^{a}e_{\nu a} = (\det e)^{-1}\frac{\delta S}{\delta e^{\mu}{}_{a}}e_{\nu}{}^{a} \tag{A.105}$$

should work. This theory should be invariant under a local Lorentz transformation i.e. $\delta S = 0$ when $\delta e^{a} = \lambda^{a}{}_{b}e^{b}$ for any antisymmetric matrix $\lambda_{ab}(x)$. So

$$0 = \int \lambda_{ab}(x)e^{\mu[b}A_{\mu}^{a]} + \frac{\delta S}{\delta\psi}\delta\psi + \delta\bar{\psi}\frac{\delta S}{\delta\bar{\psi}} = \int \lambda_{ab}(x)e^{\mu[b}e^{|\nu|a]}T_{\mu\nu} = \int \lambda_{ab}(x)e^{\mu b}e^{\nu a}T_{[\mu\nu]} \tag{A.106}$$

for arbitrary antisymmetric λ, so require $A^{[ba]} = e^{\mu[b}A_{\mu}{}^{a]} = 0$ and $T_{\mu\nu}$ symmetric. Under

an infinitesimal diffeomorphism $\delta e^a = \mathcal{L}_\xi e^a = \xi \lrcorner \mathrm{d}e^a + \mathrm{d}\left(\xi \lrcorner e^a\right)$

$$\begin{aligned}
\delta S &= \int \delta e^a \wedge \star A^c \eta_{ac} \\
&= \int \xi \lrcorner \mathrm{d}e^a \wedge \star A^a - (\xi \lrcorner e^a)\mathrm{d} \star A^c \eta_{ac} \\
&= \int \xi \lrcorner (-\omega^a{}_b \wedge e^b) \wedge \star A^c - \xi^a \mathrm{d} \star A^c \eta_{ac}. \qquad \text{(A.107)} \\
&= \int (-\xi \lrcorner \omega^a{}_b)(e^b \wedge \star A^c)\eta_{ac} + (\omega^a{}_b)(\xi \lrcorner e^b) \wedge \star A^c \eta_{ac} - \xi^a \mathrm{d} \star A^c \eta_{ac}. \\
&= \int (-\xi \wedge \star \omega_{ab})(A^{[ba]}) + (\omega_{ab})(\xi \lrcorner e^b) \wedge \star A^a - \xi^a \mathrm{d} \star A^c \eta_{ac} \\
&= \int \xi^b \left(\omega_{ab} \wedge \star A^a - \mathrm{d} \star A^a \eta_{ab}\right). \qquad \text{(A.108)}
\end{aligned}$$

so for diffeomorphism invariance we require that

$$\nabla^\mu A_\mu{}^a + \omega_\mu{}^a{}_b A^{\mu b} = 0, \qquad \text{(A.109)}$$

which after contracting with $e_{\nu a}$ gives $\nabla^\mu T_{\mu\nu} = 0$. So to have a theory that is invariant under local Lorentz transformations and diffeomorphisms, the stress tensor must be symmetric and conserved. These are constraints on the quantum stress tensor operator. We now derive this operator for the free Dirac fermion. To do so, its conventient express the action in the more symmetric form

$$\mathcal{L} = \frac{i}{2}\bar{\psi}\left(\gamma^\mu D_\mu - \overleftarrow{D}_\mu \gamma^\mu\right)\psi + m\bar{\psi}\psi. \qquad \text{(A.110)}$$

So

$$\delta S = \int -\mathcal{L} e_\mu{}^a \delta e^\mu{}_\alpha + \frac{i}{2}\bar{\psi}\left(\gamma^a D_\mu - \overleftarrow{D}_\mu \gamma^a\right)\psi\, \delta e^\mu{}_a + \frac{i}{2}\bar{\psi}\gamma^{\mu\nu\rho}\psi e_\nu{}^a e_\rho{}^b \delta\omega_{\mu ab} \qquad \text{(A.111)}$$

where $\gamma^{abc} = \{\gamma^a, S^{bc}\}/2$ is totally antisymmetric in its indices. The (Heisenberg) equations of motion for ψ imply that $\mathcal{L} = 0$, so we need not consider this term. Looking in more detail at the variation of the spin connection

$$\begin{aligned}
\gamma^{\mu\nu\rho}\psi e_\nu{}^a e_\rho{}^b \delta\omega_{\mu ab} &= \gamma^{\mu\nu\rho}\psi e_\nu{}^a e_\rho{}^b \left(\delta e^\sigma{}_a \omega_\mu{}^c{}_b e_{\sigma c} + e^\sigma{}_a \delta\Gamma^\alpha_{\sigma\mu} e_{\alpha b} + e^\sigma{}_a \nabla_\mu \delta e_{\sigma b}\right) && \text{(A.112)} \\
&= \gamma^{\mu\nu\rho}\psi e_\rho{}^b \left(\delta e^\sigma{}_a \omega_\mu{}^c{}_b e_{\sigma c} e_\nu{}^a + \delta\Gamma^\alpha_{[\nu\mu]} e_{\alpha b} + \nabla_\mu \delta e_{\nu b}\right) && \text{(A.113)} \\
&= \gamma^{\mu\nu\rho}\psi e_\rho{}^b \left(-\delta e_{\nu c}\omega_\mu{}^c{}_b + D_\mu \delta e_{\nu b} + \omega_\mu{}^c{}_b \delta e_{\nu c}\right) && \text{(A.114)} \\
&= \gamma^{\mu\nu\rho}\psi e_\rho{}^b D_\mu \delta e_{\nu b} && \text{(A.115)} \\
&= -\gamma^{\rho\nu}{}_\mu \psi e_\nu{}^a D_\rho \delta e^\mu{}_a. && \text{(A.116)}
\end{aligned}$$

So

$$\delta S = \int \left(\frac{i}{2}\bar{\psi}\left(\gamma_\nu D_\mu - \overleftarrow{D}_\mu \gamma_\nu\right)\psi + \frac{i}{2} D_\rho \bar{\psi}\gamma^\rho{}_{\nu\mu}\psi \right) e^{\nu a}\delta e^\mu{}_a \tag{A.117}$$

which with the constraint $T_{[\mu\nu]} = 0$ gives

$$T_{\mu\nu} = \frac{i}{2}\bar{\psi}\left(\gamma_{(\nu} D_{\mu)} - \overleftarrow{D}_{(\mu}\gamma_{\nu)}\right)\psi \tag{A.118}$$

with the constraint

$$0 = \frac{i}{2}\bar{\psi}\left(\gamma_{[\nu} D_{\mu]} - \overleftarrow{D}_{[\mu}\gamma_{\nu]}\right)\psi + \frac{i}{2} D_\rho \bar{\psi}\gamma^\rho{}_{\nu\mu}\psi. \tag{A.119}$$

Noting that

$$\frac{i}{2} D_\rho(\bar{\psi}\gamma^\rho{}_{\nu\mu}\psi) = \frac{i}{8} D_\rho[\bar{\psi}(\gamma^\rho\gamma_{[\nu}\gamma_{\mu]} + \gamma_{[\mu}\gamma_{\nu]}\gamma^\rho)\psi] \tag{A.120}$$

$$= \frac{i}{8}\bar{\psi}(\gamma^\rho\gamma_{[\nu}\gamma_{\mu]} D_\rho + \overleftarrow{D}_\rho\gamma_{[\mu}\gamma_{\nu]}\gamma^\rho)\psi + \frac{1}{4} m\bar{\psi}\gamma_{[\nu}\gamma_{\mu]}\psi \tag{A.121}$$

$$= \frac{i}{8}\bar{\psi}(-4\gamma_{[\mu} D_{\nu]} + 4\gamma_{[\mu}\overleftarrow{D}_{\nu]} + \gamma_{[\nu}\gamma_{\mu]}\gamma^\rho D_\rho + \overleftarrow{D}_\rho\gamma^\rho\gamma_{[\mu}\gamma_{\nu]})\psi + \frac{1}{4} m\bar{\psi}\gamma_{[\nu}\gamma_{\mu]}\psi \tag{A.122}$$

$$= \frac{i}{2}\bar{\psi}\left(\gamma_{[\nu} D_{\mu]} - \overleftarrow{D}_{[\mu}\gamma_{\nu]}\right)\psi, \tag{A.123}$$

we see the constraint is satisfied. Moreover,

$$(-i\not{D} + m)(i\not{D} + m)\psi = (-D^2 - R/4 + m^2)\psi = 0 \tag{A.124}$$

which gives that $\nabla^\mu T_{\mu\nu} = 0$.

A.8.1 Matrix elements

The stress tensor for the massive Dirac fermion of mass m is

$$T_{ij}(x;\epsilon) = \frac{i}{2}\bar{\psi}\left(\gamma_{(i}\partial_{j)} - \overleftarrow{\partial}_{(j}\gamma_{i)}\right)\psi. \tag{A.125}$$

Now we wish to quantise the Dirac field using the interaction picture. To this, we seek the classical solutions to the Dirac equation in flat space. Firstly, positive frequency solutions $\psi(x) = u(\mathbf{p})\mathrm{e}^{ip\cdot x}$ with $p^0 = E(\mathbf{p}) = \sqrt{\mathbf{p}^2 + m^2}$ must have

$$(\not{p} + m)u(\mathbf{p}) = 0, \tag{A.126}$$

and negative frequency solutions $\psi(x) = v^s(\mathbf{p})\mathrm{e}^{-ip\cdot x}$ with $p^0 = E(\mathbf{p}) = \sqrt{\mathbf{p}^2 + m^2}$

$$(\not{p} - m)v(\mathbf{p}) = 0, \tag{A.127}$$

solutions to which are boosts of the solutions to

$$(\mathbb{1}_N - \gamma^0)u(\mathbf{0}) = 0 \text{ and } (\mathbb{1}_N + \gamma^0)v(\mathbf{0}) = 0. \tag{A.128}$$

Using the representation of gamma matrices

$$\gamma^0 = \sigma_1 \otimes \mathbb{1}_2 \otimes \mathbb{1}_2 \otimes \dots \tag{A.129}$$
$$\gamma^1 = i\sigma_2 \otimes \mathbb{1}_2 \otimes \mathbb{1}_2 \otimes \dots \tag{A.130}$$
$$\gamma^2 = i\sigma_3 \otimes \sigma_1 \otimes \mathbb{1}_2 \otimes \dots \tag{A.131}$$
$$\gamma^3 = i\sigma_3 \otimes \sigma_2 \otimes \mathbb{1}_2 \otimes \dots \tag{A.132}$$
$$\dots = \dots \tag{A.133}$$

its easy to see that

$$\mathrm{Rank}(\mathbb{1}_N \pm \gamma^0) = \mathrm{Rank}\begin{pmatrix} 1 & \pm 1 \\ \pm 1 & 1 \end{pmatrix} \mathrm{Rank}(\mathbb{1}_2)^{\lfloor (d+1)/2 \rfloor - 1} = N/2, \tag{A.134}$$

and thus the number of solutions for $u^s(\mathbf{p})$ and $v^s(\mathbf{p})$ is $\mathrm{Nullity}(\mathbb{1}_N \pm \gamma^0) = N - N/2 = N/2$ each. These spinors can be chosen to form an orthogonal basis of eigenstates for the hermitian matrix γ^0, satisfying

$$u^\dagger u = 2m \text{ and } v^\dagger v = 2m, \tag{A.135}$$

then using the eigenvalue equations to introduce γ^0 to the inner product and boosting to a frame with momentum $\mathbf{p}$ gives that

$$\bar{u}^s(\mathbf{p})u^r(\mathbf{p}) = 2m\delta^{sr},\ \bar{v}^s(\mathbf{p})v^r(\mathbf{p}) = -2m\delta^{sr} \text{ and } \bar{v}^s(\mathbf{p})u^r(\mathbf{p}) = 0. \tag{A.136}$$

Note also that the operators $(\mathbb{1}_N \pm \gamma^0)/2$ project onto the postive and negative frequency parts of the zero momentum solutions, respectively. These projections can also be represented in terms of the bases of the space that they project onto right multiplied by γ^0 and then boosted to give

$$\sum_s u^s(\mathbf{p})\bar{u}^s(\mathbf{p}) = -\not{p} + m \text{ and } \sum_s v^s(\mathbf{p})\bar{v}^s(\mathbf{p}) = -\not{p} - m. \tag{A.137}$$

The Dirac field operator satisfies the Dirac equation so can be written as

$$\psi(t,\mathbf{x}) = \int \frac{\mathrm{d}^d k}{(2\pi)^d} \sum_s \frac{1}{2E(\mathbf{k})} \left(b^s(\mathbf{k}) u^s(\mathbf{k}) \mathrm{e}^{ik\cdot x} + c^{s\dagger}(\mathbf{k}) v^s(\mathbf{k}) \mathrm{e}^{-ik\cdot x} \right) \tag{A.138}$$

where the relativistically normalised creation and annihilation operators satisfy

$$\{b^s(\mathbf{p}), b^{s\dagger}(\mathbf{q})\} = \{c^s(\mathbf{p}), c^{s\dagger}(\mathbf{q})\} = \delta^{s,r}_{\mathbf{p},\mathbf{q}} \equiv (2\pi)^d 2E(\mathbf{p}) \delta_{s,r} \delta^{(d)}(\mathbf{p}-\mathbf{q}) \tag{A.139}$$

and the compact notation

$$\sum_{\mathbf{k},s} \equiv \int \frac{\mathrm{d}^d k}{(2\pi)^d} \sum_s \frac{1}{2E(\mathbf{k})} \tag{A.140}$$

has been used. The normal-ordered stress tensor operator is then

$$\begin{aligned} :T_{ij}(0,\mathbf{0}):= \frac{1}{4} \sum_{\mathbf{k},\mathbf{p},s,r} & (k_j+p_j) \bar{v}^s(\mathbf{k}) \gamma_i v^r(\mathbf{p}) c^s(\mathbf{k}) c^{r\dagger}(\mathbf{p}) + (k_j+p_j)(\bar{u}^s(\mathbf{k}) \gamma_i u^r(\mathbf{p}) b^r(\mathbf{p}) b^{s\dagger}(\mathbf{k})) \\ & + (k_j-p_j)(\bar{v}^s(\mathbf{k}) \gamma_i u^r(\mathbf{p}) c^s(\mathbf{k}) b^r(\mathbf{p}) - \bar{u}^s(\mathbf{k}) \gamma_i v^r(\mathbf{p}) b^{s\dagger}(\mathbf{k}) c^{r\dagger}(\mathbf{p})) + (i \leftrightarrow j). \end{aligned}$$

To calculate the spectral densities in Section 7.3.2 we require the contractions of the stress tensor with the vacuum and the two-particle states. The two-particle states consist of a particle and antiparticle with some momenta, $u^\mu = (E(\mathbf{u}), \mathbf{u})$ and $v^\mu = (E(\mathbf{v}), \mathbf{v})$, and some spins, s and r, respectively:

$$|\mathbf{u}, s; \mathbf{v}, r\rangle = b^{s\dagger}(\mathbf{u}) c^{r\dagger}(\mathbf{v}) |0\rangle, \tag{A.141}$$

that therefore give matrix elements

$$\langle 0| :T_{ij}(0,\mathbf{0}): |\mathbf{u}, s; \mathbf{v}, r\rangle = \frac{1}{2}(v-u)_{(i} \bar{v}^r(\mathbf{v}) \gamma_{j)} u^s(\mathbf{u}). \tag{A.142}$$

From the spin-sum formulae (A.137) it follows that

$$\begin{aligned} \sum_{s,r} \langle 0| :T_{ij}(0,\mathbf{0}): |\mathbf{u}, s; \mathbf{v}, r\rangle \langle 0| :T_{k\ell}(0,\mathbf{0}): |\mathbf{u}, s; \mathbf{v}, r\rangle^\star = \\ \frac{1}{4}(u-v)_{(k} \mathrm{tr}\left(\gamma_{\ell)} (-\not{p} - m) \gamma_{(j} (\not{q} + m) \right) (u-v)_{i)}. \end{aligned} \tag{A.143}$$

Using the anticommutation relations between the γ matrices (A.99) and, in particular, the fact that traces of odd numbers of spatial gamma matrices are zero and

$$\mathrm{tr}\left(\gamma_j \gamma_\ell \gamma_a \gamma_b \right) = N \left(\delta_{j\ell} \delta_{ab} - \delta_{ja} \delta_{\ell b} + \delta_{jb} \delta_{\ell a} \right), \tag{A.144}$$

it follows that $A_{ijkl}(\mathbf{u},\mathbf{v}) \equiv (u-v)_i(u-v)_k \mathrm{tr}(\gamma_j(-\not{u}+m)\gamma_\ell(-\not{v}-m))$ can be expressed in terms the momenta of the particles as

$$A_{ijkl}(\mathbf{u},\mathbf{v}) = N(u-v)_i(u-v)_k\left[u_\ell v_j + v_\ell u_j - \frac{1}{2}(u+v)^2\delta_{j\ell}\right] \tag{A.145}$$

and therefore

$$\begin{aligned}\sum_{s,r}\langle 0|\, :T_{ij}(0,\mathbf{0}):\, |\mathbf{u},s;\mathbf{v},r\rangle\langle 0|\, :T_{k\ell}(0,\mathbf{0}):\, |\mathbf{u},s;\mathbf{v},r\rangle^\star &= \frac{1}{4}A_{(ij)(k\ell)}(\mathbf{u},\mathbf{v}) \\ &= \frac{N}{4}(u-v)_{(i}(\mathbf{u}\mathbf{v}^{\mathrm{T}} + \mathbf{v}\mathbf{u}^{\mathrm{T}} - \frac{1}{2}(u+v)^2\delta_{j)(\ell)})(u-v)_{k)}. \end{aligned}\tag{A.146}$$

Taking $d = 2$ and relabelling the two-particle in states in terms of their total spatial momentum and the spatial momentum of the particle in the rest frame gives the key result (7.42) in Section 7.3.2.

Appendix B

Numerical Methods

In the following sections, we describe the numerical methods used to compute the heat kernels and free energy in Section 5.5 and Section 5.6, closely following the work in [3].

B.1 Setup

We will always restrict to axisymmetric deformations of the sphere; almost all will be metrics of the form (5.89) obtained from an embedding $r = R(\theta)$, though we will also consider metrics of the form (5.106) to allow us to consider conical excesses (which cannot be embedded in $\mathbb{R}^3$). In what follows, it will be convenient to work with the function $f = \ln R$, so that the deformed metric (5.89) can be written as

$$\mathrm{d}s^2 = \mathrm{e}^{2f}\left[\left(1+f'(\theta)^2\right)\mathrm{d}\theta^2 + \sin^2\theta\,\mathrm{d}\phi^2\right]. \tag{B.1}$$

We will always use spherical coordinates $\{\theta,\phi\}$ with ranges $\theta\in[0,\pi]$ and $\phi\in[0,2\pi)$.

To compute the differenced heat kernel we use the form given in (3.13),

$$\Delta K_L(t) = \sum_I \left(\mathrm{e}^{-t\lambda_I} - \mathrm{e}^{-t\bar{\lambda}_I}\right). \tag{B.2}$$

Due to the axisymmetry, the eigenfunctions of L are separable and can thus be written as $h(\theta,\phi) = w(\theta)\mathrm{e}^{im\phi}$, where m takes integer values for the scalar and half-integer values for the fermion. We then have that $L(w\mathrm{e}^{-im\phi}) = \mathrm{e}^{-im\phi}D_m w$, with D_m a second-order ordinary differential operator given explicitly on the geometry (B.1) by

$$D_m w = \mathrm{e}^{-2f}\left[-\frac{w''}{1+(f')^2} + \frac{f''f' - \cot\theta\left(1+(f')^2\right)}{\left(1+(f')^2\right)^2}w' + \left(A(\theta) + mB(\theta) + m^2\mathrm{cosec}^2\theta\right)w\right], \tag{B.3}$$

where for the scalar

$$A(\theta) = -2\xi \frac{\left(f'' - (f')^2 - 1\right)\left(1 - \cot\theta f'\right)}{\left(1 + (f')^2\right)^2}, \tag{B.4}$$

$$B(\theta) = 0, \tag{B.5}$$

while for the fermion

$$A(\theta) = -\frac{1}{2}\frac{\left(f'' - (f')^2 - 1\right)\left(1 - \cot\theta f'\right)}{\left(1 + (f')^2\right)^2} + \frac{1}{4}\frac{\left(\cot\theta + f'\right)^2}{1 + (f')^2}, \tag{B.6}$$

$$B(\theta) = -\frac{\operatorname{cosec}\theta\left(\cot\theta + f'\right)}{\sqrt{1 + (f')^2}}. \tag{B.7}$$

The operator D_m on the conical geometry (5.106) can be obtained analogously, so we do not explicitly write it here.

We index the eigenvalues λ_I as follows. Since λ_I is an eigenvalue of L if and only if it is also an eigenvalue of D_m for some allowed m, it is natural to take m to index the corresponding subspaces of eigenvalues. Within each subspace (that is, for each fixed m), we then introduce an integer $l \geqslant 0$ to index the eigenvalues of the operator D_m in ascending order. We therefore label the eigenvalues as $\lambda_{m,l}$: for any given m, the $\lambda_{m,l}$ for $l = 0, 1, \ldots$ are all the eigenvalues of D_m. With this notation, the eigenvalues of $\overline{L}$ (on the sphere with unit radius) are given by

$$\bar{\lambda}_{m,l} = \begin{cases} (|m| + l)(|m| + l + 1) + 2\xi, & \text{scalar,} \\ \left(|m| + l + \frac{1}{2}\right)^2, & \text{fermion;} \end{cases} \tag{B.8}$$

in other words, the usual quantum number ℓ is replaced by $|m| + l$, enforcing that for a fixed m, $\ell \geqslant |m|$.

The eigenvalues $\lambda_{m,l}$ are determined numerically by discretising the operators D_m over the interval $\theta \in [0, \pi]$ using standard pseudo-spectral differencing from Section 5.4 with a Chebyshev grid of $N + 2$ lattice points including the two boundary points $\theta = 0, \pi$ (see for example [104]). One subtlety is the appropriate treatment of the poles $\theta = 0$ and π. Regularity of the metric (B.1) requires that $f'(0) = 0 = f'(\pi)$, and hence an expansion of f around these points has a vanishing linear term. Using (B.3) for the scalar field, it then follows from a Frobenius expansion that near $\theta = 0$ any solution to $D_m w = \lambda_{m,l} w$ admits a regular behaviour that goes like

$$w = \theta^{|m|}\left(w_0 + \theta^2 w_2 + \cdots\right) \tag{B.9}$$

with $w_0 \neq 0$, in addition to a singular behaviour that goes like $\theta^{-|m|}$. At the other pole,

we have an analogous behaviour:

$$w = (\pi - \theta)^{|m|} \left(\tilde{w}_0 + (\pi - \theta)^2 \tilde{w}_2 + \cdots \right). \tag{B.10}$$

Hence when we difference the operators D_m with $m \neq 0$, we impose Dirichlet boundary conditions at the poles, while when we difference the operator D_0 we impose Neumann boundary conditions. On the other hand, for the fermion we instead have the allowed behaviours

$$w = \theta^{|m-\frac{1}{2}|} \left(w_0 + \theta^2 w_2 + \cdots \right), \tag{B.11}$$

$$w = (\pi - \theta)^{|m+\frac{1}{2}|} \left(\tilde{w}_0 + (\pi - \theta)^2 \tilde{w}_2 + \cdots \right). \tag{B.12}$$

Thus for $|m| \neq 1/2$ we discretise with Dirichlet boundary conditions at both poles, while for $m = 1/2$ we take a Neumann boundary condition at $\theta = 0$ and Dirichlet at $\theta = \pi$, and likewise for $m = -1/2$ a Neumann condition at $\theta = \pi$ and Dirichlet at $\theta = 0$.

Thus for each m we obtain an $N \times N$ matrix representing the discretisation of D_m; for large N, the N eigenvalues of this matrix should approximate the eigenvalues $\lambda_{m,l}$ for sufficiently low $l < N$. Of course, a finite N will not be able to keep track of eigenvalues with m too large, so some cutoff on m must be imposed. A natural one is suggested by the spherical harmonics: on the round sphere, we might wish to keep all eigenvalues up to a fixed $\ell = |m|+l$; since $l < N$, the strongest constraint is obtained by considering the lowest allowed $|m|$, which fixes a cutoff $\ell < N$. Implementing this same cutoff procedure on the deformed sphere leads us to keeping all eigenvalues satisfying $|m|+l < N$: for each allowed (i.e. integer or half-integer) m with $|m| < N$, we compute the eigenvalues of the discretised operator D_m and keep only the ones with $l < N - |m|$. The actual computation of the eigenvalues of the discretised D_m is conveniently done with the Arnoldi algorithm which is implemented in the `Mathematica` matrix eigenvalue finder. We also note that for the minimally-coupled scalar (i.e. $\xi = 0$), we explicitly drop the lowest eigenvalue $m = 0, l = 0$ because as discussed in Section 5.5.1 it is the same for both L and $\overline{L}$ and thus cancels exactly in the differenced heat kernel.

For a given N, a truncated differenced heat kernel can then be defined:

$$\Delta K_L^{(N)}(t) = \sum_{|m|<N} \sum_{l<N-|m|} \left(\mathrm{e}^{-t\lambda_{m,l}^{(N)}} - \mathrm{e}^{-t\bar{\lambda}_{m,l}} \right), \tag{B.13}$$

where $\lambda_{m,l}^{(N)}$ are the eigenvalues of the discretised operators D_m, as described above. Increasing N should yield a better approximation to the exact heat kernel. We expect this approximation to be best at large t, in which the sum is dominated by the smallest eigenvalues, while the approximation should fail for sufficiently small t, when many eigenvalues make non-trivial contributions to the sum. Since the heat kernel time t can be thought of

as an inverse square of a length scale, we expect that for a fixed N the agreement should fail for t smaller than order $\sim \ell_{\max}^{-2} \sim N^{-2}$.

However, the differenced free energy *is* sensitive to the small-t behaviour of the differenced heat kernel. To accurately compute the free energy, we therefore implement a cutoff time t_{cut} above which we integrate (5.20) with the truncated heat kernel $\Delta K_L^{(N)}$, and below which we integrate (5.20) using the leading-order behaviour $\Delta b_4 t$ from the heat kernel expansion (5.22). For each N and choice of cutoff t_{cut}, this gives an approximation to the free energy:

$$\Delta F^{(N,t_{\text{cut}})} = \sigma T \left(\Delta b_4 \int_0^{t_{\text{cut}}} \mathrm{d}t\, \mathrm{e}^{-M^2 t} \Theta_\sigma(T^2 t) + \int_{t_{\text{cut}}}^{\infty} \frac{\mathrm{d}t}{t}\, \mathrm{e}^{-M^2 t} \Theta_\sigma(T^2 t) \Delta K_L^{(N)}(t) \right). \tag{B.14}$$

The accuracy of this approximation relies on $\Delta K_L^{(N)}$ being well-approximated by the linear behaviour $\Delta b_4 t$ around $t = t_{\text{cut}}$, so that $\Delta F^{(N,t_{\text{cut}})}$ is in fact independent of t_{cut}. With our choice of $N = 600$, the truncated heat kernel $\Delta K_L^{(N)}$ gives a good approximation down to $t \sim 2 \times 10^{-4}$. For moderate deformations of the sphere (up to around $\varepsilon = 0.5$-0.7 for the deformations (5.90), depending on ℓ), $\Delta K_L^{(N)}$ agrees well with the leading-order behaviour $\Delta b_4 t$ around this lowest value of t, and we may therefore compute the free energy as described. In this case, typically we take $t_{\text{cut}} = 2.5 \times 10^{-4}$, and then varying t_{cut} gives an estimate of the systematic error in $\Delta F^{(N,t_{\text{cut}})}$ (for all plots in Chapter 5, this error is no greater than a few percent). For larger deformations, however, $\Delta K_L^{(N)}$ is *not* well-approximated by the leading-order behaviour of the heat kernel expansion around $t \sim 2 \times 10^{-4}$, and therefore we are unable to accurately compute the differenced free energy for such deformations.

We now discuss in more detail the convergence of $\Delta K_L^{(N)}$ with N, agreement with the heat kernel expansion at small t, and agreement with the perturbative results for small deformations of the sphere.

B.2 Convergence

Since we are using pseudo-spectral differencing, we expect the error in a given eigenvalue to fall exponentially with N until a limit from machine precision is reached. Since the truncated differenced heat kernel is constructed directly from the eigenvalues, it too should converge to ΔK_L exponentially until hitting machine precision. This convergence is fast at large t, since there ΔK_L is sensitive to only the smallest eigenvalues, whereas at small t convergence (which is still exponential) requires larger N to achieve the same accuracy.

To exhibit this convergence, let us order the eigenvalues of L in ascending order;

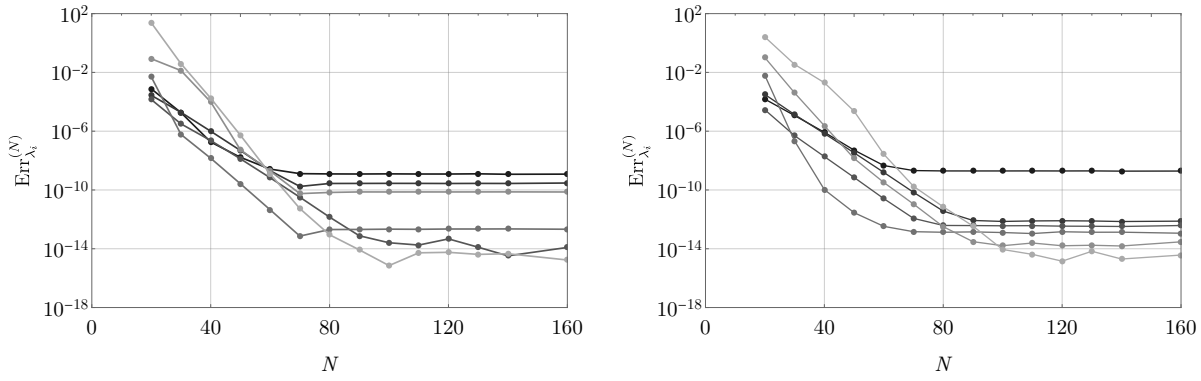

(a) Minimally-coupled scalar (b) Fermion

Figure B.1: Plots of estimated fractional error (B.15) for the eigenvalues of L on the geometry given by the embedding (5.90) with $\ell = 3$ and $\varepsilon/\varepsilon_{\max} = 0.5$. From dark to light grey, each curve corresponds to the i^{th} eigenvalue of L with $i = 2, 10, 25, 100, 200, 400$.

for a given resolution N, we then define the fractional error in the i^{th} eigenvalue as

$$\mathrm{Err}_{\lambda_i}^{(N)} = \left| \frac{\lambda_i^{(N)} - \lambda_i^{(N_{\max})}}{\lambda_i^{(N_{\max})}} \right|, \tag{B.15}$$

where the maximum resolution we use is $N_{\max} = 600$. We plot this fractional error in Figure B.1 for several eigenvalues in the geometry corresponding to the $\ell = 3$, $\varepsilon = 0.5\varepsilon_{\max}$ embedding (5.90). This corresponds to a non-linearly deformed sphere, although one that still is not very close to being singular. We see that all the eigenvalues converge exponentially with N until reaching machine precision around $N \sim 100$. As we would expect, it is the lower eigenvalues that suffer most from machine precision limitations in terms fractional error since they have a smaller absolute value (roughly the magnitude of the eigenvalues goes as $\lambda_i \sim i$). The data indicates that at the resolution $N_{\max} = 600$ used in Chapter 5, the eigenvalues have a fractional error less than $\sim 10^{-8}$ compared to their exact values.

We may likewise define the fractional error in the differenced heat kernel as

$$\mathrm{Err}_{\Delta K_L(t)}^{(N)} = \left| \frac{\Delta K_L^{(N)}(t) - \Delta K_L^{(N_{\max})}(t)}{\Delta K_L^{(N_{\max})}(t)} \right|. \tag{B.16}$$

This fractional error is shown in Figure B.2 (in the same $\ell = 3$, $\varepsilon = 0.5\varepsilon_{\max}$ geometry (5.90)) for several different values of t. Again, we observe initial exponential convergence before we become machine precision limited by $N \sim 80$. Note that smaller t requires a larger N to reach the same accuracy, but the rate of convergence is roughly independent of t. We can estimate that for $t > 0.05$ the fractional error in the differenced heat kernel at $N_{\max} = 600$ is better than $\sim 10^{-7}$, which is commensurate with the error in the individual eigenvalues.

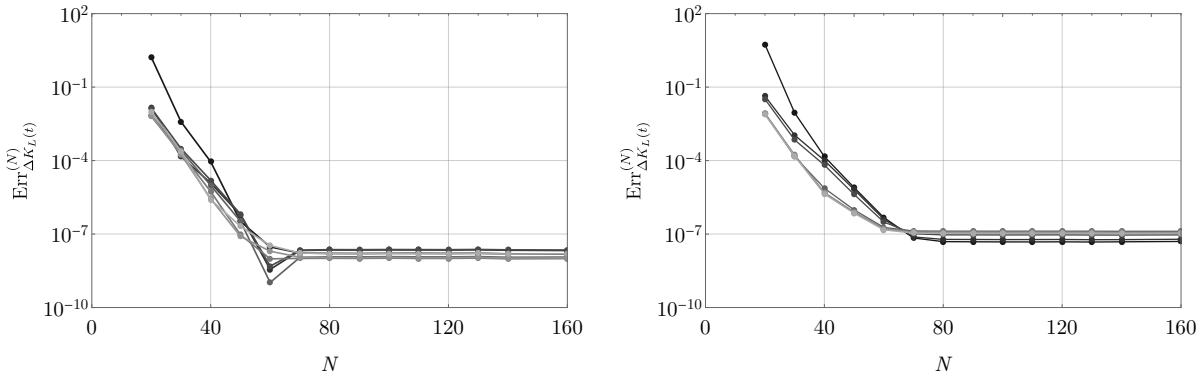

(a) Minimally-coupled scalar

(b) Fermion

Figure B.2: The fractional error (B.16) in the differenced heat kernel on the geometry given by the embedding (5.90) with $\ell = 3$ and $\varepsilon/\varepsilon_{\max} = 0.5$; from dark to light grey, the curves correspond to $t = 0.05, 0.1, 0.2, 1, 2, 4, 8$.

B.3 Comparison to Heat Kernel Expansion and to Perturbative Results

In addition to allowing us to compute the differenced free energy via (B.14) as described above, verifying that the heat kernel approaches the behaviour predicted from the heat kernel expansion at small t also provides a check of our numerical methods. To that end, in Figure B.3 we compare the small-t behaviour of $\Delta K_L^{(N)}$ for various N to the linear behaviour $\Delta b_4 t$ expected from the heat kernel expansion; again we are taking the $\ell = 3$, $\varepsilon = 0.5\varepsilon_{\max}$ embedding (5.90) as a typical example. There are two features to highlight. Firstly, even the lowest value $N = 40$ recovers the heat kernel well above $t \sim 0.1$, but computing the heat kernel accurately at very small t clearly requires using larger values of N. In particular, with the choice of $N_{\max} = 600$ used in Chapter 5, we can reliably compute the heat kernel down to $t \sim 2 \times 10^{-4}$ (with some variation depending on the deformation). Second, while the linear approximation $\Delta b_4 t$ does agree with the truncated heat kernel for sufficiently large N, for even moderate deformations of the sphere this agreement is only valid for very small t (for the case shown here, the fractional error between the linear behaviour and the heat kernel is less than about two percent for $t < 5 \times 10^{-4}$, but grows much larger for larger t). For larger deformations this agreement moves to smaller and smaller t, eventually leaving the domain in which we can reliably approximate the exact heat kernel. It is for this reason that (B.14) cannot be used to approximate the differenced free energy for very large deformations.

As an additional check of our numerical method, we may compare the truncated heat kernel for very small deformations of the sphere to the perturbative heat kernels (5.28) and (5.36). We show this agreement in Figure B.4, again for the $\ell = 3$ embedding (5.90) but now only with a weak deformation of $\varepsilon = 0.01$. Even for modest N, $\Delta K_L^{(N)}$ is very

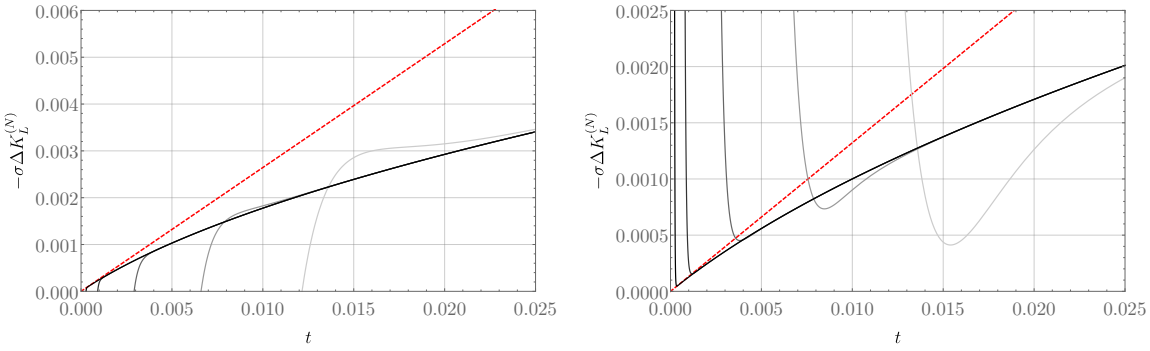

(a) Minimally-coupled scalar (b) Fermion

Figure B.3: Small-t behaviour of the truncated differenced heat kernel $\Delta K_L^{(N)}$ for various N; as in Figures B.1 and B.2, here we show the result for the geometry given by the embedding (5.90) with $\ell = 3$ and $\varepsilon/\varepsilon_{\max} = 0.5$. From light to dark grey, the curves correspond to $N = 40, 60, 100, 200, 400$, while the dashed red line shows the linear behaviour $\Delta b_4 t$ expected from the heat kernel expansion. Note that the linear behaviour only approximates the differenced heat kernel for quite small t, and we need to take $N \gtrsim 400$ to reach this linear regime.

close to the perturbative result for reasonably large t. Increasing N gives agreement with the perturbative results to smaller t, as expected. We also show a comparison with the leading-order heat kernel expansion; unlike the moderate deformation $\varepsilon/\varepsilon_{\max} = 0.5$ shown in Figure B.3, here we see good agreement with the expected linear behaviour up to almost $t \sim 0.1$.

B.4 Details on Calculating the Vacuum Energy

In this section (based on [4]) we include more details on the numerics in Chapter 6, discussing specifically the heat kernel approach to computing the vacuum energies of the free theories, and commenting on the accuracy of our numerical computations.

For the free scalar and fermion, the Casimir energy is computed from heat kernels as described in Chapter 5. In short, because for a CFT the renormalised Casimir energy of the round sphere vanishes, the renormalised Casimir energy of the deformed sphere can be defined as a difference between the energies of the deformed sphere and the round sphere. This difference is given by

$$E[h] = \frac{\sigma}{\sqrt{4\pi}} \int_0^\infty \frac{\mathrm{d}t}{t^{3/2}} \left[\mathrm{Tr}\, \mathrm{e}^{-tL} - \mathrm{Tr}\, \mathrm{e}^{-t\overline{L}} \right], \tag{B.17}$$

where $\sigma = -1/2$ for the scalar and $+1$ for the fermion, L is an elliptic differential operator on Σ, and $\overline{L}$ is the same differential operator on the round sphere. To obtain the Casimir energy, we therefore need to compute the spectrum of L numerically and then perform the above integral (the spectrum of $\overline{L}$ is known). This is done as in Appendix B.1 but with a

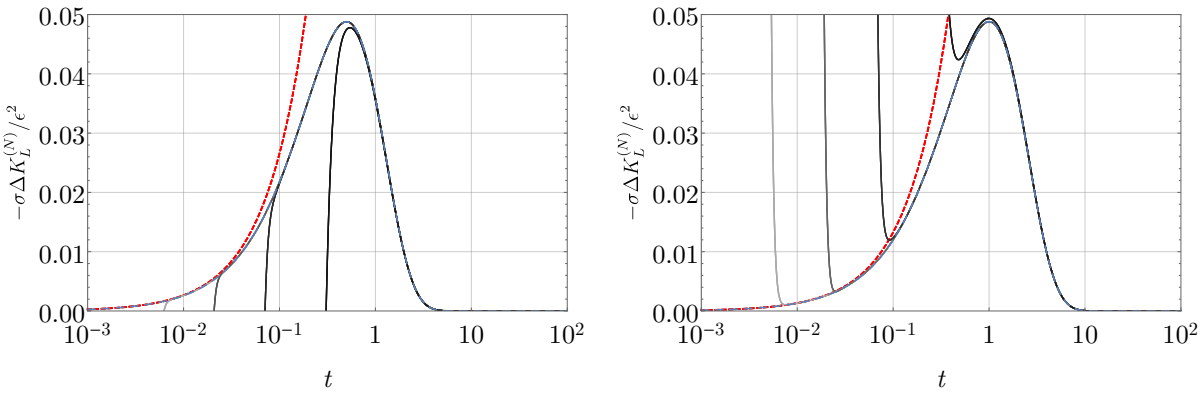

(a) Minimally-coupled scalar

(b) Fermion

Figure B.4: The convergence of the numerically-computed truncated heat kernel $\Delta K_L^{(N)}$ to the perturbative results, for the $\ell = 3$ deformation (5.90) with $\varepsilon = 0.01$. The blue dashed curves show the perturbative heat kernels (5.28) and (5.36), while the dark to light grey curves show the truncated differenced heat kernel for $N = 10, 20, 40, 80$. As in Figure B.3 we see that accuracy at small t requires larger N. We also show the leading linear behaviour $\Delta b_4 t$ from the heat kernel expansion (dashed, red).

minor enhancement allowed by the restriction to zero temperature. For the metrics (6.5) and (6.7), the lowest-lying eigenvalues in the spectrum of L are obtained by exploiting the axisymmetry and using standard pseudo-spectral methods on a grid of 800 points in θ, which allows us to approximate the above traces by summing over the first $\gtrsim 10^5$ eigenvalues. Performing the integral over t is more subtle, as the traces in (B.17) do not commute with the integral. Moreover, the small-t behaviour of the integrand is sensitive to the contributions of many eigenvalues of L; hence for any approximation in which we truncate to the lowest-lying eigenvalues of L, we are not able to accurately evaluate the integrand of (B.17) all the way to $t = 0$. Instead, we again make use of the heat kernel expansion to approximate the behaviour of the traces at small t (2.15):

$$\operatorname{Tr} \mathrm{e}^{-tL} - \operatorname{Tr} \mathrm{e}^{-t\bar{L}} = at \int \mathrm{d}^2 y \sqrt{h} \left(R - \bar{R}\right)^2 + \mathcal{O}(t^2), \tag{B.18}$$

where R and $\bar{R}$ are the Ricci scalars of the deformed and round spheres, and a is a theory-dependent (but geometry-independent) constant. We then evaluate (B.17) by introducing a cutoff t_*: for $t > t_*$ we directly integrate the integrand of (B.17) using the (many) numerically-calculated lowest-lying eigenvalues of L, but for $t < t_*$ we instead integrate the expected linear small-t behaviour (B.18):

$$E_{t_*} \equiv \frac{\sigma}{\sqrt{4\pi}} \left[2a\sqrt{t_*} \int \mathrm{d}^2 y \sqrt{h} \left(R - \bar{R}\right)^2 + \int_{t_*}^{\infty} \frac{\mathrm{d}t}{t^{3/2}} \left(\operatorname{Tr}_N \mathrm{e}^{-tL} - \operatorname{Tr}_N \mathrm{e}^{-t\bar{L}} \right) \right], \tag{B.19}$$

where the subscripts on the traces indicate that they are approximated by using only

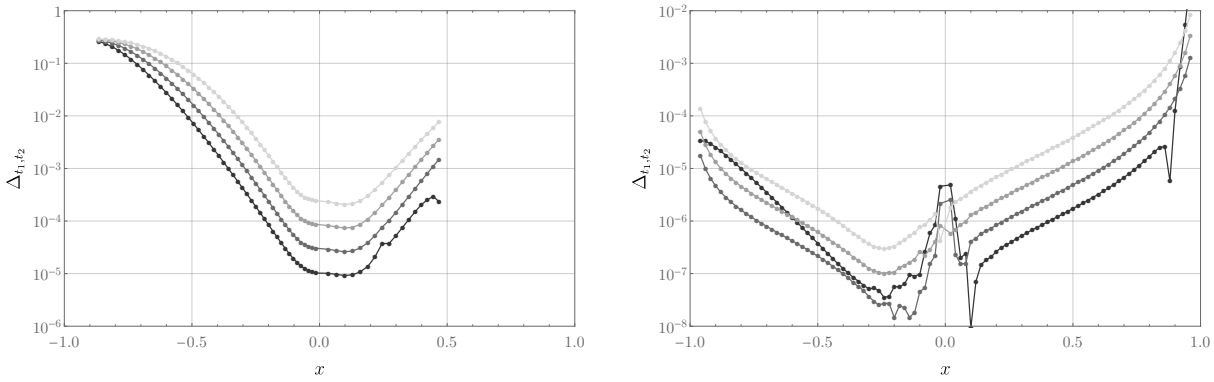

(a) Type 1, $l = 6$ (b) Type 2, $n = 1$

Figure B.5: Example behaviour of Δ_{t_1,t_2} for the Dirac fermion (the behaviour for the scalar is very similar). (a) shows the Type 1 deformation (6.5) with $l = 6$, while (b) shows the Type 2 deformation (6.7) with $n = 1$. For both we use a grid size of $N = 800$ and t_1 and t_2 are adjacent elements from the set $\{0.000125, 0.00025, 0.0005, 0.001, 0.002\}$ with $t_2 < t_1$; from light grey to black the curves correspond to decreasing t_1, t_2.

the lowest eigenvalues of L, as described above. Note here that integral involving the eigenvalues can be performed analytically, in contrast with the finite temperature case. The above procedure was implemented using MATLAB.

For E_{t_*} to be a good approximation to the actual value of the Casimir energy, we must include sufficiently many eigenvalues in the traces in (B.19) that the integrand in the second line recovers the linear behaviour (B.18) at $t \sim t_*$; this is the reason we must include hundreds of thousands of eigenvalues (and therefore use a large grid size of 800 points). For a given geometry, at a fixed and sufficient grid size N, decreasing t_* should then show convergent behaviour before we eventually reach values of t_* smaller than those accessible at the given resolution, and the convergence should cease. In this way we may determine the optimal cutoff t_* for a given N. To quantify this behaviour, we define

$$\Delta_{t_1,t_2} = \left| 1 - \frac{E_{t_*=t_1}}{E_{t_*=t_2}} \right| \tag{B.20}$$

as the relative change between two choices of cutoff. In Figure B.5 we show examples of how Δ_{t_1,t_2} varies as t_1 and t_2 are decreased for the Dirac fermion at our fiducial grid size of $N = 800$; Figure B.5a shows the worst behaviour of any of our deformations, while Figure B.5b shows the best. The scalar field exhibits analogous behaviour, so we do not include additional plots showing it. It is worth noting that while the holographic gravity solutions generally limit the range of geometries we can access for all the theories, even in the free cases systematic error can become large for the more singular geometries as illustrated in B.5a for $x \sim -1$.

As an additional check of the numerics, we also perform the same computation of

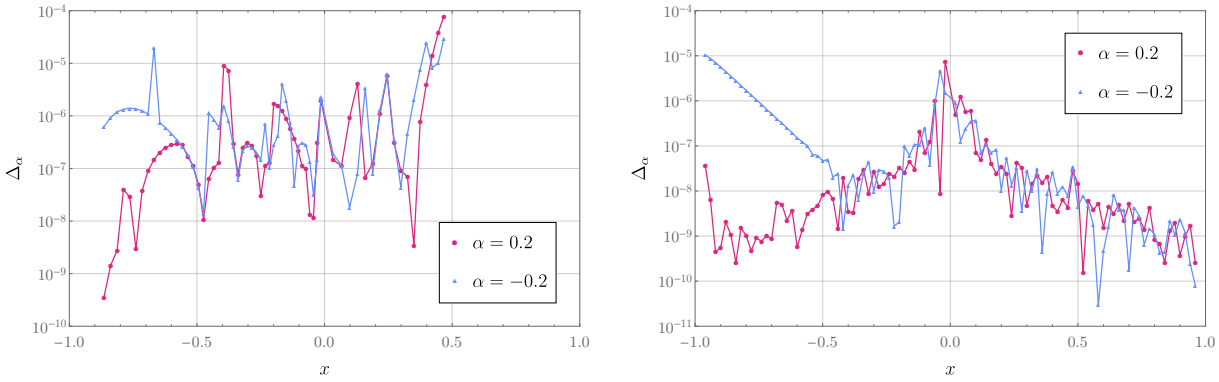

(a) Type 1, $l = 6$ (b) Type 2, $n = 1$

Figure B.6: The relative error Δ_α of the fermion Casimir energy for $\alpha = \pm 0.2$ for two representative deformations, computed with a resolution of $N = 800$. Figure (a) shows the Type 1 deformation with $l = 6$, while Figure (b) shows the Type 2 deformation with $n = 1$.

the energy under a change of coordinates

$$\theta' = \theta + \alpha \sin^3(2\theta), \tag{B.21}$$

where α is a parameter we are free to vary. Of course the energy should be independent of any change of coordinates (and therefore independent of α); any variation with α therefore offers another estimate of numerical accuracy. We therefore introduce the relative error

$$\Delta_\alpha \equiv \left| 1 - \frac{E_\alpha}{E_{\alpha=0}} \right|, \tag{B.22}$$

where E_α denotes the Casimir energy computed using the deformed coordinate θ' defined by (B.21). In Figure B.6 we show this relative error for the fermion for two representative deformations. While the values of $\alpha = \pm 0.2$ naïvely seem quite small, if one looks explicitly at the transformed metric function $b(\theta')$, $s(\theta')$ in the new coordinate θ', they are very substantially changed from those in the original θ coordinate. The good numerical independence on α is then excellent confirmation that the results are reliable and accurate.

Appendix C

The Lorentzian Yamabe Problem

Here, we present some minor modifications to the arguments presented in [126] in order to show that (2+1)-dimensional ultrastatic geometries whose conformal Laplacians have a negative eigenvalue are not Weyl equivalent to any static spacetimes with positive Ricci scalar — this is relevant to the discussion in Section 6.3.

Consider Lorentzian manifolds $\mathbb{R}\times\Sigma$, where $\Sigma = (S^2, h)$, with ultrastatic geometry

$$g = -\mathrm{d}t^2 + h_{ij}(y)\mathrm{d}y^i\mathrm{d}y^j. \tag{C.1}$$

Let ∇_Σ and R_Σ be the Levi-Civita connection on Σ and Ricci scalar, respectively. Under a Weyl transformation $g \mapsto \bar{g} = \varphi^4 g$ where $\varphi \in \mathcal{C}^\infty(\Sigma, \mathbb{R}_{>0})$, the Ricci scalar transforms as

$$\frac{1}{8}\bar{R}\varphi^{s-1} = L_\Sigma\varphi \tag{C.2}$$

with $s = 6$ where

$$L_\Sigma\varphi = -\nabla^2_\Sigma\varphi + \frac{1}{8}R_\Sigma\varphi. \tag{C.3}$$

The task to determine for which geometries Σ there exist $\bar{R}$ smooth and positive such that (C.2) admits a smooth positive solution for φ. An auxiliary problem (that turns out to be equivalent) is to find which Σ admit positive smooth solutions for φ when $\bar{R}$ is a positive constant. This is closely related to the Yamabe problem [143] and can be proven in an identical way using a small modification of a result in [144].

Theorem C.1. *Let $s \in (2, \infty)$ and*

$$\begin{aligned}\mathcal{Q}^s : L^2_1(\Sigma)\setminus\{0\} &\to \mathbb{R}\\ f \;&\mapsto \mathcal{Q}^s[f] = \frac{\displaystyle\int_\Sigma h^{ij}\partial_i f\partial_j f + a_3 R_\Sigma f^2}{\|f\|_s^2},\end{aligned}$$

where $\|\cdot\|_s$ is the L^s norm on Σ and $a_3 = 1/8$. Then we have the following:

(i) *f is a critical point of $\mathcal{Q}^s$ iff f is a weak solution to $L_\Sigma f = \frac{\mathcal{Q}^s[f]}{\|f\|_s^{s-2}} f^{s-1}$*

(ii) *There exists a $\varphi \in C^\infty(\Sigma, \mathbb{R}_{>0})$ with $\|\varphi\|_s = 1$ that minimises $\mathcal{Q}^s$, thus satisfies $L_\Sigma \varphi = \lambda_s(\Sigma)\varphi^{s-1}$ where $\lambda_s(\Sigma) = \inf_{f \in L^2_1(\Sigma)} \mathcal{Q}^s[f]$.*

Proof. Note that $\mathcal{Q}^s[c\varphi] = \mathcal{Q}^s[\varphi]$ for any positive constant c. Hölder's inequality implies that

$$\left| \int_\Sigma R_\Sigma \varphi^2 \right| \geqslant \|\varphi\|_s^2 \|R_\Sigma\|_{\frac{s}{s-2}} \tag{C.4}$$

so $\mathcal{Q}^s$ is bounded below by $-a_3\|R_\Sigma\|_{\frac{s}{s-2}}$ and thus $\lambda_s = \inf_{\varphi \in L^2_1(\Sigma)\setminus\{0\}} \mathcal{Q}^s[\varphi]$ is finite. Let $(u_i)_{i=1}^\infty$ be a sequence of $L^2_1(\Sigma) \setminus \{0\}$ functions such that $\mathcal{Q}^s[u_i] \to \lambda_s(\Sigma)$ monotonically and $\|u_i\|_s = 1$. Since $u_i \in L^2_1(\Sigma) \Rightarrow |u_i| \in L^2_1(\Sigma)$ and $\mathcal{Q}^s[|u_i|] = \mathcal{Q}^s[u_i]$ means that we can choose such a sequence with $u_i \geqslant 0$ and since

$$\|u_i\|^2_{1,2} = \int_\Sigma \partial_k u_i \partial_\ell u_i h^{k\ell} + u_i^2 \tag{C.5}$$

$$= \mathcal{Q}^s[u_i] + \int_\Sigma (1 - a_3 R_\Sigma)\, u_i^2 \tag{C.6}$$

$$\leqslant \sup_{i \geqslant 1} \mathcal{Q}^s[u_i] + \|1 - a_3 R_\Sigma\|_{\frac{s}{s-2}} \tag{C.7}$$

(u_i) is a bounded a sequence in $L^2_1(\Sigma)$ (a Hilbert Space) so by the Banach-Alaoglu Theorem, has a subsequence which converges weakly to some $\varphi_s \in L^2_1(\Sigma)$. $L^2_1(\Sigma)$ is compactly embedded in L^s (Kondrachov Embedding Theorem C.3), thus the subsequence converges strongly to $\varphi_s \in L^s(\Sigma)$ and $\|\varphi_s\|_s = 1$ (norms are continuous). By Hölder's inequality, $\|\cdot\|_1 \leqslant C\|\cdot\|_s$ for some positive constant C, so $\int R_\Sigma u_i^2 \to \int R_\Sigma \varphi_s^2$ and weak convergence in $L^2_1(\Sigma)$ means that

$$\begin{aligned}\int_\Sigma (\nabla_\Sigma \varphi_s)^2 &= \lim_{i\to\infty} \int_\Sigma \nabla_\Sigma \varphi_s \cdot \nabla_\Sigma u_i \\ &\leqslant \lim_{i\to\infty} \left(\int_\Sigma (\nabla_\Sigma \varphi_s)^2 \right)^{1/2} \left(\int_\Sigma (\nabla_\Sigma u_i)^2 \right)^{1/2}\end{aligned}$$

and thus

$$\int_\Sigma (\nabla_\Sigma \varphi_s)^2 \leqslant \lim_{i\to\infty} \int_\Sigma (\nabla_\Sigma u_i)^2$$

and so the non-negative function $|\varphi| \in L^2_1(\Sigma) \subset L^s(\Sigma)$ satisfies $\mathcal{Q}^s[|\varphi_s|] = \mathcal{Q}^s[\varphi_s] \leqslant \lim_{i\to\infty} \mathcal{Q}^s[u_i] = \lambda_s(\Sigma)$ so $|\varphi_s|$ is extremal and thus is a weak solution of (C.2) with $\bar{R} = \lambda_s(\Sigma)$. By the Regularity Theorem C.6, $|\varphi_s|$ is strictly positive and smooth. □

A key consequence of this result is that we can *always* Weyl transform an ultrastatic metric to a static geometry with constant Ricci scalar. Moreover, any given static geometry can only have *either* static geometries with positive Ricci scalar *or* static geometries with non-positive constant Ricci scalar within its conformal class. Indeed, the

Ricci scalar, $\tilde{R}$, of a Weyl transformed static metric, $\tilde{g} \mapsto \Omega^4 g$ with

$$g = -A^2 \mathrm{d}t^2 + h_{k\ell}(y)\mathrm{d}y^k \mathrm{d}y^\ell, \tag{C.8}$$

$A, \Omega \in \mathcal{C}^\infty(\Sigma, \mathbb{R}_{>0})$ and Ricci scalar $R > 0$, satisfies

$$-\frac{1}{A\sqrt{h}}\partial_k \left(A h^{k\ell} \sqrt{h} \partial_\ell \Omega \right) = \frac{1}{8}\tilde{R}\Omega^5 - \frac{1}{8}R\Omega \tag{C.9}$$

which after integrating over any constant t hypersurface gives

$$\int \sqrt{h} A \tilde{R} \Omega^5 = \int \sqrt{h} A R \Omega > 0. \tag{C.10}$$

Thus $\tilde{R}$ must be positive somewhere. Therefore, our family of metrics partitions into those which are Weyl equivalent to a static metric with positive Ricci scalar and those which are Weyl equivalent to a static metric with non-positive constant Ricci scalar. To deduce whether a metric is Weyl equivalent to a static metric with positive Ricci scalar, we need only compute the lowest eigenvalue of L_Σ. This is because of the following result from [126]. Let $\mu(\Sigma)$ be the lowest eigenvalue of L_Σ and $\psi \in \mathcal{C}^\infty(\Sigma)$ its corresponding eigenfunction. Using that $\mu(\Sigma)$ is a lower bound for the Rayleigh quotient of the operator L_Σ and $\lambda_s(\Sigma)$ is a lower bound of $\mathcal{Q}^s$, evaluating $\mathcal{Q}^s$ at its minimiser, φ, and ψ, respectively, gives that

$$\mu(\Sigma)\frac{\|\varphi\|_s^2}{\|\varphi\|_2^2} \leqslant \lambda_s(\Sigma) \leqslant \mu(\Sigma)\frac{\|\psi\|_2^2}{\|\psi\|_s^2} \tag{C.11}$$

and thus the lowest of eigenvalue of L_Σ has the same sign as $\lambda_s(\Sigma)$.

Thus, the Lorentzian manifold $\mathbb{R} \times \Sigma$ is conformally equivalent to a static metric with positive Ricci scalar *if and only if* the lowest eigenvalue of $L_\Sigma = -\nabla_\Sigma^2 + R_\Sigma/8$ is positive. Interestingly, these are the precisely the geometries that support a conformal scalar theory.

C.1 Glossary

$L^p(M) \equiv \left\{ f : M \to \mathbb{R} \text{ s.t. } \int_M |f|^p < \infty \right\}$

$L^p_k(M) \equiv$ Functions in $L^p(M)$ with k weak derivatives (Sobolev space)

$\mathcal{C}^k(M) \equiv$ Functions that are k times differentiable on M with continuous kth derivative

$\mathcal{C}^{k,\alpha}(M) \equiv \mathcal{C}^k$ functions for which $\|f\|_{k,\alpha} = \sum_{i=0}^{k} \sup_M |\nabla^i_M f| + \sup_{x,y\in M} \frac{|\nabla^k_M f(x) - \nabla^k_M f(y)|}{|x-y|^\alpha}$ is finite, where comparison is made between different points by parallel transport along radial geodesics

C.2 Useful Theorems

We include here for reference some useful theorem for the proof of Theorem C.1 from [145].

Theorem C.2 (Sobolev Embedding Theorem). *Suppose* $0 < \alpha < 1$, *and*

$$\frac{1}{q} \leqslant \frac{k-\alpha}{n}. \tag{C.12}$$

Then $L^q_k(M)$ *is continuously embedded in* $\mathcal{C}^{0,\alpha}(M)$.

Theorem C.3 (Kondrachov Embedding Theorem). *Let* M *be a compact manifold of dimension* n, $k > \ell$ *and* $k - n/p > \ell - n/q$. *Then* $L^p_k(M)$ *is compactly embedded in* $L^q_\ell(M)$.

Theorem C.4 (Global Elliptic Regularity). *Let* M *be a compact Riemannian manifold and suppose* $u \in L^1_{\text{loc}}(M)$ *is a weak solution to* $\Delta u = f$.

(i) If $f \in L^q_k(M)$, *then* $u \in L^q_{k+2}(M)$ *and*

$$\|u\|_{q,k+2} \leqslant C(\|u\|_{q,k} + \|u\|_q) \tag{C.13}$$

(ii) If $f \in \mathcal{C}^{k,\alpha}(M)$, *then* $u \in \mathcal{C}^{k+2,\alpha}(M)$ *and*

$$\|u\|_{C^{k+2,\alpha}(M)} \leqslant C(\|u\|_{C^{k,\alpha}(M)} + \|u\|_{C^\alpha(M)}) \tag{C.14}$$

Theorem C.5 (Strong Maximum Principle). *Suppose* h *is non-negative, smooth function on a connected manifold* M, *and* $u \in \mathcal{C}^2(M)$ *satisfies* $(\Delta + h)u \geqslant 0$. *If* u *attains its minimum* $m \leqslant 0$, *then* u *is constant on* M.

Theorem C.6 (Regularity Theorem). *Let* $\varphi \in L^2_1(M)$ *be a non-negative weak solution of* (C.2) *with* $2 \geqslant s$. *If* $\varphi \in L^s(M)$ *then* φ *is either identically zero or strictly positive and* $\mathcal{C}^\infty$.

Proof. $\varphi^{s-1} \in L^{\frac{s}{s-1}}(\Sigma)$ so by the Elliptic Regularity Theorem $\varphi \in L_2^{\frac{s}{s-1}}(\Sigma) \subset \mathcal{C}^{0,2/s}(\Sigma)$. Thus $\varphi^{s-1} \in \mathcal{C}^{0,2/s}(\Sigma)$ and so elliptic regularity gives that $\varphi \in \mathcal{C}^{2,2/s}$.

Taking $m_0 = \max\{0, \sup_\Sigma \left(a_3 R_\Sigma - \lambda_s \varphi^{s-2}\right)\}$, $(\Delta + m_0)\,\varphi \geqslant 0$ then by the strong maximum principle φ must either be zero everywhere (therefore smooth) or positive everywhere. In the latter case we also get that $\varphi^{s-1} \in \mathcal{C}^{2,2/s}(\Sigma)$ and repeated application of elliptic regularity gives that φ is smooth. □